JAEA-Technology
2018-004
DOI:10.11484/jaea-technology-2018-004

Excellent Feature of Japanese HTGR Technologies

Tetsuo NISHIHARA, Xing YAN, Yukio TACHIBANA, Taiju SHIBATA
Hirofumi OHASHI, Shinji KUBO, Yoshitomo INABA, Shigeaki NAKAGAWA
Minoru GOTO, Shohei UETA, Noriaki HIROTA, Yoshiyuki INAGAKI
Kazuhiko IIGAKI, Shimpei HAMAMOTO and Kazuhiko KUNITOMI

HTGR Hydrogen and Heat Application Research Center
Sector of Nuclear Science Research

July 2018

Japan Atomic Energy Agency

日本原子力研究開発機構

JAEA-Technology

本レポートは国立研究開発法人日本原子力研究開発機構が不定期に発行する成果報告書です。
本レポートの入手並びに著作権利用に関するお問い合わせは、下記あてにお問い合わせ下さい。
なお、本レポートの全文は日本原子力研究開発機構ホームページ（http://www.jaea.go.jp）
より発信されています。

国立研究開発法人日本原子力研究開発機構 研究連携成果展開部 研究成果管理課
〒319-1195 茨城県那珂郡東海村大字白方 2 番地4
電話 029-282-6387, Fax 029-282-5920, E-mail:ird-support@jaea.go.jp

This report is issued irregularly by Japan Atomic Energy Agency.
Inquiries about availability and/or copyright of this report should be addressed to
Institutional Repository Section,
Intellectual Resources Management and R&D Collaboration Department,
Japan Atomic Energy Agency.
2-4 Shirakata, Tokai-mura, Naka-gun, Ibaraki-ken 319-1195 Japan
Tel +81-29-282-6387, Fax +81-29-282-5920, E-mail:ird-support@jaea.go.jp

JAEA-Technology 2018-004

Excellent Feature of Japanese HTGR Technologies

Tetsuo NISHIHARA, Xing YAN, Yukio TACHIBANA, Taiju SHIBATA, Hirofumi OHASHI, Shinji KUBO, Yoshitomo INABA, Shigeaki NAKAGAWA, Minoru GOTO, Shohei UETA, Noriaki HIROTA, Yoshiyuki INAGAKI, Kazuhiko IIGAKI[+], Shimpei HAMAMOTO[+] and Kazuhiko KUNITOMI

HTGR Hydrogen and Heat Application Research Center
Sector of Nuclear Science Research
Japan Atomic Energy Agency
Oarai-machi, Higashiibaraki-gun, Ibaraki-ken

(Received March 30, 2018)

Research and development on High Temperature Gas-cooled Reactor (HTGR) in Japan started since late 1960s. Japan Atomic Energy Agency (JAEA) in cooperation with Japanese industries has researched and developed system design, fuel, graphite, metallic material, reactor engineering, high temperature components, high temperature irradiation and post irradiation test of fuel and graphite, high temperature heat application and so on. Construction of the first Japanese HTGR, High Temperature engineering Test Reactor (HTTR), started in 1990. HTTR achieved first criticality in 1998. After that, various test operations have been carried out to establish the Japanese HTGR technologies and to verify the inherent safety features of HTGR.

This report presents several system design of HTGR, the world-highest-level Japanese HTGR technologies, JAEA's knowledge obtained from construction, operation and management of HTTR and heat application technologies for HTGR.

Keywords: HTGR, HTTR, Reactor Design, Licensing, Operation and Maintenance, Heat Application

＋ Department of HTTR

JAEA-Technology 2018-004

日本の高温ガス炉技術の優位性

日本原子力研究開発機構　原子力科学研究部門
高温ガス炉水素・熱利用研究センター
西原　哲夫、ヤン　ジングロン、橘　幸男、柴田　大受、大橋　弘史、久保　真司、
稲葉　良知、中川　繁昭、後藤　実、植田　祥平、広田　憲亮、稲垣　嘉之、
飯垣　和彦[+]、濱本　真平[+]、國富　一彦

(2018 年 3 月 30 日　受理)

日本における高温ガス炉の研究開発は 1960 年代後半に開始した。原子力機構は国内メーカーと協力して、システム設計、燃料、黒鉛、金属材料、原子炉技術、高温機器、燃料・黒鉛の照射試験、高温熱利用技術等の研究開発を実施してきた。1990 年に日本初の高温ガス炉である高温工学試験研究炉 HTTR の建設を開始し、1998 年に初臨界に達し、その後、様々な試験運転を行い、日本の高温ガス炉技術を確立するとともに、高温ガス炉が有する固有の安全性を実証してきた。

本報告書では、高温ガス炉システムの設計例、日本が有する世界最高の高温ガス炉技術及び HTTR の建設、運転保守を通じて得られた知見、熱利用技術について紹介する。

大洗研究開発センター：〒311-1393　茨城県東茨城郡大洗町成田町 4002
＋　高温工学試験研究炉部

Contents

1. Introduction ----------1
2. General Features of High Temperature Gas-cooled Reactor ----------4
2.1 Safety ----------4
2.2 Economy ----------6
2.3 Adaptability to environment ----------7
3. Design of HTGR Plant ----------8
3.1 High Temperature engineering Test Reactor (HTTR) ----------8
3.2 Gas Turbine High Temperature Reactor for Cogeneration (GTHTR300) ---------- 29
3.3 Small-sized cogeneration HTGR (HTR50S) ---------- 39
3.4 Mitsubishi Small Module HTGR (MHR-50/100is) ---------- 47
4. Japanese Technologies of HTGR and Heat Application ---------- 52
4.1 Nuclear design ---------- 52
4.2 Thermal hydraulics design ---------- 59
4.3 Fuel ---------- 70
4.4 Graphite ---------- 79
4.5 Heat exchanger ---------- 87
4.6 High Temperature Resistant Alloy ---------- 96
4.7 Experience of HTTR Licensing ----------102
4.8 Operation and Maintenance of HTTR ----------118
4.9 Gas Turbine System for Power Generation ----------150
4.10 Iodine-Sulfur Process for Hydrogen Production ----------155
4.11 Steam Reforming System for Hydrogen Production ----------163
5. Concluding Remarks ----------174
Acknowledgements ----------174

目　次

1. 序論 ----1
2. 高温ガス炉の概要と特長 ----4
2.1 安全性 ----4
2.2 経済性 ----6
2.3 環境適合性 ----7
3. 高温ガス炉プラントの設計 ----8
3.1 高温工学試験研究炉 (HTTR) ----8
3.2 ガスタービン発電高温ガス炉 (GTHTR300) ---- 29
3.3 小型コジェネレーション高温ガス炉 (HTR50S) ---- 39
3.4 三菱小型モジュール高温ガス炉 (MHR-50/100is) ---- 47
4. 日本の高温ガス炉技術及び熱利用技術 ---- 52
4.1 炉心設計 ---- 52
4.2 熱流力設計 ---- 59
4.3 燃料 ---- 70
4.4 黒鉛 ---- 79
4.5 熱交換器 ---- 87
4.6 耐熱金属材料 ---- 96
4.7 HTTR の許認可 ----102
4.8 HTTR の運転保守 ----118
4.9 ガスタービン発電 ----150
4.10 IS プロセス水素製造 ----155
4.11 水蒸気改質水素製造 ----163
5. 結論 ----174
謝辞 ----174

1. Introduction

High temperature gas-cooled reactor (HTGR) is one of thermal reactors. It has superior safety features by using coated fuel-particle, graphite moderator and helium coolant as shown in Fig.1.1 and potential to supply high temperature heat at 950°C so that it can be used not only for power generation but also for process heat in several industrial field. Development of HTGR power generation plant started in early 1960s in USA and Germany. They constructed and operated experimental reactor and demonstration reactor with steam turbine power generation system. But they terminated to construct a commercial reactor because of political and economic reasons. In 2000s, HTGR attracts attention again as a small-medium reactor with safety and economics. It was selected one of generation IV nuclear systems by US DOE. Now many countries have been conducted research and development for commercial HTGR.

Japan Atomic Energy Agency (JAEA) started research and development of HTGR in 1969. In the first stage, essential technologies of HTGR such as fuel and material test, core physics test, thermal hydraulic test and so on as well as experimental test reactor design were conducted. Since 1985, JAEA started HTTR (High Temperature engineering Test Reactor) project which is the first HTGR in Japan. JAEA got a construction permission of HTTR in 1990 and started construction in 1991. HTTR achieved the first criticality in 1998 and the world's first operation of 950°C reactor outlet coolant temperature in 2004. JAEA completes the world-highest-level HTGR technologies. Furthermore, JAEA conducted long-term high temperature operation (950°C /50days operation) to demonstrate the capability of high temperature heat supply and the loss of forced cooling (LOFC) test at reactor power of 30% to demonstrate the inherent safety feature of HTGR in 2010. The LOFC test simulates the severe accident in which the reactor coolant flow is reduced to zero and the reactor scram is block. The test result shows that reactor shuts down by Doppler Effect and keeps stable condition without any operation management. JAEA has accumulated useful data for development of future commercial HTGR system though design, construction and operation of HTTR. History of HTGR development in Japan is shown in Fig. 1.2.

In this report, we introduce typical HTGR system designs and describe HTGR technologies developed by JAEA in collaboration with Japanese industries.

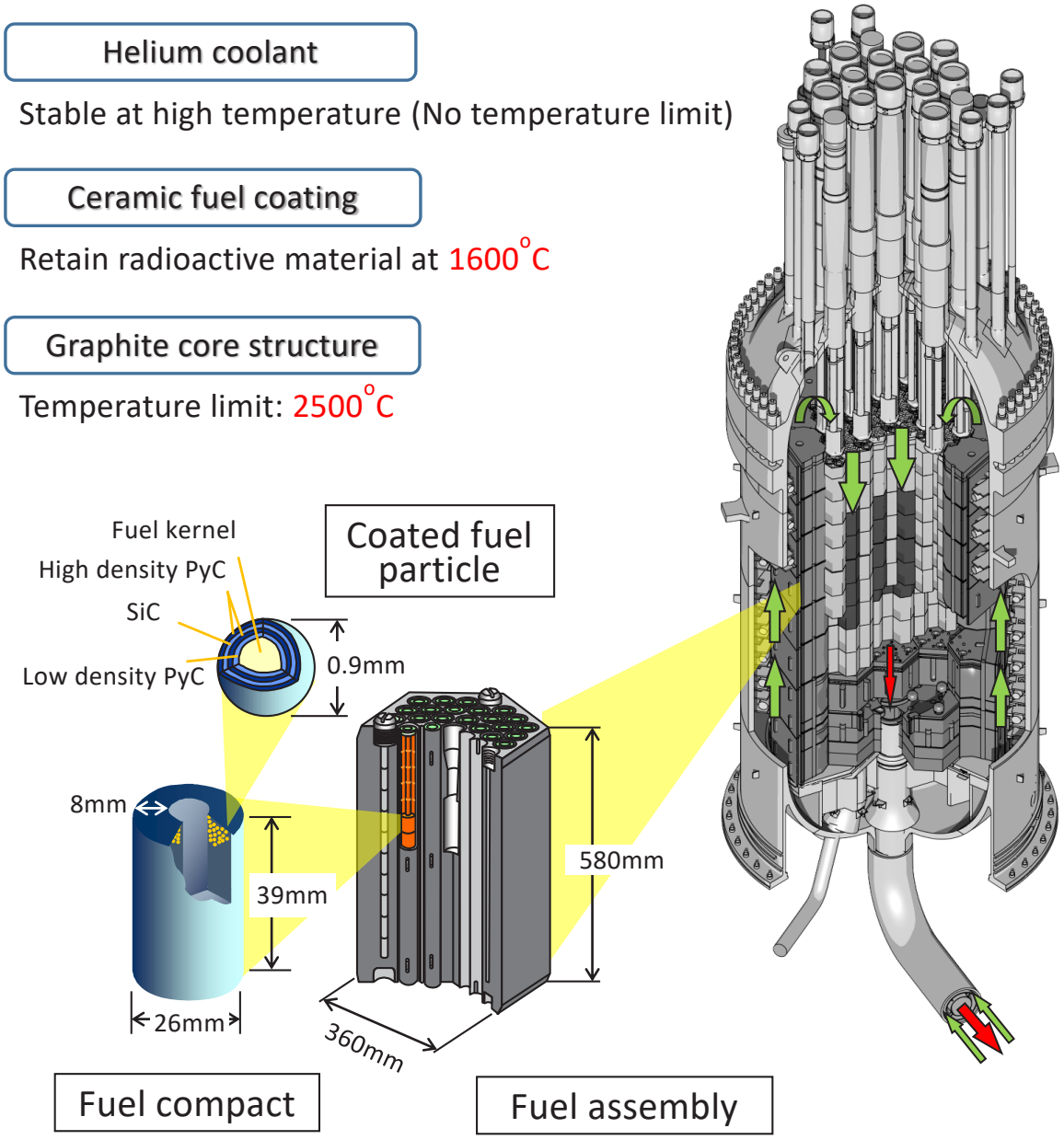

Fig.1.1 Structure of HTGR

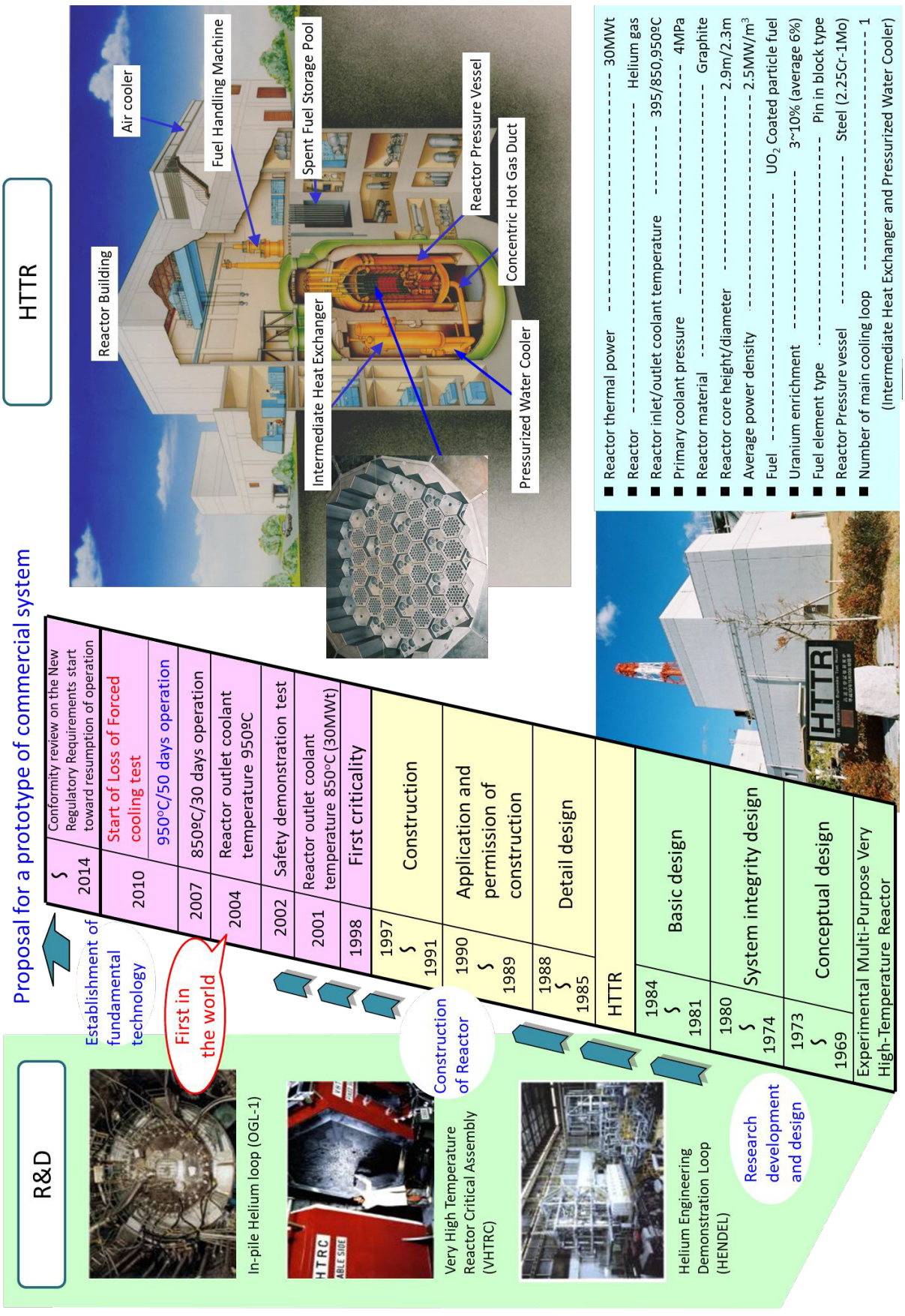

Fig.1.2 History of HTGR development in Japan

2. General Features of High Temperature Gas-cooled Reactor

2.1 Safety

As shown in Fig.1.1, helium coolant is chemically stable, ceramic-coated particle of HTGR fuel has excellent heat-resistant property and contain fission products (FP) within its coating, and graphite core structure also can withstand up to 2500°C without any thermal damage.

Helium gas does not react chemically with fuel and core structures so that hydrogen gas is not produced by chemical reaction of fuel element in accident like a LWR as shown in Fig.2.1. A large amount of water or air ingress can be eliminated by design of secondary water cooling system and reactor confinement building to prevent oxidation of fuel and core graphite material. HTGR does not need to consider the hydrogen explosion and vapor explosion.

Ceramics coated particle fuel can bear very high temperature condition over 2200°C without any FP release as shown in Fig.2.2. It can be recycle use under 1600°C by taking the safety margin. HTGR can be designed that the fuel temperature does not exceed 1600°C in any accident to prevent fuel damage. HTGR does not need to consider the core melt accident.

HTGR can remove the residual heat of the core indirectly because of optimized low reactor power density and graphite core structure. Core graphite has large heat capacity and high thermal conductivity. As the forced cooling performance is gone in a loss of coolant accident, decay heat of fuel transfers to reactor vessel through the core graphite structure slowly by thermal conduction and emission as shown in Fig.2.3. This performance restricts to rise the fuel temperature up to design limit of 1600°C. HTGR does not need to consider the immediate accident management and to provide excess emergency safety system.

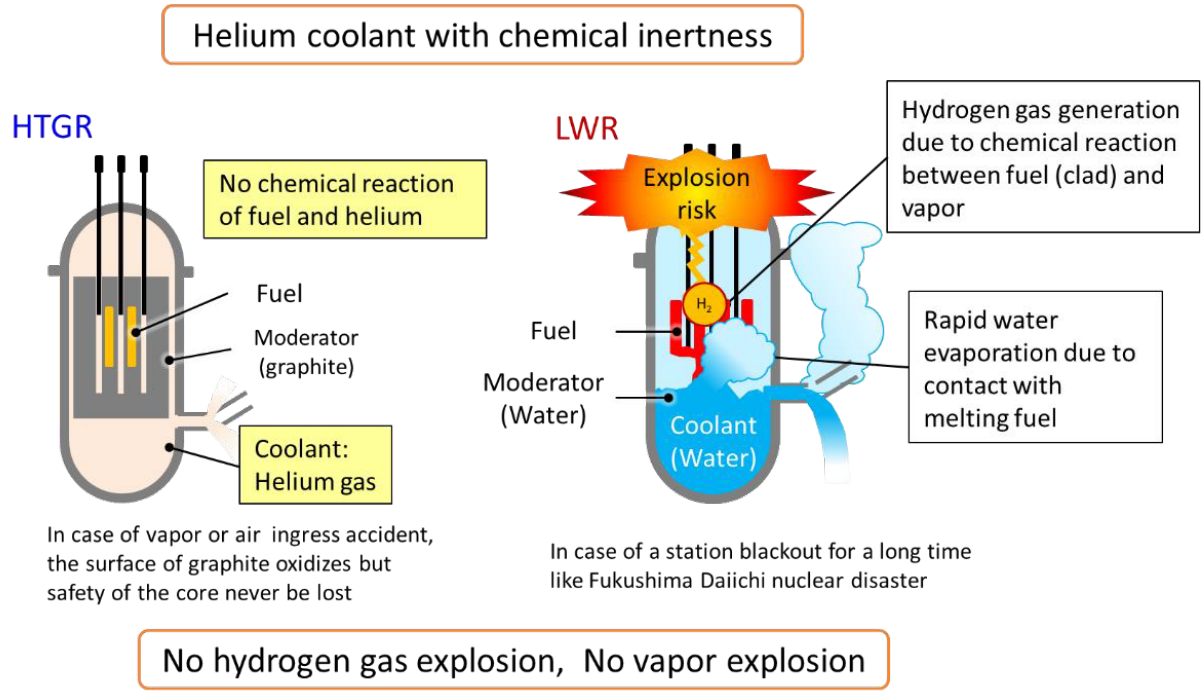

Fig.2.1 Safety feature of HTGR against hydrogen explosion

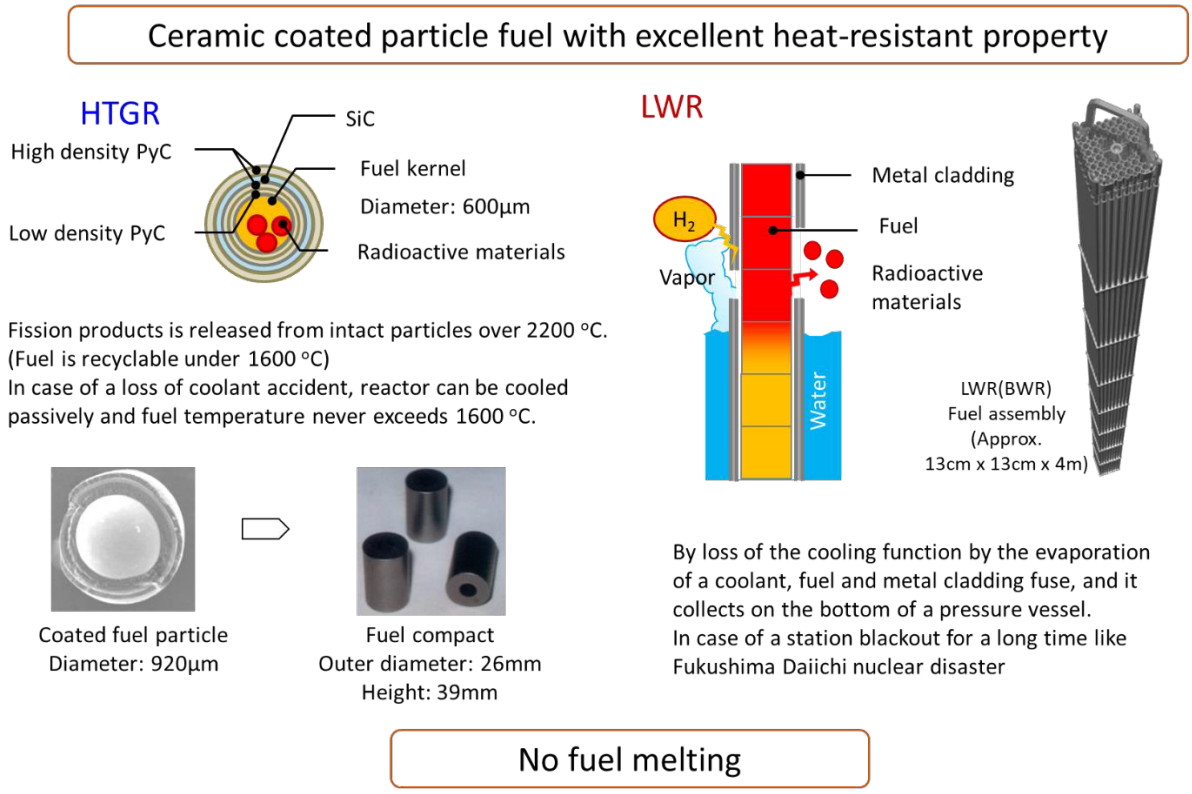

Fig.2.2 Safety feature of HTGR against fission products release

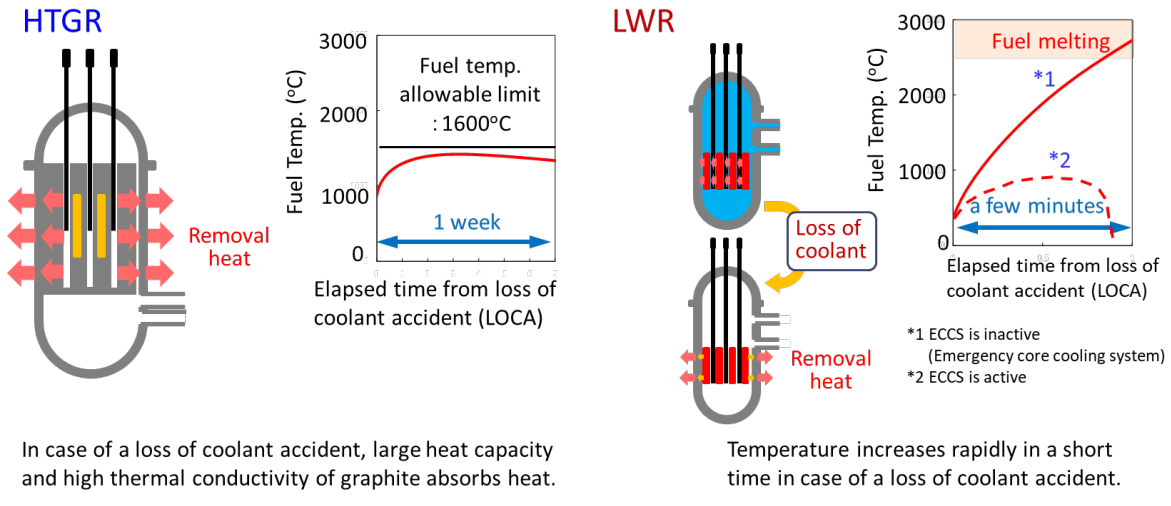

Fig.2.3 Safety feature of HTGR against accident management

2.2 Economy

Helium coolant of HTGR enable to use a gas turbine power generation system. HTGR gas turbine power generation system can achieve high energy efficiency of 46% at 850°C of reactor coolant. High power generation efficiency brings low energy consumption and excellent energy security performance. Inherent safety features of HTGR also offer low construction cost by reducing safety equipment because HGTR can ignore the occurrence of severe accident and consequent core damage as mentioned in Section 2.1. Preliminary cost estimation shows that power generation cost of HGTR is 30% lower than that of LWR as shown in Fig.2.4.

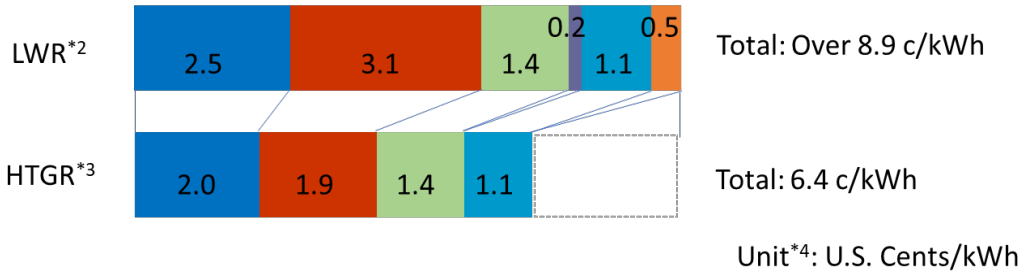

By fully utilizing advantage of HTGR of high thermal efficiency, high retention performance of fission products and excellent inherent reactor safety,

- costs of management for accident risks and additional safety measures are eliminated.
- capital, operating and maintenance costs are lower.

*1 When the HTGR was used only for power generation.
*2 Cost Evaluation Committee Report, National Strategy Office, Energy and Environmental Council, Cost Evaluation Committee (eds.), December 19th, 2011: http://www.cas.go.jp/jp/seisaku/npu/policy09/archive02_hokoku.html
*3 JAEA estimation
*4 Based on the exchange rate in June 2014: 102 JPY/USD

- Capital cost (-0.5 c/kWh)
  The cost is lower owing to fewer number of facilities by small number of water and steam system facilities and higher thermal efficiency of the plant.
- Operating and maintenance costs (-1.2 c/kWh)
  The cost is lower owing to fewer number of facilities in the whole plant and very little radiation exposure to plant operators and maintenance workers because of greater retention of fission products inside four-layer coated fuel particles.
- Fuel cycle cost
- Cost of additional safety measures (-0.2 c/kWh)
  Emergency safety measures, emergency power generation facilities, reliability assurance of external power supply, measures for severe accidents, etc. are eliminated owing to the inherent safety design.
- Expenses related to policy measures
  The cost is not changed for siting, disaster prevention, public relations, development of human resources, assessment and investigation, development of current/future technology for power generation, etc.
- Cost of management for accident risks (-0.5 c/kWh)
  Compensation for damage, decommissioning of accident reactor, decontamination, etc. are eliminated owing to the inherent safety design.

Fig.2.4 Economy of HTGR in power generation

2.3 Adaptability to environment

Coated particle of HTGR fuel has high radiation resistance and high FP containment performance. Average burn-up ratio of HTGR can be 120GWd/t which is 3 times higher than the metal cladding tube fuel like LWR. HTGR power generation system offers low amount of uranium waste in combination with high burn-up fuel and high power generation efficiency. Preliminary estimation shows that the amount of waste can be reduced to one-fourth of LWR as shown in Fig.2.5.

HTGR also can supply high temperature heat and steam through secondary cooling system. This heat can be used as a heat source of chemical plant like hydrogen production plant. The replacement of HGTR from fossil fuel plant can contribute to reduce fossil fuel consumption and carbon dioxide emission. This contributes to resolve the global warming issue.

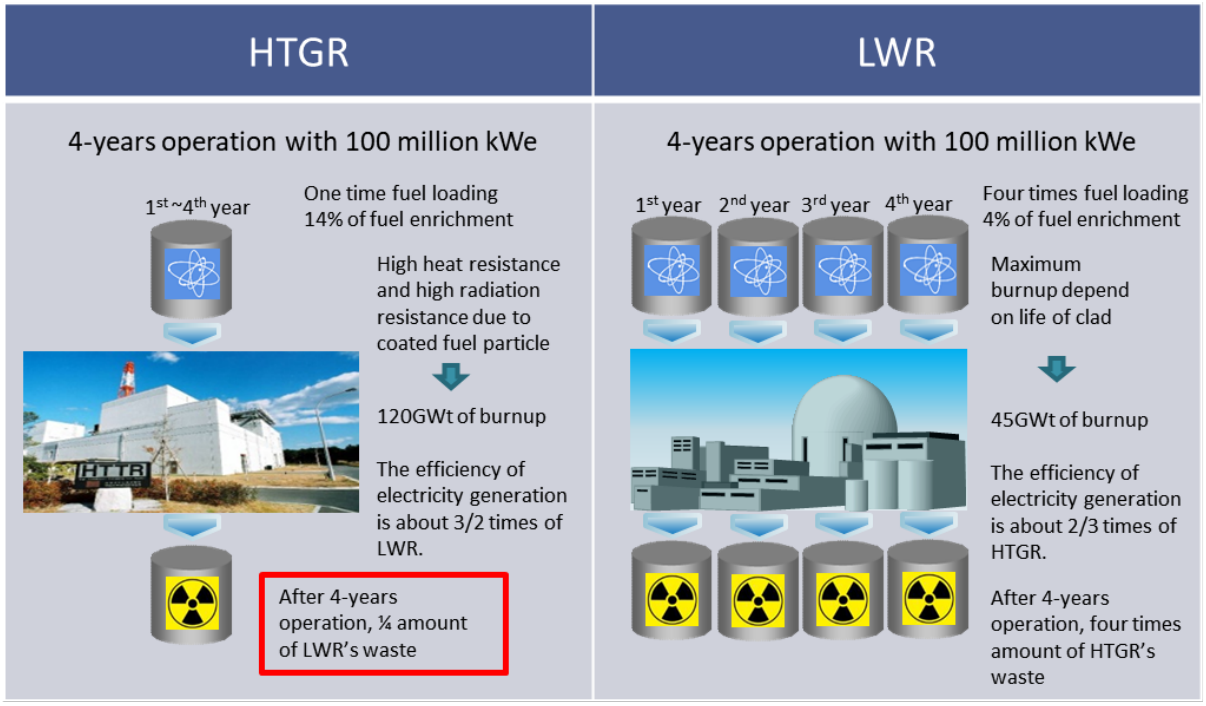

Fig.2.5 Low amount of waste in HTGR

3. Design of HTGR Plant

3.1 High Temperature engineering Test Reactor (HTTR)

3.1.1 HTTR

(1) Outline

A bird's-eye view of the HTTR site is shown in Fig. 3.1.1. The plant area is 200m × 300m in size, including the reactor building, spent fuel storage building, cooling towers, exhaust stack, laboratory building and other auxiliary facilities. The reactor building of 48m × 50m in size is located in the center of the plant. The exhaust stack of 80m in height is in the north side of the reactor building to ventilate the air from the reactor building to the atmosphere. The laboratory building and the development building are on the west of the reactor building. On the east of the reactor building locates the spent fuel storage building.

The reactor building design is illustrated in Fig. 3.1.2 with five levels of three lower ground floors and two upper ground floors. The reactor building contains an 18.5m diameter, 30m height reactor containment vessel made of steel, which is formed in vertical cylinder shape. The reactor pressure vessel, the intermediate heat exchanger (IHX), the pressurized water cooler (PWC) and other heat exchangers in the cooling system are installed in the reactor containment vessel.

The HTTR is the first HTGR in Japan. It is a helium gas cooled and graphite moderated test reactor with 30MW thermal power, and outlet coolant temperature of 850˚C at the rated operation and 950˚C in high temperature test operation. The HTTR uses pin-in-block type fuel assembly and is capable of demonstrating nuclear process heat utilization. The purposes of the HTTR are establishment of the HTGR and nuclear heat utilization technologies. The major specifications of the HTTR are shown in Table 3.1.1. The design life-time of permanent structure components in the HTTR is based on 20 years with a load factor of 60% full power operation.

1) Reactor pressure vessel

The reactor pressure vessel (RPV), 13.2m in inner height and 5.5m in diameter, is fabricated of $2^{1}/_{4}$ Cr-1Mo steel and consists of a vertical cylinder, a hemispherical top lid and a bottom dome. The RPV contains the core components such as fuel blocks, graphite reflectors, reactivity control system, core support structures, etc.

The schematic structure of the RPV is shown in Fig. 3.1.3. The top lid of the RPV is bolted to the flange of the vertical cylinder. Thirty-one stand-pipes, including the control rod and the irradiation stand-pipes, are welded to the top lid. A stand-pipe closure is installed on the top of each stand-pipe and is removed during refueling. Thermal shields are installed on the inner surface of the top lid to protect against high temperatures in accident conditions.

Core support ribs and a core support ring are welded to the bottom dome to support the vertical load of the core components and reactor internals. The RPV is supported by a RPV skirt, stabilizers and a stand-pipe support beam. The RPV skirt is welded to the bottom dome. The stabilizers surround the vertical cylinder and are supported by the side concrete structure. The stand-pipe support beam is located near the top of the stand-pipes. Special stand-pipe fixing devices are located at the top of some of the stand-pipes to prevent the

stand- pipe internal structure from being ejected in the event of a stand-pipe rupture accident.

As a material for the RPV, $2^1/_4$ Cr- 1Mo steel is employed because this steel has better creep strength at high temperature than Mn-Mo steel which is widely used in the pressure vessels of light water reactors. As the RPV constitutes a part of the reactor coolant pressure boundary and is subjected to a higher temperature than those of light water reactor plants, its integrity is of prime importance in the safety of the HTTR. Thus the high-temperature structural design guidelines for the HTTR have been established based on the well-established design guidelines for the fast breeder reactor plants taking into account the characteristics of the material and HTTR service conditions.

2) Containment structure

The containment structure consists of a reactor containment vessel (CV), service area (SA) and an emergency air purification system which reduce the release of FP to the environment during the postulated accidents. The CV is designed to withstand the temperature and pressure transients and to be leak-tight within the specified limits in the case of concentric hot gas duct rupture.

a) Reactor containment vessel

The CV made of steel is 30.3m in height, 18.5m in inner diameter and has 2800m^3 free volume. Its configuration is shown in Fig. 3.1.4. The CV is comparatively small, to minimize the amount of air which may react with graphite components during the depressurization accident (rupture of the concentric hot gas duct).

The CV is designed to have a maximum leak rate of 0.1% of the total volume per day at room temperature and 0.9 times of 0.4MPa, which is the maximum service pressure. The specification of the CV is shown in Table 3.1.2.

b) Service area

The SA is the space surrounding the CV where the fuel handling and storage systems and the primary and the secondary helium purification systems are located. The pressure inside the SA is maintained slightly lower than that of the atmosphere by the ventilation system and the emergency air purification system in normal and accident conditions, respectively.

c) Emergency air purification system

The emergency air purification system removes airborne radioactivity and maintains proper pressure in the SA during the accidents. The system consists of two lines as shown in Fig. 3.1.5. Each line consists of an exhaust filtering unit, an exhaust blower and butterfly valves. The system filters and discharges the air to atmosphere through an exhaust duct at a volume flow of 56m^3/min/unit. The specification of the emergency air purification system is shown in Table 3.1.3.

Table 3.1.1 Major specification of the HTTR

Thermal Power	30MW
Outlet coolant temperature	850˚C/950˚C
Inlet coolant temperature	395˚C
Fuel	Low enriched UO_2
Fuel element type	Prismatic block
Direction of coolant flow	Downward flow
Pressure vessel	Steel
Number of main cooling loop	1
Heat removal	Intermediate heat exchanger (IHX)
	Pressurized water cooler (PWC)
Primary coolant pressure	4MPa
Containment type	Steel containment
Plant lifetime	About 20 years

Table 3.1.2 Specification of reactor containment vessel

Containment type	Steel containment
Maximum service pressure	0.4MPa
Maximum service temperature	150˚C
Major size	
Inner diameter	18.5m
Overall height	30.3m
Body thickness	30mm
Top lid thickness	38mm
Refueling hatch diameter	8.5m
Free volume	2800m^3
Material	Carbon steel
Maximum leak rate	Less than 0.1% per day at room temperature and 0.9 times as high as maximum service pressure

Table 3.1.3 Specification of emergency air purification system

Exhaust filtering unit	
Type	Dust and iodine removal filter
Number	2
Volume velocity	56m^3/min/unit
Charcoal thickness	50mm
Removal efficiency	
Iodine	More than 95% at 50˚C and relative humidity of 80%
Metallic FP	More than 99% for 0.7 micron of particle

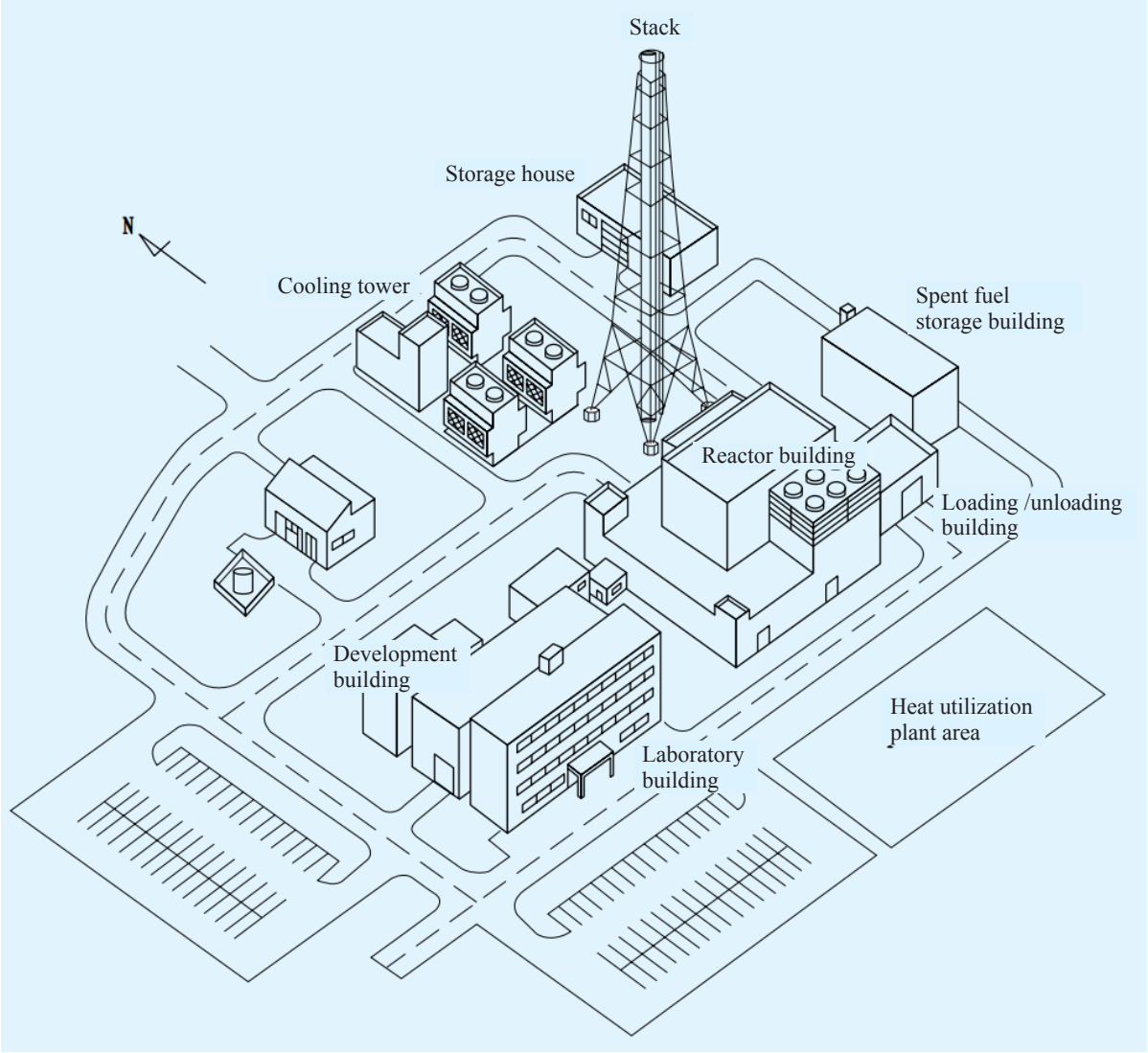

Fig. 3.1.1 Bird's eye view of HTTR site

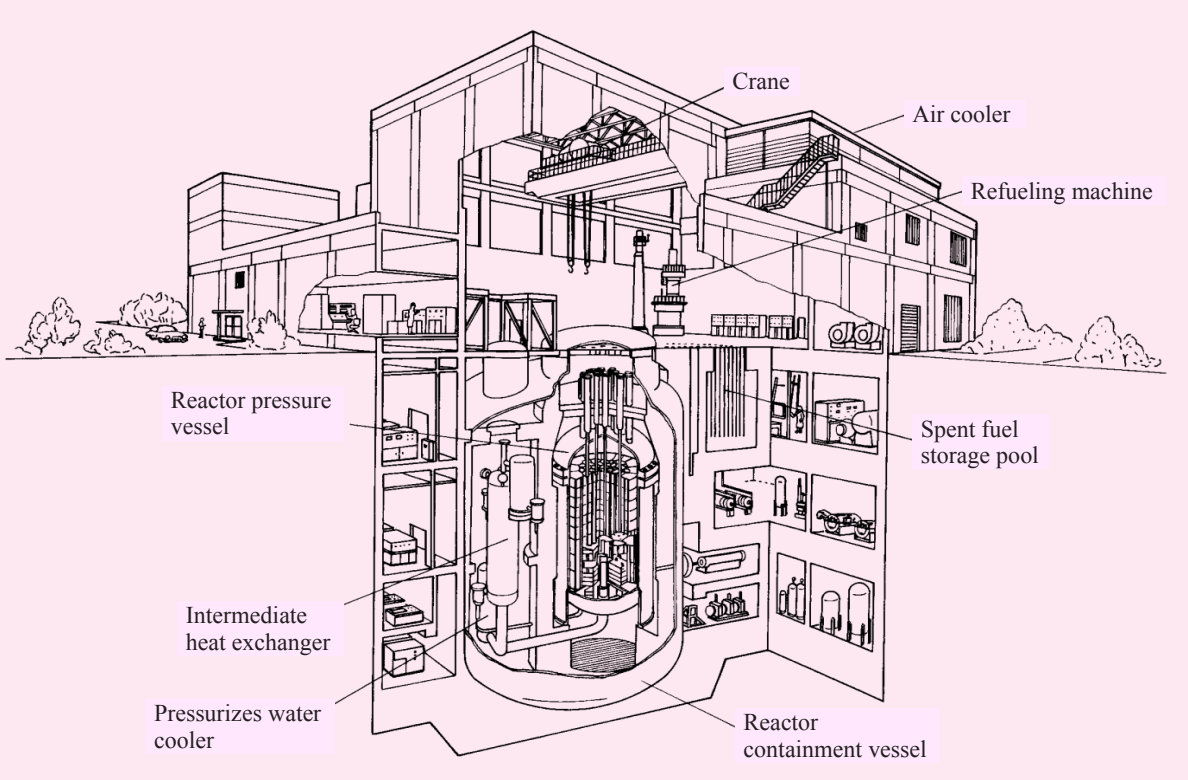

Fig. 3.1.2 Cutaway view of the HTTR reactor building

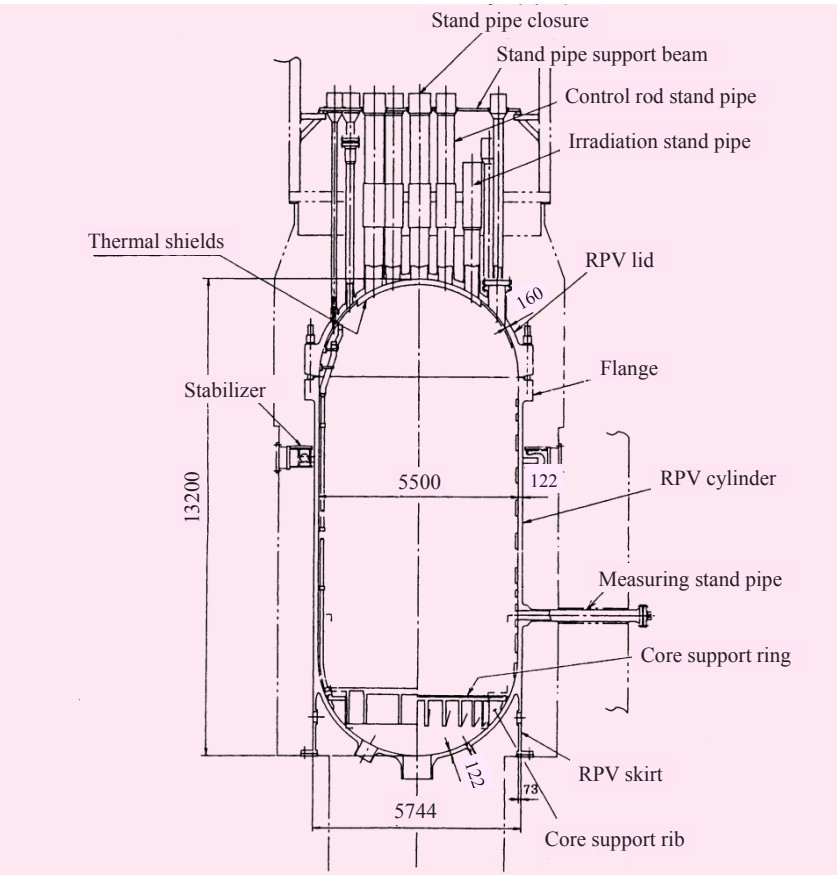

Fig. 3.1.3 Schematic diagram of reactor pressure vessel (unit: mm)

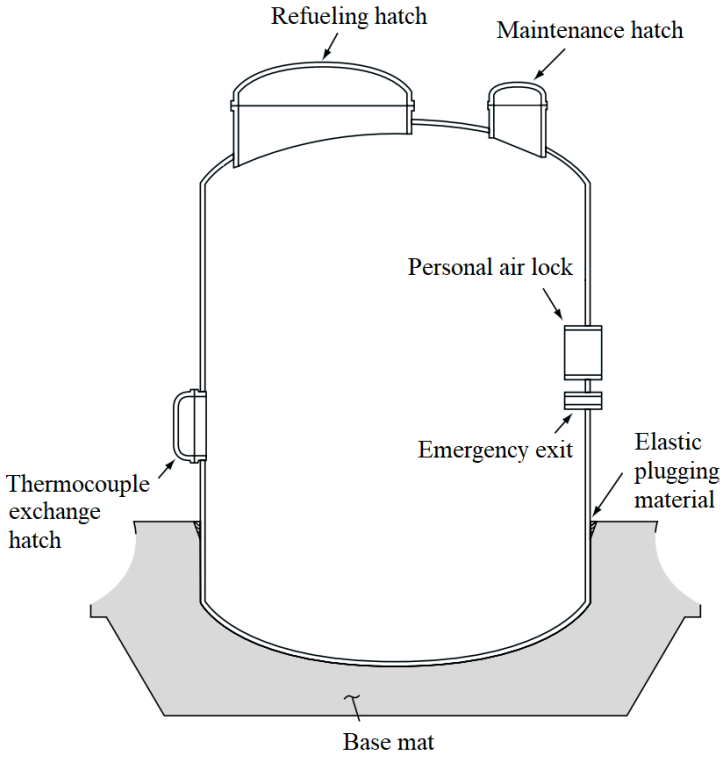

Fig. 3.1.4 Reactor containment vessel

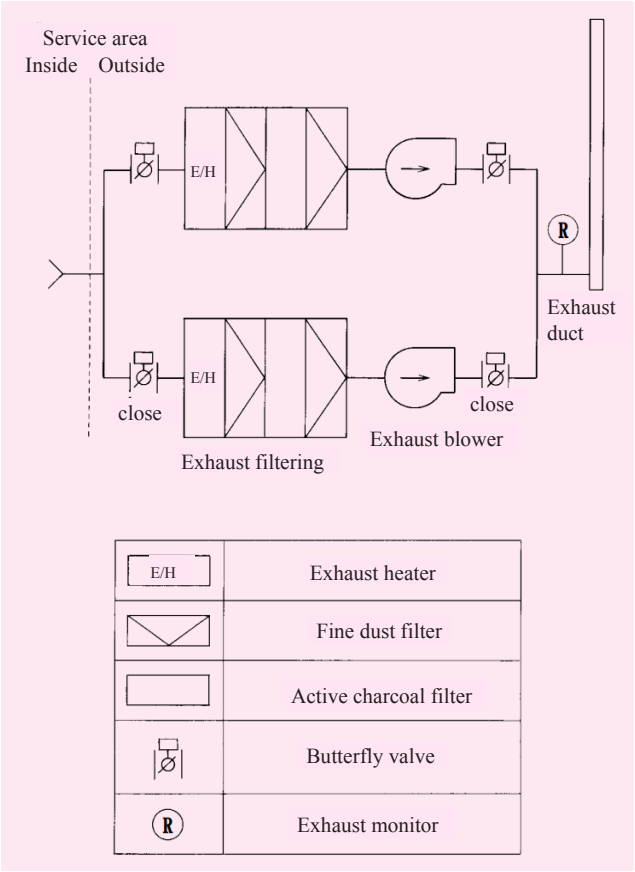

Fig. 3.1.5 Emergency air purification

(2) Nuclear design

1) Nuclear code system

The nuclear characteristics (power distribution, control rod worth, shut down margin, etc.) were calculated by the HTTR nuclear design code system which consists of the computer codes, including DELIGHT[3.1.1)], TWOTRAN-II[3.1.2)], and CITATION-1000VP[3.1.3)].

The analysis of core characteristics was carried out considering the ^{235}U enrichment and burnable poison zoning optimized to minimize the maximum fuel temperature. The calculation flow is shown in Fig. 3.1.6. The DELIGHT code developed in JAEA especially for the nuclear design of the HTTR, is a one-dimensional cell burnup code to produce the few-group constants for core analysis. The TWOTRAN-II is a two-dimensional transport code to produce the average group constants of the burnable poison and graphite block with the control rods. The analysis was conducted by the three-dimensional core analysis code CITATION-1000VP with group constants.

Currently, the burnup and criticality calculation for the HTTR has been performing by using the modern neutronic codes such as deterministic SRAC code, Monte-Carlo MVP and MCNP codes. The calculation results showed a good agreement with the experimental results of the HTTR[3.1.4-3.1.7)].

2) Reactor core

The vertical view of the HTTR is shown in Fig. 3.1.7. The reactor core consists of the reactor internal and the core components. The reactor internal (Fig. 3.1.8) comprises the graphite and metallic core support structures, shielding blocks to support and arrange the core components inside the reactor pressure vessel.

The graphite support structures consist of hot plenum blocks, core bottom structures, core support posts etc. The hot plenum blocks provide lateral and vertical positioning and support of the core array. The blocks contain flow paths which guide the primary coolant from the outlet of the fuel columns and distribute it into the hot plenum beneath the hot plenum blocks.

The core support posts are designed to support the core and hot plenum block arrays which form the hot plenum. The permanent reflector is a graphite structure surrounding the replaceable reflector and control rod guide column located in the circumference of the core. The metallic core support structures are composed support plates, a core support grid and core restraint mechanisms. The core support plate and the core support grid are placed below the thermal insulation layers. The core restraint mechanism surrounds the permanent reflector blocks. These components were assembled in a factory to check the assembly procedure and to test its sealing performance. After the test, these components were dismantled and transported to the site and assembled inside the reactor pressure vessel.

The core components are formed in the same prismatic shape with 36cm in across flat and 58cm in height, including replaceable reflector blocks, irradiation blocks, control rod guide blocks, and fuel assembly blocks. They are cylindrically piled up to form the core. The 290cm height, 230cm diameter active core is surrounded by a permanent reflector made of graphite as presented in Fig. 3.1.9. There are 30 fuel columns and 7 control rod guide columns inside the active core. The reflector region contains 9 additional control rod guide columns, 12 replaceable reflector columns, and 3 irradiation columns. Each fuel column is stacked by 2 bottom graphite

blocks, 5 fuel assembly blocks, and 2 top graphite blocks.

Before loading the fuel blocks into the active core, the whole fuel region is filled with the graphite dummy blocks. After that the fuel blocks is loaded into the fuel region by clockwise replacing the dummy blocks. The fuel blocks are loaded from the periphery to center of the core.

3) Fuel

The configuration of the fuel elements in the HTTR is shown in Fig. 3.1.10. The hexagonal prism fuel block, which is 360mm in width and 580mm in height, consists of 31 or 33 fuel rods. The fuel rods are inserted into fuel holes with a diameter of 41 mm. Each fuel rod is formed from a graphite sleeve containing 14 fuel compacts, in which about 13000 coated fuel particles (CFPs) are stochastically embedded in an annular graphite matrix corresponding to approximately 30% volume packing fraction. Each CFP contains a spherical fuel kernel of low-enriched uranium.

There are four layers surrounding the fuel kernel, including a low-density porous pyrolytic carbon (PyC) buffer layer, followed by a high-density PyC layer, a SiC layer, and an outer high-density PyC layer. The CFPs are fabricated in the graphite matrix of fuel compact. There are 12 different enriched uranium fuels in the HTTR, with 6wt% on average. The more detailed characteristics of the CFPs is shown in Table 3.1.4.

The fabrication of the first-loading fuel started in June 1995. A total of 66,780 fuel compacts, corresponding to 4,770 fuel rods, were successfully produced through the fuel kernel, coated fuel particle and fuel compact processes. The fuel rods were transferred to the reactor building of the HTTR, where the fuel rods were inserted into the graphite blocks to form the fuel assemblies. In December 1997, 150 fuel assemblies were completely formed and stored in new fuel storage cells.

The second-loading fuels were fabricated from 2002 to 2005. About 30,000 fuel compacts have been fabricated successfully. They show as good quality as the first-loading fuels.

4) Reactivity control system

The reactivity control system of the HTTR is shown in Fig. 3.1.11(a). The control rods (CRs) are individually supported by control rod drive mechanisms (CRDMs) located in stand-pipes connected to the hemispherical top lid of the reactor pressure vessel. The CRs are inserted into the channels in the active core and replaceable reflector regions. Reactor shutdown is made at first by inserting 9 pairs of CRs into the reflector region, and then by inserting the other 7 pairs of the CRs into the active core region after the temperature is reduced, so that the CRs should not exceed their design temperature limit.

The CRDM withdraws and inserts a pair of the CRs. During normal operation, the position of the CRs is sustained by the torque of the motor. The maximum withdrawal velocity is limited to a value below 70mm/s by the decelerator. At the reactor shutdown, the CRs are released from the CRDMs by separating the clutch gear teeth, and inserted into the core by gravity. Reserve shutdown capability is provided by insertion of B_4C/C pellets into holes in the CR guide blocks.

Various tests have been performed to evaluate the reliability of the reactivity control system. Fig. 3.1.11(b) shows the typical reactor shutdown time under seismic conditions. The verification tests were

performed to make sure that the CR should not be damaged after the reactor shutdown. The maximum temperature for the verification tests was about 1100˚C.

Concerning the reactivity control system, various tests were carried out to assure the performance, for example, CR driving speed and detection of CR position.

Table 3.1.4 Designs of CFPs

Kernel diameter	600 μm
Fuel kernel material	UO_2
Enriched uranium	6 wt% (Avg.)
Kernel density	10.61 g/cm^3
Coating material	PyC/PyC/SiC/PyC
Layer thickness	60/30/25/45 μm

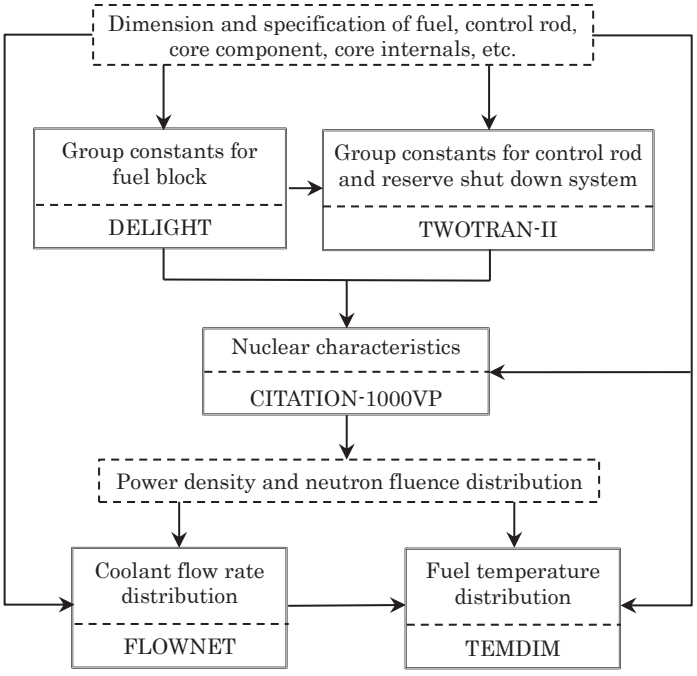

Fig. 3.1.6 Calculation flow of nuclear and thermal-hydraulic design

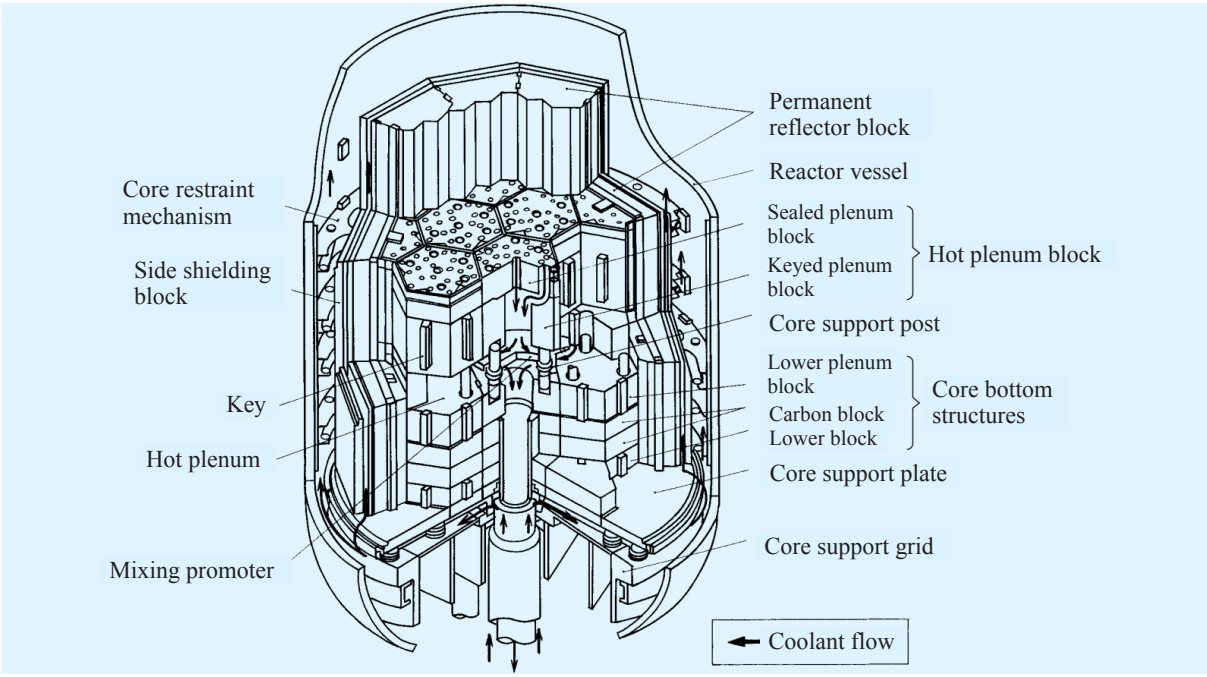

Fig. 3.1.7 Vertical view of the HTTR

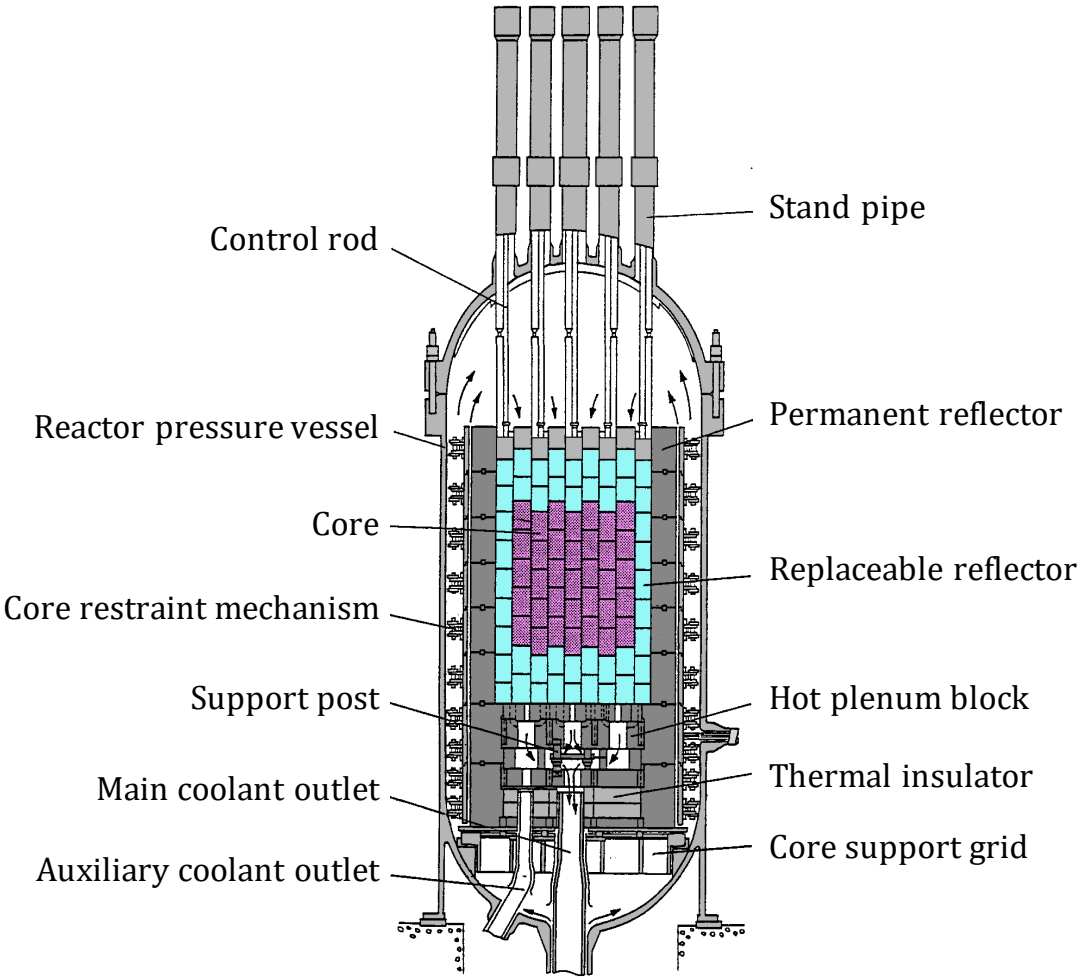

Fig. 3.1.8 Structure of reactor internal

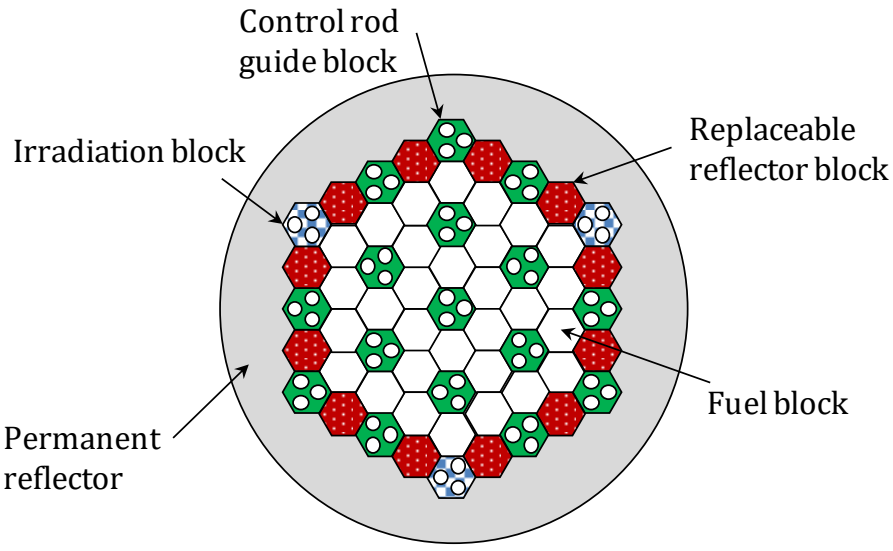

Fig. 3.1.9 Top view of the HTTR core

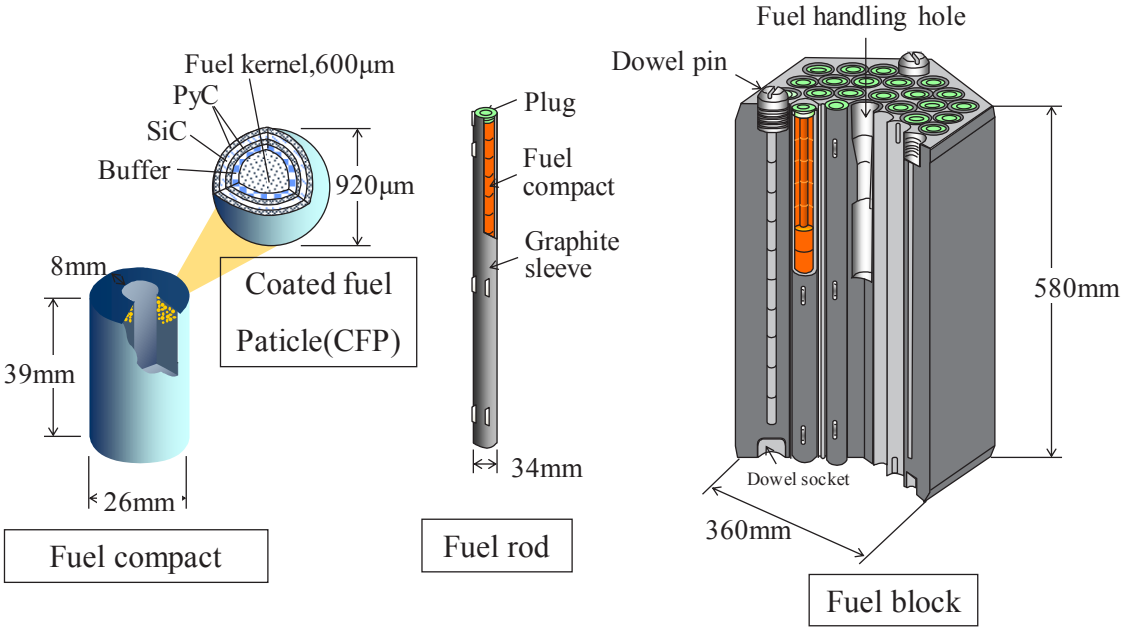

Fig. 3.1.10 Structure of HTTR fuel assembly

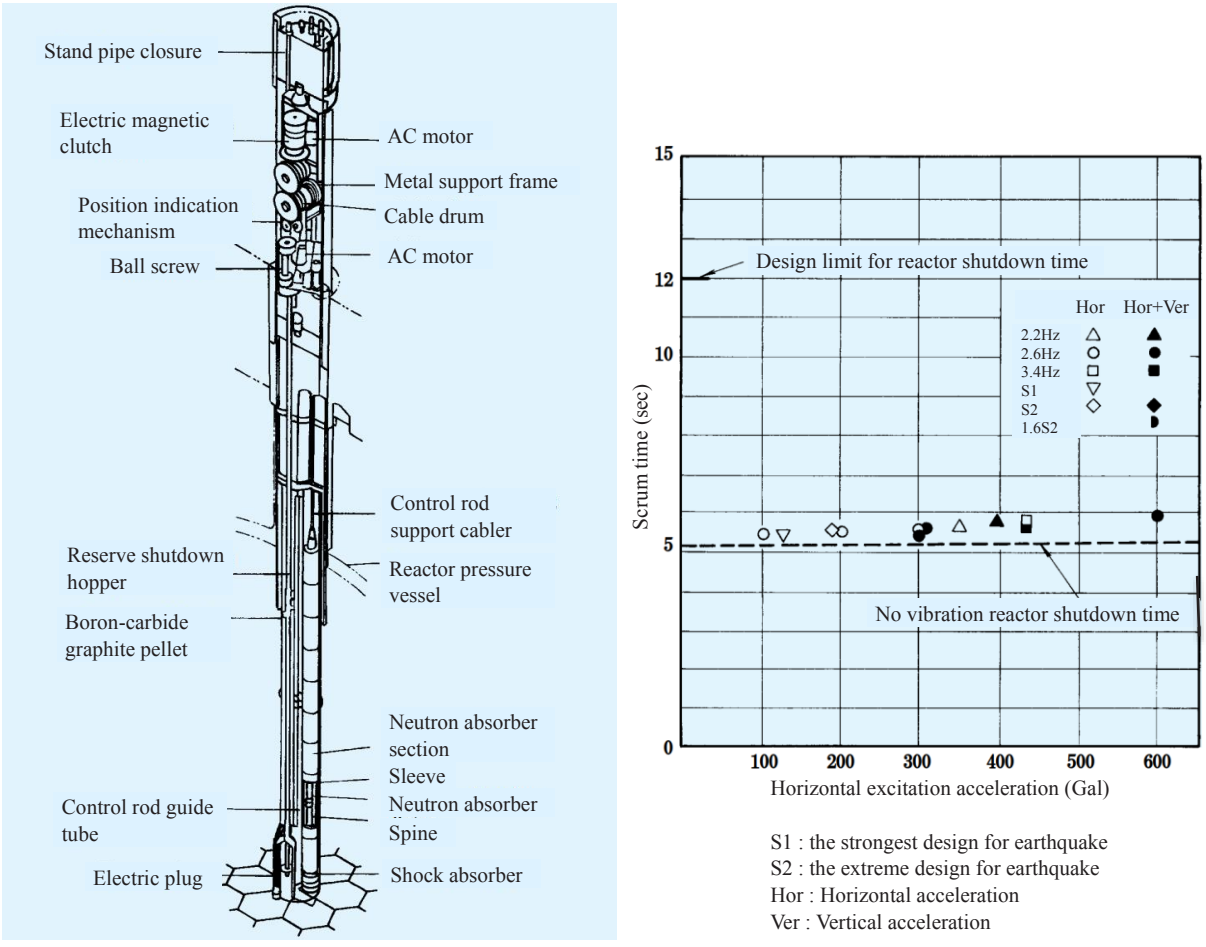

(a) (b)

Fig. 3.1.11 (a) Reactivity control system; (b) Typical results for reactor shutdown time

(3) Thermal design

1) Thermal hydraulic code

The core thermal and hydraulic code diagram can also be seen in Fig. 3.1.6. The thermal-hydraulic characteristics (distribution of coolant flow rate, fuel temperature, etc.) were calculated considering the main coolant flow in the graphite blocks, bypass flow in the inter-column gap, leakage flow through the permanent reflectors and cross flow in the interface of graphite blocks. The distribution of coolant flow rate was calculated by the flow network analysis code FLOWNET[3.1.8)] with the network model. The fuel temperature distribution is estimated using the TEMDIM code[3.1.9)]. The power density and neutron flux distributions are achieved from the neutronic calculations. The thermal behavior and characteristics of the HTTR are also calculated by using the 3-dimentional codes such as RELAP5[3.1.10)], ANSYS FLUENT[3.1.11)], or STAR-CCM+[3.1.12)].

2) Main cooling system

The main cooling system (MCS) of the HTTR is composed of a primary cooling system (PCS), a secondary helium cooling system (SHCS) and pressurized water cooling system (PWCS) as schematically shown in Fig. 3.1.12. The PCS, which has gas circulators and two heat exchangers, i.e. a helium-helium intermediate heat exchanger (IHX) and a primary pressurized water cooler (PPWC), removes the heat from the reactor core to the SHCS and PWCS. Primary helium gas is transferred from the core to the IHX and the PPWC through a primary concentric hot gas duct. The SHCS, composed of the secondary pressurized water cooler (SPWC) and a gas circulator, removes the heat from the primary helium gas through the IHX. The PWCS consists of an air cooler and water pumps. The air cooler cools the pressurized water for both the PPWC and the SPWC, and transfers the heat from the reactor core to the final heat sink of atmosphere.

The HTTR is operated in two loading modes. One is a parallel loaded operation in which the IHX and the PPWC are operated simultaneously. Their heat removal rates are 10 and 20MW, respectively. The other is a single loaded operation in which the reactor is cooled only by the PPWC of 30MW.

3) Auxiliary cooling system

The auxiliary cooling system (ACS) consists mainly of the AHX, auxiliary gas circulators and an air cooler as shown in Fig. 3.1.12. The ACS has a heat transfer capacity of about 3.5MW.

The ACS automatically starts up when the reactor is scrammed and the MCS is stopped in abnormal events. Core cooling by a forced circulation is possible with the ACS. The ACS consists of redundant dynamic components such as gas circulators, water pumps and valves that are also operated with emergency power supply.

The residual heat of the core can be removed even by the vessel cooling system (VCS) without the ACS. The ACS, however, is needed from the viewpoint of operational flexibility, because it takes a very long time to cool down the core by the VCS.

4) Vessel cooling system

The VCS consists of upper, lower, and side cooling panels and heat removal adjustment panels around the RPV, as shown in Fig. 3.1.13, and cooling water circulation systems. The amount of heat removal should be adjusted to be less than 0.6MW during normal operation to accomplish the reactor outlet gas temperature of 950˚C, and to be more than 0.3MW during accidents to cool down the reactor and not to exceed the limits of fuel and RPV temperature. The VCS is used as a residual heat removal system when the forced circulation by the MCS cannot be maintained due to the rupture of the inner pipe or both pipes in the concentric hot gas duct. The VCS is also an engineered safety feature composed of two independent complete sets that are backed up with emergency power supply. They are operated even in normal operation to cool the biological shielding concrete wall.

Each cooling panel consists of several parts. Pressure proof and leakage tests were performed at each fabrication process.

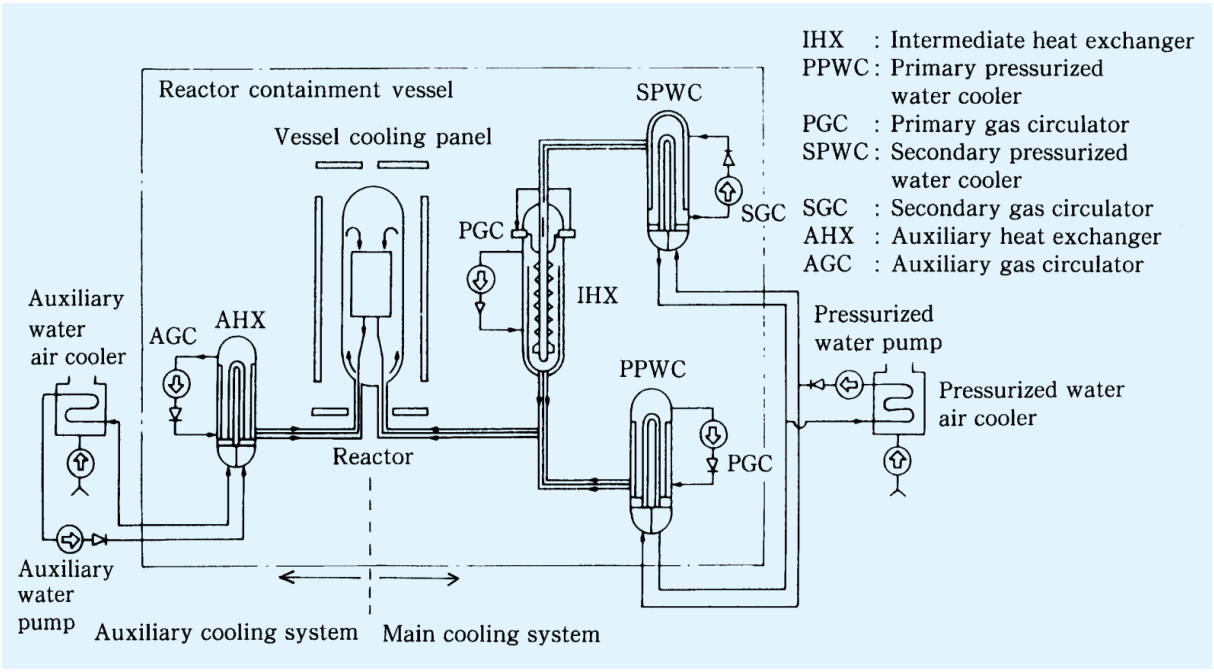

Fig. 3.1.12 Cooling systems

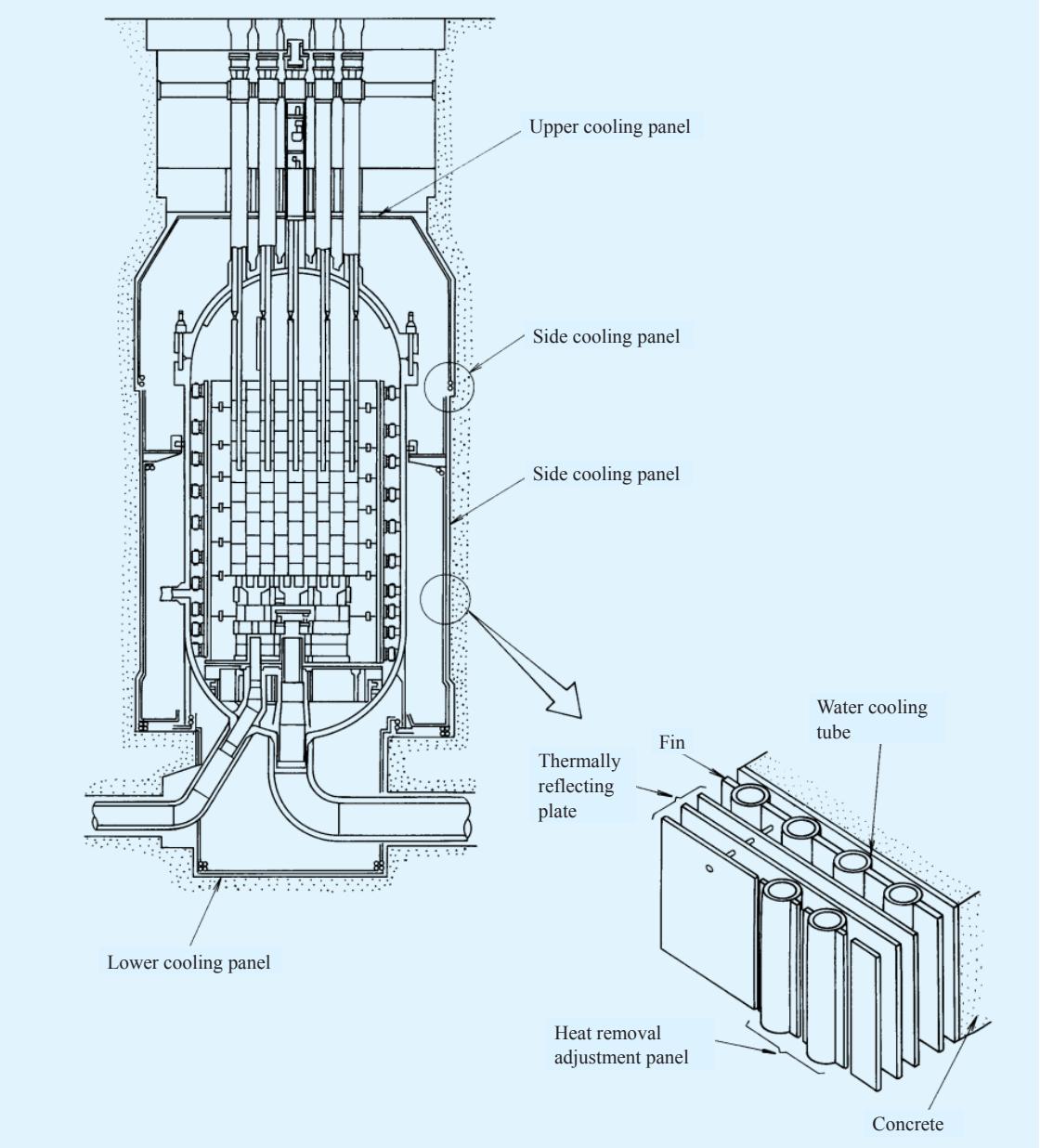

Fig. 3.1.13 Cooling panels of the vessel cooling system around the reactor pressure vessel

References

3.1.1) R. Shindo, et al., “DELIGHT-7: One dimensional fuel cell burnup analysis code for High Temperature Gas-cooled Reactors (HTGR)”, JAERI-M 90-048 (1990), 225p (in Japanese).

3.1.2) K. D. Latherop, F. W. Brinkley. “TWOTRAN-2: An interfaced exportable version of the TWOTRAN code for two-dimensional transport”, LA-4848-MS, Los Alamos National Laboratory (1973).

3.1.3) H. Harada, K. Yamashita, “The reactor core analysis code CITATION-1000VP for high temperature engineering test reactor”, JAERI-M 89-135 (1989), 83p (in Japanese).

3.1.4) M. Goto, et al., “Neutronics calculations of HTTR with several nuclear data libraries”, Journal of Nuclear Science and Technology, 43, 10, pp.1237-1244 (2006).

3.1.5) International Atomic Energy Agency, “Evaluation of High Temperature Gas Cooled Reactor Performance: Benchmark Analysis Related to Initial Testing of the HTTR and HTR-10”, IAEA-TECDOC-1382 (2003).

3.1.6) H.Q. Ho et al., “Investigation of uncertainty caused by random arrangement of coated fuel particles in HTTR criticality calculations”, Annals of Nuclear Energy, 112, pp.42-47 (2018).

3.1.7) J.D. Bess, N. Fujimoto, “Benchmark Evaluation of Start-Up and Zero-Power Measurements at the High-Temperature Engineering Test Reactor”, Nuclear Science and Engineering, 178, pp.414-427 (2014).

3.1.8) S. Maruyama, et al., “Verification of in-vessel thermal and hydraulic analysis code “FLOWNET””, JAERI-M 88-138 (1988), 39p (in Japanese).

3.1.9) S. Maruyama, et al., “Verification of fuel temperature analysis code “TEMDIM””, JAERI-M 88-170 (1988), 72p (In Japanese).

3.1.10) H. Sato, et al., “Validation and application of thermal hydraulic system code for analysis of helically coiled heat exchanger in high-temperature environment”, Journal of Nuclear Science and Technology, 51, 11-12, pp.1324-1335 (2014).

3.1.11) N. Tsuji, et al., “Study of the applicability of CFD calculation for HTTR reactor”, Nuclear Engineering and Design, 271, pp.564-568 (2014).

3.1.12) K. Takamatsu, “Thermal-hydraulic analyses of the High-Temperature engineering Test Reactor for loss of forced cooling at 30% reactor power”, Annals of Nuclear Energy, 106, pp.71-83 (2017).

3.1.2 HTTR gas turbine cogeneration test plant (HTTR-GT/H_2 plant)

With the aim of completion in system technology of an HTGR helium gas turbine as well as hydrogen cogeneration for commercial plant construction, we are planning to couple heat application system consist of helium gas turbine and hydrogen production plant to the HTTR. The objective of HTTR gas turbine cogeneration test plant (HTTR-GT/H_2 plant) construction is to obtain first-of-a-kind license for nuclear-heated helium gas turbine and hydrogen cogeneration plant. Also, we aim to demonstrate economical and reliable operation as a prerequisite for licensing of a commercial plant. The basic design of HTTR-GT/H_2 plant was started in 2015. System design, and major component design has been performed. In addition, auxiliary system design and preliminary safety analysis was completed to show the feasibility of demonstration program.

Table 3.1.5 shows major specifications. Figure 3.1.14 depicts the configuration of HTTR-GT/H_2 plant. The configurations are determined in order to minimize the modification of the existing HTTR facility as well as to simulate the configuration of commercial system. A helium gas turbine and a second intermediate heat exchanger (2nd IHX), which provides heat to the hydrogen production plant, are installed in the secondary helium cooling system. The 2nd IHX and helium gas turbine are installed in cascade. The HTTR is operated in parallel operation mode and one-third of the heat is transported to the secondary loop via the IHX. The heated helium from IHX firstly flows through the inner side of co-axial hot gas duct and introduced to piping with internal insulation. In cogeneration operation, helium from the IHX enters the 2nd IHX to export heat to the tertiary helium loop for hydrogen production and is guided to the helium gas turbine. On the contrary, the heated helium bypasses the 2nd IHX in sole power generation operation, directly flows into the turbine. The turbine exhaust helium is introduced to a recuperator in order to recover heat. Then the flow is delivered to a precooler, enters a compressor, reheated at the recuperator and returns to the IHX via a cooler through the outer side of co-axial hot gas duct. In hydrogen cogeneration operation, a part of flow in the high pressure side of recuperator is provided to the turbine inlet to maintain the temperature as required. The rejected heat from the secondary helium cooling system is dissipated to two cooling water systems via coolers and is exhausted to ambient air through an air cooler and a cooling tower, respectively.

Figure 3.1.15 shows the cross sectional view of an integrated heat exchanger. The integrated heat exchanger consists of a recuperator and a precooler and their connecting flow paths. The recuperator is offset-fin type plate heat exchanger and used to recover heat from turbine exhaust gas. The precooler is a helically-coiled heat exchanger with low finned tubes and aims to cool helium gas to reduce compression work in the compressor. Pressurized cooling water flows through inside of the heat transfer tubes and helium flows outside of the tube bundle. Figure 3.1.16 shows the configuration of turbomachinery. The helium gas turbine consists of turbines, compressors, and generators. The turbines are radial type and devised at either end of a generator shaft. Figure 3.1.17 shows the plant layout. The gas turbine building is sufficient offset distance to ensure the integrity of reactor building which includes safety-related systems, structures and components and habitability of the reactor control room against leakages of combustible and hazardous chemicals.

Table 3.1.5 Major specifications of the HTTR-GT/H_2 plant

Parameters	Specifications
Reactor thermal power [MWt]	30
Reactor outlet temperature [°C] (Sole power generation/cogeneration)	850/950
IHX heat exchange rate [MWt]	10
Power generate rate (max.) [MWe]	1
H_2 production rate (max.) [Nm^3/h]	30
Reactor coolant pressure [MPa]	4
Turbine inlet temperature [°C]	570
Gas turbine pressure ratio	1.3
Turbine flow rate [kg/s]	9-10
H_2 plant heat supply [MWt]	0.7
H_2 plant inlet helium temperature [°C]	820

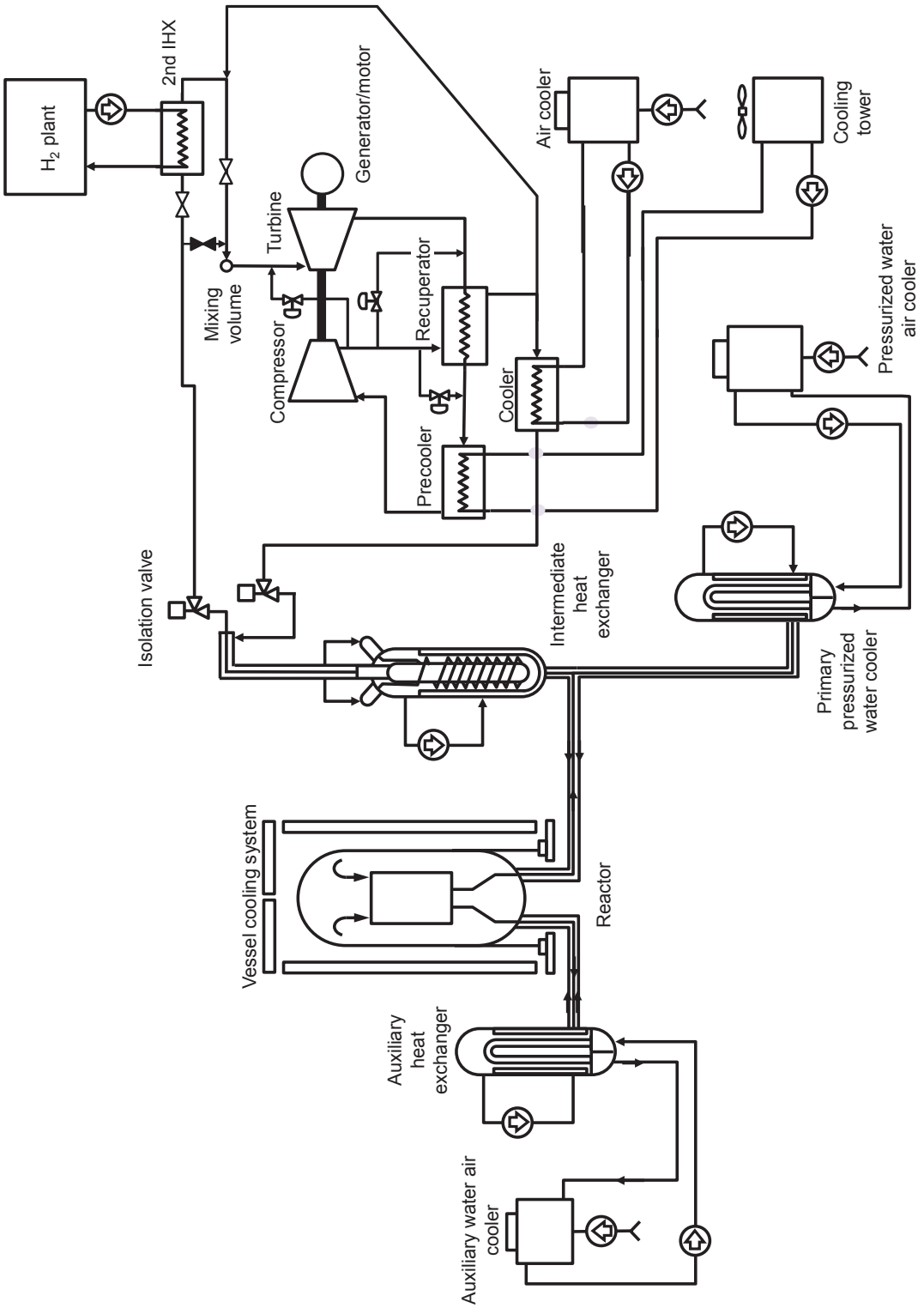

Fig.3.1.14 System configuration of the HTTR-GT/H_2 plant

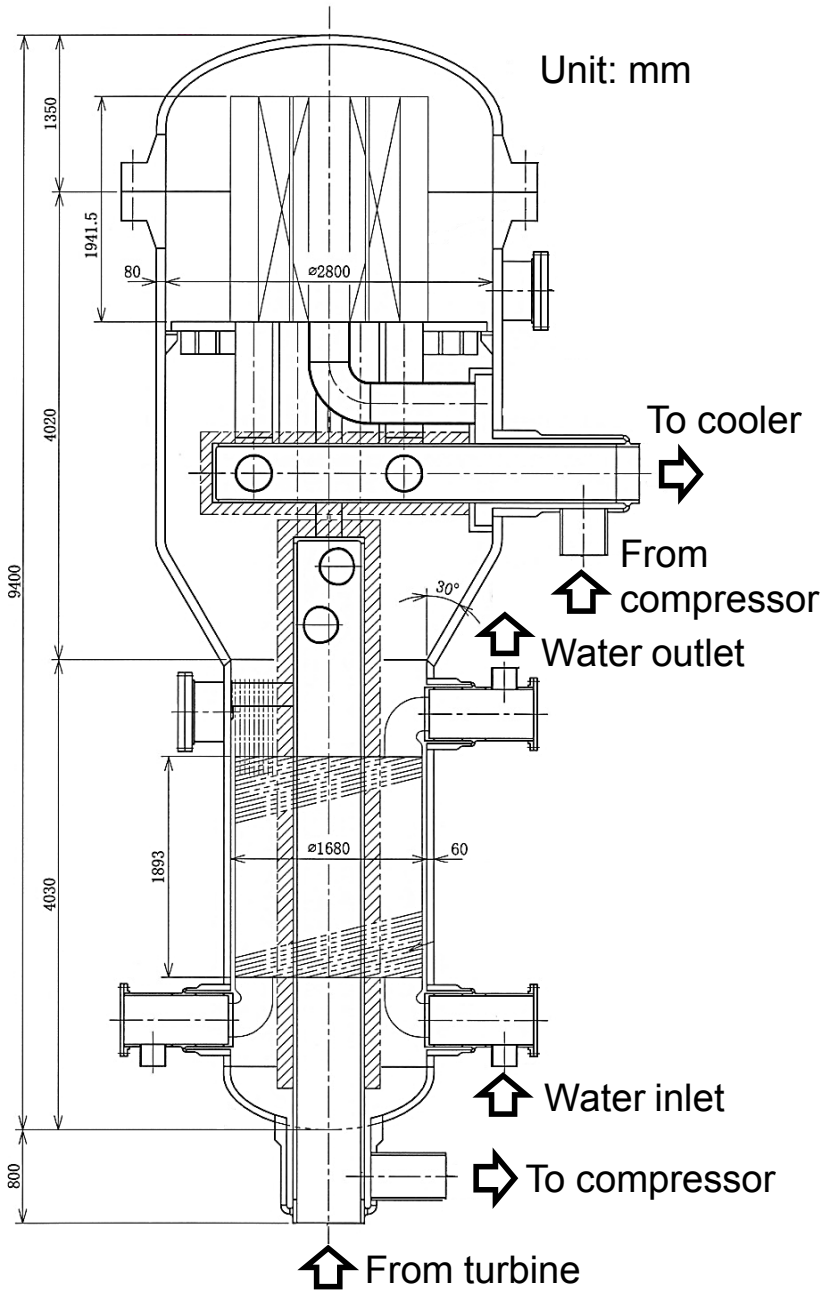

Fig.3.1.15 Cross sectional view of integrated heat exchanger

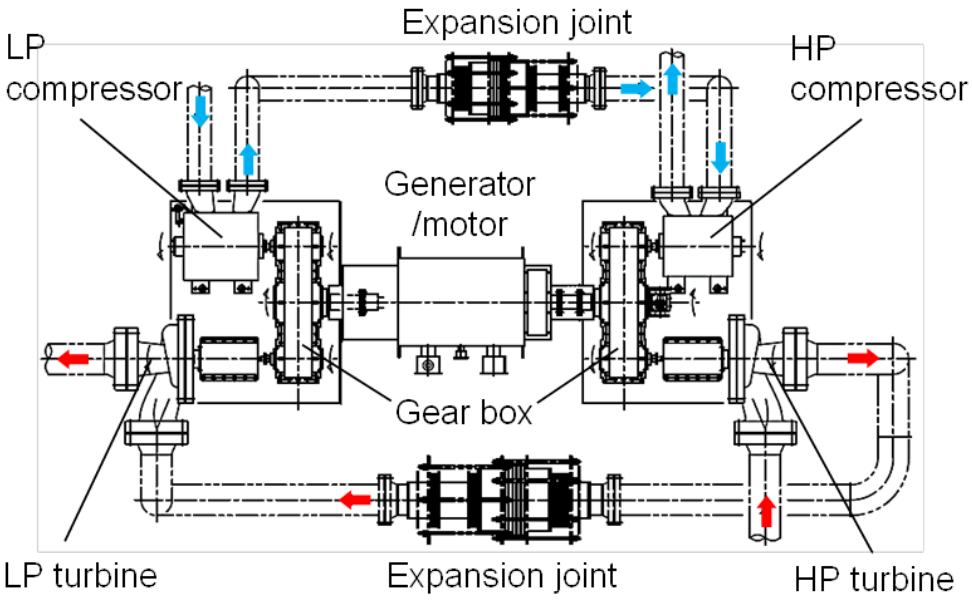

LP: Low pressure, HP: High pressure

Fig.3.1.16 Helium gas turbine layout

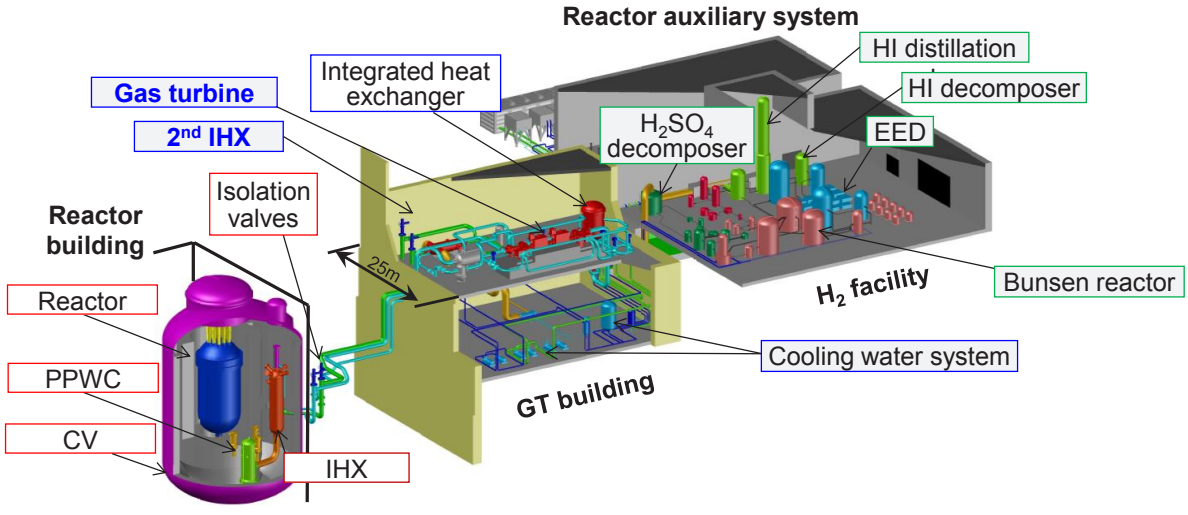

PPWC: Primary pressurized water cooler, CV: Containment vessel,

IHX: Intermediate heat exchanger, GT: Gas turbine, EED: Electro-electrodialysis

Fig.3.1.17 Plant layout of the HTTR-GT/H_2 plant

3.2 Gas Turbine High Temperature Reactor for Cogeneration (GTHTR300C)

3.2.1 Design Overview

GTHTR300C (Gas turbine High Temperature Reactor 300 MWe for Cogeneration) is a multi-purpose, inherently-safe, site-flexible commercial HTGR design under current development in JAEA. The development milestones in Table 3.2.1 target commercialization around 2030 [3.2.1-3.2.3)].

As a Generation-IV technology, the GTHTR300C offers important advances comparing to current light water reactors. The reactor coolant temperature is significantly higher in the range of 850-950°C. Such high temperature capability as proven in JAEA's HTTR test reactor operation enables a wider range of applications such as high temperature heat applications. The design employs a direct-cycle helium gas turbine to simplify the plant by eliminating water and steam systems while delivering 45-50% generating efficiency comparing to about 33% efficiency by current reactors. The design incorporates all ceramic fuel, low power density but high thermal conductivity graphite core, and inert helium coolant to secure inherent reactor safety. The inherent safety permits siting proximity to customers, in particular to industrial heat users so as to minimize the cost and loss of high temperature heat supply. Dry cooling becomes economically feasible due to the use of gas turbine. The waste heat from the gas turbine cycle is rejected from 200°C, creating a large temperature difference from ambient air making the dry cooling tower size per unit of power generation comparable to the wet cooling towers used in nuclear plants today. The economical dry cooling permits inland and remote reactor siting even without a large source of cooling water.

Typical applications include electric power generation, thermochemical hydrogen production, desalination cogeneration using waste heat only, and steelmaking. Figure 3.2.1 shows two of the plant application arrangements. The reactor thermal power may be rated up to 600 MWt maximum. The maximum product output per reactor is 120 t/d hydrogen enough to fuel about one million cars, 280-300 MWe electricity generation with additional seawater desalination cogeneration of 55,000 m^3/d potable water for about a quarter million of population, and annual production of 0.65 million tons of steel. All these are produced without CO_2 emission.

Table 3.2.1 Development Milestones

2003	Pre-licensing basic design for GTHTR300 completed
2004	Design development started
2005	Design extended to cogeneration system - GTHTR300C
2014	Hydrogen production IS-process test facility constructed
2015	HTTR-connected demonstration program HTTR-GT/H_2 started (section 3.1)
2025	HTTR-GT/H_2 test operation (planned)
2030	Construction of lead commercial plant (planned)

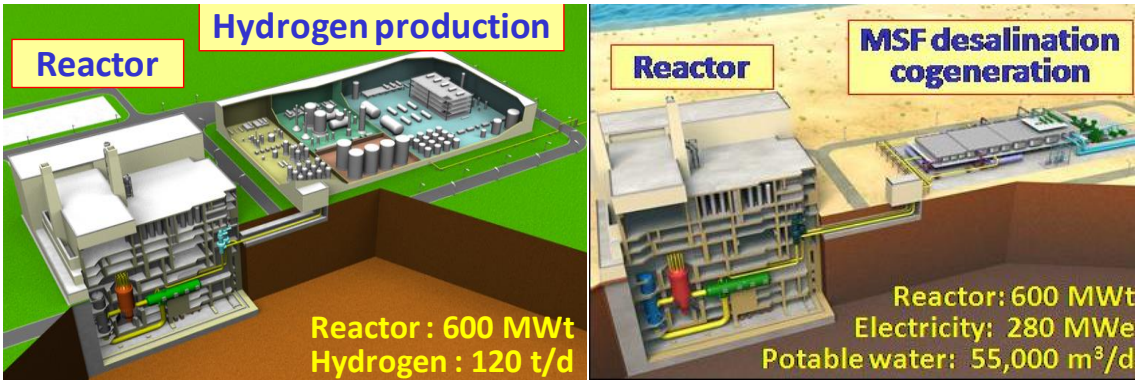

MSF: Multi-stage flash

Fig. 3.2.1 **GTHTR300C**
Cogeneration applications for hydrogen production (left) and for desalination (right)

3.2.2. Design Description

3.2.2.1 Design Philosophy

The overall goal of the commercial plant design is to provide a family of system options capable of producing competitive electricity, hydrogen, desalination, other products, and yet deployable in the near term. The development of the multiple systems simultaneously does not necessarily suggest having investment and risk multiplied. Rather, the development requirement is minimized thanks to a design philosophy of system simplicity, economical competitiveness and originality, namely the SECO philosophy. There are three major elements to this design philosophy.

The first element is technology simplification. All design variants are built on the premise that they share common system technologies to the maximum extent possible. As a result, the design variants share a unified reactor and primary coolant circuit, an aerodynamically and mechanically similar line of helium gas turbines used for electricity production, and the IS process selected to produce hydrogen. The helium gas turbine and the IS process are compatible application systems with the high temperature reactor heat source to enable economically competitive energy production.

The second element of the SECO design philosophy has been incorporating unique design attributes that are less demanding on the system technologies required. The efforts in this area have resulted in such original design simplification as conventional steel reactor pressure vessel construction, horizontal gas turbine installation, and system modular arrangement among others (see Fig. 3.2.2).

The third element that has been made possible by constant pursuit of technology and design simplification is a focused technological development scope that comes with low risk and investment of overall development. Furthermore, since the technologies to be developed are shared by several systems, the benefit of investing in any one development is increased. On the site where the HTTR is constructed for acquiring the reactor technology, JAEA has also been carrying out research and development on the helium gas turbine and the IS process.

3.2.2.2 System Design

The reactor system combines a high temperature gas-cooled reactor with direct-cycle gas turbine to generate power while circulating the reactor coolant. The system design (Fig. 3.2.2) consists of three functionally-oriented pressure vessel units, housing the reactor core, the gas turbine, and the heat exchangers respectively. The multi-vessel system facilitates modular construction and independent maintenance access to the functional vessel units. The reactor system is placed below grade in the reactor building. The pre-application basic design of the system was completed in 2003 by JAEA and domestic industrial partners Mitsubishi Heavy Industries, Fuji Electric, Nuclear Fuel Industries and others. The design added cogeneration capabilities in a GTHTR300C design that can accept various roles of cogeneration while sharing equipment designs with the GTHTR300. Finally, the system design is updated that demonstrated the potential of 50% thermal efficiency power generation upon completion of the current technology developments in JAEA [3.2.4)]. The major technical parameters for the GTHTR300C are given in Table 3.2.2.

3.2.2.3 Fuel Design

The fuel design is coated fuel particle of less than 1 mm in diameter (Fig. 3.2.3). Each particle consists of a UO_2 kernel coated by four layers of low and high density pyro-carbon and silicon carbide. The all ceramic particle fuel is heat resistant up to 1600°C. Approximately ten-thousand particles are packaged into a compact of the size of a thumb. The compacts are then assembled into graphite-clad integrated fuel rods. The fuel rods are inserted into the bore holes of a hexagonal graphite fuel block of about 1 m long and 41 cm across, where the annulus formed between the fuel rod and the bore hole provides coolant flow channels. The fuel blocks are loaded into the reactor core. The more fuel blocks are placed in the core, the higher the power output of the reactor.

3.2.2.4 Research and Development

While the reactor technologies required for the GTHTR300 are developed mainly with construction and operation of JAEA's 30 MWt and 950°C test reactor, we are separately developing and testing all key balance of plant technologies (see Fig. 3.2.4) needed for the commercial system, including test validation of the helium gas turbine equipment at one-third to full scale, production-scale fuel fabrication lines, thermochemical hydrogen production process, and the superalloy heat exchanger capable of transferring 950°C reactor heat to the hydrogen production process.

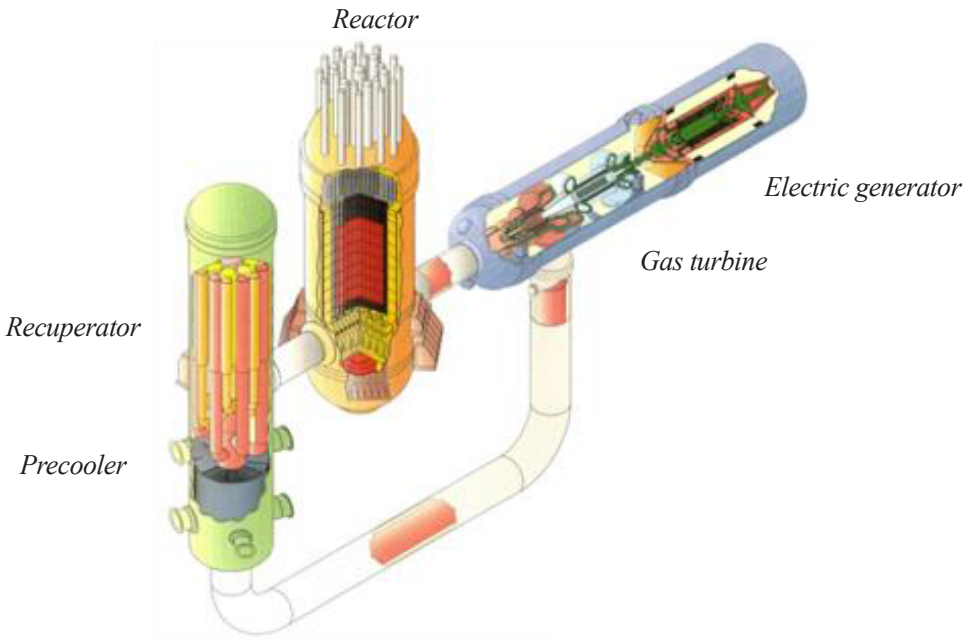

Fig. 3.2.2 Functionally-oriented pressure vessel units of the reactor primary system

Table 3.2.2 GTHTR300C Technical Parameters

Parameter	Value
Technology developer:	JAEA jointly with MHI, Toshiba/IHI, Fuji
Country of origin:	Japan
Reactor type:	Prismatic HTGR
Electrical capacity (MWe):	100~300 MWe
Thermal capacity (MWth):	< 600 MWth
Design capacity factor:	>90%
Design life (years):	60
Coolant:	helium
Moderator:	graphite
Primary circulation:	forced circulation
System pressure:	7 MPa
Reactivity control mechanism:	control rod
RPV height (m):	23
RPV diameter (m):	8
Coolant temperature, core Outlet (°C):	850-950
Coolant temperature, core Inlet (°C):	587-633
Integral design:	No
Power conversion process:	direct Brayton cycle
High temperature process heat:	Yes
Low temperature process heat:	Yes
Cogeneration capability:	Yes
Design configured for process heat	Yes
Safety features:	Inherent
Fuel type/assembly array:	UO_2 TRISO ceramic coated particle
Fuel block length (m):	1
Number of fuel columns in core:	90
Average fuel enrichment:	14%
Average fuel burnup (GWd/t):	120
Fuel Cycle (months):	48
Number of safety trains:	4
Emergency safety systems:	inherent
Residual heat removal systems:	inherent
Refueling Outage (days):	30
Distinguishing features:	Multiple applications of power generation, hydrogen production, process heat supply, steelmaking, desalination, district heating.
Modules per plant:	Up to 4 reactors
Estimated construction schedule (months):	24-36
Seismic design:	>0.18 g automatic shutdown
Predicted core damage frequency:	$<10^{-8}$/reactor year
Design Status:	Basic design

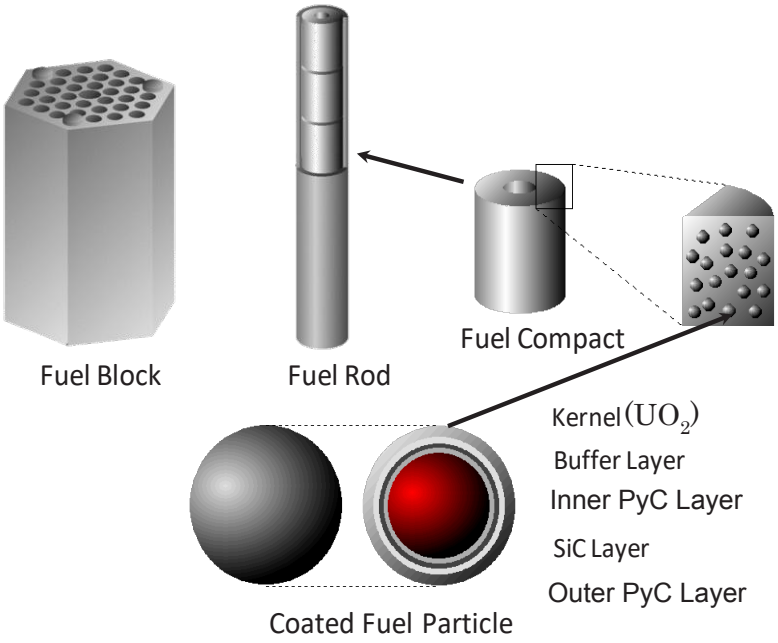

Fig. 3.2.3 Fuel design features

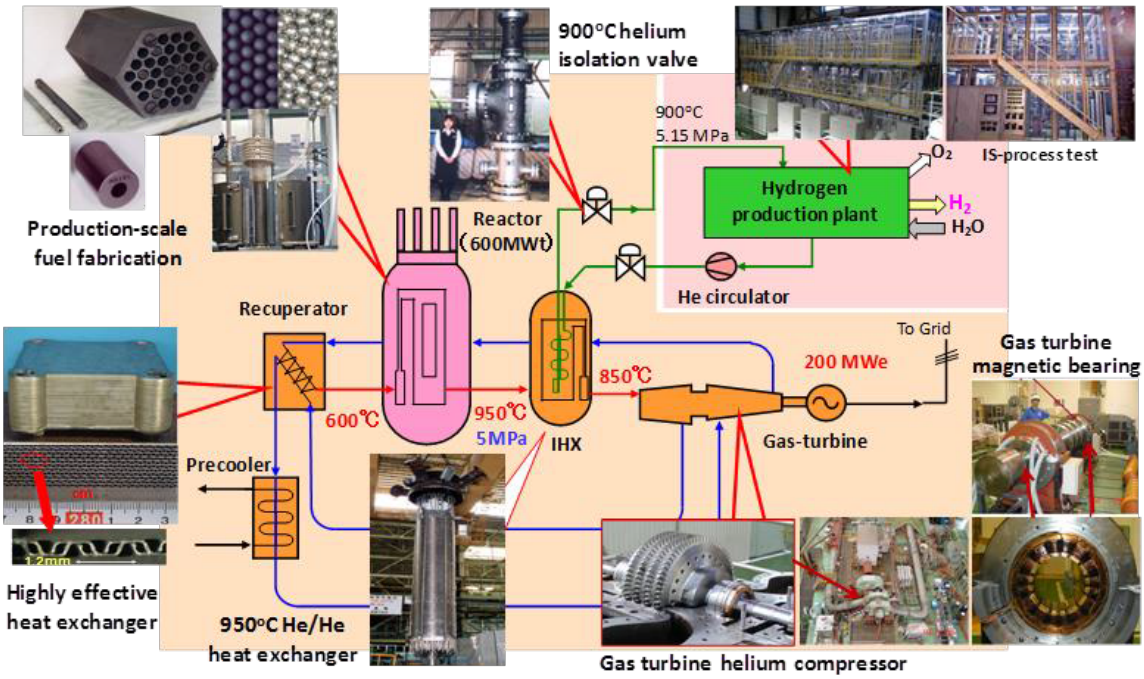

Fig. 3.2.4 Plant technologies developed for GTHTR300C

3.2.3 Plant Inherent Safety Design

The reactor delivers fully inherent safety due to three enabling design features:

- The ceramic coated particle fuel maintains its containment integrity under the design temperature limit of 1600°C.
- The reactor helium coolant is chemically inert and thus absent of explosive gas generation or phase change.
- The graphite-moderated reactor core is designed having characterises of negative reactivity coefficient, low-power density and high thermal conductivity.

As a result of these features, the decay heat of the reactor core can be removed by natural draft air cooling from outside of the reactor vessel for a period of days or months without reliance on any equipment or operator action even in such severe accident cases as loss of coolant or station blackout, while the fuel temperature will remain below the fuel design limit (see the illustration in Fig. 3.2.5).

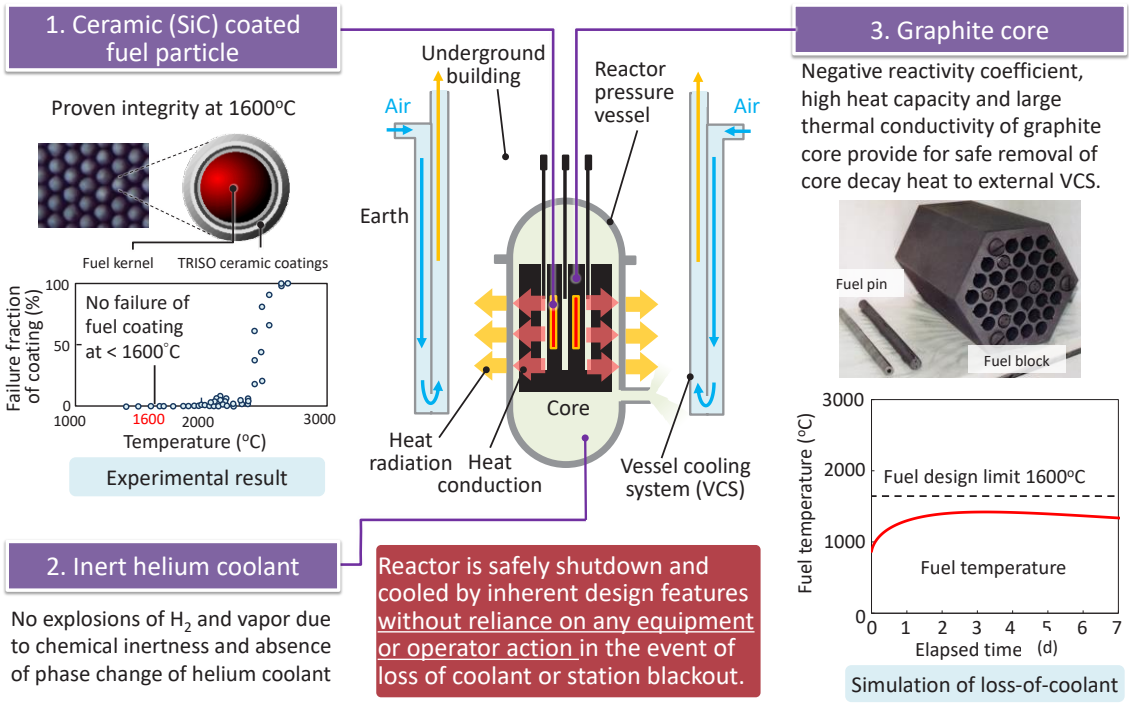

Fig. 3.2.5 Inherent reactor safety design

3.2.4. Plant Operational Performances

3.2.4.1 Control and Instrumentation System

The plant control and instrumentation system needed to enable load following in power generation mode as well as in cogeneration mode is shown in Fig. 3.2.6 [3.2.5)]. The overall approach to dynamic operation integrates the following four load control strategies:

1) Control of turbine speed, Sd, through flow bypass valve CV1.
2) Control of recuperator low-pressure-side inlet temperature, Tx, through flow bypass valve CV2.
3) Control of turbine inlet temperature, Tt, by flow bypass valve CV3.
4) Control of turbine inlet temperature and pressure, Tt and Pt, by bypass valve CV4, and inventory flow valves IV1 and IV2.

The first two strategies are used to control rapid transients such as a sudden loss of electric generator load. They are effective to protect the gas turbine from excess overspeed and prevent thermal shock in the recuperator.

The third strategy is used to automate heat rate to follow slow or fast changes in the heat load of the IHX when it is perturbed by the thermal production plant. As the IHX primary exit flow temperature rises or falls in response to a change in the IHX secondary heat load, the flow valve CV3 opens or closes to introduce more or less cold flow upstream of the turbine (from the compressor discharge to the turbine inlet) to keep the turbine inlet temperature constant. The overall control strategy aims to continue normal power generation, unaffected by any heat load change in the IHX.

The fourth control strategy is applied to automate cogeneration load follow. The conditions to be met include (1) constant reactor temperature to avoid thermal stress in high temperature structure; (2) constant reactor thermal power to yield base load economics; and (3) constant power generation efficiency over a broad range of load follow.

3.2.4.2 Operation Performance

The ability to follow variable power and heat loads is simulated as shown in Fig. 3.2.7. The simulation examines the plant response to an electric demand increase of 5% of the base rate per minute with corresponding reduction of the heat rate, which is the maximum requirement for cogeneration load follow. The reactor remains at 100% power at all times. Starting from the base cogeneration rates, the turbine power generation is increased to follow the electric load demand increase by increasing the primary coolant inventory through the inventory control valve IV1. The IHX heat rate to the thermal production plant is lowered by lowering the intermediate loop flow circulation rate with the variable speed gas circulator. As the primary exit temperature of the IHX begins to rise, the valve CV4 is opened, by active or prescheduled control to follow load demand, to direct cold flow from the compressor discharge to mix with the hot exit gas of the IHX primary side. By applying flow bypass via CV4 the goal to maintain the turbine inlet temperature near the rated 850^{o}C is achieved, as shown in Fig. 3.2.7. The electricity generation rate increases to 280 MWe from 203 MWe in as little as 7 minutes. The pressure in the reactor and at turbine inlet increases to 7 MPa

from 5 MPa. To return to the base cogeneration state, the control is reversed by reducing primary coolant inventory through another inventory control valve IV2 and simultaneously by closing the bypass valve CV4.

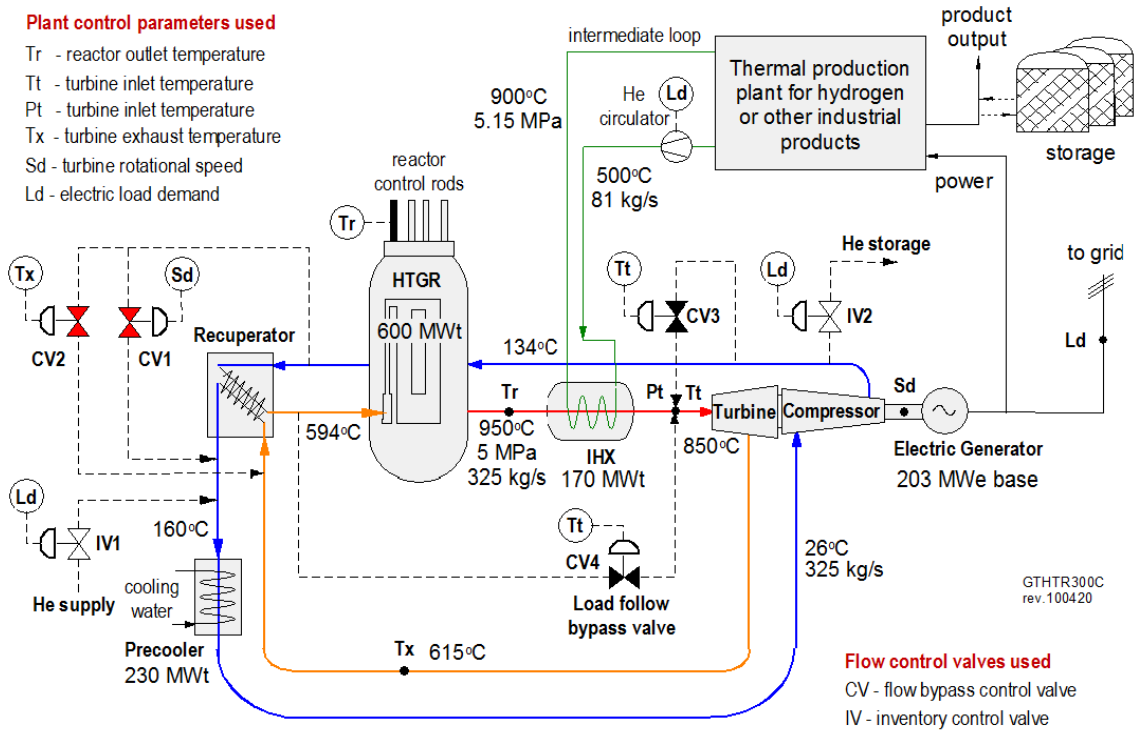

Fig.3.2.6 Control system for GTHTR300

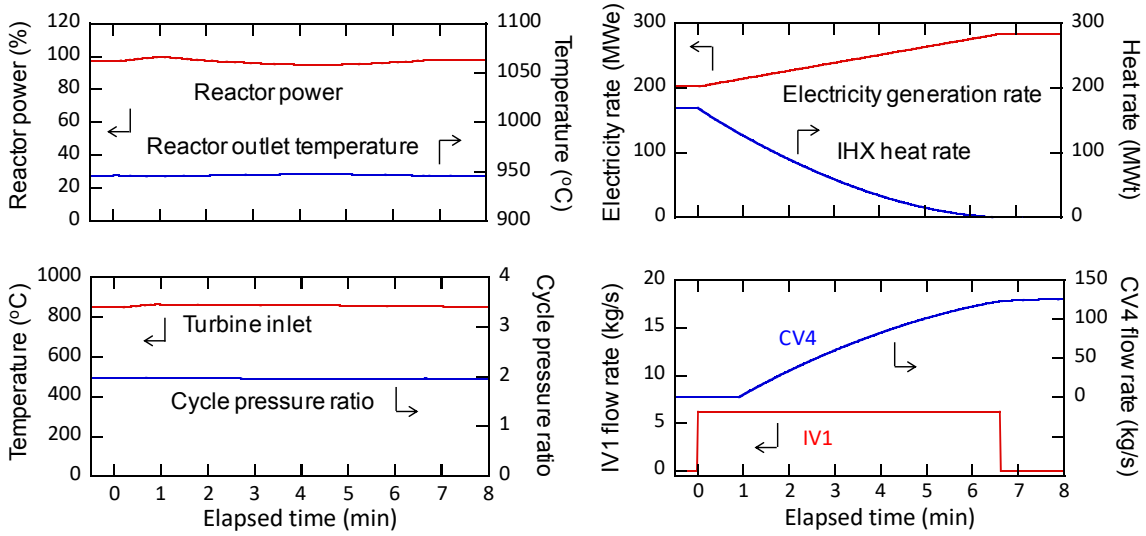

Fig.3.2.7 Simulation of cogeneration plant load follow to +5%/min electric load increase

References

3.2.1) X. Yan, K. Kunitomi, T. Nakada and S. Shiozawa, “GTHTR300 design and development”, Nuclear Engineering and Design, 222, 2-3, pp.247-262 (2003).

3.2.2) K. Kunitomi, X. Yan, T. Nishihara, N. Sakaba And T. Mouri, “JAEA’s VHTR for hydrogen and electricity cogeneration: GTHTR300C”, Nuclear Engineering and Technology, 39, 1, pp.9-20 (2007).

3.2.3) S. Kasahara, N. Tanaka, H. Noguchi, J. Iwatsuki, H. Takegami, X. L. Yan And S. Kubo, “JAEA’s R&D on the thermochemical hydrogen production IS process”, HTR2014, Weihai, China, pp.27-31 Oct., Paper HTR2014-21233, Institute of Nuclear and New Energy Technology (2014).

3.2.4) H. Sato, X. Yan, Y. Tachibana, K. Kunitomi, “GTHTR300—A nuclear power plant design with 50% generating efficiency”, Nuclear Engineering and Design, 275, pp.190-196 (2014).

3.2.5) X. Yan, H. Sato, Y. Tachibana, K. Kunitomi, R. Hino, “Evaluation of High Temperature Gas Reactor for Demanding Cogeneration Load Follow”, Journal of Nuclear Science and Technology, 49, 1, pp.121-131 (2012).

3.3 Small-sized cogeneration HTGR (HTR50S)

3.3.1 Introduction

JAEA has conducted a conceptual design of a 50 MWt small-sized HTGR, as shown in Fig. 3.3.1, for multiple heat applications (HTR50S) with dual reactor outlet coolant temperatures of 750°C and 900°C with maximum use of conventional and proven technologies in order to deploy HTGR in developing countries the 2020s. [3.3.1-3.3.3)]

3.3.2 Design philosophy

The design philosophy of the HTR50S is a high advanced reactor, which is reducing the R&D risk based on the HTTR design, upgrading the performance for commercialization by utilizing the knowledge obtained by the HTTR operation and the GTHTR300 design. The balance of plant shall be designed for the heat application of district heating and process heat supply based on the steam turbine system and for the demonstration of the power generation by helium gas turbine (GT) and the hydrogen production by the thermochemical water splitting IS process to satisfy the user requirement for multiple heat applications. The HTR50S is to be upgraded its performance as FOAK commercial plant or a demonstration plant and expanded its application as the following steps:

(i) Phase I: Power generation by a conventional steam turbine at the reactor outlet temperature of 750 °C using the performance-proven HTTR fuel to demonstrate the technologies improved from HTTR

(ii) Phase II: Extension of the burn-up by employing shuffling refueling using a higher performance fuel

(iii) Phase III: Increase the reactor outlet temperature to 900°C and install an intermediate heat exchanger (IHX) to demonstrate helium GT and hydrogen production using the IS process.

The philosophy of safety design is the adoption of the defense-in-depth concept and the utilization of the inherent features of HTGR to protect people and the environment from the harmful effect of the radioactive materials as well as HTTR. However, the safety design of HTR50S is different from that of HTTR as follows: (i) the vessel cooling system (VCS) is designed as a passive means and (ii) the shutdown cooling system (SCS), of which role is to remove decay heat by forced cooling in the core, is designed as non-safety class system.

3.3.3 Major specification

The major design specification of HTR50S is listed in Table 3.3.1. The reactor outlet temperature in Phase I was determined as 750 °C taking into account that the conventional heat-resistant alloy, Alloy 800H, of which the restrictive temperature is 760 °C, can be applied to the heat exchanger tube of the steam generator (SG). The reactor outlet temperature will be increased to 900°C in Phase II so that the helium gas turbine, of which inlet temperature is 850°C, can be demonstrated at the same temperature condition as the commercial plant. The higher reactor inlet temperature is better for the core thermal design because the coolant flow rate is increased due to the decrease of temperature

difference between the core inlet and outlet. However, it affects the material selection for RPV. The reactor inlet temperature was determined as 325°C to apply the low-alloy steel for LWR, e.g., SA533B and SA508 to the RPV, of which restrictive temperatures are 370°C at normal operation and 540°C in accidents. Temperature margin is about 45 °C considering the HTTR design. The primary coolant pressure affects the thickness of RPV, that is, the RPV weight. The RPV, the most heavy component, of HTR50S will be transported to the developing countries not only the coast country but also the inland country. Whereas the primary coolant pressure of GTHTR300 is 7 MPa, the primary coolant pressure of HTR50S was determined as 4 MPa as the same pressure of HTTR to reduce the weight of RPV and utilize the experience obtained by the HTTR design and construction. The number of fuel blocks in axial direction was increased from 5 of HTTR to 6 in order to apply the two-batch shuffling refueling for axial direction to demonstrate the high burn-up fuel after the 2nd step of Phase I. The size of the fuel block is same as that of HTTR. These design specifications result in the effective core height of 3.48 m. The number of column is 30, which is same as that of HTTR. Therefore the equivalent core diameter is same as that of HTTR of 2.30 m.

3.3.4 System configuration

To satisfy the user requirement for the multiple heat applications, the system was designed so as to use heat from HTR50S for district heating and process heat based on the steam turbine system in Phase I, for the demonstration of the helium GT in Phase II and for the demonstration of the hydrogen production technology in Phase III. Figure 3.3.2 shows the overall plant configuration. The GT system and IHX, and the hydrogen production system will be installed in Phase II and Phase III, respectively. The products in each system are also listed in Table 3.3.1. The condition of steam at the inlet of steam turbine was determined as 533 °C at 12.0 MPa taking into account of the proven technology of the Japanese vendor and the condition in the former HTGR steam turbine system in USA (i.e., 538 °C at 16.6 MPa). The steam turbine system was designed so as to adjust the thermal duty for the district heating network and the process heat from 0 to 25 MW. It means the thermal duty of steam turbine can be adjusted from 50 to 25 MWt as 50% partial load operation. The gross electricity generation varies from 17.2 MWe at full load operation of steam turbine to 13.5 MWe at 50% partial load operation for district heating. The overall nuclear reactor thermal power utilization is 77% at 50% partial load operation of steam turbine with the 25 MW heat supply to district heating network.

3.3.5 Reactor design

Figure 3.3.3 shows the configuration of the reactor. The reactor core is a prismatic cylindrical core and consists of 30 fuel columns, 18 replaceable reflector columns and 13 control rod (CR) guide columns, surrounded by the permanent reflector block made of PGX graphite for upper and middle side part and IG-11graphite for lower side part. The irradiation blocks and the outermost three columns of CR guide blocks in the HTTR were replaced to the replaceable reflector blocks in the HTR50S design. The number of the fuel block layers was increased from 5 of HTTR to 6. The primary

concentric hot gas duct is connected to not at the bottom of RPV as HTTR but at the side of RPV to layout the primary system vessels inline side-by-side arrangement. Whereas the RPV diameter is same as that of HTTR, the length is increased due to the increase of the number of the fuel blocks in axial direction. The design target is to reduce the weight of RPV in mode of packing less than 300 tons from the view pint of shipping to the inland countries. The reactor inlet temperature was reduced from 395°C of HTTR to 325°C. It enables to employ Mn-Mo steel instead of 2¼Cr-1Mo steel used in HTTR. The wall thickness of the vessel body could be reduced from 122.0 mm of HTTR to 77.0 mm under the same design pressure condition of HTTR, 4.7 MPa. In this result, the approximate RPV weight from the bottom to the flange sheet was evaluated as 180 tons. It means total weight of RPV including the transport cradle satisfies the design target of less than 300 tons.

As for the core design, the number of uranium enrichments can be reduced from 12 to 3. The average core power density and the burn-up days can be increased from 2.5 MW/m^3 to 3.5 MW/m^3 and from 660 days to 730 days (i.e., 2 years) satisfying the maximum fuel temperature less than 1495°C, respectively.

3.3.6 Steam generator design

The SG to produce superheated steam is a unique component of HTR50S, because SG is not installed in HTTR and GTHTR300 series. The helical-coiled counter flow type heat exchanger that is used for the HTTR IHX was applied to the SG design as shown in Fig.3.3.4 because it can reduce the size of component. Both evaporator and super heater parts are installed inside the inner shell. The primary helium gas flows on the shell side and water/steam in the tube side. The major specification of SG is listed in Table 3.3.2. The Alloy 800H steel are used only for the super heater part, and the 2¼Cr-1Mo steel are employed for the evaporate part and welded using heterogeneous material joint to connet the heat exchanger tubes made of Alloy 800H steel, so as to reduce the amount of expensive heat-resistance alloy (i.e., Alloy 800H).

3.3.7 Summary

Conceptual design of a 50 MWt small-sized HTGR, HTR50S, for multiple heat applications with high level of safety has been conducted by JAEA with support of Japanese vendors. HTR50S can satisfy the user requirements for multiple heat applications and its performance is upgraded compared to that of HTTR without significant R&D utilizing the knowledge obtained by the HTTR design and operation.

References

3.3.1) H. Ohashi, H. Sato, et al., “Conceptual design of small-sized HTGR system for steam supply and electricity generation (HTR50S)”, Proceedings of SMR2011, SMR2011-6558 (2011).

3.3.2) X. Yan, Y. Tachibana, et al., “A small modular reactor design for multiple energy applications: HTR50S”, Nuclear Engineering and Technology, 45, 3, pp.401-414 (2013).

3.3.3) H. Ohashi, H. Sato, et al., “A Small-Sized HTGR System Design for Multiple Heat Applications for Developing Countries”, International Journal of Nuclear Energy, 2013, Article ID 918567, (2013).

Table 3.3.1 Major design specification of HTR50S

Parameters	Single operation mode (Phase I)			Serial operation mode (Phase II and III)
Thermal power (MW)	50			50
Coolant	Helium			Helium
Reactor inlet temperature (°C)	325			325
Reactor outlet temperature (°C)	750			900
Coolant pressure (MPa)	4			4
Coolant flow rate (kg/s)	22.3			16.5
Core structure material	Graphite			Graphite
Core type	Prismatic / Pin-in-block			Prismatic / Pin-in-block
Effective core height (m)	3.48			3.48
Equivalent core diameter (m)	2.30			2.30
Numbers of fuel blocks	180			180
Fuel	Low enriched UO_2 TRISO Coated fuel particle			Low enriched UO_2 TRISO Coated fuel particle
	HTTR type fuel	High burn-up fuel		High burn-up fuel
Refueling	Whole	Half core		Half core
Reactor pressure vessel	Mn-Mo steel (SA533B/SA508)			Mn-Mo steel (SA533B/SA508)
Number of main cooling loop	1			1
Heat removal (SG / IHX (MWt))	Single mode (50 / 0)			Serial mode (30 / 20)
Steam turbine power generation (MWe)	17.2	13.5	8.6	10.3
Gas turbine power generation (MWe)	—	—	—	6.9
District heating (MWt) (water at 95°C and 0.1MPa (t/h))	—	25 (857)	—	7.6 (259)
Process heat (MWt) (helium at 850°C and 4MPa (t/h))	—	—	—	20 (47.3)
Process heat (MWt) (helium at 310°C and 10MPa (t/h))	—	—	25 (45)	—
Hydrogen (Nm^3/h)	—	—	—	800 (Phase III only)

Table 3.3.2 Major specifications of Steam Generator

Parameters		Values
Thermal duty (MW)		50
Primary helium	Temperature (inlet / outlet) (°C)	750 / 325
	Flow rate (kg/s)	22.4
Water/steam	Temperature (inlet / outlet) (°C)	200 / 538
	Pressure (inlet / outlet) (MPa)	13.3 / 12.5
	Flow rate (kg/s)	19.3
Heat exchanger tube	Material	Evaporator: 2¼Cr-1Mo steel Super heater: Alloy 800H
	Outer diameter (mm)	31.8
	Thickness (mm)	3.5
	Number of tubes	36
Helical tube bundle	Number of layers	8
	Outer diameter (m)	1.4
	Inner diameter (m)	0.7
	Effective heat transfer area (m^2)	260

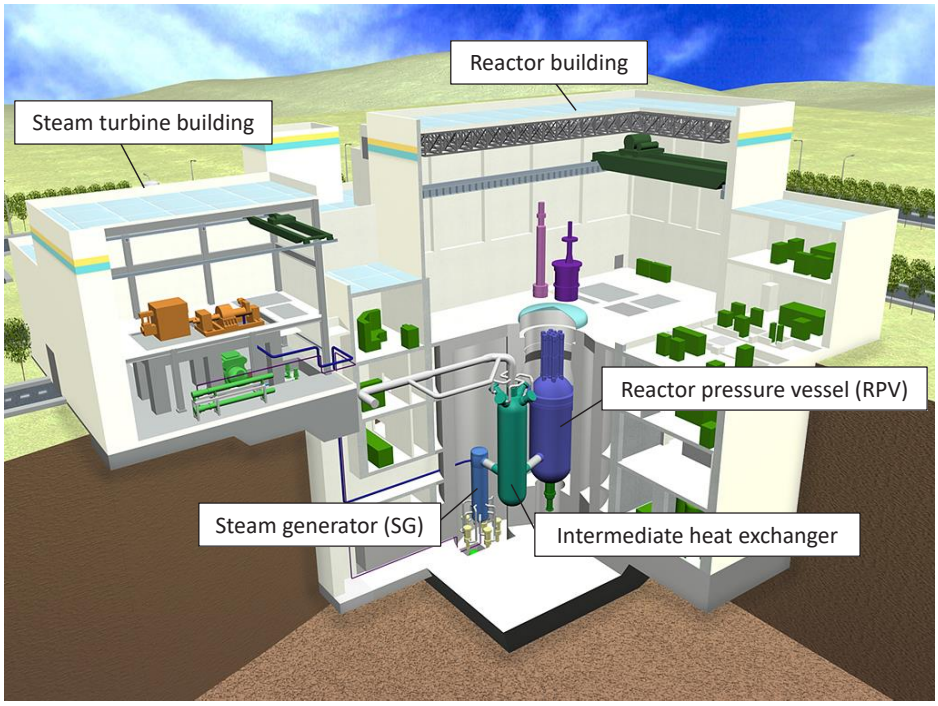

Fig. 3.3.1 HTR50S

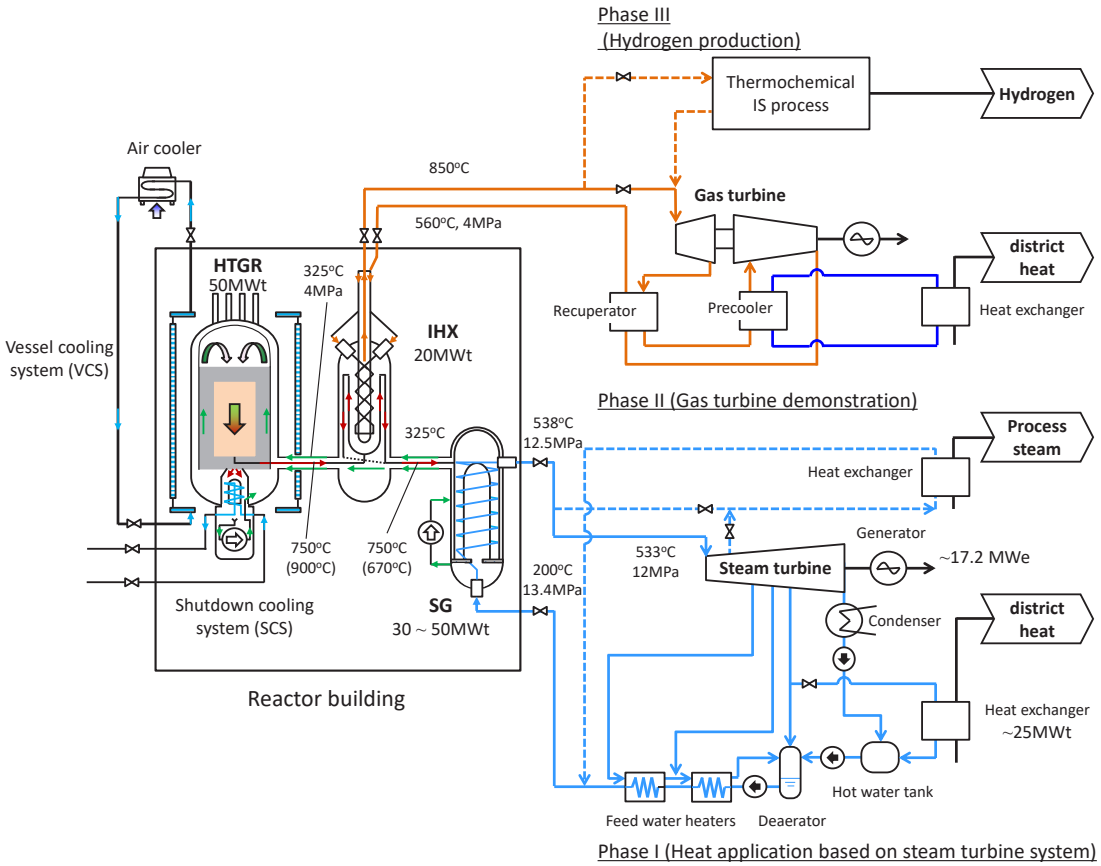

Fig. 3.3.2 HTR50S plant configuration

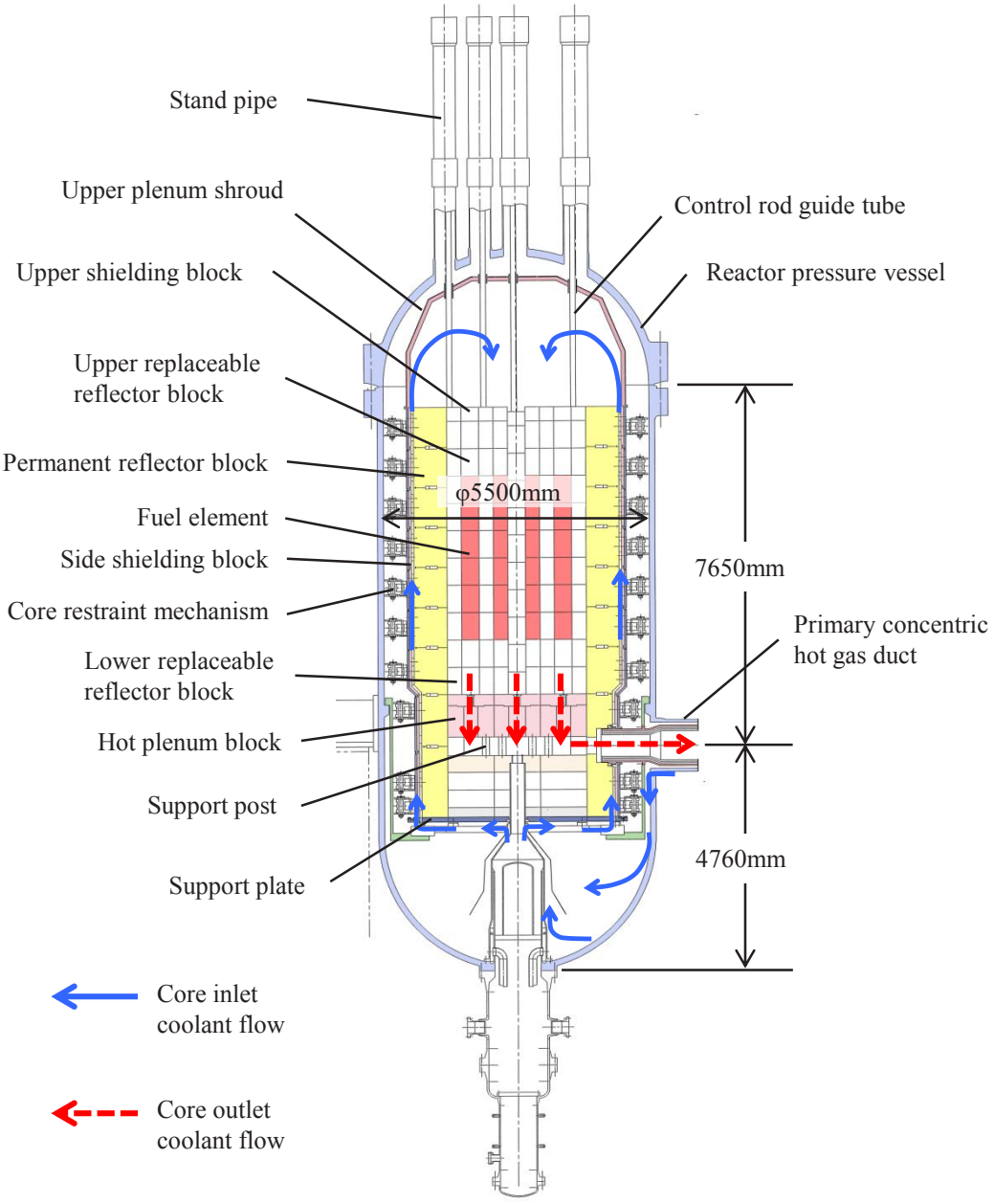

Fig. 3.3.3 Structure of the reactor

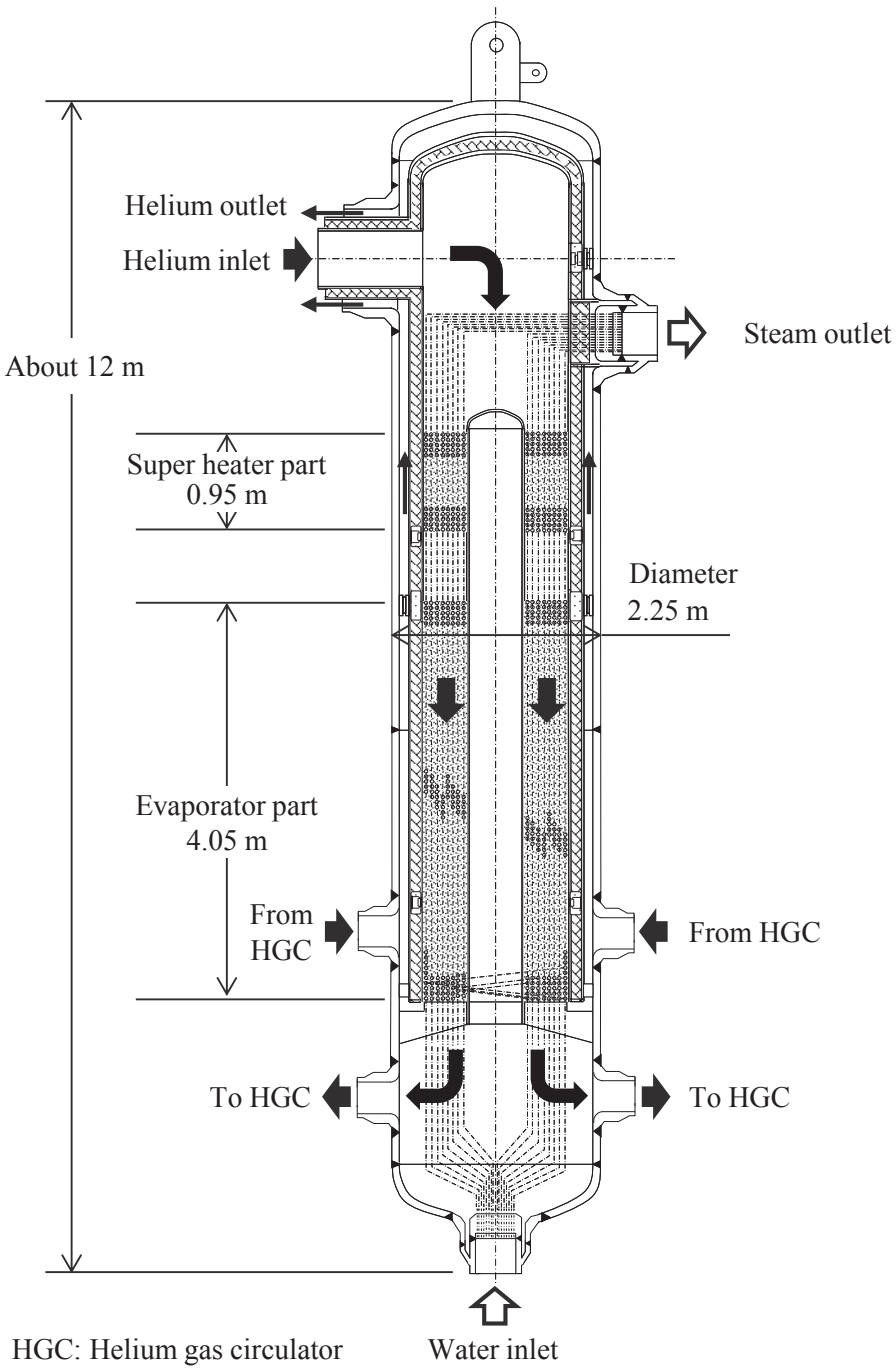

Fig. 3.3.4 Structure of the steam generator (SG)

3.4 Mitsubishi Small Module HTGR (MHR-50/100is) [3.4.1)]

Mitsubishi Heavy Industries, Ltd. (MHI) and JAEA have proposed a small sized HTGR design for steam turbine power generation. The system of MHR-50/100 (Mitsubishi small-sized High temperature gas-cooled modular Reactor of 50-100 MWe nominal output) aims at high inherent safety and high economical advantage for commercialization. The conceptual design reflected on the following results of market research and financial analysis.

a. Lower development and construction cost
b. Minimum R&D requirements
c. Shorter construction period: Less than 36 months
d. Inherent safety feature application

Furthermore, in response to greater safety requirement to nuclear plants following the Fukushima Daiichi Nuclear Power Station Accident on March 2011, the inherent safety of the plant concept is improved in a design of MHR-50/100is, which eliminates the need for a steam/water dump system during a water ingress accident.

Major specifications of MHR-50/100 are shown in Table 3.4.1. The fuel of a pin-in-block type developed by JAEA for the HTTR was selected. For the power conversion system, a steam turbine power generation system was selected. Fig. 3.4.1 shows the system flow diagram with heat and mass balance of MHR-100. The reactor was found capable of maintaining stability during long-term Station Black-Out (SBO) with protection of only passive devices during a depressurization accident and with additional motion of steam/water dump system during a water ingress accident. In order to simplify license approval for FOAK (First Of A Kind), a sealed type of containment vessel was selected for a containment system whereas for NOAK (Nth Of A Kind) a confinement building system might be adopted following the design philosophy in the MHTGR and GTHTR300, etc. Figure 3.4.2 shows the general overview of MHR in FOAK. In response to the requirements for Fukushima Daiichi Accident, MHI developed the improved plant concept known as MHR-50/100is. More specifically, design improvements were made in which the pressure of secondary system was changed to be the same as that of primary system. A new SG internal structure was proposed and introduced to minimize the amount of the water ingress to the primary helium circuit with providing a water storage plenum in the lower part of SG during SG heat-transfer tube rupture as well as system pressure changing. Figure 3.4.3 shows SG cross cut view. The improved design concept can be significantly effective to reduce the amount of water ingress into the reactor core in case of an accident without active functions except feed water isolation. Table 3.4.2 shows the major specifications of MHR-50/100is. Figure 3.4.4 shows the plant building arrangement of MHR-100is.

MHI recently started conceptual design of MHR-100 Gas Turbine system (MHR-100GT) to achieve further safety and economic superiority. The innovativeness of MHR-100GT design is to optimize current and traditional technologies into the MHR-100 design. JAEA contributes the part of activities concerning the core physics design and safety evaluation of MHR-50/100 series.

Reference

3.4.1) S. Oyama, et al., “Mitsubishi Small Module High Temperature Gas-cooled Reactor “MHR” conceptual design - A comparison analysis between a steam turbine cycle and a gas turbine cycle –”, Proceedings of the 2017 International Congress on Advances in Nuclear Power Plants (ICAPP 17), 17630, (2017).

Table 3.4.1 Major specifications of MHR-50/100

Items	Unit	MHR-50	MHR-100
Reactor power	MWt	120	250
Reactor inlet/outlet temperature	ºC	300/750	350/750
Primary helium gas pressure	MPa	6	
Core type	-	Pin-in-block type	
Main steam temperature/pressure	ºC/MPa	538/10	538/12.6
Number of steam generator	-	1	2

Table 3.4.2 Major specifications of MHR-50/100is

Items	Unit	MHR-50is	MHR-100is
Reactor power	MWt	120	250
Reactor inlet/outlet temperature	ºC	300/750	350/750
Primary helium gas pressure	MPa	6	
Core type	-	Pin-in-block type	
Main steam temperature/pressure	ºC/MPa	538/6	538/6
Number of steam generator	-	1	2

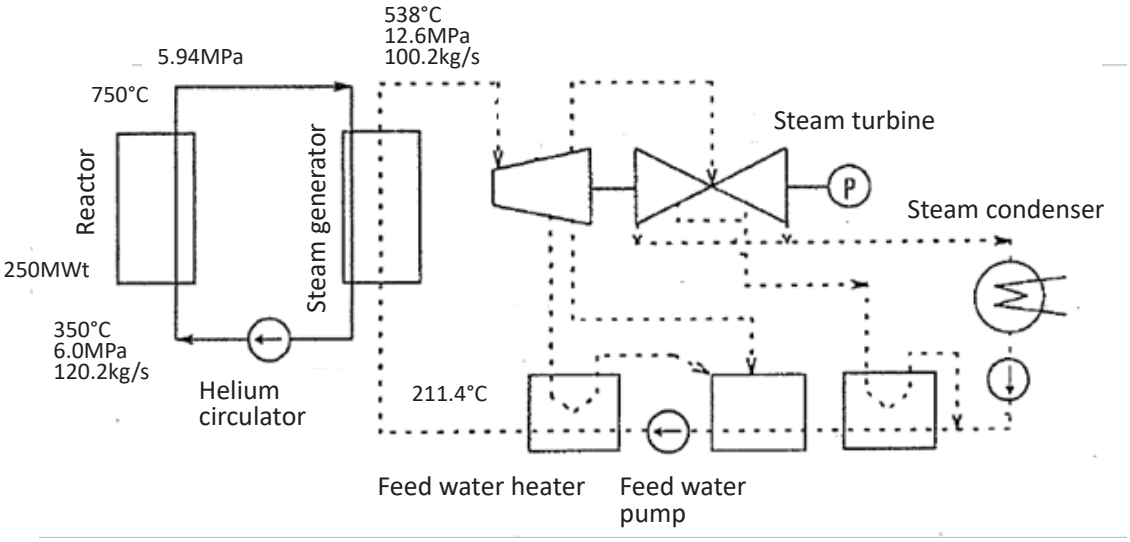

Fig.3.4.1 Flow diagram with heat and mass balance of MHR-100

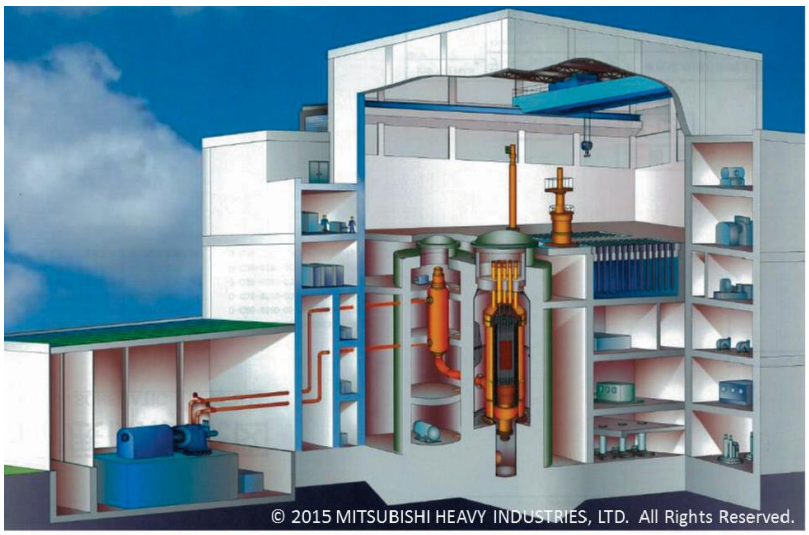

Fig.3.4.2 General overview of MHR-50

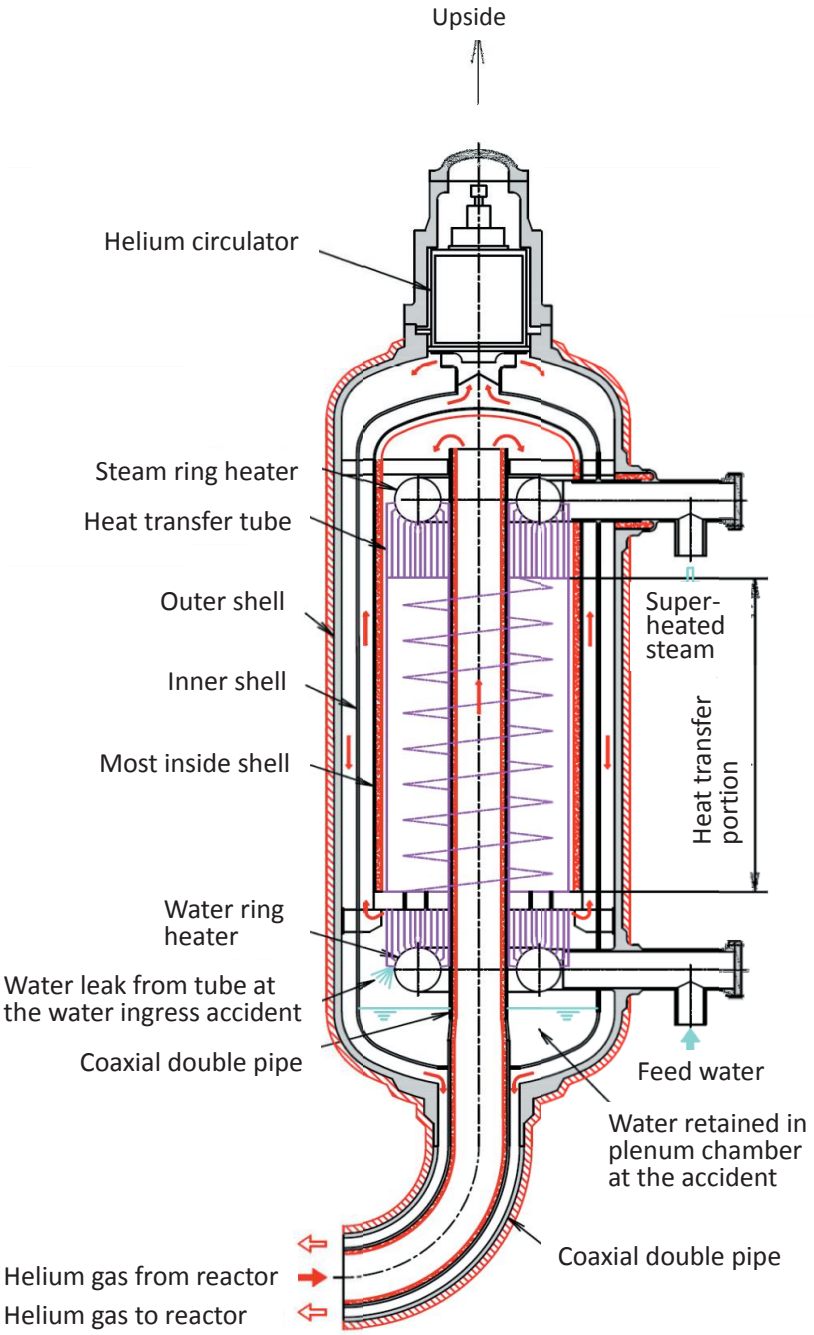

Fig.3.4.3 Cross cut view of SG

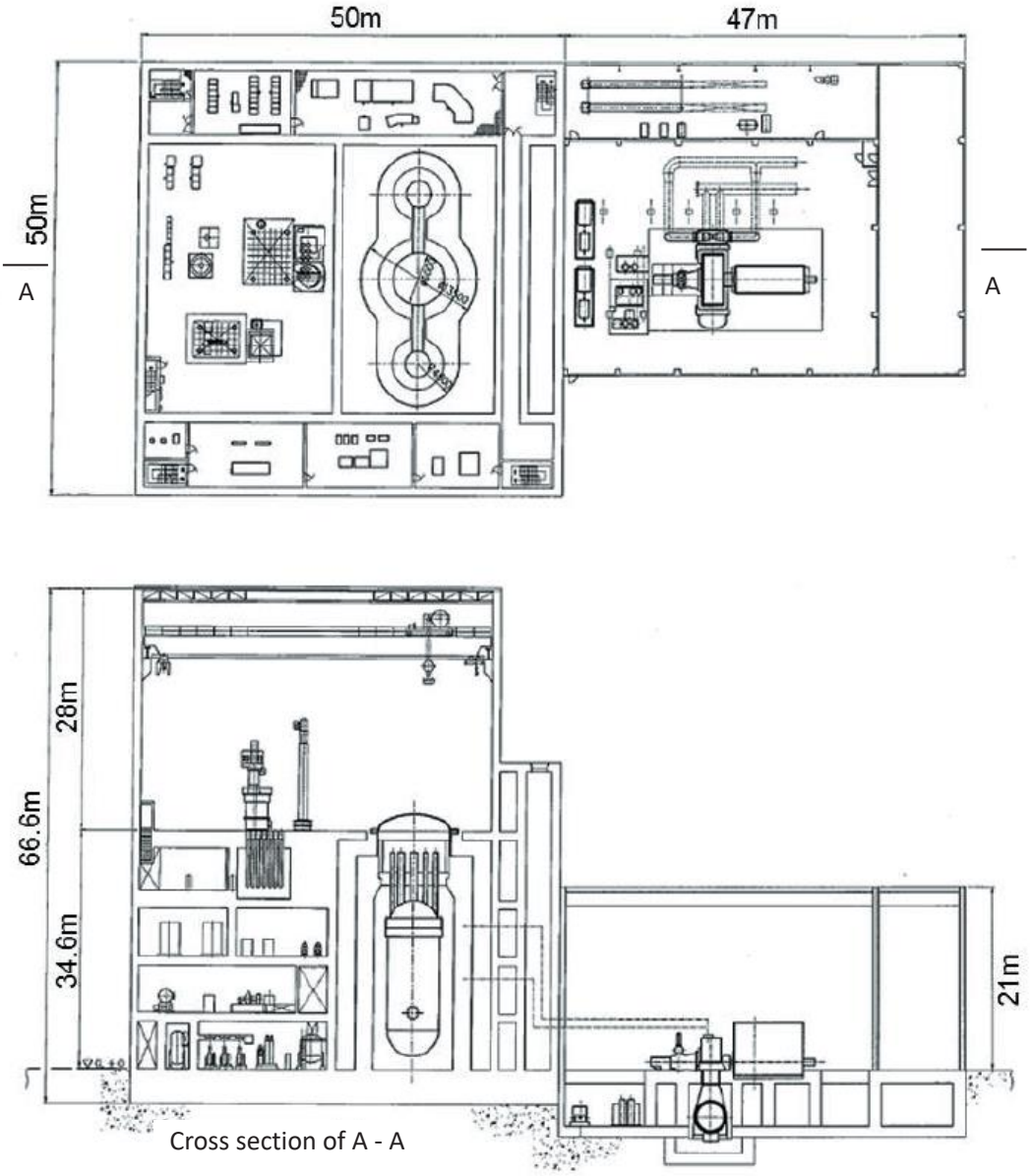

Fig.3.4.4 Plant building arrangement of MHR-100is

4. Japanese Technologies of HTGR and Heat Application

4.1 Nuclear design

4.1.1 Nuclear design code system for HTTR [4.1.1- 4.1.2)]

Unlike the earlier HTGRs (FSV, AVR and THTR) that has used high enriched uranium (HEU) mixed with thorium, the HTTR is based on low enriched uranium (LEU) fuel to improve nuclear proliferation resistance. Therefore, a nuclear design code system has been developed in JAEA to allow for the LEU based core design.

The nuclear design code system consists of the DELIGHT, TWOTRAN-2, and CITATION-1000VP computer codes. The DELIGHT calculates group constants of fuel and graphite blocks for succeeding core calculations. Resonance, neutron spectrum, neutron flux distribution, criticality, and burnup calculations are carried out sequentially. In the resonance range, the code employs intermediate resonance approximation and considers the effect of double heterogeneity caused by coated fuel particles and assembled fuel rods. The TWOTRAN-2 transport code calculates the average group constants of graphite blocks where control rods (CRs) are inserted. The CITATION-1000VP, developed from the CITATION, performs nuclear characteristics analyses in three-dimensional whole-core model of the HTTR in relatively short run time.

The nuclear design code system was developed on the very high temperature reactor critical assembly (VHTRC) [4.1.2)] which was used to generate experimental data for the code validation. Calculation uncertainties of effective multiplication factor, neutron flux distribution, burnable poison (BP) reactivity worth, CR worth and temperature coefficients by the nuclear design code system were considered as shown in Table 4.1.1. Calculation uncertainties of Monte Carlo code were also evaluated. The Monte Carlo code showed good agreement with experimental data of the VHTRC. The Monte Carlo code could be applied for the evaluation of various HTGR designs developed by JAEA.

4.1.2 Nuclear design of HTTR [4.1.3)]

It is important in the nuclear design to suppress the fuel temperature rise by optimizing the power distribution, which is carried out in the following steps. Firstly, JAEA planned to replace each fuel block with a fresh fuel block after every burnup cycle. The axial and radial power distribution is optimized to flatten by allocating optimally the fuel blocks with 12 different uranium enrichments of fresh fuel throughout the core (Fig. 4.1.1). Secondly, the loading of fresh fuel blocks throughout the core caused large initial excess reactivity, which resulted in the deep insertion of CRs into the core and resulted in high fuel temperatures. Greater excess reactivity is necessary because fast reactivity depletion resulted from the low conversion ratios of the LEU fuel. Thus, it is important for the nuclear design of the HTTR to reduce the excess reactivity adequately. The problem with the excess reactivity was solved by optimizing BPs in the core as shown in Fig. 4.1.1. The optimization kept the excess reactivity to the minimum necessary for reactor operations. Thirdly, deviation from the optimum power distribution due to burnup of fissile materials was avoided by optimizing the specifications of the BPs, namely, the poison atom density and the radius for each local area. The excess reactivity of the core was maintained constant.

It becomes possible, then, to operate the reactor without changing the insertion position of CRs during power operation at 950ºC.

4.1.3 HTTR data

4.1.3.1 Critical approach [4.1.4)]

The critical approach of the HTTR was carried out by the fuel addition method at room temperature. In the critical approach, dummy graphite blocks previously placed in the core were replaced with fresh fuel blocks from the outer core region in the form of fuel columns as shown in Fig. 4.1.2. The first criticality was achieved using an annular form core comprising 19 fuel columns. After the first criticality, the fuel loading was carried out additionally to construct the fully loaded core at room temperature. The fully loaded core was constructed using a cylindrical form core comprising 30 fuel columns.

The criticality calculations of the core loaded with 12–30 fuel columns, which were constructed in the critical approach, were performed the MVP [4.1.5)] with JENDL-4.0 [4.1.6)], JENDL-3.3 [4.1.7)], ENDF/B-VII.0 [4.1.8)], and JEFF-3.1 [4.1.9)]. Table 4.1.2 shows that JENDL-4.0 yields k_{eff} values that are 0.5–0.9%Δk smaller than those yielded by JENDL-3.3, and 1.0–1.5%Δk smaller than those yielded by ENDFL/B-VII.0 or JEFF-3.1. The k_{eff} values calculated with ENDF/B-VII.0 and JEFF-3.1 are the same for all the core states. The discrepancies between the experimental and calculation results on the following two issues were resolved as expected by replacing the nuclear data libraries with JENDL-4.0, in which the thermal capture cross section of carbon was revised for the first time in 27 years. This fact shows that the applicability of JENDL-4.0 to the HTTR criticality calculations is excellent. JENDL-4.0 promises to improve the accuracy of the HTGR criticality calculations, which allows the design of the commercial HTGR with lower cost and higher performance.

- Loaded number of fuel columns achieving the first criticality
- Excess reactivity of the fully loaded fuel column core

4.1.3.2 Neutron flux distribution and power distribution [4.1.10)]

(a) Measurement of neutron flux distribution in the reflector region

The axial neutron flux distribution for three irradiation columns in the reflector region are measured by fission chambers. The fission chambers were axially traversed by manually from the bottom of the fuel region to the upper surface of the second top reflector block. The output of fission chamber was affected by small reactivity change caused by the movement of the fission chamber. The count rate at each step was normalized with the count rate of the other fission chamber fixed at a certain position.

(b) Measurement of the power distribution [4.1.10-4.1.11)]

The power distribution of the core is an important property determining the maximum fuel temperature. Hence, the axial and radial shape of the power distribution is designed to be exponential and flat, respectively, to keep the maximum fuel temperature as low as possible. Therefore, the measurement

was conducted to provide a basis for determination of the actual power distribution. The experiment was performed by measuring the gross gamma ray emitted from the fuel assembly when withdrawn from the core during reactor shutdown. The measured fuel assemblies were in service and their average burn-up was about 4400 MWd/t. Prior to the measurement, a proportional relation between the gross gamma ray intensity and the power density of fuel assemblies was confirmed. A fuel assembly was withdrawn by the fuel handling machine up to the side where the Geiger-Muller counter was mounted. The 20 fuel assemblies were measured and reloaded into the core after the experiment. The radial and axial distributions are normalized with the average of the core and the column, respectively.

4.1.3.3 Control rod position [4.1.12)]

The HTTR has 16 pairs of 32 CRs consisting of one pair of the central CR (C-CR), six pairs of the first ring CR (R1-CR), six pairs of the second ring CR (R2-CR) and three pairs of the third ring CR (R3-CR). All of the CRs are same in material and geometry. The location in the core on the radial direction is illustrated in Fig. 4.1.1. The CRs are inserted into the core from the upper region of the core to the bottom of the fuel region through vertical holes which is placed in the CRs guide blocks. During normal operation, C-CR, R1-CRs and R2-CRs are used to control reactivity, meanwhile, R3-CRs, which are only used at scram, are withdrawn from the core and not used. In order not to disturb the optimized power distribution form in radial direction, all the CRs except R3-CRs are operated so that their insertion depths into the core are the same. The CR position is defined as the distance from the fully inserted CR. The CR position data has been measured continuously from the BOC (Beginning Of Cycle) to the current burnup. In the HTTR, reactivity control during normal operation is conducted with CRs and BPs. No other reactivity control systems are installed, such as chemical shims or recirculation flow controls in LWRs. The change of the CR position with burnup shows the change of the excess reactivity with burnup, and hence this data is very useful to validate burnup calculation methods.

Figure 4.1.3 shows the changes in the CR positions with burnup for both zero power and full power in high-temperature test operation mode. We plotted the experimental data for full power from 200 EFPD (Effective Full Power Day), at which the first full power high-temperature test operation was carried out, to the current 370 EFPD of burnup. For zero power, we plotted the experimental data from 0 EPFD to 300 EFPD. The experimental data for full power operation show that the CR position decreases with burnup, which suggests that the CR insertion depth increases with burnup. For zero power, meanwhile, the CR position is almost constant with burnup, which is different from the trend for full power.

For the HTTR full power operation, the experimental data and the analytical result showed the same trend for the change in the CR position with burnup. They agree within 10 cm throughout the burnup period, which corresponds to about 1%Δk/k in reactivity. Meanwhile, for zero power, both the experimental data and the calculation results show that the CR position is almost constant throughout the burnup period. They agree within 15 cm, which corresponds to about 1.5%Δk/k in reactivity, during the burnup period. Hence, although there is still room for improvement, the validity of the whole core burnup calculation for the HTTR was confirmed by the experimental data.

References

4.1.1) K. Yamashita, R. Shindo, I. Murata, et al., “Nuclear Design of the High-Temperature Engineering Test Reactor (HTTR)”, Nuclear Science and Engineering, 122, 2, pp.212-228 (1996).

4.1.2) N. Fujimoto, N. Nojiri and K. Yamashita, “Validation of the nuclear design code system for the HTTR using the criticality assembly VHTRC”, Nuclear Engineering and Design, 233, 1-3, pp.155-162 (2004).

4.1.3) N. Fujimoto, N. Nojiri, H. Ando, et al., “Nuclear design”, Nuclear Engineering and Design, 233, 1-3, pp.23-36 (2004).

4.1.4) M. Goto, S. Shimakawa and Y. Nakao, “Impact of revised thermal neutron capture cross section of carbon stored in JENDL-4.0 on HTTR criticality calculation”, Journal of Nuclear Science and Technology, 48, 7, pp.965-969 (2011).

4.1.5) Y. Nagaya, K. Okumura, T. Mori, et al., “MVP/GMVPII: General Purpose Monte Carlo Codes for Neutron and Photon Transport Calculations Based on Continuous Energy and Multigroup Methods”, JAERI 1348 (2005), 388p.

4.1.6) K. Shibata, O. Iwamoto, T. Nakagawa, et al., “JENDL-4.0: A New Library for Nuclear Science and Engineering”, Journal of Nuclear Science and Technology, 48, 1, pp.1-30 (2011).

4.1.7) K. Shibata, T. Kawano, T. Nakagawa, et al., “Japanese Evaluated Nuclear Data Library Version 3 Revision-3: JENDL-3.3”, Journal of Nuclear Science and Technology, 39, 11, pp.1125-1136 (2002).

4.1.8) M.B. Chadwick, P. Oblozinský, M. Herman, et al., “ENDF/B-VII.0: Next Generation Evaluated Nuclear Data Library for Nuclear Science and Technology”, Nuclear Data Sheets, 107, 12, pp.2931-3060 (2006).

4.1.9) A. Koning, R. Forrest, M. Kellett, et al., “The JEFF-3.1 Nuclear Data Library”, JEFF Report 21 (2006).

4.1.10) N. Nojiri, S. Shimakawa, N. Fujimoto, et al., “Characteristics test of initial HTTR core”, Nuclear Engineering and Design, 233, 1-3, PP.283-290 (2004).

4.1.11) N. Nojiri, S. Shimakawa, K. Takamatsu, et al., “Power Distributions in the High Temperature Engineering Test Reactor (HTTR) by Measuring Gross Gamma Ray from the Fuel Assembles”, JAERI-Tech 2003-086 (2003), 136p (In Japanese).

4.1.12) M. Goto, M. Shinohara, D. Tochio, et al., “Long-term high-temperature operation of the HTTR”, Nuclear Engineering and Design, 251, pp.181-190 (2012).

Table 4.1.1 Calculation uncertainties of the HTTR design

Items	Difference between the experimental and analytical results	Calculation uncertainty considered in the HTTR nuclear design
Effective multiplication factor	1%Δk	1%Δk
CR worth	2.6%	10%
BP worth	~0%	10%
Power and neutron flux distribution	2.9%	3%
Temperature coefficient of reactivity	6%	10%

Table 4.1.2 Comparison between experimental and calculation results

	Experiment	JENDL-4.0	JENDL-3.3	ENDF/B-VII.0	JEFF-3.1
Number of fuel columns at achieving the first criticality	19	19	18	17	17
Excess reactivity of the fully loaded core (%Δk/k)	12.0	12.0	12.4	12.8	12.7

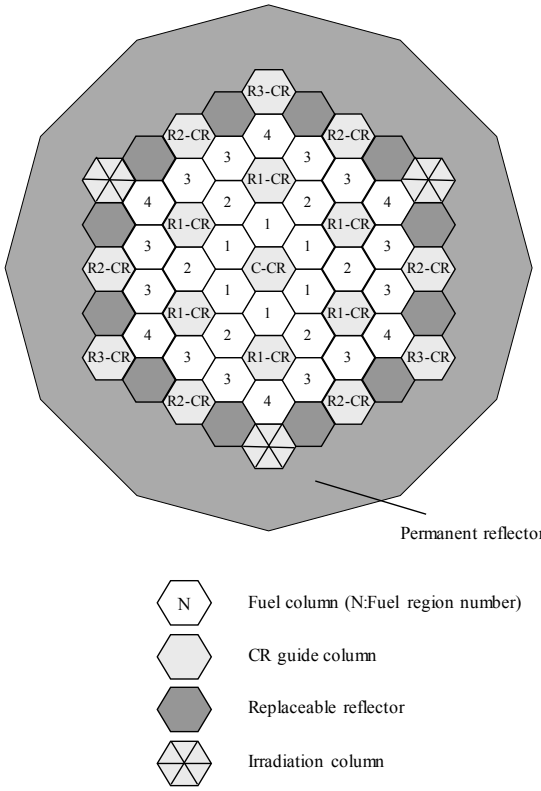

Layer*3	Fuel region number*1				BP*2
	1	2	3	4	
1	6.7	7.9	9.4	9.9	2.0
2	5.2	6.3	7.2	7.9	2.5
3	4.3	5.2	5.9	6.3	2.5
4	3.4	3.9	4.3	4.8	2.0
5	3.4	3.9	4.3	4.8	2.0

*1 ^{235}U enrichment (wt%)

*2 Natural boron concentration (wt%)

*3 The number indicates the layer number from the top fuel block.

Fig. 4.1.1 Fuel and BP allocating plan of the HTTR

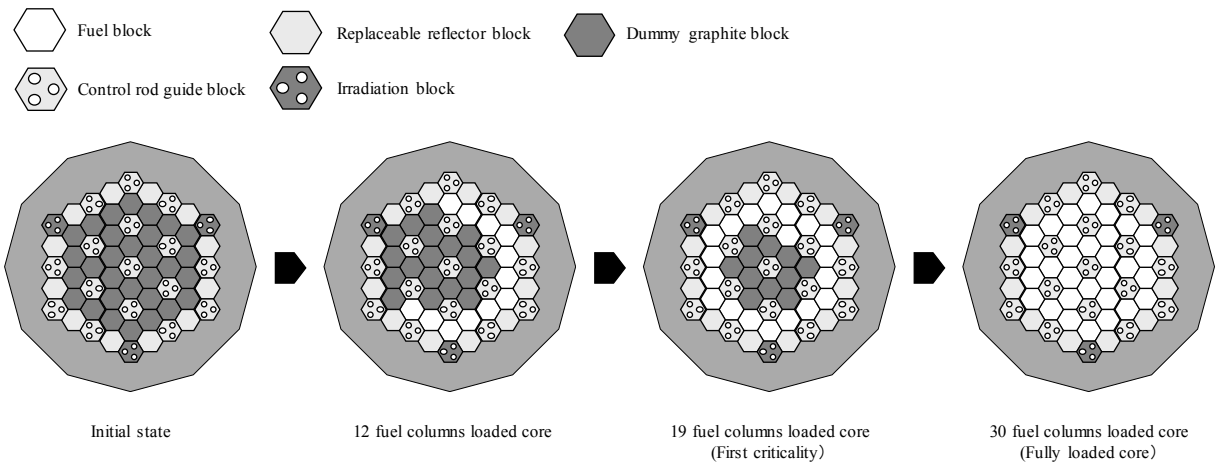

Fig. 4.1.2 Procedure of the HTTR critical approach

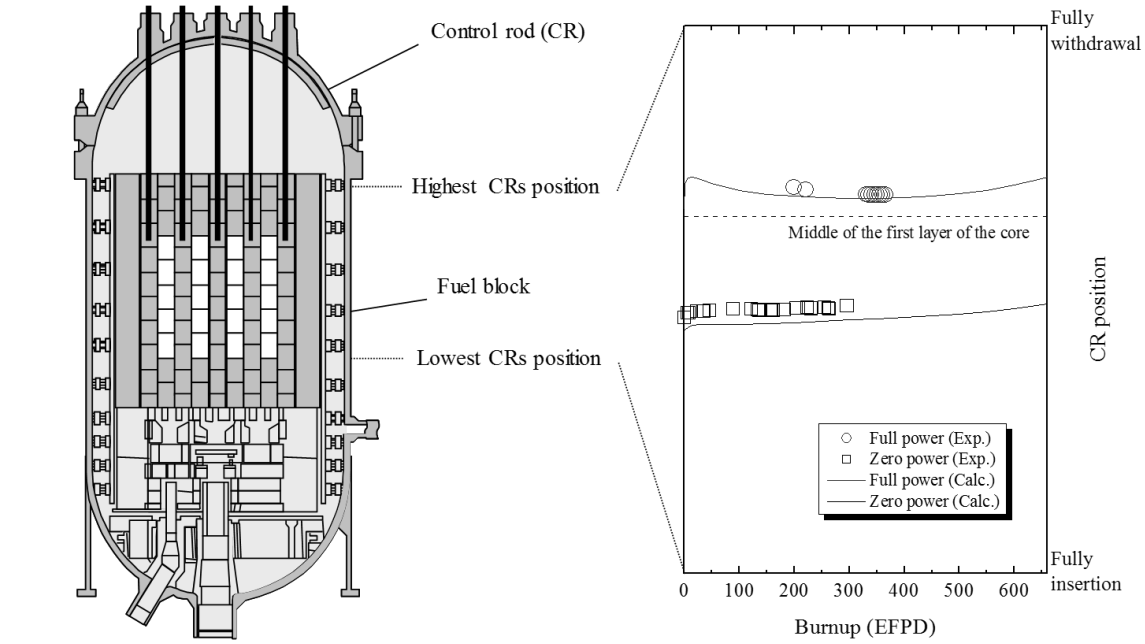

Vertical sectional view of HTTR pressure vessel

Changes in control rod position with burnup

Fig. 4.1.3 Changes of CR position with burnup

4.2 Thermal hydraulics design

4.2.1 Procedure of thermal hydraulic design

The design procedure shown in Fig. 4.2.1 is followed in JAEA to design the HTTR and other reactors presented in Chapter 3. The procedure is based on the flow network calculation code FLOWNET [4.2.1)] and the fuel temperature calculation code TEMDIM [4.2.2)]. The objective of the procedure is confirmation of the maximum fuel temperature in normal operation to be lower than a thermal design target to ensure the structural integrity of the coated fuel particles. The distribution of fuel temperature is calculated by using the input of power density and neutron fluence distributions obtained by the nuclear design and by using the input of the core coolant flow distribution obtained by the flow network calculation.

4.2.2 Outline of flow network code

4.2.2.1 Calculation model

The calculation model of a flow network code consists of one-dimensional flow branches and pressure nodes which are the junctions or terminals of the branches, as shown in the Fig. 4.2.2. Each branch has the cross-sectional area, length, equivalent diameter and pressure loss coefficient of an actual flow passage. A detailed coolant flow rate distribution is determined on the basis of the power density and neutron fluence distributions obtained by the nuclear design and the dimensions of the core components and reactor internals. Furthermore, not only the main coolant flow in the fuel cooling channels but also the gap flow between hexagonal graphite columns, the leakage flow through permanent reflectors, and the crossflow in the horizontal interface gap between hexagonal graphite blocks are considered as flow passages in the core region. Every gap width is calculated on the basis of the core temperature and neutron fluence distributions and the thermal expansion of the components.

4.2.2.2 Calculation method

In the flow network code, the following equations are used for each node and branch, steady temperature, pressure and flow distributions in a flow network are calculated. The thermal properties in the flow network code have temperature dependency:

● Equation of continuity

$$\sum_i m_{ij} + S_j = \sum_k m_{jk} \tag{4.2.1}$$

● Equation of motion (pressure loss between nodes i and j)

$$\Delta p_{ij} = p_i - p_j = \frac{1}{2\bar{\rho}_{ij}}\left(\frac{m_{ij}}{A_{ij}}\right)^2 \times \left\{4 f_{ij}\frac{L_{ij}}{D_{ij}} + K_{ij} + 2\bar{\rho}_{ij}\left(\frac{1}{\rho_{ij}^{out}} - \frac{1}{\rho_{ij}^{in}}\right)\right\} \tag{4.2.2}$$

● Energy equation

$$C_p \sum_i T_{ij} m_{ij} + C_p T_{S_j} S_j + Q_{ij} = C_p T_j \sum_k m_{jk} \tag{4.2.3}$$

Each node pressure and branch flow is obtained by solving the non-linear simultaneous equations on pressure p from Eq. (4.2.1) and Eq. (4.2.2). Regarding Eq. (4.2.2) as a linear equation about m, the following equation is obtained:

$$p_i - p_j = m_{ij} R_{ij} \tag{4.2.4}$$

where,

$$R_{ij} = \frac{|m_{ij}|}{2\bar{\rho}_{ij} A_{ij}^{\,2}} \left[\lambda_{ij} \frac{L_{ij}}{D_{ij}} + K_{ij} + 2\bar{\rho}_{ij} \left(\frac{1}{\rho_{ij}^{out}} - \frac{1}{\rho_{ij}^{in}} \right) \right] \tag{4.2.5}$$

Substituting Eq. (4.2.4) into Eq. (4.2.1), the following pressure equation is obtained:

$$\left(\sum_i \frac{p_i}{R_{ij}} + \sum_k \frac{p_k}{R_{jk}} \right) + S_j - p_j \left(\sum_i \frac{1}{R_{ij}} + \sum_k \frac{1}{R_{jk}} \right) = 0 \tag{4.2.6}$$

Re-evaluating factors with mass flow dependency, the repeating calculation of Eq. (4.2.6) is carried out, each node pressure and branch flow is obtained. Each node temperature is calculated by using Eq. (4.2.3) with the pressure and mass flow obtained from Eq. (4.2.6). The above steps are repeated to obtain the steady pressure, temperature and flow distributions in a flow network.

In Eqs. (4.2.1) to (4.2.6), the upper-lowercase letters mean m: mass flow rate, S: source term, p: pressure, ρ: density, A: cross-sectional area, f: Fanning's friction factor, L: length, D: equivalent diameter, K: parasitic pressure loss coefficient, $\bar{\rho}$: average density, C_p: specific heat at constant pressure, T: temperature, Q: heat, R: equation defined by Eq. (4.2.5), λ: Darcy's friction factor and the subscripts mean i, j, k: node number, ij: branch number, jk: branch number, out: outlet, in: inlet.

4.2.2.3 Evaluation of Flow Gap Width

Every gap width is calculated on the basis of the core temperature and neutron fluence distributions and the thermal expansion of the graphite blocks. Fig. 4.2.3 shows the calculation procedure of the gap widths between columns. The gap widths between columns and the crossflow gap width are calculated by the following equations [4.2.3)]:

● Gap width between columns, δ_{g1}

$$\delta_{g1} = \delta_{g1,0} - \frac{1}{2} P_b \left(T_{h,i}\, \alpha_{h,i} + T_{h,j}\, \alpha_{h,j} \right) - \frac{1}{2} W_b \left(T_{b,i}\, \alpha_{b,i} + T_{b,j}\, \alpha_{b,j} \right) + \frac{1}{2} W_b \left(\zeta_{b,i} + \zeta_{b,j} \right) \tag{4.2.7}$$

● Gap width between columns, δ_{g2}

$$\delta_{g2} = \delta_{g2,0} + P_b\, T_h\, \alpha_h - \frac{1}{2} W_b \left(T_{b,i}\, \alpha_{b,i} + T_{b,j}\, \alpha_{b,j} \right) + \frac{1}{2} W_b \left(\zeta_{b,i} + \zeta_{b,j} \right) \tag{4.2.8}$$

● Crossflow gap width between i and i+1 blocks, δ_c

$$\delta_c = \frac{1}{2} \left(\xi_{b,i} + \xi_{b,i+1} \right) + \delta_h \tag{4.2.9}$$

In Eqs. (4.2.7) to (4.2.9), the upper-lowercase letters mean δ: gap width, P: average pitch, T: temperature, α: thermal expansion coefficient, W: block width across flat, ζ: irradiation deformation

coefficient, ξ: thermal and irradiation deformation, and the subscripts mean 0: initial value, b: core block, h: hot plenum block, i, j: core block number.

4.2.3 Outline of fuel temperature calculation code

A fuel temperature calculation code can calculate fuel temperature in the steady state operation of the block-type HTGRs. In this section, the core configuration of the block-type HTGRs, the calculation objects, calculation models, basic equations and calculation conditions of the fuel temperature calculation code, are described.

4.2.3.1 Calculation objects

The calculation objects of the fuel temperature calculation code are the fuel columns which consist of stacked fuel assemblies with the fuel rods. The fuel columns in the same positional relation in relation to the core center column are regarded as the same groups. Due to specific layout arrangement for fuel and control rods, the core is subdivided into several groups. The power density and neutron fluence distributions of the representative one channel with the maximum peaking factor are selected from each fuel column group, and these are used for fuel temperature calculation. The channel means a triangular prism divided into 24 in horizontal cross-sectional view of the fuel column in the nuclear design, and the channel selection is carried out through the data conversion program shown in Fig. 4.2.1.

4.2.3.2 Calculation model

The calculation model of the fuel temperature calculation code is the multi-cylindrical model which consists of a central void or central helium gas, fuel compacts, a helium gap, graphite sleeves, helium gas in a main fuel cooling channel, and graphite blocks, as shown in Fig. 4.2.4. The thermal radiation heat transfer between the fuel compacts and the graphite sleeves and that between the graphite sleeves and the graphite blocks are considered. The periphery of the model is surrounded by the adiabatic boundary in order to achieve conservative solutions.

4.2.3.3 Basic equations

The temperature distributions of the fuel columns are obtained by solving the following system of equations based on boundary conditions:

Solid rejoin: $$\frac{1}{r}\frac{d}{dr}\left(rk\frac{dT}{dr}\right)+\ddot{q}=0 \tag{4.2.10}$$

Coolant region: $$dq=\dot{m}C_p\,dT \tag{4.2.11}$$

where r: position in radial direction, k: thermal conductivity, T: temperature, $\ddot{q}$: volumetric heat source, q: heat flowing in coolant from wall, $\dot{m}$: coolant flow rate, C_p: coolant's specific heat at constant pressure, dT : coolant's temperature gradient in flow direction. The thermal conduction of the solid region in the circumferential and axial directions is ignored because of low one.

Hot spot factors are considered in the fuel temperature calculation in order to evaluate the maximum

fuel temperature with a sufficient margin, and they are used to account for various uncertainties and to assure that the specified maximum fuel temperature in the core does not exceed the thermal design target at any time and any location during the normal operation condition [4.2.4-4.2.5)].

Fuel temperature at an arbitrary evaluation point is obtained by adding on inlet coolant temperature to temperature difference at each position, as shown in Fig. 4.2.5. Based on this way of thinking, the fuel temperature T_f is evaluated by the following equation with the nominal values obtained by the fuel temperature calculation:

$$T_f = T_{in} + \sum_{i=1}^{5}\left(F_i \cdot \Delta T_i^N\right) \tag{4.2.12}$$

where,

T_{in} : core inlet coolant temperature

F_i : overall hot spot factor for component *i*

ΔT_i^N : nominal temperature rise

i = 1: coolant temperature rise
2: film temperature rise
3: temperature rise in graphite sleeve
4: gap temperature rise
5: temperature rise in fuel compact.

Thus, the maximum fuel temperature is obtained by the following equation:

$$T_f^{\max} = \max(T_f) \tag{4.2.13}$$

In order to determine F_i, the systematic and random factors are determined individually according to the functional relationship between the uncertainty and the temperature. The total systematic factor F_i^S is given by combining the systematic factors f_{ij}^S:

$$F_i^S = \prod_{j=1}^{n} f_{ij}^S \tag{4.2.14}$$

where, *n* is the number of systematic factors. The random factors f_{ik}^R are combined to give the total random factor F_i^R:

$$F_i^R = 1 + \sqrt{\sum_{k=1}^{m}\left(f_{ik}^R\right)^2} \tag{4.2.15}$$

where, *m* is the number of random factors. Then, F_i is calculated by the following definition that is the product of the total systematic and random factors:

$$F_i = F_i^S \times F_i^R \tag{4.2.16}$$

By using equations (4.2.14), (4.2.15) and (4.2.16), equation (4.2.12) can be rewritten to the following equation:

$$T_f = T_{in} + \sum_{i=1}^{5}\left[\prod_{j=1}^{n} f_{ij}^{S} \cdot \left\{1 + \sqrt{\sum_{k=1}^{m}\left(f_{ik}^{R}\right)^2}\right\} \cdot \Delta T_i^{N}\right] \tag{4.2.17}$$

Basically, the systematic and random factors for each component *i* are determined by sensitivity analyses [4.2.6) 4.2.7)]. Table 4.2.1 shows the hot spot factors, as example, used in the HTR50S, one of the reactor designs presented in Chapter 3.3.

4.2.3.4 General calculation conditions

The general calculation conditions used in the fuel temperature calculation code are shown in Fig. 4.2.4 and Table 4.2.2.

(1) Gap conductance with thermal radiation

The gap conductance h_{gap} (W/(m^2•K)) between the fuel compact outer surface and the graphite sleeve inner surface is calculated from the following equation:

$$h_{gap} = \frac{k_{He}}{\Delta_{gap}} + \frac{\sigma\left(T_{fo}^{\ 2} + T_{si}^{\ 2}\right)\left(T_{fo} + T_{si}\right)}{\dfrac{1}{\varepsilon_{fo}} + \dfrac{r_{fo}}{r_{si}}\left(\dfrac{1}{\varepsilon_{si}} - 1\right)} \tag{4.2.18}$$

where k_{He}: thermal conductivity of helium gas (W/(m•K)), $\Delta_{gap} = r_{si} - r_{fo}$: gap width (m), r_{fo}, r_{si}: outer and inner radii of fuel compact and graphite sleeve (m), σ: Stefan-Boltzmann constant $= 5.67 \times 10^{-8}$ (W/(m^2•K^4)), T_{fo}, T_{si}: temperatures of fuel compact outer surface and graphite sleeve inner surface (K) and ε_{fo}, ε_{si}: emissivities of fuel compact outer surface and graphite sleeve inner surface. The emissivities ε_{fo} and ε_{si} are set at 0.8 as the default values, which include the lower limit of the experimental values. Users can change the values if necessary.

The gap width Δ_{gap}, which is important to evaluate the fuel temperature, is calculated from the following equations [4.2.7)]:

$$\Delta_{gap} = 1.569 \times 10^{-4} + 2.047 \times 10^{-5}\phi - 1.430 \times 10^{-6}\phi^2 + 4.088 \times 10^{-8}\phi^3 \quad (\phi \le 16 \times 10^4) \tag{4.2.19}$$

$$\Delta_{gap} = 2.0752 \times 10^{-4} + 4.87 \times 10^{-6}\phi \quad (\phi > 16 \times 10^4) \tag{4.2.20}$$

where ϕ is neutron fluence ($\times 10^{24}$ n/m^2). The equations (4.2.19) and (4.2.20) were determined on the basis of the thermal expansion and irradiation deformation of the fuel compact and graphite sleeve.

(2) Convective heat transfer

The convective heat transfer is considered for the annular flow path between the graphite sleeve outer surface and the graphite block inner surface. The equation of the convective heat transfer is as follows [4.2.8)].

$$Nu = 0.020 Re^{0.8} Pr^{0.4} \left(\frac{D_i}{D_o}\right)^{-0.16} \left(\frac{T_W}{T_b}\right)^{-0.5} \qquad \text{(Re>2,000)} \tag{4.2.21}$$

where Nu: Nusselt number, Re: Reynolds number, Pr: Prandtl number, D_i, D_o: inner and outer diameters of annular flow path (m), T_W: wall temperature (K) and T_b: coolant bulk temperature (K).

When the center holes of the fuel compacts are cooled by the coolant, the following equation is used

for the fuel compact inner surface:

$$Nu = 0.020 Re^{0.8} Pr^{0.4} \qquad (\mathrm{Re}>2{,}000) \qquad (4.2.22)$$

In the case of $Re \leq 2{,}000$, the constant values obtained by substituting Re=2,000 into Eqs. (4.2.21) and (4.2.22) are used.

(3) Thermal radiation heat transfer

The thermal radiation heat transfer h_r (W/(m^2•K)) between the graphite sleeve outer surface and the graphite block inner surface is evaluated from the following equation:

$$h_r = \frac{\sigma\left(T_{so}^{\ 2} + T_{bi}^{\ 2}\right)\left(T_{so} + T_{bi}\right)}{\dfrac{1}{\varepsilon_{so}} + \dfrac{A_{so}}{A_{bi}}\left(\dfrac{1}{\varepsilon_{bi}} - 1\right)} \qquad (4.2.23)$$

where T_{so}, T_{bi}: temperatures of graphite sleeve outer surface and graphite block inner surface (K), A_{so}, A_{bi}: areas of graphite sleeve outer surface and graphite block inner surface (m^2), ε_{so}, ε_{bi}: emissivities of graphite sleeve outer surface and graphite block inner surface. The emissivities ε_{so} and ε_{bi} are set at 0.8 as well as Eq. (4.2.18).

(4) Adiabatic wall

The adiabatic wall condition is used for the graphite block outer surface. When the center holes of the fuel compacts are a void, the condition is also adopted for the fuel compact inner surface.

4.2.4 Validation of HTTR design codes [4.2.8)]

The validation of FLOWNET was made by a comparison of experimental data obtained by the thermal hydraulic experiments with HENDEL (Helium Engineering Demonstration Loop) core component test section (T_2) and the one-column test facility and their analytical results. The HENDEL T_2 was a full scale mock-up of metallic and graphite core support structures for HTTR. A coolant leakage test, in which coolant flow characteristics through the gaps between the permanent reflector blocks was investigated, was carried out simulating the operation condition of HTTR.

The validation of TEMDIM was carried out by comparing the analytical results to experimental data obtained by the HENDEL fuel stack test section (T_1). The HENDEL T_1 was the simulation of a fuel stack in the core which consists of a single-channel test rig and a multi-channel test rig; the former simulates one fuel cooling channel and the latter one fuel column.

References

4.2.1) S. Maruyama, T. Murakami, Y. Kiso, Y. Sudo, “Verification of In-Vessel Thermal and Hydraulic Analysis Code “FLOWNET””, JAERI-M 88-138 (1988), 39p (in Japanese).

4.2.2) S. Maruyama, N. Fujimoto, S. Fujii, T. Watanabe, Y. Sudo, “Verification of Fuel Temperature Analysis Code “TEMDIM””, JAERI-M 88-170 (1988), 72p (in Japanese).

4.2.3) Y. Inaba, H. Sato, M. Goto, H. Ohashi, Y. Tachibana, “Conceptual Design of Small-sized HTGR System, 3; Core Thermal and Hydraulic Design”, JAEA-Technology 2012-019 (2012), 142p (in Japanese).

4.2.4) S. Maruyama, K. Yamashita, N. Fujimoto, et al., “Evaluation of Hot Spot Factors for Thermal and Hydraulic Design of HTTR”, Journal of Nuclear Science and Technology, 30, 11, pp.1186-1194 (1993).

4.2.5) N. Fujimoto, S. Maruyama, S. Fujii, et al., “Evaluation of Parameters Effect on the Maximum Fuel Temperature in the Core Thermal and Hydraulic Design of HTTR”, JAERI-M 88-187 (1988), 79p (in Japanese).

4.2.6) S. Maruyama, K. Yamashita, N. Fujimoto, et al., “Determination of Hot Spot Factors for Calculation of the Maximum Fuel Temperatures in the Core Thermal and Hydraulic Design of HTTR”, JAERI-M 88-250 (1988), 88p (in Japanese).

4.2.7) Y. Inaba, K. Isaka, T. Shibata, “Development of Fuel Temperature Calculation Code “FTCC” for High Temperature Gas-cooled Reactors”, JAEA-Data/Code 2017-002 (2017), 74p (in Japanese).

4.2.8) S. Saito, et al., “Design of high temperature engineering test reactor (HTTR)”, JAERI 1332 (1994), 247p.

Table 4.2.1 Example of hot spot factors as used in HTR50S design

(a) Systematic factors (unit: -)

Items	Coolant temperature rise	Film temperature rise	Sleeve temperature rise	Gap temperature rise	Fuel compact temperature rise
Thermal power	1.00	1.02	1.02	1.02	1.02
Radial power distribution	1.03	1.03	1.03	1.03	1.03
Axial power distribution	1.0	1.0	1.0	1.0	1.0
Coolant flow rate	1.01	1.008	1.0	1.0	1.0
Flow rate distribution	1.02	1.016	1.0	1.0	1.0
Inlet coolant temperature	+20˚C				

(b) Random factors (unit: -)

Items	Coolant temperature rise	Film temperature rise	Sleeve temperature rise	Gap temperature rise	Fuel compact temperature rise
Dimension					
Compact internal diameter	0.0	0.0	0.0	0.0	0.01
Compact external diameter	0.0	0.0	0.0	0.37	0.012
Sleeve internal diameter	0.0	0.0	0.015	0.37	0.0
Sleeve external diameter	0.0	0.017	0.012	0.0	0.0
Cooling channel diameter	0.0	0.014	0.0	0.0	0.0
Effective heating length	0.0	0.002	0.002	0.002	0.002
Fissile content					
Fuel kernel diameter	0.001	0.001	0.001	0.001	0.001
Fuel kernel density	0.001	0.001	0.001	0.001	0.001
Enrichment	0.035	0.035	0.035	0.035	0.035
Uranium content	0.02	0.02	0.02	0.02	0.02
Coolant physical property					
Specific heat	0.002	0.001	0.0	0.0	0.0
Thermal conductivity	0.0	0.018	0.0	0.03	0.0
Viscosity	0.0	0.012	0.0	0.0	0.0
Irradiation induced deformation	0.0	0.0	0.0	0.21	0.0
Gap conductance	0.0	0.0	0.0	0.10	0.0
Eccentricity of compact-sleeve	0.0	0.041	0.041	0.041	0.041
Power distribution	0.02	0.02	0.02	0.02	0.02
Flow rate distribution	0.04	0.032	0.0	0.0	0.0

Table 4.2.2 General calculation conditions used in fuel temperature calculation code

Items	Fuel compact		Graphite sleeve		Graphite block	
	Inner surface	Outer surface	Inner surface	Outer surface	Inner surface	Outer surface
Calculation condition	Adiabatic wall or convective heat transfer	Gap conductance including thermal radiation		Convective heat transfer and thermal radiation		Adiabatic wall
Emissivity	-	0.8	0.8	0.8	0.8	-

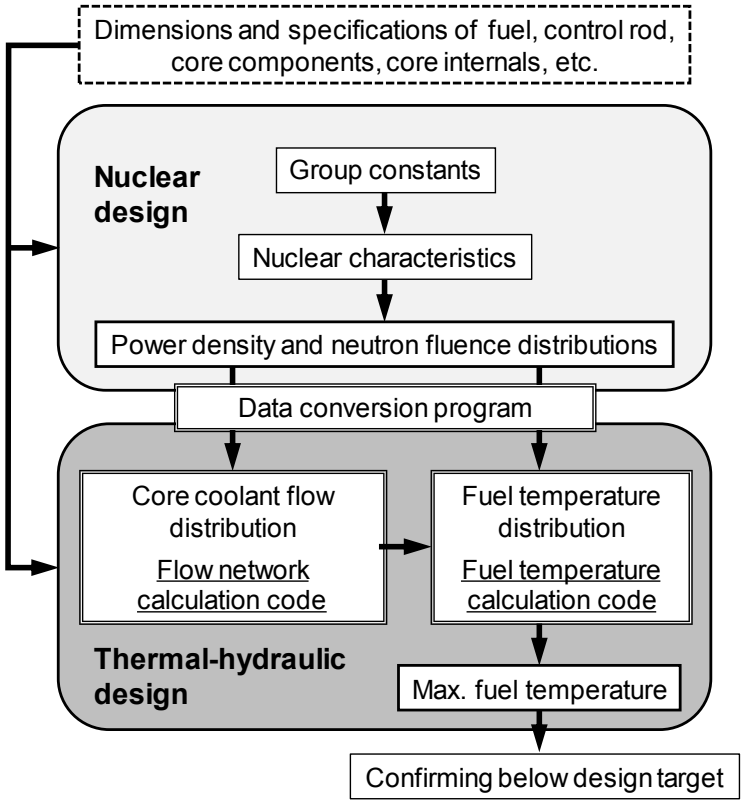

Fig. 4.2.1 Procedure of core thermal hydraulic design for block-type HTGRs

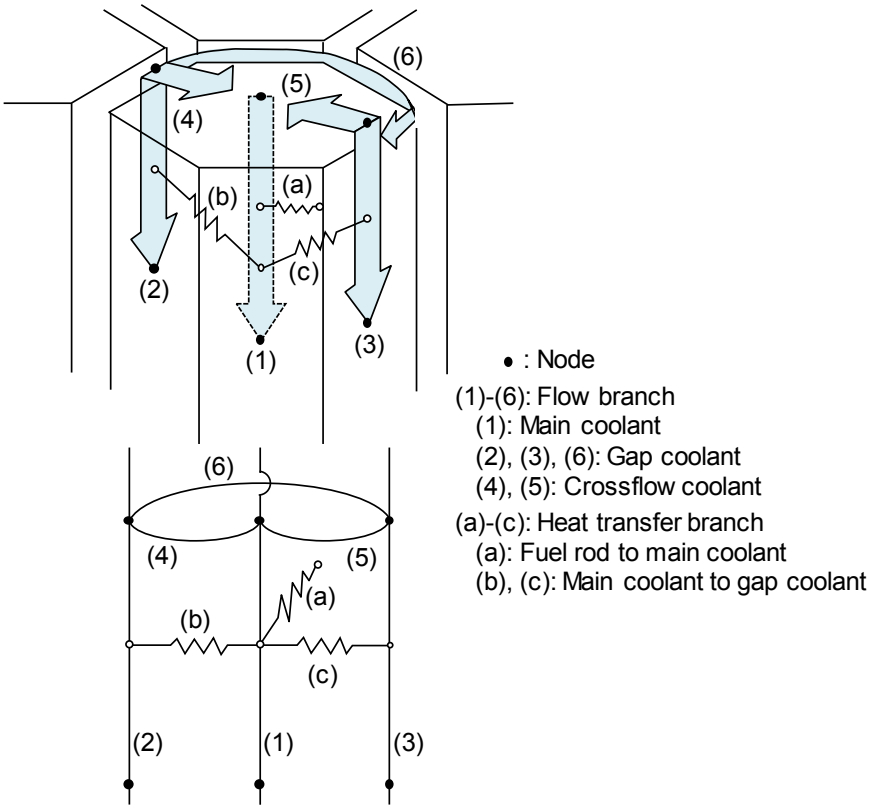

Fig. 4.2.2 Flow around fuel assemblies and flow network model of Flow network

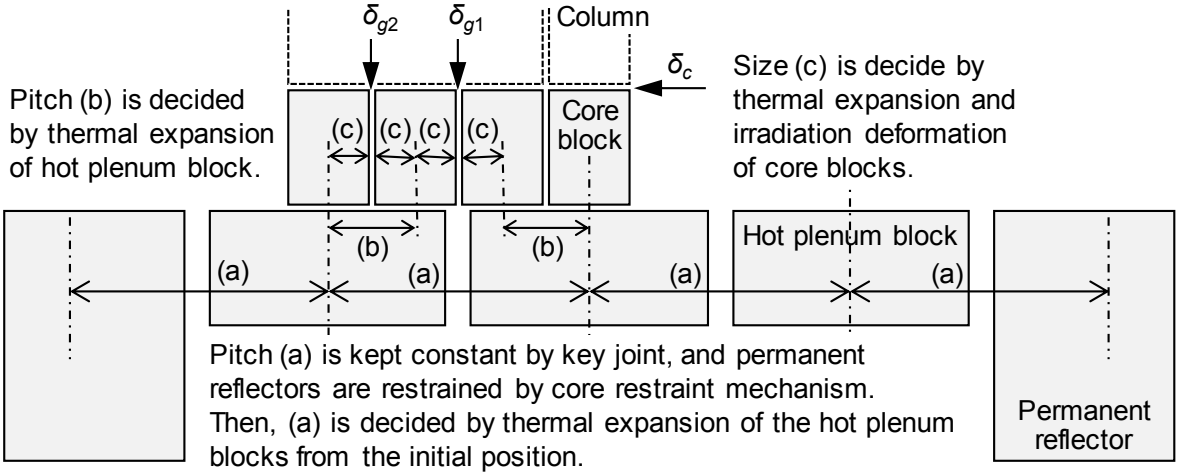

Fig. 4.2.3 Calculation procedure of gap width between columns

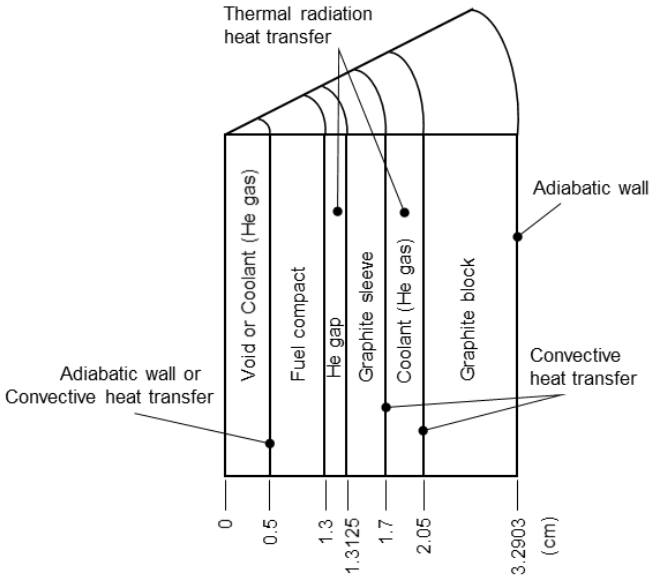

Fig. 4.2.4 Fuel temperature calculation model with size as representative example

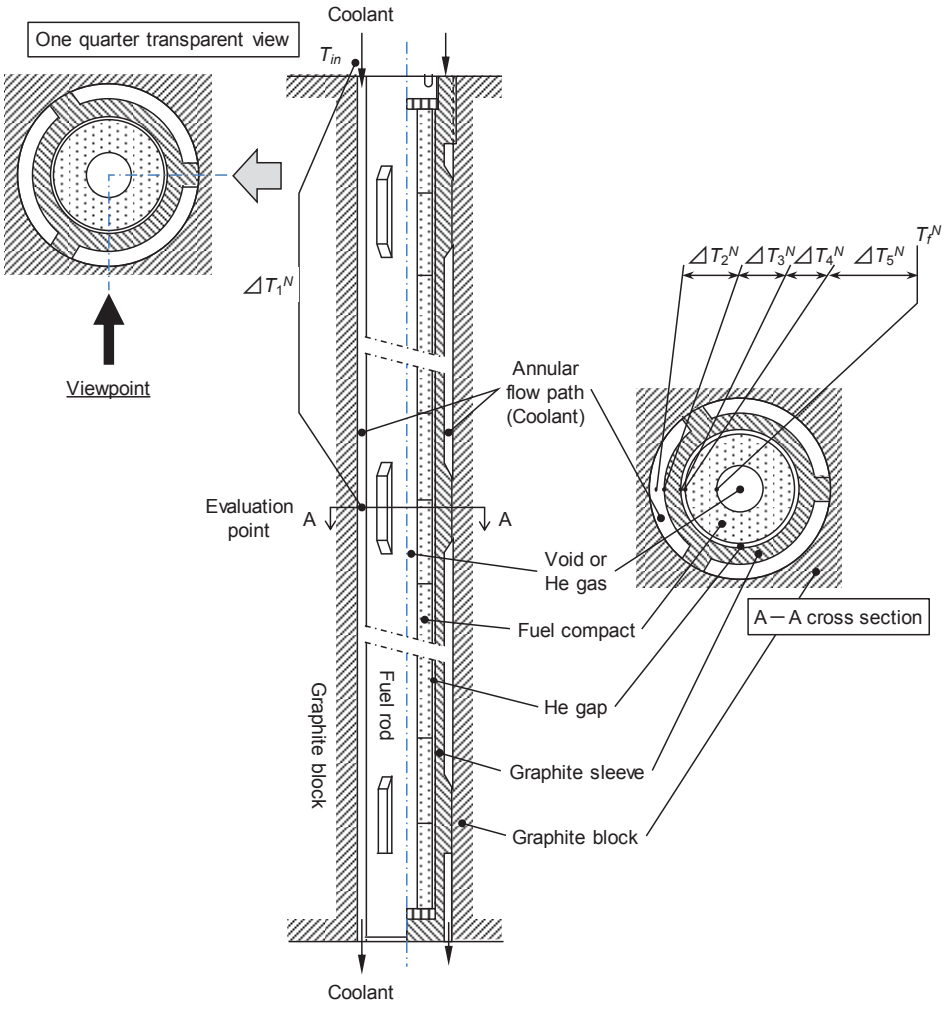

Fig. 4.2.5 Concept of fuel temperature evaluation

4.3 Fuel

4.3.1 Fuel design

Two fuel element concepts, the spherical fuel element and the block-type fuel element as shown in Fig. 4.3.1, are presently in use in HTGR. In either concept, the high temperature capability and the inherent safety design of the HTGRs rely mainly on the integrity of the fuel design of the refractory TRISO (Tri-Structural Isotropic)-coated fuel particles, in which the inner fuel kernel is coated successively with the low-density carbon buffer, the inner isotropic high-density carbon (IPyC), the silicon carbide (SiC) and the outer isotropic high-density carbon (OPyC) layers.

Both the HTTR and GTHTR300 employ the TRISO-coated fuel particles with UO_2 kernel. The fuel particles are dispersed in the graphite matrix and sintered to form a fuel compact as shown in Fig. 4.3.1. Each fuel rod contains a number of fuel compacts. The design of the fuel rod differs between the HTTR and GTHTR300. In HTTR, the fuel compacts are inserted in a graphite sleeved tube to form a fuel rod. In the GTHTR300, the fuel rod is a monolithic structure where the graphite sleeve is eliminated as shown in Fig.4.3.2 to permit an increase in core power density without increasing fuel temperatures in operation or accident. Table 4.3.1 summarizes major specifications of each fuel of the HTTR and GTHTR300 [4.3.1-4.3.3].

4.3.2 Fuel fabrication

4.3.2.1 TRISO-coated fuel particle

In safety design of the HTGR fuels, it is important to retain fission products within particles so that their release to primary coolant does not exceed an acceptable level. From this point of view, the basic design criteria for the fuel are to minimize the failure fraction of as-fabricated fuel coating layers and to prevent significant additional fuel failures during operation [4.3.1]. HTTR criterion is less than 0.2 % for as-fabricated fuel failure fraction which is sum of fractions both of through-coatings failure and SiC-defective [4.3.1]. GTHTR300 criterion is less than 5×10^{-4} for as-fabricated fuel failure fraction, how is equivalent to limitation of radiation exposure evaluation [4.3.4].

Technologies for reducing as-fabricated failure fraction of TRISO coated fuel particle to limit radiation release [4.3.1]. The UO_2 kernels were fabricated in a gel-precipitation process. After formation of uranyl nitrate solution containing methanol and an additive, spherical droplets are produced by a vibration dropping technique. Following the drying and calcinating, reduction of the calcinated kernels to UO_2 was carried out. Kernel fabrication was completed by a sintering process to produce dense UO_2 kernels. The coating layers were deposited on the kernels in a chemical vapor deposition process using a fluidized coater. The TRISO-coating process is divided into four coating processes for the porous PyC, IPyC, SiC and OPyC layers. The buffer and high-density PyC coating layers were derived from pyrolysis of C_2H_2 and C_3H_6, respectively, and the SiC layer from CH_3SiCl_3. The amount of charged particles corresponded to 3.4kg uranium per a coating batch. At a desired temperature, reactants were put into the coater to produce a coating layer on the particles fluidized in the coater. After a certain time to produce the desired thickness of the layer, the reactant gas supply was replaced by argon. The coater and the coated fuel

particles were cooled down, and then the coated fuel particles were removed from the bottom of the coater. All UO_2 kernels and coated fuel particles are classified by means of a vibrating table to exclude odd shape particles.

The as-manufactured quality of the fuel has been improved by the modification of fabrication conditions and processes. The coating failure during coating process was mainly caused by the strong mechanical shocks to the particles given by violent particle fluidization in the coater and by the unloading procedure of the particles. The coating process was improved by optimizing the mode of the particle fluidization and by developing the process without unloading and loading of the particles at the intermediate coating process [4.3.6)] .

4.3.2.2 Fuel compact

Technologies for optimizing condition of fuel compaction process to prevent yield loss (HTTR experiences: 2.5×10^{-6} for through-coatings failure fraction, 8×10^{-5} for SiC-defective fraction [4.3.5)] which satisfy criteria of commercial reactor GTHTR300 [4.3.4)]). The fuel compacts of the HTTR are produced by warm-pressing of the coated fuel particles with graphite powder. In the first step, the coated fuel particles are overcoated by resinated graphite powder with alcohol. The resinated graphite powder is prepared by mixing electro-graphite powder, natural graphite powder, and phenol resin as a binder in the ratio 16:64:20, followed by grinding the mixture to powder. The aim of the overcoating is to avoid direct contact with neighboring particles in the fuel compact. The thickness of overcoating layer is about 200 μm, which is determined by the specification for the volume fraction of the coated fuel particles in the fuel compact (30vol%). Then the overcoated particles are warm-pressed by metal dies to form annular green fuel compacts. The final step of the compaction process is the heat-treatment of the green fuel compacts at 800˚C in flowing N_2 to carbonize the binder and at 1800˚C in vacuum to degas the fuel compacts. Then the fabrication process was modified to reduce the defective particle fraction during the compaction process [4.3.5)].

The compaction process was improved by optimizing the combination of the pressing temperature and the pressing speed of the overcoated particles to avoid the direct contact with neighboring particles in the fuel compact [4.3.6)]. In addition, there were odd-shaped overcoated particles in which two or three coated fuel particles were included. The odd-shaped overcoated particles failed during compaction process because they could not keep distance to each other. Then, they were removed before compaction process. Furthermore, by analyzing relations between the measured SiC-failure fractions and fabrication parameters, such as coating layer thickness, overcoating layer thickness, pressing speed, etc., it was concluded that the SiC layer thickness should be thicker than 27 μm to avoid as-fabricated SiC-failure to reduce unexpected large SiC-failure fractions during the compaction process. As shown in Fig. 4.3.3, as-fabricated fuel compacts contained almost no through-coatings failed particles and few SiC-defective particles. Average through-coatings and SiC defective fractions were 2×10^{-6} and 8×10^{-5} respectively [4.3.5)].

4.3.2.3 Know-hows for fuel fabrication possessed in Japan

JAEA's patent/ know-how / data for the fuel fabrication technologies have been developed through collaboration with Nuclear Fuel Industries, Ltd. The major items are as follows;

- Continuous coating method
- Design of fluidized bed
- Coating condition of each coating layer
- Optimizing fluidized particle condition
- Relationship between coating duration and internal flaw
- Compaction press temperature and velocity
- Removal of odd overcoated particle
- Control of compaction press condition

On the other hand, Manufacturers have developed unique technologies, exclusive of those jointly developed and owned with JAEA. Mojor patent / know-how are the followings;

- Mass production technologies of external gelation method (4.3kg-U per a batch)
- Vibrated dropping method
- Technologies to select good sphericity
- Mass production technologies of fluidized bed and chemical vapor deposition method (3.4kg-U per a batch)
- In-situ sampling system for TRISO coating inspection
- Fluidized particle condition
- Mass production technologies of overcoating device (3.4kg-U per a batch x 3 per 3 compact lots)
- Overcoated particle condition
- Sintering condition of fuel compact

4.3.3 Fuel inspection

The inspection items for the HTTR fuel were determined to confirm specifications, which certify nuclear and thermal-hydraulic design, irradiation performance and so on. From the viewpoint of purposes, the inspection items are divided into three categories, namely (1) compulsory, (2) user's requirement or optional and (3) vender's quality control [4.3.7)]. The sampling rate was also determined by considering the uniformity of inspected data. Three categories are basically classified as (a) small-scattering data, (b) medium-scattering data and (c) large-scattering data. One sample is measured from an inspection lot for the small-scattering data. For the inspection lot with medium-scattering data, three samples are measured and all of them should satisfy criterion. For the large-scattering data, measured data should meet statistically required criterion with 95% confidence. The inspection item, purpose, method and sampling rate in the HTTR fuel fabrication are summarized in Table 4.3.2 [4.3.7)]. JAEA and Japanese manufacturers have developed HTGR technologies to achieve those criteria, and own the following patents, know-hows and data.

4.3.4 Fuel performance under HTTR test operations

Also JAEA has developed technologies and accumulated data through HTTR test operations such as;

- Fission gas sampling data (Manually sampling measuring/evaluating technologies)
- Circulated radioactivity measuring data (Automated measuring technology by Fuel Failure Detection System)
- Plated-out fission products measuring data (Surface dose measuring technologies when exchanging filter of Primary Gas Circulator)

During the rise-to-power tests performed from 1999 to 2004 and several service operations of the HTTR, primary coolant sampling measurements were carried out to measure fission gas concentration. The concentrations of fission gas nuclides of ^{85m}Kr, ^{87}Kr, ^{88}Kr, ^{133}Xe, ^{135}Xe, ^{135m}Xe and ^{138}Xe were less than 0.1MBq/m^3. The release rate to birth rate ratios, (R/B)s, of fission gases were calculated based on the measured concentrations. Figure 4.3.4 shows (R/B)s of ^{88}Kr as a function of the reactor power. The (R/B) values are as low as 2×10^{-9} up to 60% of the reactor power, then increase to 7×10^{-9} at full power operation. During the high temperature test operation, where the outlet coolant temperature is 950˚C, the (R/B) became 1.5×10^{-8} at full reactor power. The obtained data were analyzed by fission gas release model, and the fission gas release mechanism is recoil from the contaminated uranium in the fuel compact matrix in lower reactor power. Beyond 60% of the reactor power, fractional release increases because diffusion release becomes main release mechanism. The increase of (R/B) in the high temperature operation is caused by increase of diffusion release according to fuel temperature elevation [4.3.8)].

References

4.3.1) S. Saito, et al., “Design of high temperature engineering test reactor (HTTR)”, JAERI 1332 (1994), p.247.

4.3.2) T. Nakata, et al., “Nuclear, Thermal and Hydraulic Design for Gas Turbine High Temperature Reactor (GTHTR300)”, Transactions of the Atomic Energy Society of Japan, 2, 4, pp.478-489 (2003) (in Japanese).

4.3.3) S. Katanishi, et al., “Feasibility Study on High Burnup Fuel for Gas Turbine High Temperature Reactor (GTHTR300), (II)”, Transactions of the Atomic Energy Society of Japan, 3, 1, pp.67-75 (2004) (in Japanese).

4.3.4) S. Katanishi and K. Kunitomi, “Safety evaluation on the depressurization accident in the gas turbine high temperature reactor (GTHTR300)”, Nuclear Engineering and Design, 237, 12-13, pp.1372-1380(2007).

4.3.5) K. Sawa, et al., “Fabrication of the first-loading fuel of the High Temperature Engineering Test Reactor”, Journal of Nuclear Science and Technology, 36, 8, pp.683-690 (1999).

4.3.6) K. Minato, et al., “Improvements in quality of as-manufactured fuels for high-temperature gas-cooled reactors”, Journal of Nuclear Science and Technology, 34, 3, pp.325-333(1997).

4.3.7) K. Sawa, et al., “Safety criteria and quality control of HTTR fuel”, Nuclear Engineering and Design, 208, 3, pp.305-313(2001).

4.3.8) S. Ueta, et al., “Fuel and fission gas release behavior during rise-to-power test ot the high temperature engineering test reactor (HTTR)” Journal of Nuclear Science and Technology, 40, 9, pp.679-686(2003).

Table 4.3.1 Major specifications of the fuels of the HTTR and GTHTR300

	HTTR [4.3.1-4.3.5]	*GTHTR300* [4.3.2- 4.3.3]
Fuel kernel		
Diameter (μm)	600±55	550
Density (g cm^{-3})	10.63±0.26	10.80
^{235}U enrichment (%)	3.4-9.9	14
Impurity (ppm EBC [a])	≤ 3	
Coating layers		
Buffer layer thickness (μm)	60±12	140
IPyC layer thickness (μm)	30±6	25
SiC layer thickness (μm)	25^{+12}_{0}	40
OPyC layer thickness (μm)	45±6	25
Buffer layer density (g cm^{-3})	1.10±0.10	1.15
IPyC layer density (g cm^{-3})	$1.85^{+0.10}_{-0.05}$	1.85
SiC layer density (g cm^{-3})	≥3.20	3.20
OPyC layer density (g cm^{-3})	$1.85^{+0.10}_{-0.05}$	1.85
OPTAF [a] of IPyC and OPyC layers	≤1.03	
Coated fuel particle		
Diameter (μm)	920^{+50}_{-30}	1010
Sphericity	≤1.2	
Fuel compact		
Coated fuel particles packing fraction (vol.%)	30±3	29
Impurity (ppm EBC [b])	≤5	
Exposed uranium fraction	$\leq 1.5\times10^{-4}$	
SiC-failure fraction	$\leq 1.5\times10^{-3}$	
Outer diameter (mm)	26.0±0.1	26.0 including 1 mm coating layer
Inner diameter (mm)	10.0±0.1	9.0
Height (mm)	39.0±0.5	83.0
Matrix density (g cm^{-3})	1.70±0.05	
Compressive strength (N)	≥4900	
Fuel rod		
Uranium content (gU)	188.58±5.66	
Total length (mm)	577±0.5	1000
Fuel compact stack length (mm)	≥544	83

[a] Optical anisotropy factor. [b] Equivalent boron content.

Table 4.3.2 The inspection item, purpose, method and sampling rate in the HTTR fuel fabrication

Inspection item	Major purpose*	Method	Sampling rate
Fuel kernel			
^{235}U enrichment	B	Mass spectrometer analysis and gamma-ray spectrometer analysis	1 sample/enrichment
Diameter	B	Optical particle size analysis	1 sample (100 particles) /fuel kernel lot
Sphericity	A	Optical particle size analysis	3 samples (100 particles /sample)/fuel kernel lot
Density	B	Mercury substitution	3 samples/fuel kernel lot
O/ U ratio	A	Oxidation and weighing	1 sample/fuel kernel lot
Impurities	A, B	Emission spectrometer analysis	1 sample/enrichment
Coated Fuel Particle (CFP)			
Layer thickness	A	Solvent substitution or sink-float	3 samples/ CFP lot
Optical anisotropy factor	A	Polarization photometer	1 sample (5 particles/ sample) /enrichment
Diameter	B	Optical particle size analysis	1 sample (100 particles) /CFP lot
Appearance	A	Visual observation	1 sample (2000 particles) /CFP lot
Cross section	A	Ceramography	1 sample (20 particles) /CFP lot
Sphericity	A	Selection by vibration table	All Coated fuel particles
Strength	A	Point crushing	30 particles/ enrichment
Fuel compact			
^{235}U enrichment	D	Mass spectrometer analysis and gamma-ray spectrometer analysis	1 sample/ enrichment
U content	B	gamma-ray spectrometer analysis	All fuel compacts
O/ U ratio	A	Oxidation and weighing	1 sample/ fuel compact lot
Graphite powder	A	Density, impurities, grain size and water content	1 sample/ graphite powder lot
Binder	A	Contents, ash, melting point and impurities	1 sample/ binder lot
Exposed uranium fraction	A	Deconsolidation and acid leaching	2 samples/ fuel compact lot
SiC-failure fraction	A	Burn and acid leaching	3 samples/ fuel compact lot
Packing fraction	B	Weighing and calculation	3 samples/ fuel compact lot
Matrix density	A	Weighing and calculation	3 samples/ fuel compact lot
Dimensions	C	Micrometer	All fuel compacts
Appearance	A	Visual observation	All fuel compacts
Marking	D	Visual observation	All fuel compacts
Strength	A	Compression	3 samples/ enrichment
Cross section	A	Ceramography	1 sample/ fuel compact lot
Impurities	B	Emission spectrometer analysis	1 sample/ enrichment

* A: Irradiation performance, B: Nuclear design, C: Thermal–hydraulic design, D: Process control

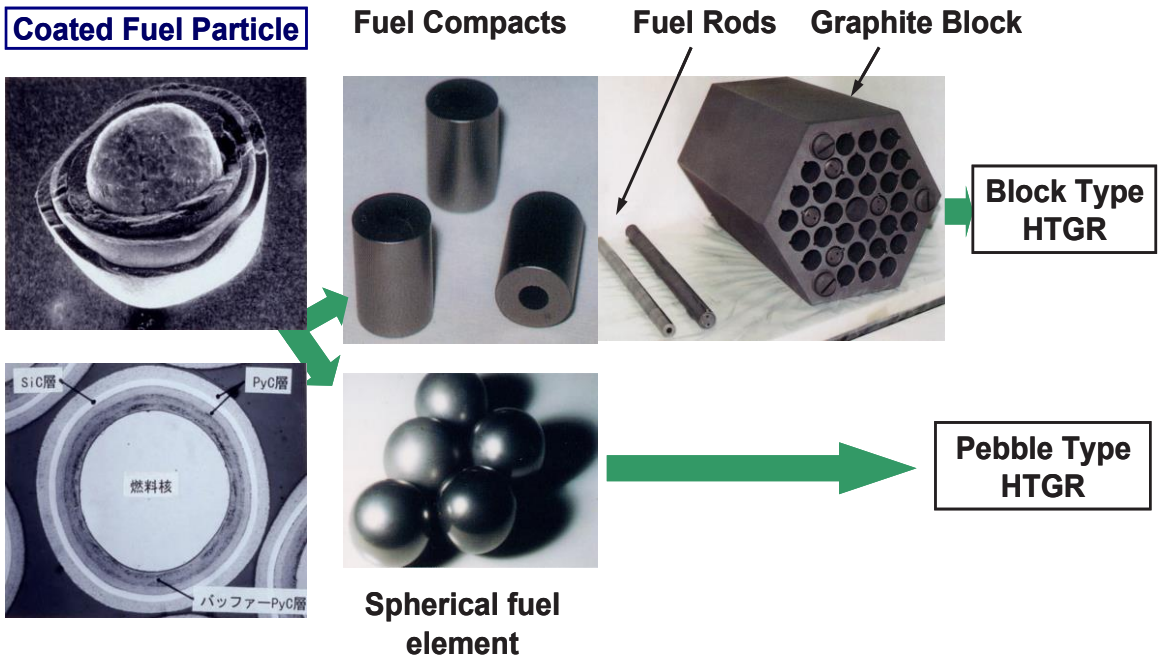

Fig. 4.3.1 High Temperature Gas-cooled Reactor Fuel

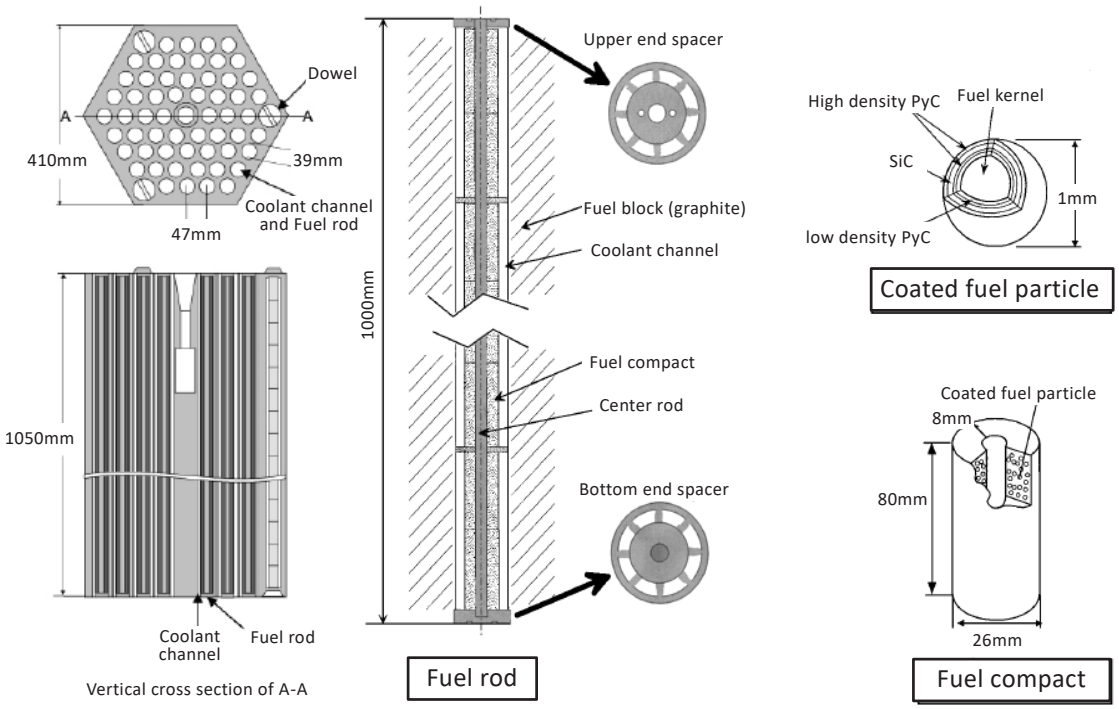

Fig. 4.3.2 Schematic of GTHTR300 fuel

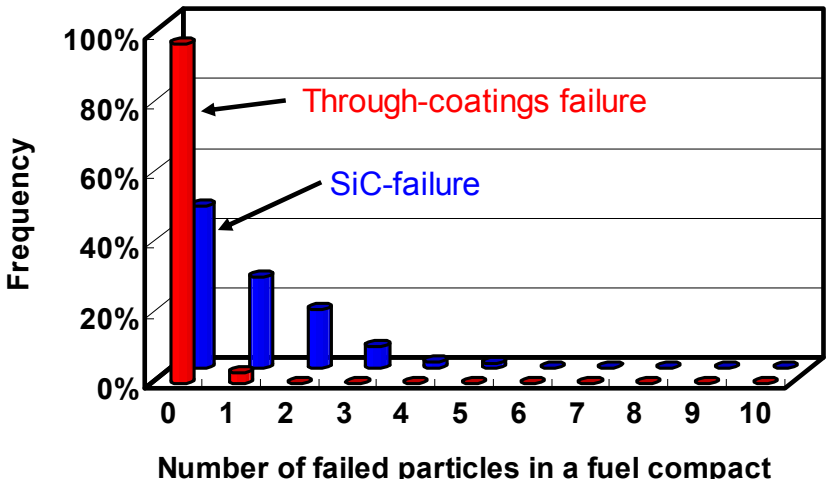

Fig.4.3.3 Number of failed particles in a fuel compact in the first-loading duel fabrication

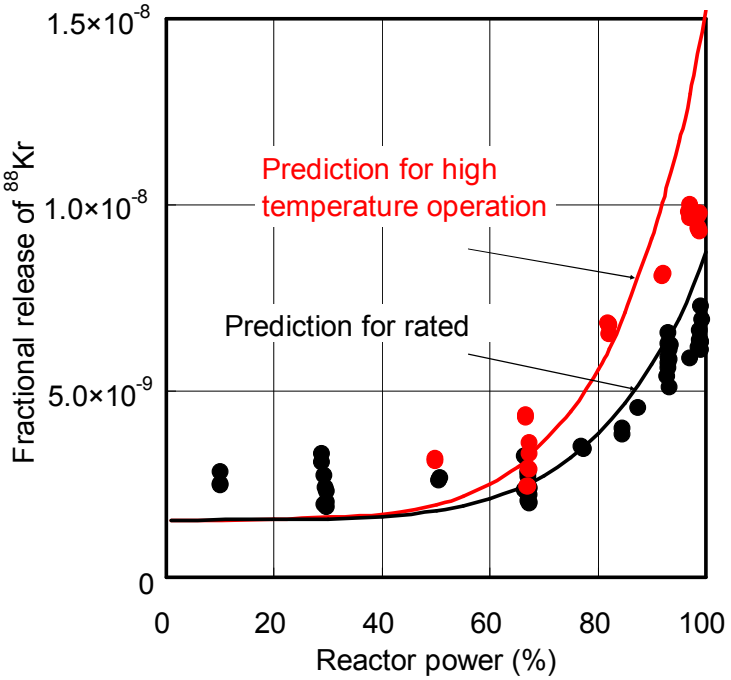

Fig. 4.3.4 Release rate to birth rate ratios in HTTR during 950˚C and 850˚C operations

4.4 Graphite

The material properties including irradiation effects of the graphite, which is the in-core structural components of the HTGR, depend highly on the raw material and forming processes. JAEA had established the material database including irradiation effects of the lG-110 graphite, PGX graphite and ASR-0RB carbon, all of which are used for various in-core component constructions of the HTTR [4.4.1, 4.4.2].

IG-110 graphite, provided by Toyo Tanso Co., is fine-grained isotropic graphite with high purity and high strength. It is used for the major components in HTGR under high temperature and high neutron irradiation condition. To obtain high quality graphite, the manufacture controls parameters in the following production process;

Grinding/mixing: Rotor speed

Mixing: temperature, number of mixing

Grinding/sieving: rotor speed

Cold isostatic pressure isotropic press (CIP) molding: pressure, time

Primary firing: temperature, time

Pitch impregnation: pressure, temperature, time

Secondary firing: temperature, time

Graphitization and high purity: temperature, time, halogen gas flow rate.

The quality of law material coke such as, bulk density, true density, ash content, volatile content, linear expansion coefficient, graphitization property will affect the quality of graphite. By strict acceptance inspections about raw material coke, dispersion in product quality could be suppressed. CIP molding technology with water pressure can make graphite blocks to have isotropic properties in a macroscopic view point. In the graphitization process, temperature control up to about 3000°C can provide graphite blocks with predetermined physical properties.

The graphite components for the GTHTR-300 are designed based on the established lG-110 material database. The fuel graphite blocks of GTHTR-300 are replaced within the range of neutron fluence of 5 dpa(displacement per atom) and it is covered by the HTTR database without extension of irradiation effect. The IG-110 is also used for the Chinese demonstration HTR-PM reactors. The IG-11 graphite, an unpurified grade of lG-110, is used for the reflector blocks of the Chinese test reactor HTR-10.

In this section, the HTGR technologies for in-core graphite components is summarized following the experiences in the HTTR.

4.4.1 In-core Graphite and Carbon Structures in the HTIR

The in-core components are categorized based on their safety function, replaceability, etc. The arrangement of graphite components in the HTTR is shown in Fig. 4.4.1 [4.4.1]. The reactor core consists of hexagonal fuel blocks, control rod guide blocks, and replaceable reflector blocks. The active core is surrounded by replaceable reflector blocks and permanent reflector blocks and supported by the core support components. IG-110 graphite, PGX graphite and ASR-0RB carbon are used for the in-core

components.

The graphite components are categorized into two kinds taking their safety function and replaceability into account as shown in Fig. 4.4.2 [4.4.2)]. One is core graphite component, the other is core support graphite component.

(1) Core graphite components

The fuel blocks are graphite hexagonal prisms with an array of fuel holes. The fuel blocks are 360mm in across flats and 580mm in height as shown in Fig. 4.4.3 [4.4.1)]. Coolant helium gas of the reactor flows gap between the holes and the rods. The fuel blocks are fabricated from the lG-110 graphite, isotropic fine-grained nuclear grade. Table 4.4.1 [4.4.1)] shows typical thermomechanical properties of the lG-110 graphite. Control rod guide blocks and replaceable reflector blocks have the same external dimensions as the fuel blocks. They are also fabricated from the IG-110 graphite.

(2) Core support graphite components

The assembly of core support is shown in Fig. 4.4.1 [4.4.1)]. The hexagonal hot plenum block assembly contains passages, which collect the primary coolant flow from the outlet the columns and distribute it into the high-temperature plenum beneath the hot plenum blocks. These blocks are fabricated from grade PGX, medium- to -fine grained molded graphite. Typical thermomechanical properties of the PGX graphite are shown in Table 4.4.1 [4.4.1)]. The core support posts and seats are designed to support the core and hot plenum block array. The posts and seats are made of the lG-110 graphite with higher strength than the PGX graphite.

The thermal insulation layer at the core bottom consists of three blocks: lower plenum block, carbon block, and bottom block. Table 4.4.1 [4.4.1)] shows typical thermomechanical properties of the ASR-0RB carbon.

The permanent reflector is a graphite structure surrounding the replaceable reflector and control rod guide columns. These blocks are made of PGX graphite.

4.4.2 Design criteria for graphite components

(1) Outline of the design criteria for the HTTR

For the construction of the HTTR, JAEA (formerly, JAERI) established the graphite structural design code [4.4.2)]. The JAEA's design code contains a set of material property data for the IG-110 graphite, PGX graphite, and ASR-0RB carbon being used in the HTTR core. The specified minimum ultimate strength is determined from statistical treatment of strength data such that the survival probability is 99% at a confidence level of 95%, because the ultimate strength exhibits considerable statistical scatter. It is important to suppress the scatter of the data by product control to keep the reference strength in high.

As the environmental effect on the strength, both the increase of strength by neutron irradiation and the decrease of strength by oxidation are considered. On the other hand, the increases of strength by temperature and strain rate are not considered due to a conservative design view point.

The quality assurance of in-core components of the HTTR [4.4.3)] was carried out on the basis of the requirement from reactor design. Their quality has been controlled during production and after machining with respect to their properties and specifications. Fig. 4.4.4 shows the flow diagram of acceptance test program for the manufacturing process of IG-110 graphite in the HTTR [4.4.3, 4.4.4)]. In-service inspection program was determined for the core graphite components by using a TV camera and surveillance test specimens [4.4.5)].

(2) Irradiation effects on graphite

For the application of graphite materials to the in-core components, one of the important subjects is to take into account the neutron irradiation induced property changes. The fundamental mechanisms on the irradiation effects on graphite were widely studied. However, the material properties of graphite are dependent highly on their grades based on raw materials and forming process. Hence, the irradiation effects on the graphite are also dependent on their grades.

The properties, considering the irradiation effects, are the dimensional change, longitudinal elastic modulus, mean coefficient of thermal expansion, thermal conductivity, strength, and steady -state irradiation creep coefficient. In the design code for the HTTR, they are expressed in the graphical expressions of material property data as a function of fast neutron fluence about several irradiation temperatures. The design curves in the graphical expressions were determined based on the irradiation experimental results at the JMTR of JAEA, etc.

The irradiation induced dimensional change is a fundamental neutron irradiation effect. Fig. 4.4.5 [4.4.6)] shows the relative dimensional change of the IG-110 as a function of fast neutron fluence for several irradiation temperatures. The dimensional change depends on irradiation temperature. The curves in this figure are obtained by the interpolation and extrapolation of the experimental data with evaluation. At the first stage of the neutron irradiation, the bulk of the graphite shows shrinkage. Then neutron fluence is increased, the shrinkage is attained to the minimum point ‘turn-around’. Then, the dimensional change has turned out to increase. The turn-around point depends on the graphite grade and irradiation temperature.

(3) Standard for the graphite components of HTGR

For the design of the graphite components in the HTTR, the graphite structural design code for the HTTR [4.4.2)] and inspection standard of graphite for the HTTR [4.4.3)] were applied. For the commercial HTGR, a "special committee on research on preparation for codes for graphite components in HTGR" at Atomic Energy Society of Japan (AESJ) had established the draft of standard for graphite components in HTGR in March 2009 [4.4.7)]. For the establishment of the standard, the standards for the graphite components of HTTR and design code for graphite components in ASME were reviewed. The established standard is based on the HTTR graphite design code and the inspection standard of the graphite components for the HTTR, as shown in Fig. 4.4.6. The draft of standard for graphite core components in high temperature gas-cooled reactor" is composed of (1) general rules, (2) design standard, (3) material

and product standards, (4) in-service inspection and maintenance standard, and (5) appendix and explanation. As an appendix of the design standard, the graphical expressions of material property data of IG-110 graphite as a function of fast neutron fluence are expressed. The graphical expressions were determined through the interpolation and extrapolation of the irradiated data.

References

4.4.1) S. Saito, et al., “Design of high temperature engineering test reactor (HTTR)”, JAERI 1332 (1994), 247p.

4.4.2) HTTR Designing Laboratory, et al., “Graphite structural design code for the high temperature engineering test reactor”, JAERI-M 89-006 (1989), 37p (in Japanese).

4.4.3) J. Toyota, et al., “An Inspection standard of graphite for the High Temperature Engineering Test Reactor”, JAERI-M 91-102(1991), 61p (in Japanese).

4.4.4) M. Ishihara, et al., “Principle design and data of graphite components”, Nuclear Engineering and Design, 233, 1-3, pp.251-260(2004).

4.4.5) J. Sumita, et al., “Reactor internals design”, Nuclear Engineering and Design, 233, 1-3, pp.81-88(2004).

4.4.6) T. Shibata, et al., “Interpolation and extrapolation method to analyze irradiation-induced dimensional change data of graphite for design of core components in very high temperature reactor (VHTR)”, Journal of Nuclear Science and Technology, 47, 7, pp.591-598 (2010).

4.4.7) T. Shibata, et al., “Draft of Standard for Graphite Core Components in High Temperature Gas-cooled Reactor”, JAEA-Research 2009-042(2010), 119p.

Table 4.4.1 Typical thermomechanical properties of IG-110 graphite, PGX graphite and ASR-0RB carbon [4.4.1)]

	IG-110	PGX	ASR-0RB
Bulk density (Mg/m^3)	1.78	1.73	1.65
Mean tensile strength (MPa)*	25.3	8.1	6.8
Mean compressive strength (MPa)*	76.8	30.6	50.4
Young's modulus (GPa) ($\pm 1/3S_u$)**	7.9	6.5	8.7
Mean thermal expansion coefficient ($10^{-6}K$) (293～673K)	4.06	2.34	4.40
Thermal conductivity (W/m･K) (673K)	80	75	10
Ash (ppm)	Max. 100	Max. 7000	Max. 5000
Grain size (μm)	Mean 20	Max. 800	Max. 2000

* : at room temperature
** : Determined from the cord joining two points (one point is the one-third of the specified minimum tensile strength and the other is the one-third of the specified minimum compressive strength) on the stress-strain curve.

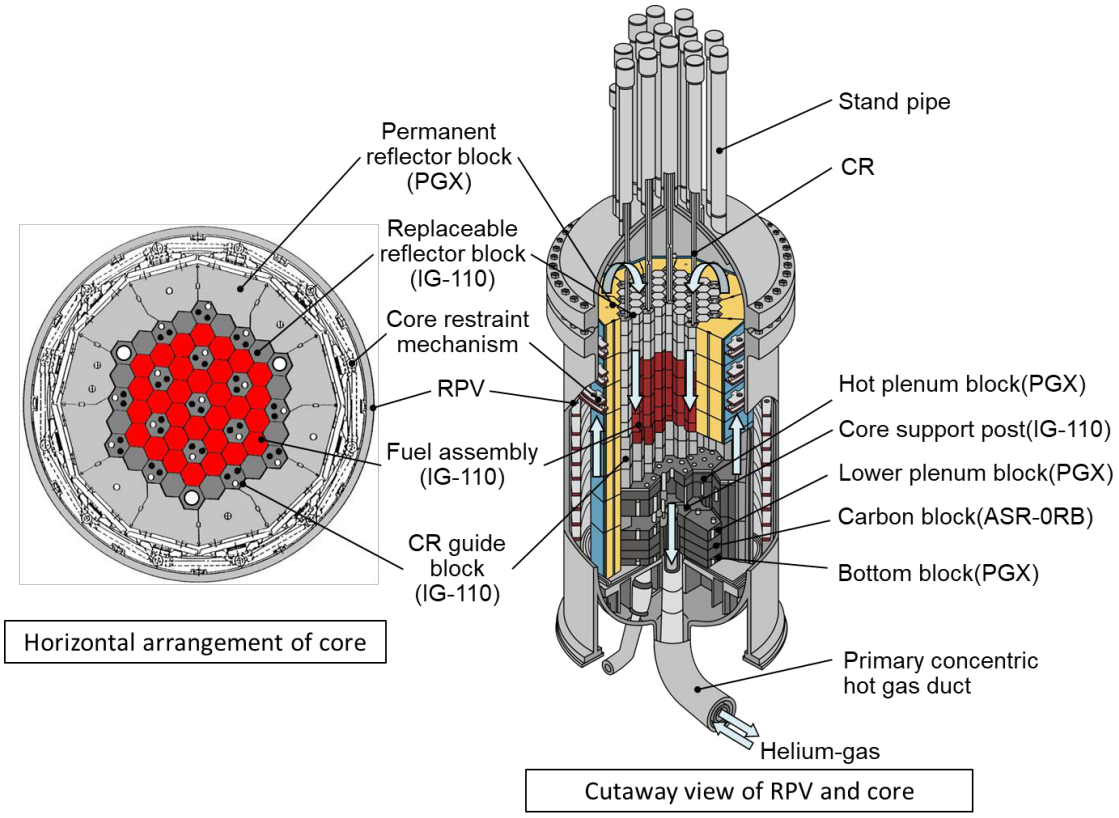

Fig. 4.4.1 The arrangement of graphite components in the HTTR [4.4.1)]

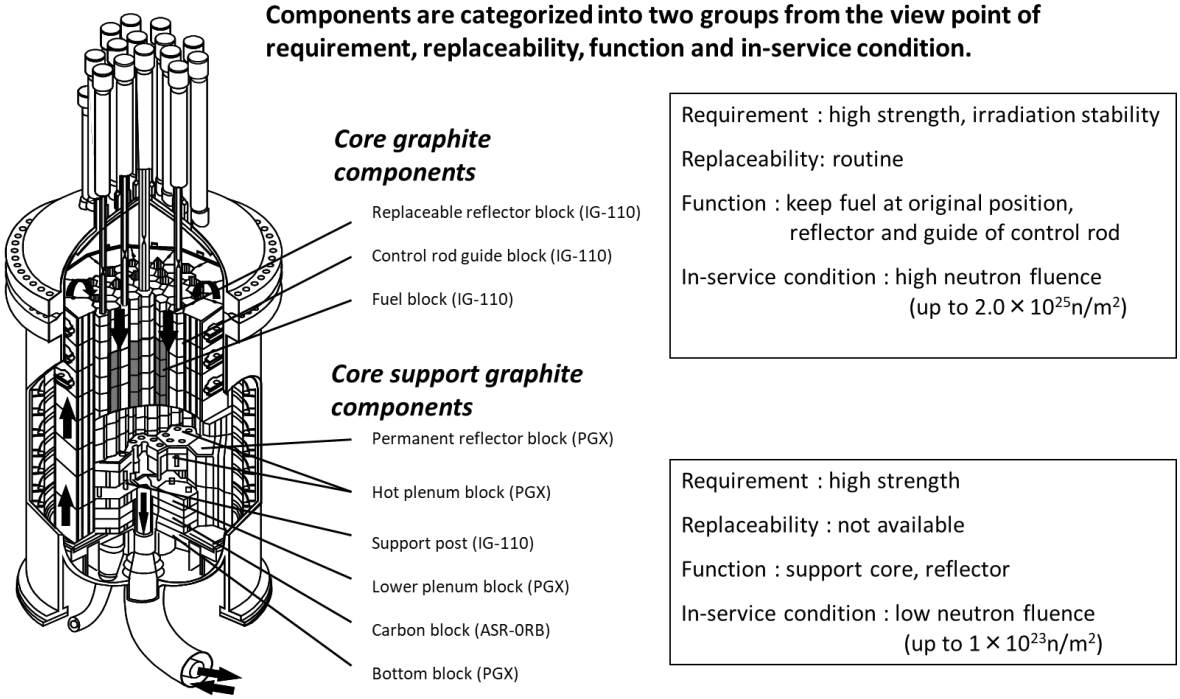

Fig. 4.4.2 Category of graphite components [4.4.2)]

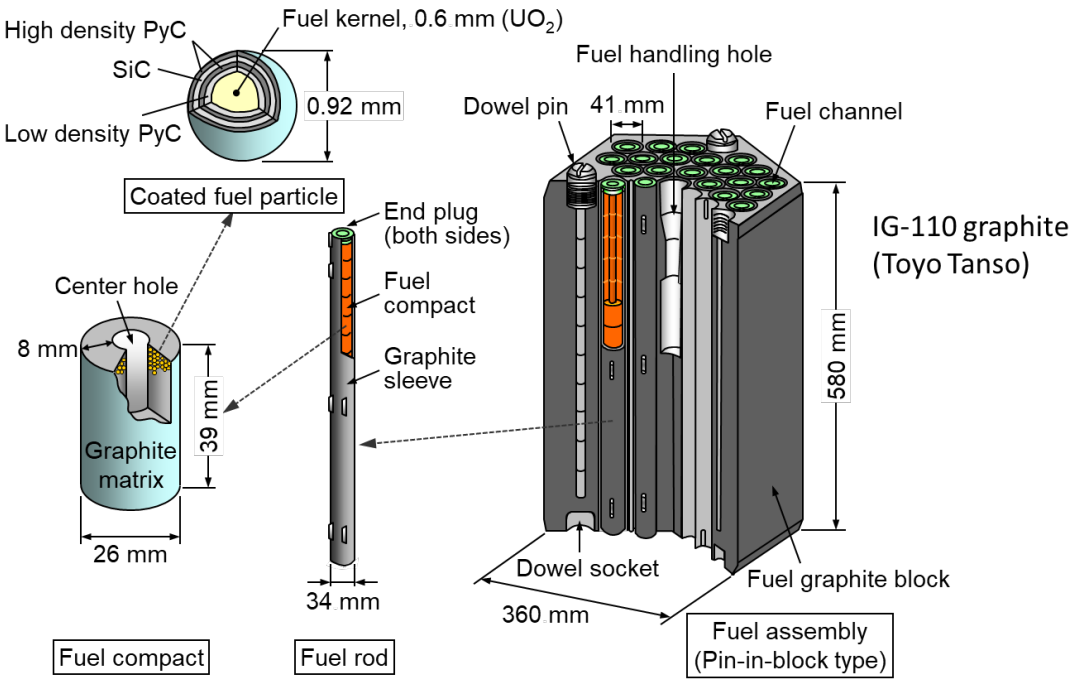

Fig.4.4.3 Fuel block of HTTR [4.4.1)]

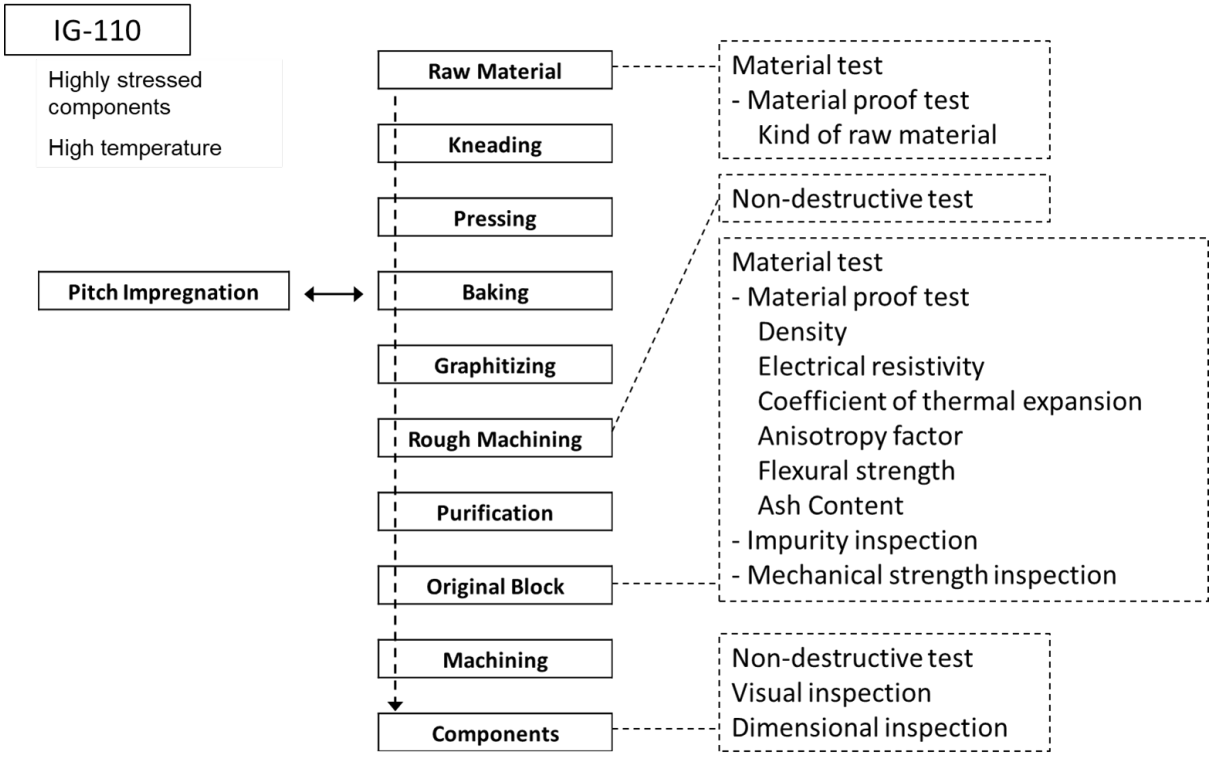

Fig. 4.4.4 Flow diagram of acceptance test program [4.4.3, 4.4.4)]

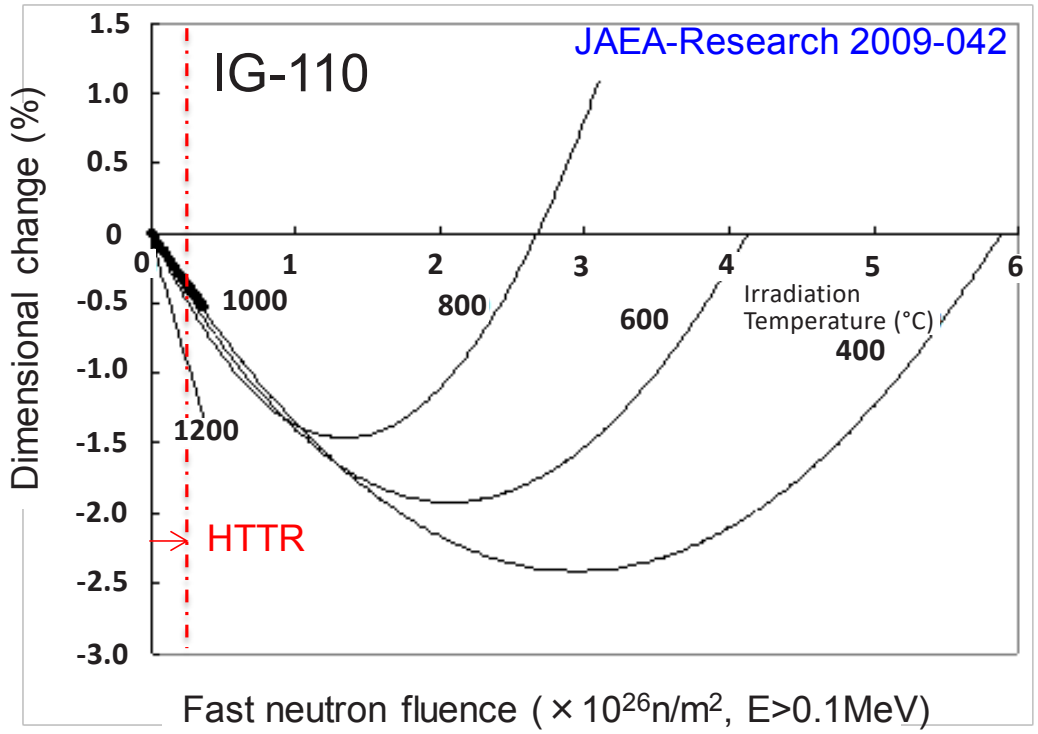

Fig. 4.4.5 Irradiation induced dimensional change of IG-110 graphite at high neutron fluence [4.4.6)]

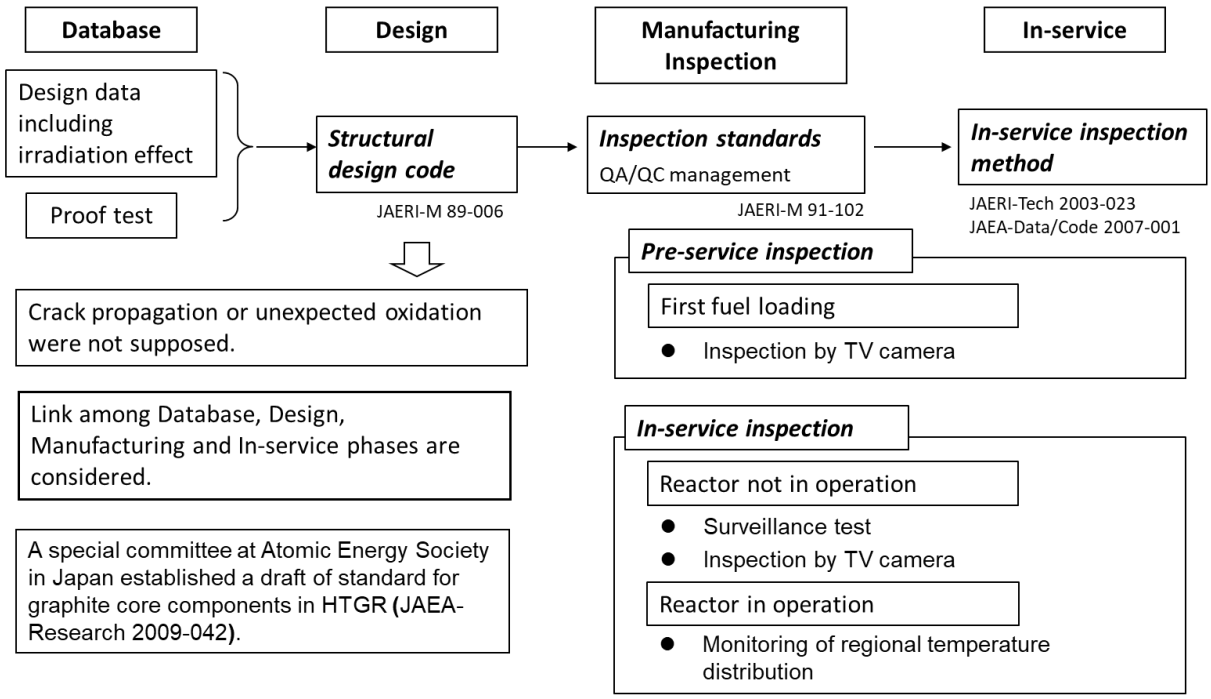

Fig. 4.4.6 Structure of standard for graphite components in HTGR [4.4.7)]

4.5 Heat exchanger

4.5.1 Introduction

An intermediate heat exchanger (IHX) is used to transfer nuclear heat to heat utilization system. Addition, an IHX acts as a part of the physical coupling between the reactor system and the heat utilization system. The coupling is required to.

- Prevent or mitigate transfer of fission products from the reactor primary system to the heat utilization system.
- Isolate or mitigate disturbance from the operation event or accident of the nuclear system to the heat utilization system and vice versa.

This chapter highlights several IHXs designed or constructed by JAEA.

4.5.2 The IHX for HTTR

In the HTTR, a 10 MWt (thermal) IHX is installed to transfer heat from the primary coolant to secondary system. Table 4.5.1 gives the main specifications. Figure 4.5.1 shows the IHX structure. The helical tube bundle contains six layers in the radial direction of heat transfer tubes. Each tube is about 30m long and has 8 welded joints. The tubes are fabricated of the high temperature heat resistance material Hastelloy XR developed from Hastelloy X by JAEA so as to improve the creep strength and corrosion resistance by optimizing its chemical composition[4.5.1)]. Moreover, a filler metal for tungsten inert gas (TIG) welding of Hastelloy XR was developed and a welding process corresponding to B which causes embrittlement phenomenon was investigated [4.5.2)]. And this Hastelloy XR tube is composed of helical type as mentioned above. This type is springy, and it absorbs the difference in thermal expansion[4.5.3)]. Each tube is fixed at both ends of the hot and cold headers and supported by six tube supporters in the tangential direction. The primary coolant flows on the shell side, and the secondary coolant flows in the tubes. The structure integrity of the IHX tubes for the vibration of tube bundles, friction by fluid is very important for the safety of the HTTR because they form the reactor coolant pressure boundary [4.5.4)]. Therefore an in-service inspection (ISI) of the tubes will be carried out with eddy current testing (ECT). The ECT probe is moved in the tubes by probe-inserting equipment (PIE) [4.5.5)].

Performance evaluation using HTTR is actually carried out for IHX with the reactor outlet coolant temperature of 850 °C or 950 °C. As a result, the exchanged heat was almost 10MW, which is 1/3 of the generated heat at the reactor and design value, and there was no difference between the heat transfer coefficient derived from the design formula and the experimental value. It was confirmed that the heat occurred in the reactor could be transported to the secondary system through IHX without problems [4.5.6-4.5.8)].

4.5.3 Commercial IHX designs for GTHTR300C

Several IHXs have been designed for use in the commercial reactor of GTHTR300C. The basic technologies developed on the HTTR IHX are applied. Major challenges of these commercial designs are scale up of the heat transfer capacity and extension of the life time to meet the design requirements for

the commercial reactor. The IHX design parameters are listed in Table 4.5.2.

4.5.3.1 170MWt vertical helical tube design

The structure of this design shown in Fig. 4.5.2 is essentially same as the HTTR IHX. The challenge is the increase of heat capacity and thus the size to many times that of HTTR. As self-weight of the heat transfer tube increases with the size, the primary stress increases and approaches to the stress limit of the tubing material, Hastelloy-XR, in the coolant operating temperature of 950°C. The conceptual structure of the vertical helical coil tube bundle, which has been developed with the construction of the HTTR IHX to suppress the primary stress due to the weight of the tube, has been applied to this commercial design. Furthermore, the primary stress in the tube connection to the high temperature header can be further reduced by changing the coil start position of the helical coil for each layer[4.5.9)] and by increasing tube outer diameter to 45.0 mm. As a result, a heat capacity of 170 MWt may be achieved in this design with a design life time of 20 years.

4.5.3.2 390MWt vertical helical tube design

This design as shown in Fig. 4.5.3 selects the finned heat transfer tubing, instead of smooth tubing, in order to further increase the unit heat transfer capacity[4.5.10)]. The additional design changes made from the structural concept of 170 MW IHX described earlier include:

(1) In the vicinity of the primary side inlet nozzle, a cylindrical baffle plate enclosing the heat transfer tube is provided to prevent the high temperature helium gas from directly hitting the heat transfer tube.
(2) A secondary side chamber communicating with the secondary side inlet nozzle was provided inside the top plate, and a donut shaped heat insulating tubes attached to the inner tube was installed in the outer tube.
(3) By changing the shape of the upper and lower plates from hemispherical shape to elliptical shape, the total length of the heat exchanger was reduced.

4.5.3.3 170MWt horizontal helical tube design

The main objective of the horizontal type is to extend the service life time to 40 years by further reducing the primary stress compared with the vertical design[4.5.11)]. By placing the tube bundle horizontally, the center pipe and associated header, which support and connect the tube bundle with high stress concentration in the vertical designs, are eliminated. Instead, the multiple tube headers are mounted peripherally on the outer shell, which lead to shortened tubing connection to the headers and thereby reduced primary stress in the tubes. The thermal expansion of the tube bundle is absorbed by the moving support of the tube bundle similar to the feature of the HTTR IHX. As a result, the length of the overall horizontal IHX is nearly halved from the vertical design of the same heat capacity. The 170MW IHX design in horizontal placement is shown in Fig. 4.5.4.

References

4.5.1) K. Watanabe, M. Shindo, et. al., “Evaluation on Materials Performance of Hastelloy Alloy XR for HTTR Uses-6 (Tensile and Creep Properties of Heat Exchanger Tube Base Materials and its Welded-Joints)”, JAERI-Research 97-009 (1997), 62p (in Japanese).

4.5.2) K. Watanabe, H. Nakajima, et. al., “Filler Metal Development for Hastelloy Alloy XR - Weldability and Properties of Weldment Used the Filler Metal for Thin Wall Structure-”, JAERI-M 91-181 (1991), 81p (in Japanese).

4.5.3) K. Hada, M. Oukubo and O. Baba, “Application of new design methodologies to very high-temperature metallic components of the HTTR”, Nuclear Engineering and Design, 132, 1, pp.13-21 (1991).

4.5.4) Y. Inagaki, K. Kunitomi, et. al., “R&D on high temperature components”, Nuclear Engineering and Design, 233, 1-3, pp.211-223 (2004).

4.5.5) Y. Tachibana, T. Nishihara, et.al., “Test Plan using the HTTR for Commercialization of GTHTR300C”, JAEA-Technology 2009-063 (2010), 155p.

4.5.6) S. Nakagawa, N. Fujimoto, et.al., “Rise-to-power Test in High Temperature Engineering Test Reactor -Test Progress and Summary of Test Rusults up to 30MW of Reactor Thermal Power-”, JAERI-Tech 2002-069 (2002), 87p (in Japanese).

4.5.7) K. Takamatsu, S. Nakagawa, et. al., “Rise-to-power Test in High Temperature Engineering Test Reactor in the High Temperature Test Operation Mode -Test Progress and Summary of Test Rusults up to 30MW of Reactor Thermal Power-”, JAERI-Tech 2004-063 (2004), 61p (in Japanese).

4.5.8) D. Tochio, S. Hamamoto, et. al., “Result of Long-term Operation of HTTR - High-temperature/Parallel-loaded 50-days Operation -”, JAEA-Technology 2010-038 (2010), 57p (in Japanese).

4.5.9) R. Katoh, T. Nishihara and K. Kunitomi, “Design of the Intermediate Heat Exchanger for the High Temperature Gas-cooled Reactor Hydrogen Cogeneration System, (I)”, Transactions of the Atomic Energy Society of Japan, 6, 2, pp.141-148 (2007) (in Japanese).

4.5.10) Xing L. Yan and R. Hino, “Nuclear Hydrogen Production Handbook”, Green Chemistry and Chemical Engineering (2011).

4.5.11) K. Tanaka, A. Terada, et. al., “HTTR-GT/H2 test plant - conceptual design study on new intermediate heat exchanger”, Proceedings of the 2016 International Topical Meeting on High Temperature Reactor Technology (HTR2016), HTR2016-18747, pp.419-425, November 6-10, 2016, Las Vegas, USA (2016).

Table 4.5.1 Main Specification of the IHX in HTTR

Type	Vertical helically-coiled counter flow	
Design pressure Outer shell Heat transfer tube	 4.7 MPa 0.29 MPa (differential pressure)	
Design temperature Outer shell Heat transfer tube	 430 ˚C 955 ˚C	
Operating condition	Rated operation	High temperature test operation
Flow rate of primary helium gas (max)	14.9 t/h	12.2 t/h
Inlet temperature of primary helium gas	850 ˚C	950 ˚C
Outlet temperature of primary helium gas	387 ˚C	389 ˚C
Flow rate of secondary helium gas (max)	12.8 t/h	10.8 t/h
Inlet temperature of secondary helium gas	244 ˚C	237 ˚C
Outlet temperature of secondary helium gas	782 ˚C	869 ˚C
Heat capacity	10 MW	
Heat transfer tube Number Outer diameter Thickness Length	 96 31.8 mm 3.5 mm 30 m	
Outer diameter of shell Total height	1.9 m 10 m	
Material Outer and inner shell Heat transfer tube Hot header and center pipe	 SCMV4-2NT (2.25Cr-1Mo steel) Hastelloy XR Hastelloy XR	

Table 4.5.2 IHX design parameters

Item			HTTR IHX	GTHTR300C IHXs		
Heat exchange rate			10 MWt	170 MWt	390 MWt	170 MWt
Design features			Vertical helical tube bundle w/ smooth tubes	Vertical helical tube bundle w/ smooth tubes	Vertical helical tube bundle w/ finned tubes	Horizontal helical tube bundle w/ smooth tubes
Tube out diameter/thickness		mm	31.8/3.5	45.0/5.0	31.8/4.0 (1.5 fin high)	45.0/5.0
Heat transfer area		m^2	215	144.7	3653	144.7
Shell side	Flow rate	kg/h	12240	1165680	1170360	1167000
	Inlet temperature	°C	950	950	950	950
	Outlet temperature	°C	389	850	719	850
	Pressure	MPa	4.06	5.00	4.98	5.00
	Pressure loss	kPa	4	31	30	Less than 50
Tube side	Flow rate	kg/h	10800	291600	636120	289000
	Inlet temperature	°C	237	500	475	491
	Outlet temperature	°C	869	900	900	900
	Pressure	MPa	4.21	5.15	5.13	5.15
	Pressure loss	kPa	45	58	70	Less than 60
Weight	Main tube bundle	t	5	50	125	50
	Hastelloy XR used	t	3	167	860	105
Life time		y	20	20	20	40

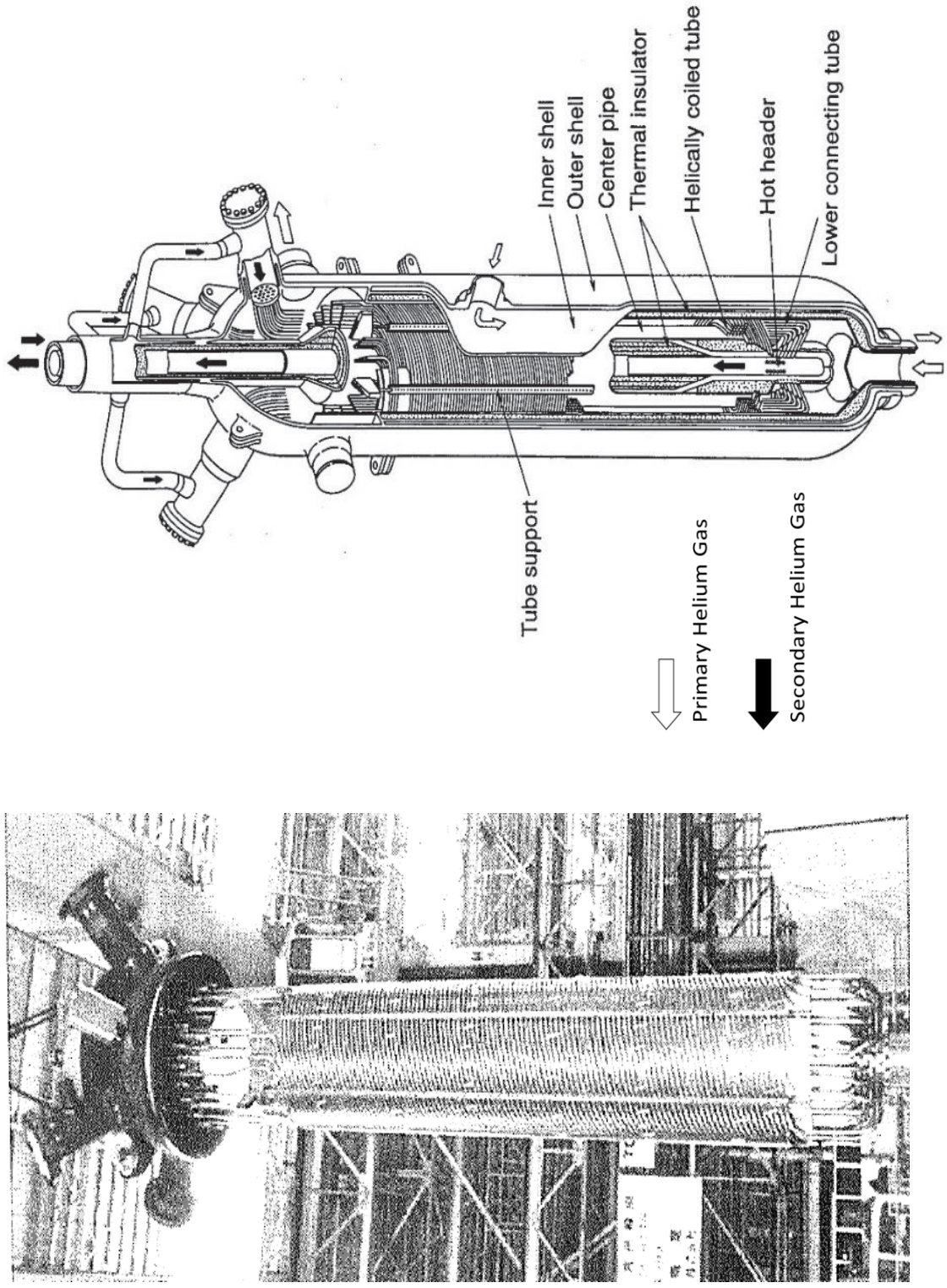

Fig. 4.5.1 10MWt Helical tube IHX installed and tested in the HTTR reactor

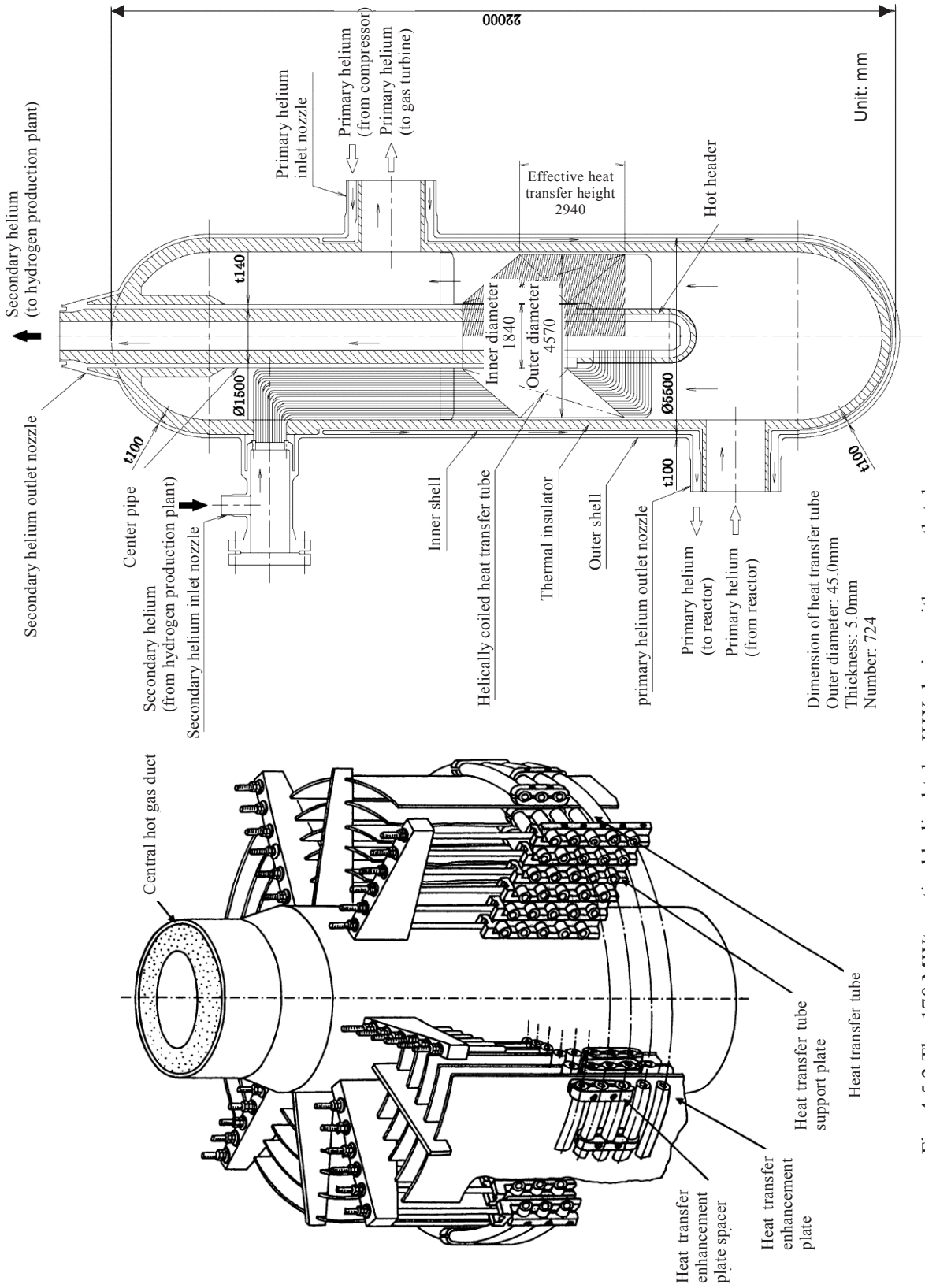

Fig. 4.5.2 The 170 MWt vertical helical tube IHX design with smooth tubes

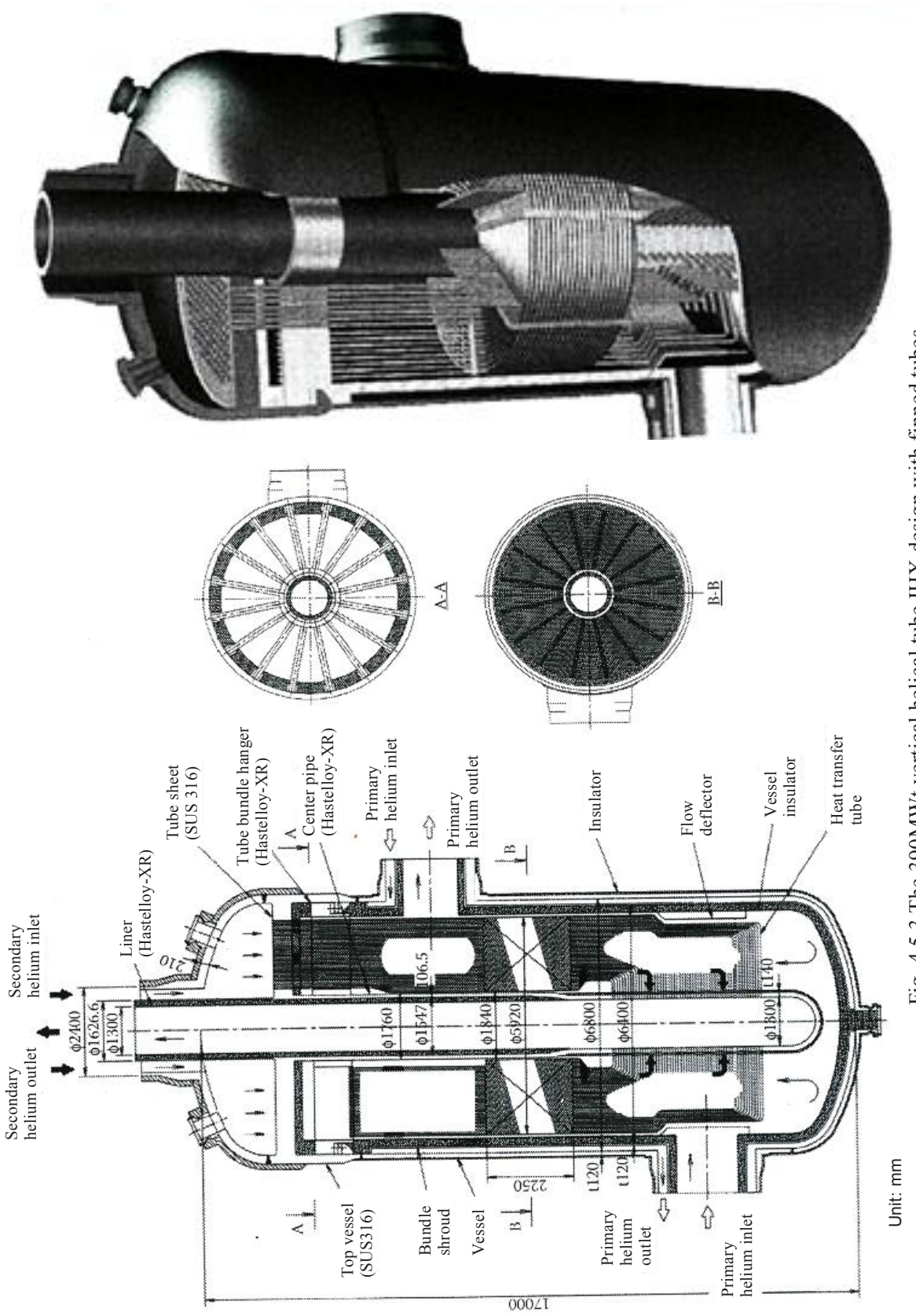

Fig. 4.5.3 The 390MWt vertical helical tube IHX design with finned tubes

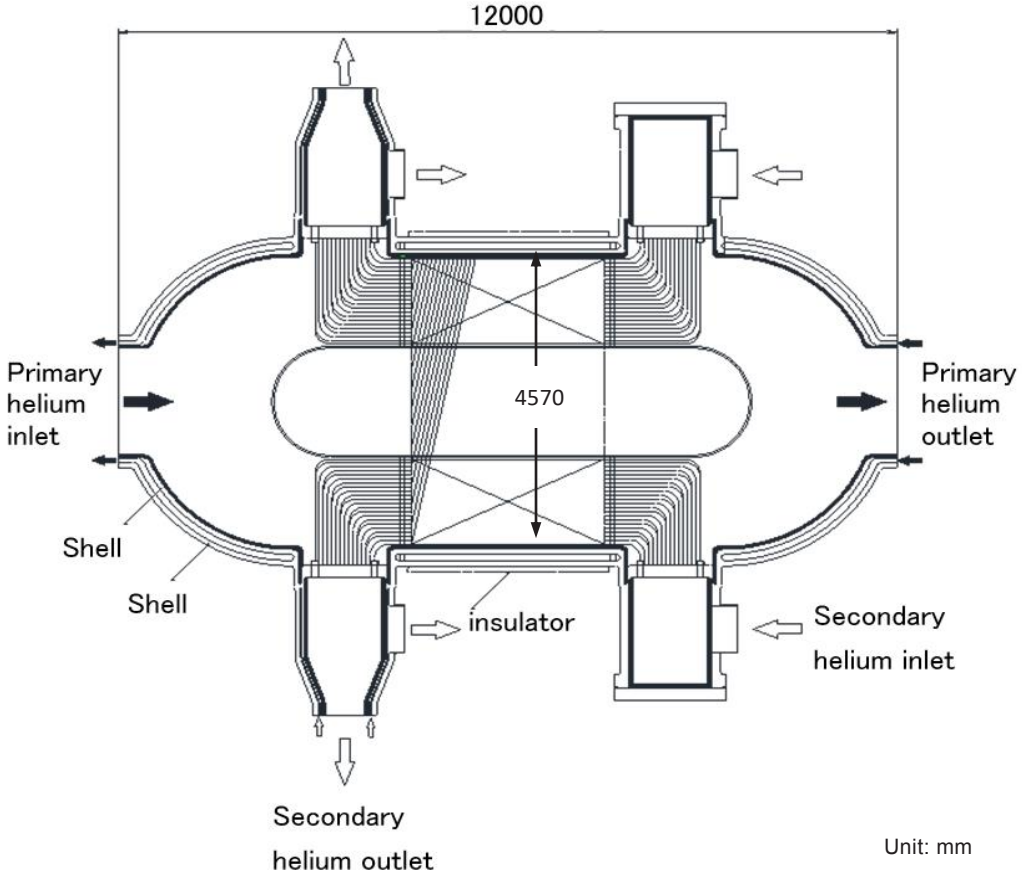

Fig .4.5.4 The 170MWt IHX horizontal helical tube IHX design with smooth tubes

4.6 High Temperature Resistant Alloy

4.6.1 Development of Hastelloy XR

In 1970s, material selection tests of heat-resistant alloys for the High-Temperature Gas-cooled Reactor (HTGR) were performed as shown in Fig.4.6.1 mainly on long-term corrosion resistance in impure HTGR helium environment. Taking into account also service conditions of the intermediate heat exchanger (IHX) of the HTGR, a nickel-base Cr-Mo-Fe superalloy Hastelloy X, which has excellent accumulated experiences in jet engines, was selected for the heat transfer tubes and the hot header in the IHX. Since Hastelloy X does not have sufficient compatibility with the primary helium coolant at very high temperatures, Hastelloy XR was developed from Hastelloy X to improve the compatibility.

It was found that for Hastelloy X, tightening the contents of some elements even within the specification of the chemical compositions results in remarkable improvements in the compatibility. The following modification items (1) and (2) were made on Hastelloy X to improve the compatibility and further modification items (3) and (4) were given to improve applicability to the HTGR.

(1) Optimizing manganese and silicon contents

Formation of stable and adherent oxidation films of $MnCr_2O_4$ spinel and SiO_2 is essential for the very high temperature components. Such an oxidation film is formed on the base metal through optimizing the Mn and Si contents for Hastelloy X.

(2) Lowering aluminum and titanium contents

Internal oxidation and intergranular attack are suppressed through lowering the A1 and Ti contents.

(3) Lowering cobalt content

Radioactive contamination in the primary cooling system by Co-containing corrosion products decreases to negligible levels through lowering the Co content.

(4) Optimizing boron content

Addition of boron improves the creep strength for Hastelloy XR, but causes contamination of the core and degradation in weldability. Optimization of the B content, therefore, is needed for a specific purpose. To a Tungsten-arc Inert-gas (TIG) welding wire, addition of boron within 40-60 ppm was made to improve the creep strength of the welded joints.

JAEA in cooperation with Mitsubishi Materials Group developed Hastelloy XR with the modifications (1) to (3) above by 1976. Then, various tests were conducted on Hastelloy XR to construct engineering database for design of the HTGR. In addition, quality of Hastelloy XR including creep strength was improved with the modification (4) above by 1984. Based on the engineering database of Hastelloy XR, JAEA developed high temperature structural design guideline including design allowable limits on Hastelloy XR by 1990.

The specification of the improved version of Hastelloy X which is called the nuclear grade alloy

Hastelloy XR is shown in Table 4.6.1, with a comparison to that of Hastelloy X. Hastelloy XR with optimization of boron content is called Hastelloy XR-II, when it is necessary to distinguish Hastelloy XR-II from Hastelloy XR. Heat transfer tubes, hot header, etc. of the intermediate heat exchanger of the High Temperature Engineering Test Reactor (HTTR) is made of Hastelloy XR-II.

Figure 4.6.2 shows results of long-term corrosion tests under severe thermal cycles, wherein superiority of Hastelloy XR to Hastelloy X is demonstrated as expected from the protective oxide film formed on Hastelloy XR.

4.6.2 High Temperature Structural Design Guideline [4.6.1)]

The primary cooling system components and related components that serve as the reactor coolant pressure boundaries of the HTTR are used at high temperatures in creep regime. In particular, the heat transfer tubes and hot header of the intermediate heat exchanger (IHX) are subjected to temperatures above 900°C. The reactor pressure vessel as well as the metallic core support structures are exposed to the reactor coolant at temperatures of around 400°C under an irradiation condition. High temperature structural materials are chosen for the high temperature components of the HTTR, taking into careful considerations the service conditions and safety functions of the components. The material used are as follows:

- A nickel-base corrosion and heat resistant superalloy Hastelloy XR,
- A normalized and tempered (NT) 2 1/4Cr-1Mo steel,
- Two types of austenitic stainless steel, SUS321TB and SUS316, and
- 1Cr-0.5Mo-V steel, an alloy steel bolting material for high temperature service.

Components and their service conditions are listed up for these structural materials in Table 4.6.2.

Some of the high temperature materials and their service temperatures are beyond the well-established high temperature structural design codes such as the Elevated Temperature Structural Design Guide for the Prototype Fast Breeder Reactor “Monju” (abbreviated as FBR Code) and the ASME Boiler and Pressure Vessel Code Case N-47[4.6.2)]. Accordingly, development of a new high temperature structural design guideline was necessary for these materials at their service temperatures. Moreover, at the very high temperatures, where creep deformation is significant, component design based on elastic analysis is not possible.

Thus, extensive R&D was carried out not only in JAEA but also in national and private research organizations in Japan to establish a reliable high temperature structural design guideline.

A high temperature structural design guideline provides design limits and rules for guarding high temperature components against failure modes. Development of a new high temperature structural design guideline, therefore, requires

1) Identification of failure modes under exposure to service environments within the guideline application temperature range for each material and
2) Development of design limits and rules for guarding against each failure mode with appropriate safety margins.

From reviewing material test results and information on failures at commercial plants and experimental facilities, the following failure modes were identified for the five structural materials used for the HTTR.

a) Ductile rupture by short-term loading
b) Creep rupture by long-term loading
c) Buckling by short-term loading
d) Creep buckling by long-term loading
e) Creep fatigue failure
f) Gross distortion by incremental collapse and ratcheting
g) Loss of function by excessive deformation.

These failure modes are the same as those considered in well-established high temperature structural design codes. It should be noted here that the long-term loading means loading at high temperatures that develops significant creep effect over a long period.

The fact that the failure modes for the new materials are the same as for those of the well-established codes suggests the possibility that fundamental philosophies on design limits and rules of the well-established codes can be applicable to the new materials. Among the well-established high temperature structural design codes, the FBR Code was the only one that had been authorized by the Japanese government, and so it was the most appropriate for discussion on applicability to new materials. We came to the conclusion that design limits and rules for the abovementioned seven failure modes and for the five materials can be developed on the basis of the fundamental philosophies of the FBR Code.

On this conclusion, the detailed design limits and rules were developed for each material, based on experimental data on material properties and structural mechanics behavior under multi-axial stress states, referring to those of the FBR Code.

The maximum metal temperature of Hastelloy XR in the HTTR reaches about 900°C even during the normal operation and is likely to exceed 950°C but less than 1000°C in events such as a loss of secondary cooling.

Taking into account the service temperature conditions, material tests and structural mechanics tests for both base metals and TIG-weld joints were conducted at temperatures ranging from room temperature to 1050°C, mainly in JAEA but also in the National Research Institute for Metals (National Institute for Materials Science (NIMS) at present) and research laboratories of private nuclear power companies. Test conditions of major material property tests for the base metals are briefly listed in Table 4.6.3. Test specimens were taken from product forms of tubes, plates, forging cylinders and bars simulating application to the HTTR high temperature components.

References

4.6.1) Y. Tachibana and T. Iyoku, “Structural Design of High Temperature Metallic Components,” Nuclear Engineering and Design, 233, 1-3, pp.261-272 (2004).

4.6.2) The American Society of Mechanical Engineers, The ASME Boiler and Pressure Vessel Code Case N-47-23 Class 1 Components in Elevated Temperature Service Section III Division I, ASME, New York (1986).

Table 4.6.1 Specifications for chemical composition of Hastelloy XR and X

Material	Chemical Compositions (wt%)															
	Range	Elements														
		C	Mn	Si	P	S	Cr	Co	Mo	W	Fe	Ni	B	Al	Ti	Cu
Hastelloy XR	max.	0.15	1.00	0.50	0.040	0.030	23.00	2.50	10.00	1.00	20.00	Rem	0.010	0.05	0.03	0.50
	min.	0.05	0.75	0.25	-	-	20.50	-	8.00	0.20	17.00	Rem	-	-	-	-
Hastelloy X	max.	0.15	1.00	1.00	0.040	0.030	23.00	2.50	10.00	1.00	20.00	Rem	0.010	0.50	0.15	0.50
	min.	0.05	-	-	-	-	20.50	0.50	8.00	0.20	17.00	Rem	-	-	-	-

Table 4.6.2 Materials and service conditions of HTTR high temperature components

Material		Components	Service conditions		Maximum allowable temperature
Material	Product form		Design temperature	Design pressure*	
2 1/4Cr-1Mo steel	Plate, forging, pipe	Reactor pressure vessel	440℃	4.8 MPa	550℃
		Shells of intermediate heat exchanger, primary pressurized water cooler, etc.	430℃	4.8 MPa	
		Outside pipe of concentric double pipe	430℃	4.8 MPa	
Hastelloy XR	Tube, plate, forging	Intermediate heat exchanger heat transfer tubes	955℃	0.29MPa	1000℃
		Intermediate heat exchanger hot header	940℃	0.29MPa	
SUS321	Tube	Primary pressurized water cooler heat transfer tubes	380℃	4.8 MPa	650℃
SUS316	Bar	Core restraint mechanism	450℃	-	650℃
1Cr-0.5Mo-V steel	Forging	Core restraint mechanism	450℃	-	450℃

***: absolute pressure**
Note: Control rod sleeves are made of Alloy 800H, whose maximum allowable temperature at a scram is 900℃.

Table 4.6.3 Mechanical properties data on Hastelloy XR obtained for high temperature structural design

Test item	Test conditions
Tensile tests	Temperatures : RT to 1000 °C, every 25 °C Strain rates : 0.3 %/min to 100 %/min
Creep tests	Temperatures : 500 to 1050 °C, every 50 °C Maximum test time : about 38,000 hours Total number of tests : about 300
Fatigue and creep-fatigue interaction tests	Temperatures : RT to 1000 °C, every 50 °C at high temperatures Strain rates : 2×10^{-5} to 1×10^{-3} /s Hold times : 0 to 1 hour Materials : as-received and thermally aged
Fracture toughness tests	Thermal aging conditions Temperatures : 800 to 1000 °C Maximum aging time : 2,000 hours Test items : V-notch charpy, fracture toughness and fatigue crack propagation rate
Corrosion tests	Environment : HTTR coolant gas-simulated helium Temperatures : 900 to 1000 °C Maximum test time : 30,000 hours
Others	Poisson's ratio, thermal expansion, etc.

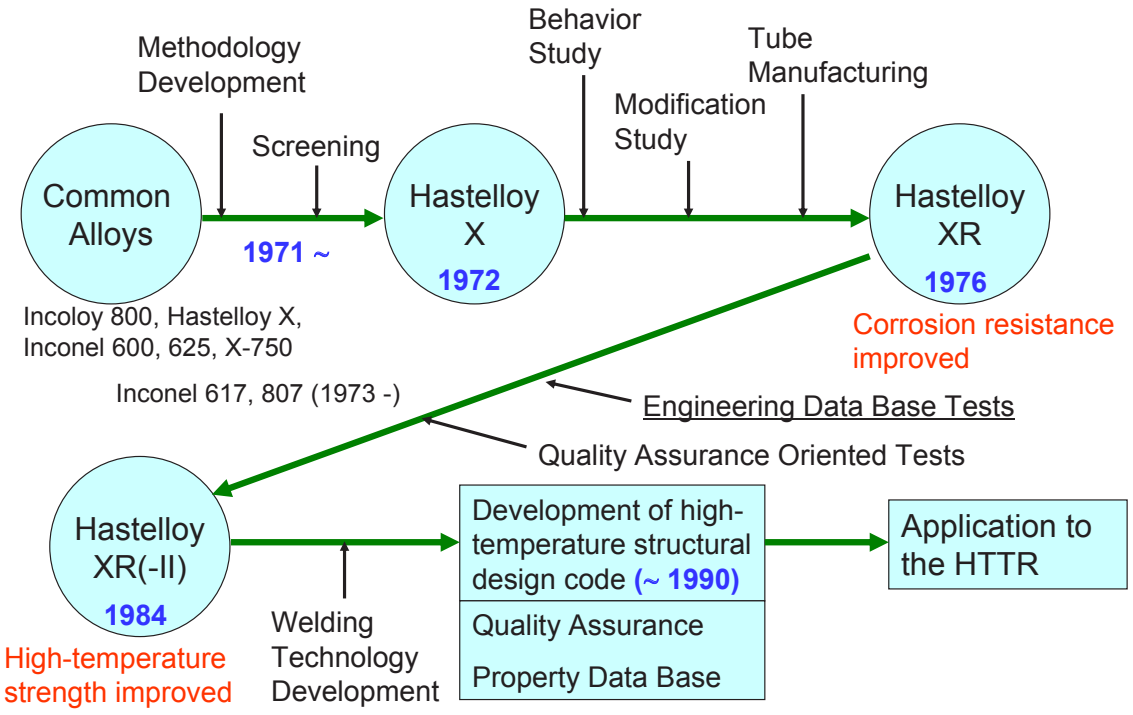

Fig. 4.6.1 Development of Hastelloy XR

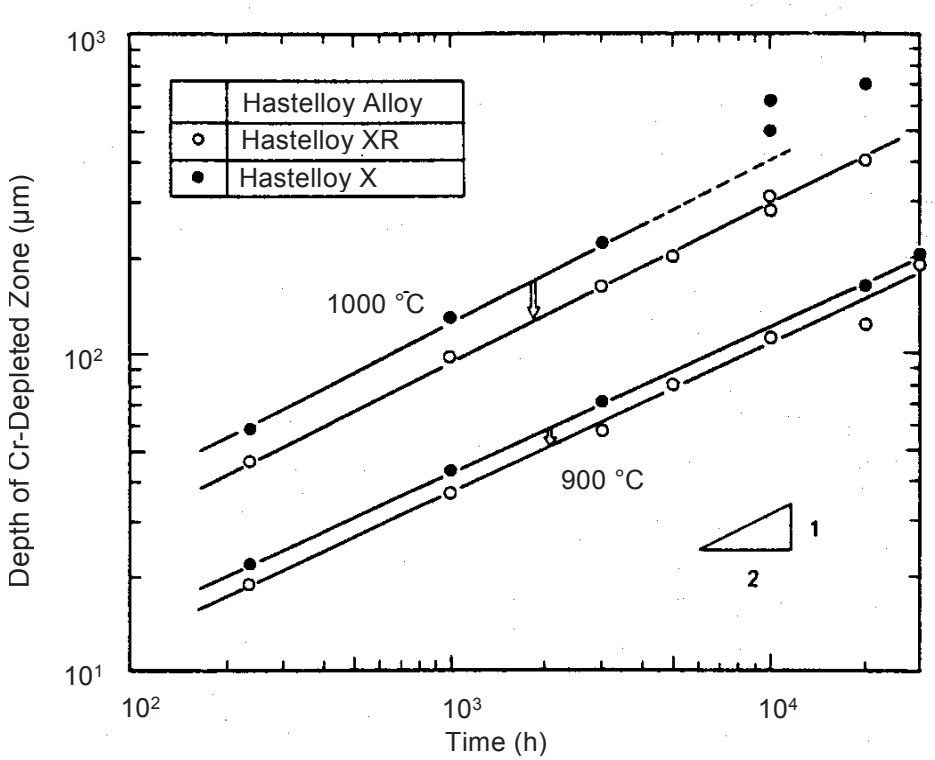

Fig. 4.6.2 Comparison of environmental effect in Cr-depleted zone depth between Hastelloy XR and Hastelloy X

4.7 Experience of HTTR Licensing

4.7.1 Outline

The HTTR has been designed to establish and upgrade the technological basis for advanced HTGRs. In February 1989, the Japan Atomic Energy Research Institute (JAERI), former name of JAEA, submitted the application for HTTR installation permit to the Prime Minister of Japan. In November 1990, the safety review was terminated by the Nuclear Safety Commission (NSC) which was the regulatory authority of the time and the Prime Minister issued the installation permit of the HTTR to JAERI. Up to now, the significant experimental data to validate the safety design of the HTTR have been accumulated through the following tests:

- Long term operation of 30 days at 850 °C
- Long term operation of 50 days at 950 °C
- Safety demonstration tests
    - Reactivity insertion test by control rod withdrawal
    - Coolant flow reduction test by tripping of gas circulators
    - Loss of forced cooling test

In this section, the outline of original safety design of the HTTR is described. After the 2011 off the Pacific coast of Tohoku Earthquake, Nuclear Regulatory Authority (NRA) established a more stringent new regulation standard. The safety review for the HTTR to confirm the conformity to the new regulation standard is undergoing. The explanation to NRA concerning the conformity of HTTR is almost completed and the HTTR is expected to pass the safety review without any additional hardware measures. As of 1st December 2017, about 60 review meetings on conformity to the new regulatory requirements of NRA were held and JAEA successfully deal with the request from those meetings

As mentioned above, the JAEA has many experiences and know-how concerning the HTGR licensing.

4.7.2 Basic safety design philosophy [4.7.1)]

Fig. 4.7.1 shows a logical flow to establish the basic safety design philosophy of the HTTR. The Top Level Regulatory Criteria for the HTTR is identical to that of the LWR. Table 4.7.1 provides the summary of the Top Level Regulatory Criteria for both the HTTR and LWRs in Japan. In addition, according to the International Commission on Radiological Protection (ICRP) recommendation [4.7.2)], the principle of ALARA (as low as reasonably achievable) was applied to reduce the radiation dose to plant personnel and members of the public around the HTTR as low as reasonably achievable. To meet the Top Level Criteria and apply the principle of ALARA, the basic safety design philosophy of the HTTR was determined based on that of the LWR stipulated in “Guidelines for Safety Design of LWR Power Plant” considering inherent safety characteristics of the HTGR. In order to ensure safety, the well-known fundamental safety functions such as control of reactivity, removal of heat from the core and confinement of radioactive materials shall be performed in normal and off-normal states. The strategy of the defense-in-depth [4.7.3)] that provides a series of level of defense is implemented to ensure that the fundamental safety functions shall be reliably achieved in normal and off-normal states. The level of the defense in depth

consists of prevention of off-normal events, control of off-normal events and mitigation of off-normal events. The newly considered premise to establish the basic safety design philosophy of the HTTR is that it considers an air ingress accident and following oxidation of the core. The HTTR safety design shall prevent the excessive oxidation of the core and fission products release to the environment.

4.7.3 Fundamental safety functions unique to HTTR [4.7.1)]

(1) Control of reactivity

The reactor is shut down safely and reliably from any operational state using the control rod system. Furthermore, the reserve shutdown system is provided, which is composed of boron-carbide/graphite (B_4C/C) pellets. The power control and normal reactor shutdown of the HTTR are achieved with 16 pairs of control rods. The control rod system can achieve subcriticality from any operation state and maintain subcriticality in the cold core conditions even when a pair of control rods stick at the operational position.

In the case of a scram during normal operation, nine pairs of control rods in the replaceable reflector region are inserted at first, and the rest of control rods are inserted after the core is cooled down to prevent exposure of the control rod cladding in a high-temperature environment of above 900 °C. The core temperature is determined by monitoring the outlet helium gas temperature. A pair of control rods are driven by the one drive mechanism. The control rods are released from the drive mechanism and inserted by gravity when the reactor is scrammed.

(2) Removal of heat from the core

The main cooling system removes residual heat from the core during a normal reactor shutdown. In addition to the main cooling system, the HTTR has two other residual heat-removal systems. The auxiliary cooling system is used for off-normal transients that coolant flow boundary is intact and a vessel cooling system is used for accidents that forced circulation of the coolant cannot be maintained.

The auxiliary cooling system automatically starts up when the reactor is scrammed in an anticipated operational occurrence and accident in which forced cooling is available, while the main cooling system is stopped. The auxiliary cooling system is classified as a safety system. It consists of two helium gas circulators, the auxiliary water cooler and an affiliated water-cooling system. In terms of the core coolablity, the residual heat can be removed by the vessel cooling system without using the auxiliary cooling system. However, it is needed from the viewpoint of operational flexibility because it takes a very long time to cool down the core without the auxiliary cooling system.

The vessel cooling system is used as a residual heat-removal system when the forced circulation in the primary cooling circuit is no longer available due to a rupture of the inner pipe or both internal and external pipes in the coaxial double primary pipes. The vessel cooling system is also a safety system equipped with two completely independent systems, which are backed up with an emergency power supply. It is operated even during normal operation to cool the reactor shielding concrete wall.

(3) Confinement of fission product release

The HTTR has multiple barriers to prevent fission product release into the environment, fuel coatings, the reactor pressure boundary, the containment vessel and the reactor building. The ceramic layers surrounding the fuel kernel act as the primary barrier for the fission product release. The integrity of these ceramic layers is sufficiently kept under 1600°C based on several experiments. JAERI carried out the irradiation test and post irradiation tests up to 33,000 MWd/t before the HTTR operation and continues to carry out irradiation tests for the HTTR initial loading fuel up to 70,000 MWd/t. So far, the heating up tests after the irradiation proved that the integrity of the fuel can be sufficiently maintained under 1600°C. It also showed that the fuel failure rate in the range from 1600°C to 1800 °C is negligibly small.

This is the major specific feature of the HTTR as well as the other HTGRs in the world. While most of the HTGRs constructed or being designed in the world do not have a containment vessel, the HTTR has a containment vessel made of steel. Its functions are to contain fission products and to limit the amount of air ingress into the core. The containment vessel is installed in the reactor building, which acts as the confinement. The confinement is maintained at a slightly negative pressure to the environment by a ventilation and air conditioning system during both normal and off-normal states.

The off-site radiation dose limit in such accident as depressurization accident is remarkably reduced by the containment vessel together with the confinement.

4.7.4 Seismic technologies especially for graphite components

This section summarizes “Vibration tests data for verification of seismic analysis code” [4.7.4)]. Aseismic studies have been performed to clarify the vibration characteristics and assess the structural integrity of the core components and the core bottom structure. These studies have been done independently through experimental and analytical methods. The coupling effects of the core components on the vibration characteristics of the core bottom structure, and vice versa are also investigated.

(1) Vibration characteristics of core components

A core seismic computer code is required for determination of the overall core response and the displacement characteristics of the core and to calculate design loads for the core components. A comprehensive research and development program was undertaken to develop a means to analyze the block-type core for aseismic design. However, no general-purpose codes met the above requirements. This was due to a number of limitations, especially the inability to efficiently treat impacts and highly nonlinear characteristics in large numbers. We, therefore, developed the SONATINA- 2V code [4.7.5)]. This code is used to predict the impact phenomena between graphite blocks and to provide information on impact forces, displacements, etc. that is required for the safety evaluation of the structural integrity of the core. To evaluate the validity of the SONATINA-2V code and to confirm the structural integrity of the core graphite blocks, many kinds of seismic tests were conducted.

(2) Validation of SONATINA-2V code

The impact of the graphite block, particularly the dowel and socket system, and the displacement of blocks were the most important items from the viewpoint of the core seismic design. Therefore, the code was verified in terms of these response values [4.7.6]. Fig. 4.7.2 shows the typical overall core response characteristics at 2.5 m/s^2. The analytical results were in good agreement with the test. Since the SONATINA-2V code is applied to a two-dimensional analytical model, it is necessary to confirm that the code can predict the seismic response of the three-dimensional full core. Fig. 4.7.3 presents the relative displacements of the core graphite blocks as a function of excitation frequency at 1.0 m/s^2, comparing the test results using the full-scale seven-column model with the analytical ones. In a low-frequency range, where the first vibration mode of the column is dominant, the columns vibrate together. When the frequency exceeds the resonance frequency, the columns exhibit different response modes where the relative displacement response is small. As the code models a two-dimensional vertical slice core (three degrees of freedom), the equivalent column stiffness becomes harder than that of a three-dimensional core (six degrees of freedom). As a result, the calculated frequency response shifts to a slightly higher frequency region in comparison with the experimental result. It can be, thus, seen that the analytical results showed good agreement with the test.

4.7.5 Acceptance criteria[4.7.1)]

Acceptance criteria for the HTTR are established fundamentally reflecting the safety requirements for LWR power plants and taking into account major features of HTGRs and the HTTR. Acceptance criteria for the anticipated operational occurrences and the accidents for the HTTR and LWRs are shown in Table 4.7.2. The maximum fuel temperature is restricted to 1600°C to avoid fuel failure during the anticipated operational occurrences. Criteria for the temperature and the pressure of the primary pressure boundary and the containment vessel are determined considering following items.

(a) Materials composing the pressure boundary and the containment vessel shall have stable strength, and their temperature range during the normal operation and abnormal condition is within the temperature range determined by the design code [4.7.7).]

(b) Materials such as 2.25Cr–1Mo and Hastelloy XR have sufficient strength below the temperature of 550°C and 1000°C, respectively.

However, the margin in their creep rupture strength decreases over 500°C for 2.25Cr–1Mo and 980°C for Hastelloy XR. The temperature limits of their materials in anticipated operational occurrences are determined to 500°C and 980°C, respectively, so that the reactor components can be re-used without any repair after an anticipated operational occurrence occurs. In the case of accidents, the core shall not be seriously damaged and shall maintain its geometry for sufficient coolability; i.e.,

(a) Fuels shall be maintained in the graphite fuel block or sleeve

(b) Structural integrity of the graphite support structures such as support posts shall prevent the core from collapsing so as to maintain subcriticality.

The radiation exposure is limited to 5 mSv as effective dose equivalent outside the site boundary of

the HTTR. For the evaluation of the radiation exposure, external gamma-ray exposure from the radioactive cloud containing noble gases and iodine, internal exposure by inhalation from the radioactive cloud, direct external gamma-ray exposure and external skyshine gamma-ray exposure from fission products such as Cesium contained in the containment vessel are considered. The total radiation exposure, which is the sum of these exposures shall be lower than the limit of 5 mSv. Based on ICRP, in special case, 5 mSv of annual radiation exposure for the public is acceptable, though a limit of 1 mSv is recommended. For accidents, which have small frequencies of those occurrences, the value of 5 mSv is applied to judge the significant risk of radiation exposure for the public. The nearest site boundary from the HTTR facility is about 200m and the site is about 5 km far from the center of Oarai town having about 20,000 inhabitants.

4.7.6 Selection of events [4.7.1)]

Abnormal events to be postulated as anticipated operational occurrences and accidents have been selected considering their frequencies of occurrence and based on the investigation of main causes which affect each item of the acceptance criteria identified for the HTTR; that is,

(a) fuel temperature
(b) core damage
(c) temperature of reactor coolant pressure boundary
(d) pressure at reactor coolant pressure boundary
(e) pressure at containment vessel boundary
(f) risk of radiation exposure for the public

The initiating abnormal events have been classified into similar event groups according to “Examination Guide for Safety Evaluation of Light Water Nuclear Power Reactor Facilities”. Then, the most severe events with respect to the acceptance criteria within each similar event group are selected as the representative postulated events. Examples of the selection of anticipated operational occurrences and accidents are shown in Figs. 4.7.4 and 4.7.5. The main causes that affect the fuel temperature are increase of power and decrease of heat removal in the core. The increase of power is caused by reactivity addition, in which four event groups are postulated.

- malfunction of the reactivity control system
- malfunction of the experimental facility
- increase of the primary coolant flow
- increase of heat removal by the secondary cooling system

Two initiating events are considered as the malfunction of the reactivity control system.

(i) abnormal control rod withdrawal
(ii) abnormal control rod insertion.

The abnormal control rod withdrawal is the more severe event with respect to the fuel temperature, and is selected as the representative postulated event. The representative postulated events concerning other acceptance criteria are selected in the same way. The postulated events considered in the safety evaluation

of the HTTR as anticipated operational occurrences and accidents are listed in Tables 4.7.3a and b.

A major accident and a hypothetical accident are evaluated to ensure the safety of the public in the case of serious accidents. “Major accidents” are postulated assuming the occurrence of the worst-case accident from a technical standpoint considering the reactor characteristics and engineered safety features. “Hypothetical accidents” are postulated assuming the occurrence of an accident more serious than a “Major Accident”, which is unlikely to occur from a technical standpoint, and shall be based on the assumption that one or more engineered safety features fail to function.

The acceptance criteria are established in “Examination Guide of Reactor Siting and Guidelines for Interpretation in their Application” as follows:

(a) effective dose equivalent to whole body shall not exceed 0.25 Sv in a major accident or a hypothetical accident

(b) effective dose equivalent to thyroid shall not exceed 1.5 Sv for a child in a major accident and 3.0 Sv for an adult in a hypothetical accident

(c) whole-population dose shall not exceed 2×10^4 man Sv in a hypothetical accident

A double-ended rupture of coaxial double pipes of the primary cooling system (depressurization accident) is postulated for the HTTR as the major accident and the hypothetical accident with respect to the risk of radiation exposure for the public.

4.7.7 Safety evaluation technologies

This section summarizes “Verified analysis codes accepted to licensing” [4.7.8]. Analytical tools for the safety evaluation were developed. All of them were validated by comparison between experimental results and analytical ones for the safety evaluation of the HTTR. Table 4.7.4 shows the representative events in the safety evaluation of the HTTR and analytical tools. Analytical code is as follows;

The BLOOST-J2 code [4.7.9] is used to analyze the effects of reactivity and flowrate change on the reactor power and temperatures of the core. The BLOOST-J2 code was modified from BLOOST5 code [4.7.10] so as to adopt the configuration of the HTTR. The validation of the BLOOST-J2 code was conducted by comparing analytical results with the data of control rod withdrawal/insertion experiments with Fort St. Vrain (FSV) at 50% of rated power.

The THYDE-HTGR code [4.7.11] is used to analyze plant dynamics of the HTTR. The THYDE-HTGR code was modified from THYDE [4.7.12] code to treat helium gas behavior in transient conditions. The THYDE code was validated by a comparison with various experiments such as LOFT experiments [4.7.13]. A new function to evaluate thermal and hydraulic transient of helium gas was added in the THYDE-HTGR code. The other functions were the same as that of the THYDE code. The validation of the THYDE-HTGR code was conducted by comparing analytical results with the data of control rod withdrawal/insertion experiments with FSV at 50% of rated power. Thermal and hydraulics behavior of helium gas was validated by comparing experimental results obtained in Engineering Research Association of Nuclear Steelmaking (ERANS) and analytical ones.

The TAC-NC code [4.7.14] modified from TAC-2D [4.7.15] is used to calculate transient thermal and hydraulic

characteristics in the core during loss of forced cooling accident such as the depressurization accident. The TAC-2D code was used for various calculations, and heat transfer calculations by conduction, convection and radiation have a sufficient reliability. The function to analyze heat transfer by natural circulation in the core is added in the TAC-NC code. This function was validated by comparing with an air ingress experiment, which simulated a rupture of the coaxial double primary pipes of the HTTR.

The RATSAM6 code [4.7.16)] is used to calculate the amount of mass and energy released from the reactor into the containment vessel with consideration given to heat transfer during the rupture of the coaxial double primary pipes. The validation of the code was performed by comparing the analytical results with experimental results, which are obtained by using a 1/8 scaled apparatus simulating the PCS (Primary Cooling System) of the Colder Hall-type Reactor. The COMPARE-MOD1 code [4.7.17)] is used to calculate pressure and temperature behavior in each compartment of the containment vessel during the depressurization accident. The code was certified by the US Nuclear Regulatory Committee as a code for safety analysis to calculate pressure and temperature behavior in the containment vessel.

The GRACE code [4.7.18)] is used to calculate axial and radial distributions of oxidation of graphite materials and concentration distribution of oxygen in a mixed gas of air and helium by analyzing the oxidation reaction between ingressed air and the graphite structures. The validation of the code was performed by using results of a graphite oxidation experiment. Input conditions for the code such as mass transfer coefficient were obtained from the heat transfer correlations obtained in the experiments.

The OXIDE-3F code [4.7.19)] is used to analyze the oxidation reaction of the graphite materials with steam ingressed in the core by a rupture of the heat transfer tubes of the Primary Pressurized Water Cooler (PPWC). The method to calculate the rate of graphite oxidation in the OXIDE-3F code is basically the same as that of the GRACE code.

The FLOWNET/TRUMP code [4.7.20)] is used to calculate the temperature distribution in the fuel block when a coolant channel was blocked. The code is the combination of the FLOWNET and TRUMP codes. The FLOWNET code is a one-dimensional flow network evaluation code. While the TRUMP code is a three-dimensional heat conduction code. The validation of the code was performed by comparing results of the uniform and non-uniform power distribution tests, which were carried out using the multi-channel test rig of the Helium Engineering Demonstration Loop (HENDEL).

4.7.8 New safety criteria

On the new regulatory standards, the safety designs for the strengthened natural phenomena such as earthquakes and volcanoes, fire and internal flooding were required. Furthermore, the mitigation measures against the beyond design basis accidents were required. In the HTTR, by considering the safety features such as the radiant core cooling even if the loss of forced cooling accident occurs, the safety designs against these accidents approved by the NRA without reinforcement of facilities.

References

4.7.1) K. Kunitomi, et al., “Safety design”, Nuclear Engineering and Design, 233,1-3, pp.45-58 (2004).

4.7.2) International Commission on Radiological protection, “Recommendations of the International Commission on Radiological protection”, ICRP publication 26, Pergamon press (1977).

4.7.3) International Atomic Energy Agency, “Basic Safety principles for Nuclear Power Plants 75-INSAG-3 Rev. 1”, INSAG-12 (1999).

4.7.4) T. Iyoku, et al., “R&D on core seismic design”, Nuclear Engineering and Design, 233, 1-3, pp.225-234 (2004).

4.7.5) T. Ikushima, ““SONATINA-2V”, a computer program for seismic analysis of the two-dimensional vertical slice HTGR core”, JAERI 1279 (1982), 63p.

4.7.6) T. Iyoku, et al., “Seismic study of high-temperature engineering test reactor core graphite structures”, Nuclear Technology, 99, 2, pp.158-168 (1992).

4.7.7) Y. Tachibana, T. Iyoku, “Structural design of high temperature metallic components”, Nuclear Engineering and Design, 233, 1-3, pp.261–272 (2004).

4.7.8) K. Kunitomi, et al., “Safety evaluation of the HTTR”, Nuclear Engineering and Design, 233, 1-3, pp.235-249 (2004).

4.7.9) S. Nakagawa, et al., “Core dynamics analysis code for high temperature gas reactor “BLOOST-J2””, JAERI-M 89-013 (1989), 44p (in Japanese).

4.7.10) M. Merrill, “BLOOST-5: A Combined Reactor Kinetics – Heat Transfer Code for the IBM-7044 Preliminary Description”, General Atomics, GAMD-6644 (1965).

4.7.11) M. Hirano, et al., “Development of THYDE-HTGR: computer code for transient thermal-hydraulics of high-temperature gas-cooled reactor”, JAERI-M 90-071 (1990), 68p.

4.7.12) Y. Asahi, et al., “THYDE-P2 Code: RCS (reactor-coolant system) Analysis Code”, JAERI 1300 (1986), 172p.

4.7.13) M. Hirano, et al., “Analysis of LOFT Small Break Experiment L3-1 with THYDE-P Code (CSNI International Standard Problem No.9 and THYDE-P Sample Calculation Run 50)”, JAERI-M 82-008 (1982), 71p.

4.7.14) K. Kunitomi, et al., “Two-dimensional thermal analysis code “TAC-NC” for high temperature engineering test reactor and its verification”, JAERI-M 89-001 (1989), 34p (in Japanese).

4.7.15) J. F. Petersen, “TAC2D: A General Purpose Two-Dimensional Heat Transfer Computer Code Users Manual”, General Atomics, GA-8868 (1969).

4.7.16) R. K. Deremer, et al., “RATSAM : A Computer Program to Analyze the Transient Behavior of the HTGR Primary Coolant System During Accidents”, General Atomics, GA-A-13705 (1977).

4.7.17) R. G. Gido, et al., “COMPARE-MOD1 : A Code for the Transient Analysis of Volumes with Heat Sinks, Flowing Vents and Doors”, Los Alamos, LA-7199-MS (1978).

4.7.18) H. Kawakami, “Air Oxidation Behavior of Carbon and Graphite materials for HTGR”, Tanso, 124, pp.26-33 (1986).

4.7.19) M. B. Peroomian, et al., “OXIDE-3 : A Computer Code for Analysis of HTGR Steam or Air

Ingress Accidents", General Atomics, GA-A-12493 (1974).

4.7.20) S. Maruyama, et al., "Verification of combined thermal-hydraulic and heat conduction analysis code FLOWNET/TRUMP", JAERI-M 88-173 (1988), 76p (in Japanese).

Table 4.7.1 Summary of Top Level Regulatory Criteria for the HTTR [4.7.1)]

Dose limits	Top Level Regulatory Criteria
Normal operation	・ 5 mSv of annual radiation exposure outside the site boundary ・ Based on "Examination Guide for Dose Goal outside the site boundary of Light Water Nuclear Reactor Facilities"
Accident	・ No significant risk of radiation exposure to the public ・ Effective dose equivalent shall not exceed 5 mSv ・ Based on "Examination Guide for Safety Evaluation of Light Water Nuclear Power Reactor Facilities"
Major accident	・ Effective dose equivalent to the whole body shall not exceed 0.25 Sv outside the site boundary ・ Effective dose equivalent to the thyroid shall not exceed 1.5 Sv for a child outside the site boundary ・ Based on "Examination Guide of Reactor Siting and Guidelines for Interpretation in their Application"
Hypothetical accident	・ Effective dose equivalent to the whole body shall not exceed 0.25 Sv outside the site boundary ・ Effective dose equivalent to the thyroid shall not exceed 3.0 Sv for an adult outside the site boundary ・ The whole-population dose shall not exceed 2 x 10^4 man Sv ・ Based on "Examination Guide of Reactor Siting and Guidelines for Interpretation in their Application"

Table 4.7.2a Acceptance criteria for anticipated operational occurrence for the HTTR [4.7.1)]

HTTR	LWR
• The peak fuel temperature shall be less than 1600 ℃.	Minimum critical heat flux (MCHF) or MCHF ratio shall not exceed the limited value. Fuel cladding shall not fail mechanically. Fuel enthalpy shall not exceed the limited value.
• Pressure on reactor pressure boundary is less than 1.1 times of maximum pressure in service.	Pressure on reactor pressure boundary is less than 1.1 times of maximum pressure in service.
• Maximum temperature of reactor pressure boundary 2.25Cr–1Mo steel < 500 ℃ Austenite stainless steel < 600 ℃ Hastelloy XR < 980 ℃	

Table 4.7.2b Acceptance criteria for accident for the HTTR [4.7.1)]

HTTR	LWR
• The reactor core shall not be seriously damaged and can be cooled sufficiently.	Minimum critical heat flux (MCHF) or MCHF ratio shall not exceed the limited value. Fuel cladding shall not fail mechanically. Fuel enthalpy shall not exceed the limited value.
• Pressure on reactor pressure boundary is less than 1.2 times of maximum pressure in service.	Pressure on reactor pressure boundary is less than 1.2 times of maximum pressure in service.
• Maximum temperature of reactor pressure boundary 2.25Cr–1Mo steel < 550 ℃ Austenite stainless steel < 650 ℃ Hastelloy XR < 1000 ℃	
• Maximum pressure on containment boundary is less than maximum pressure in service. • No significant risk of radiation exposure to public	Maximum pressure on containment boundary is less than maximum pressure in service. No significant risk of radiation exposure to public

Table 4.7.3a Selected events for anticipated operational occurrences [4.7.1)]

• Abnormal control rod withdrawal under subciritical condition
• Abnormal control rod withdrawal during rated operation
• Decrease in primary coolant flowrate
• Increase in primary coolant flowrate
• Decrease in heat removal by secondary cooling system
• Increase in heat removal by secondary cooling system
• Loss of off-site electric power
• Abnormality of irradiation specimens and experimental equipment
• Abnormality during safety demonstration tests

Table 4.7.3b Selected events for accidents [4.7.1)]

• Channel blockage in fuel block
• Rupture of inner pipe of concentric pipe in primary cooling system
• Rupture of inner pipe of concentric pipe in secondary cooling system
• Rupture of concentric pipe in secondary cooling system
• Rupture of pipe in pressurized water cooling system
• Rupture of concentric pipe in primary cooling system
• Rupture of heat tube in pressurized water cooler
• Rupture of pipe in primary coolant purification system
• Rupture of pipe in processing facilities of radioactive gaseous waste
• Rupture of sweep gas pipe in irradiation test facilities
• Rupture of standpipe

Table 4.7.4 Selected events and analytical codes [4.7.7)]

Event name	BLOOST-J2	THYDE-HTGR	TAC-NC	RATSAM6	COMPARE MOD-1	GRACE	OXIDE-3F	FLOWNET/TRUMP
Anticipated operational occurrence								
Abnormal control rod withdrawal under subcritical condition	Y							
Abnormal control rod withdrawal under rated operation	Y							
Decrease in primary coolant flowrate		Y						
Increase in primary coolant flowrate		Y						
Decrease in heat removal by secondary cooling system		Y						
Increase in heat removal by secondary cooling system		Y						
Loss of off-site electric power		Y						
Abnormality of irradiation specimens and experimental equipment	Y							
Abnormality during safety demonstration tests		Y						
Accident								
Channel blockage in fuel block								Y
Rupture of inner pipe of coaxial double pipes in primary cooling system			Y					
Rupture of inner pipe of coaxial double pipes in secondary cooling system		Y						
Rupture of coaxial double pipes in secondary cooling system		Y						
Rupture of pipe in pressurized water cooling system		Y						
Rupture of coaxial double pipes in primary cooling system		Y	Y	Y	Y	Y		
Rupture of heat tube in pressurized water cooling system		Y					Y	
Rupture of pipe in primary coolant purification system *								
Rupture of pipe in processing facilities of radioactive gaseous waste *								
Rupture of sweep gas pipe in irradiation test facilities								Y
Rupture of standpipe	Y		Y	Y	Y			

*; This event does not use any analytical code for the safety evaluation.

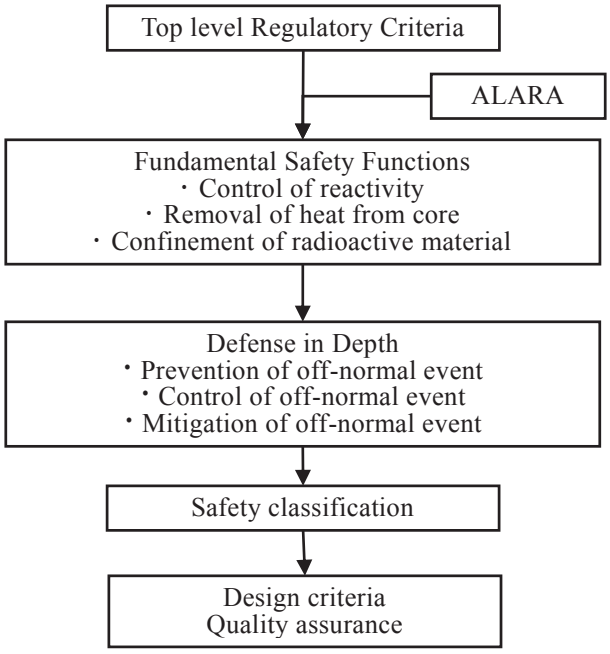

Fig. 4.7.1 Logical flow to establish a safety design philosophy of the HTTR [4.7.1)]

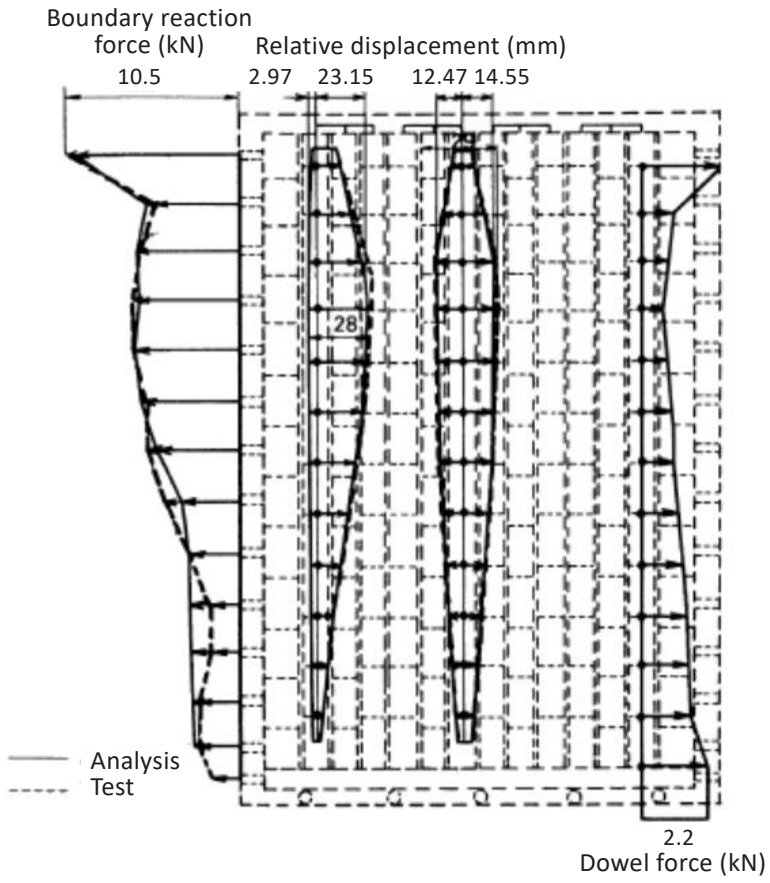

Fig. 4.7.2 Typical core overall response characteristics at resonance [4.7.4)]

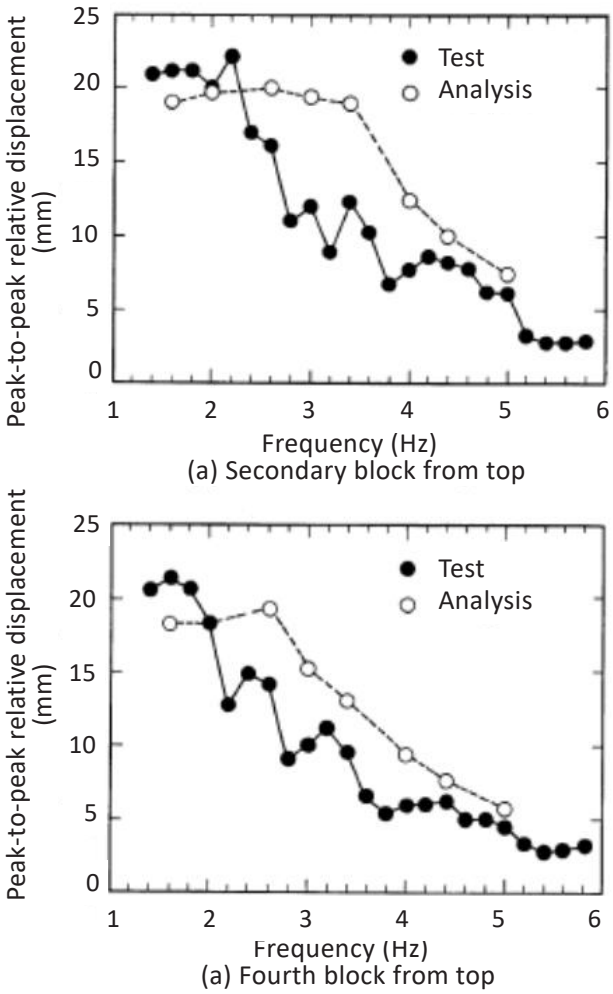

Fig. 4.7.3 Comparison between test and analytical results of relative block displacement (full-scale seven-column test) [4.7.4)]

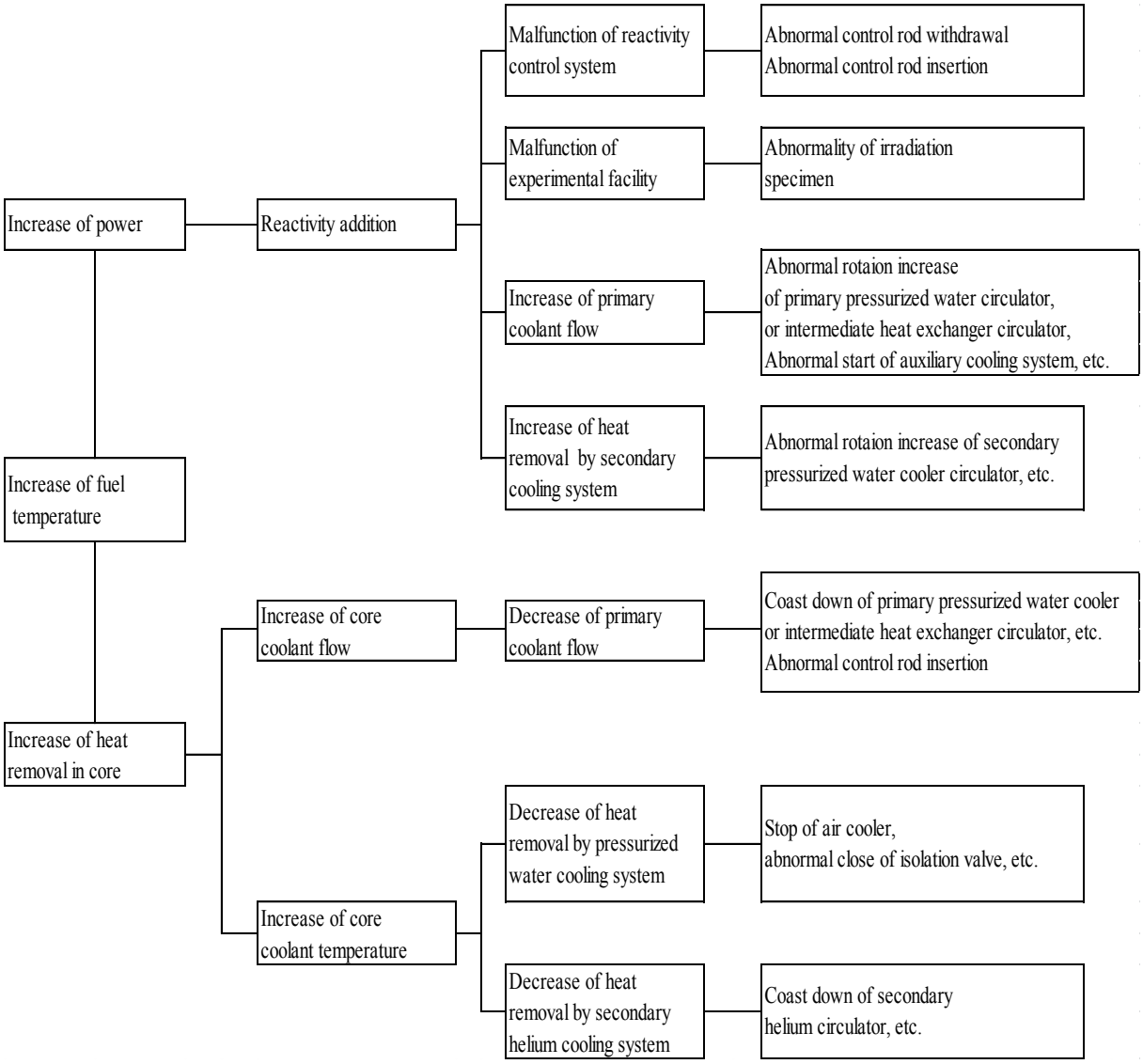

Fig. 4.7.4 Example of a selection process of anticipated operational occurrence [4.7.1)]

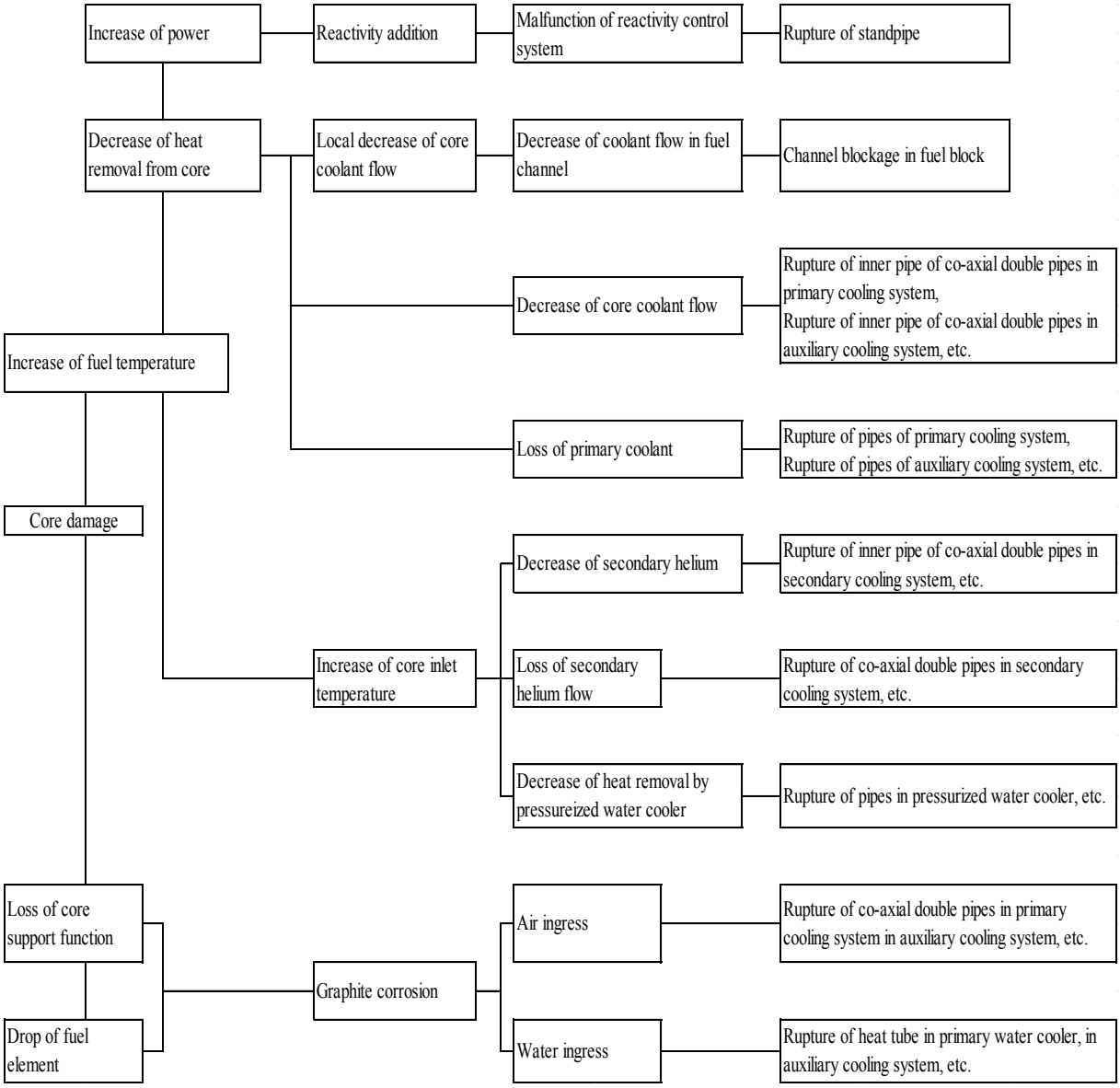

Fig. 4.7.5 Example of selection process of accident [4.7.1)]

4.8 Operation and Maintenance of HTTR

4.8.1 Outline

The HTTR, which locates at the south-west area of 5000 m^2 in the Oarai Research Establishment, had been constructed since 1991 before accomplishing the first criticality on November 10, 1998. The operation history of HTTR is shown in Table 4.8.1. Rise to power tests of the HTTR started in September, 1999 and the rated thermal power of 30 MW and the reactor outlet coolant temperature of 850℃ was attained in December 2001. HTTR is now conducted in-service operation through the rise-to power operation with rated operation or high-temperature test operation. In March 2007, HTTR was conducted rated/parallel-loaded 30-days operation, in order to demonstrate to supply stable heat to heat utilization system for long-term. This paper reports the characteristics of long-term operation for HTTR. The long term high temperature operation using HTTR was carried out to establish the technical basis of HTGR in the high temperature test operation mode during 50-days since January till March, 2010. In addition to conducting tests ending with short-term operation, we confirm the stability of the integrated system by performing long-term continuous operation and examine the knowledge necessary for upgrading the HTGR in the future.

In the current experimental program, further experiments with the power plant will realistically demonstrate that the loss of coolant accident neither endangers the environment nor the plant itself. The inherent safety properties have been demonstrated in overall plant tests. Operating results to date have confirmed the brock-type VHTR concept. In this section, we show an overview of the technology and data on design and manufacturing demonstrated through HTTR operation.

4.8.2 Know-how and remarks of construction process

Table 4.8.2 shows phases and remarks from design and manufacturing to reactor operation at full power. JAEA and manufactories have carried out the development and piled up the data for equipment and components of HTTR in phase during the design and manufacturing process. Especially, the following experiences and technologies and so on, which are special to HTGR, are valuable to construct the new HTGRs;

- Manufacturing and processing technologies for graphite and carbon components.
- Manufacturing and welding technologies for high temperature components and structures.
- Establishment of inspection standard for fuel, graphite components, and B_4C/C.

The experience of acceptance tests and installation of equipment are also valuable. Especially, testing methods and conditions of acceptance test for fuels, graphite and so on were established by JAEA and manufactories. Tests from installment of equipment to reactor operation at full power were divided into 3 phases and carried out step by step.

Water is used for LWR, but since HTGR uses helium gas, attention must be paid to radiation leakage. Also, since HTGR becomes hotter than LWR and FBR, there are many places where gap is provided in the structural material beforehand and it is important to control the leakage of helium. It is important to pay strong attention to the following points in the construction phase of HTGRs. Because coolant of

HTGRs is helium gas which leaks easily through narrow gaps by a small pressure difference and has no shielding ability.

(a) Heat leakage
(b) Helium leakage
(c) Radiation leakage

Remarks of each test also shows in Table 4.8.2. Experiences of trouble and countermeasure for heat leakage and radiation leakage are described below.

(1) Prevention of temperature rise primary upper shielding by heat leakage[4.8.1)]

In a non-nuclear heat up test, the temperature of primary upper shielding as well as helium gas temperature inside standpipes of the reactor rose much higher than expected. As the result of estimation, it was confirmed that these temperatures should exceed design values at full power operation of the HTTR.

Heat from the RPV of HTTR, which is conducted to the primary upper shielding through the standpipes and the top of the primary upper shielding, are cooled by air flowing in the standpipe room as shown in Fig. 4.8.1. The standpipe room inlet temperature of the air is about 15°C. The panel of the vessel cooling system at the bottom of the shielding, which consists of many water-cooling tubes contained in a steel casing, also removes the heat from the primary upper shielding. For the 16 standpipes of control rod drive mechanisms, small amount of purified helium gas of about 25°C, called ‘purge gas’, from helium purification system for reduction of chemical impurities and fission products in the primary cooling system, comes in through the standpipe closures, which plug the standpipes, purges control rod drive mechanisms, and cools the standpipes at the same time.

Test and analysis were carried out to investigate cause of the accident. As the results, it was indicated that the existence of upward coolant flow through an annular gap, about 2 mm in width, between the standpipe and the control rod guide sleeve by a pressure difference. It was presumed that the upward flow is heated inside of the standpipe and the primary upper shielding through the standpipes. In order to control the flow rate of primary coolant in the control rod guide block column, there is one orifice, which produces pressure drop between the plenum of the RPV top head dome, designated by A in Fig. 4.8.2, and inside the guide pipe for the control rod support cable, designated by B in the same figure. By the pressure difference primary coolant flows upward along the wall of the standpipe, change direction, and then flows downward through the graphite orifice and along the control rod support cable inside the guide pipe as shown in Fig. 4.8.2. The flow was named ‘bypass flow’.

To prevent the bypass flow mentioned above the first countermeasure was considered and taken as shown in Fig. 4.8.3. The concept of the countermeasure is to minimize the pressure drop between A and B in Fig. 4.8.2. For this purpose square holes were bored on the side of the guide pipe for the control rod support cable and new holes for coolant paths were bored in the top plate of the control rod guide tubes as designated new openings in Fig. 4.8.3.

An out-of-pile test at room temperature and atmospheric pressure was conducted to confirm the effect of the first countermeasure. A full-scale apparatus modeling the standpipe and the inner components was

utilized for the test. As a result, it was confirmed that the first countermeasure is effective. Flow direction between the standpipe and the control rod guide sleeve is downward. Thus, the bypass flow is prevented and purge gas flows properly.

Temperature analysis was also performed using a finite element method (FEM) code called SSPHEAT in order to estimate the effect of the countermeasure. As a result, it was confirmed that the flow rate of the purge gas per standpipe should be more than 0.6 g/s^{-1} to observe the design temperature of the shielding, 88°C.

After the countermeasure, non-nuclear heat test was carried out. As the result, the shielding temperature exceeds the design temperature of 88°C at full power. It was indicated that the effect of the purge gas is much less than what we expected, though the bypass flow is prevented.

The first countermeasure prevented the bypass flow and decreased enough the helium gas temperature inside the standpipe. However, the temperature of the primary upper shielding did not decrease to the acceptable level. Thus, a second countermeasure was considered. Figure 4.8.4 shows the second countermeasure, which is an installation of cylindrical copper plates and heat insulators around standpipe. The cylindrical plates in the standpipe room work as radiation fins. The lower part of the copper plates contact with the vessel cooling panel at the bottom. Inside the panel, run water-cooling tubes cool the bottom of the primary upper shielding directly and its standpipe side indirectly through the cylindrical copper plates.

The confirmation tests, which are non-nuclear heat up test, were carried out. As the result, the temperature fall, which is an effect of the second countermeasure, is confirmed. In addition, temperature analysis of the confirmation tests was carried out to estimate the temperature of primary upper shielding at full power operation. The FEM code, namely SSPHEAT, is also used for the analysis. The second countermeasure, copper plates, and heat insulators were additionally modeled. As the result, it was confirmed that the temperature of primary upper shielding at full power of 30 MW is lower than the design temperature of 88°C.

The obtained experiences and technologies will be helpful in designing new HTGRs to prevent heat leakage caused by helium leakage.

(2) Prevention of neutron streaming to upper direction[4.8.2)]

The radiation shielding design of HTTR was paid attention to avoid streaming because helium gas coolant has no shielding ability. Especially, prevention of neutron streaming to upper direction was important because up to 31 standpipes penetrate the primary upper shielding. In addition, the temperature of components including shielding rose high, and gaps are needed to prevent mechanical interaction by thermal expansion.

Figure 4.8.5 shows shielding structure of a standpipe. The carbon steel shield and carbon shield are stuffed inside the standpipes. However, the standpipe has a center hole for the wire suspending the control rod as well as a circumferential gap between the carbon steel. At the outside, a grout shield and a carbon

steel shield are provided with an offset structure to prevent neutron streaming, but narrow gaps still exist to prevent mechanical interaction by thermal expansion.

A total of 31 standpipes composing of steel guide tubes are embedded in the primary upper shield. The geometrically-complex upper shield region with the standpipe penetrations has been analyzed with a two-dimensional SN transport code DOT3.5 incorporating the mutual shielding effects of the standpipes.

The shielding performance test was carried out to find abnormal radiation exposure. In this test, dose equivalent rates were measured on the basis of the classified power levels from zero to full power. The shielding performance tests were carried out with the reactor power rising in steps to predict the condition at the higher power based on the data obtained at the lower power. Thermal reactor powers in the test were set at 0.3, 9, 15, 20, and 30MW. The dose equivalent rates were measured by the 3He proportional counters for neutron and the Geiger-Muller (GM) counters for gamma. Neutron streaming in the upper direction was carefully examined at the standpipe room. At the restricted area during operation, neutron and gamma-ray doses were continuously measured and additionally by using two different types of thermo luminescence dosimeters (TLDs) for thermal neutron and gamma. The GM counter, ^{3}He proportional counter, and TLD were installed nearby standpipe.

The measurement was carried out during the first criticality test of the HTTR. As the result, the measured dose equivalent rate was under the detection limit. No unexpected neutron streaming paths were found around the standpipes through the test. In the test at low reactor power, dose equivalent rates for neutrons and gamma were measured at the standpipe room, the operation floor, and around the containment vessel during 7.5 kW and 300 kW operation. At all of the measured points, dose equivalent rates for neutron and gamma were the same level as the background. For the test with medium reactor powers at 9 MW, 15 MW, and 20 MW, criteria was satisfied for neutron and gamma at all of the measured points. At full power, it was confirmed that the dose equivalent rates were under the detection limit for neutron and gamma. Thus, the shielding of the HTTR satisfies the requirement for human access to the reactor during operation, and it could be designed with a conservative margin on the safe side. The dose equivalent rates at the standpipe room changed according to the reactor power and the average dose equivalent rates at full power operation were approximately 120 μSv/h and 8 μSv/h for neutron and gamma, respectively.

In the shielding design of HTTR, the dose equivalent rate at the standpipe room was evaluated to be 18 mSv/h, which was two orders of magnitude higher than the measured. On the other hand, the design value employed the safety factor with 30% per each decade of neutron flux attenuation.

The criteria of dose equivalent rate were set successfully to satisfy the requirement for human access to the reactor during operation. In addition, there was no unexpected neutron streaming path around the standpipes at the standpipe room. It was confirmed that the shielding design of HTTR is valid. The obtained experiences and technologies will be helpful in shielding design of new HTGRs, in which the standpipes are employed.

4.8.3 Fabrication experience of HTTR fuel[4.8.3)]

The core of HTTR consists of 150 fuel assemblies. An HTTR fuel is a so-called pin-in-block type of hexagonal graphite block containing fuel rod as shown Fig.4.8.6. In the field of HTGR fuel, JAEA has carried out a lot of research and development works. The fuel fabrication technologies were developed with the collaboration of the Nuclear Fuel Industry Co. Ltd. (NFI). The fabrication of the first-loading fuel and the second-loading fuel were successfully produced through the fuel kernel, coated fuel particles (CFPs), and fuel compact process. Fabrication of the first-loading fuel was the first mass-production of the HTGR fuel in Japan. Because of this, JAEA and NFI experienced some technical problems during the fabrication. The problems and countermeasures are described below.

High quality and production efficiency of fuel were established through a lot of R&D activities and fabrication experiences of irradiation examination samples. Finally, it was decided to fabricate the first-loading fuel of the HTTR by the fuel kernel process using the vibration dropping technology, the continuous four-layer coating process and optimization of the compaction conditions. Fig. 4.8.7 depicts a flow diagram of the HTTR fuel production process.

(1) Fabrication process of coated fuel particle

The UO_2 kernels were fabricated in a gel-precipitation process. After formation of uranyl nitrate solution containing methanol and an additive, spherical droplets are produced by a vibration dropping technique. The UO_2 kernels were fabricated in a gel-precipitation process. After formation of uranyl nitrate solution containing methanol and an additive, spherical droplets are produced by a vibration dropping technique. Following the drying and calcinating, reduction of the calcinated kernels to UO_2 was carried out. Kernel fabrication was completed by a sintering process to produce dense UO_2 kernels. The coating layers were deposited on the kernels in a CVD process using a fluidized coater. The TRISO coating process is divided into four coating processes for the porous PyC, IPyC, SiC, and OPyC layers. The buffer and high density PyC coating layers were derived from C_2H_2 and C_3H_5, respectively, and the SiC layer from CH_3SiCl_3. All UO_2 kernels and TRISO coated particles are classified by means of a vibrating table to exclude odd shape particles.

The coating failure during coating process was mainly caused by the strong mechanical shocks to the particles given by violent particle fluidization in the coater and by the unloading procedure of the particles. The coating process was improved by optimizing the mode of the particle fluidization and by developing the process without unloading and loading of the particles at the intermediate coating process.

(2) Fabrication process of fuel compact

The fuel compacts are produced by warm-pressing of the coated fuel particles with graphite powder. In the first step, the coated fuel particles are overcoated by resinated graphite powder with alcohol. The resinated graphite powder is prepared by mixing electrographite powder, natural graphite powder, and phenol resin as a binder, followed by grinding the mixture to powder. The aim of the overcoating is to avoid direct contact with neighboring particles in the fuel compact. Then the overcoated particles are

warm-pressed by metal dies to form annular green fuel compacts. The final step of the compaction process is the heat-treatment of the green fuel compacts at 800℃ in flowing N_2 to carbonize the binder and at 1,800℃ in vacuum to degas the fuel compacts.

The coating layers should be intact before and during irradiation. However, small fractions of the particles with defective coating layers have been present during the fabrication process. Among several modes of defective coating layers, a defective SiC coating layer is the most harmful from the standpoint of fission product retention. Then the fabrication process was modified to reduce the defective particle fraction during the compaction process before fabrication of the first-loading fuel of the HTTR. The compaction process was improved by optimizing the combination of the pressing temperature and the pressing speed of the overcoated particles to avoid the direct contact with neighboring particles in the fuel compact.

(3) Assembling

Fourteen fuel compacts were encased in a long graphite sleeve, making up a fuel rod. The graphite sleeves and the graphite blocks were made of IG-110, a fine grained, low impurity, isostatic-pressed isotropic graphite. The graphite sleeves were transported from Toyo Tanso Co.Ltd. to NFI to assemble the fuel rods. The fuel rods and graphite blocks were transported to the HTTR reactor building. Assembling of the fuel blocks was carried out in the reactor building by insertion of the fuel rods into the graphite blocks. Assembled fuel blocks were stored in new fuel storage cells after inspection. The cells were filled with helium gas to keep the fuel blocks in dry condition.

(4) Inspections[4.8.4)]

The inspection items were determined to confirm specifications, which certify nuclear and thermal-hydraulic design, irradiation performance and so on. From a viewpoint of purposes, the inspection items are divided into three categories described below;

(a) Compulsory

(b) User's requirement or optional

(c) Vender's quality control

The sampling rate was also determined by considering the uniformity of inspected data. Three categories are basically classified as:

- Small-scattering data
- Medium-scattering data
- Large-scattering data

One sample is measured from an inspection lot with small-scattering data. For the inspection lot with medium-scattering data, three samples are measured and all of them should satisfy criterion. For the large-scattering data, measured data should meet a statistically required criterion with 95% confidence. Table 4.8.3 shows the inspection item, purpose, method and sampling rate in the HTTR fuel fabrication which were determined by JAEA and manufactories.

It is considered that these experiences and technologies will be helpful in fuel fabrication of new HTGRs, in which pin-in-block type fuel is employed.

4.8.4 Operation experiences

(1) Overview of HTTR test experiences[4.8.5)]

The overall test operation plan using HTTR is as follows. R&Ds are divided into two items, one is the establishment of technology basis of HTGR, and the other is R&Ds toward domestic and overseas deployment of HTGR. Establishment of technology basis of HTGR is divided into three items. Establishment of design direction of HTTR, Validation of safety of HTTR in representative events, and recently newly added item is the confirmation after the accident of Fukushima-daiichi NPS. For establishment of design direction of HTTR, Most of items were confirmed, HTGR technology base has been established.

(2) Pre-operational tests

A pre-operational test operation of the reactor cooling system was performed from May 1996 to March 1998. At the stage of the pre-operational test without nuclear heating and with dummy fuel blocks, the helium gas was heated by the gas circulators up to about 200°C at 2MPa. Pre-operational tests of the cooling system were performed at this operation condition to accumulate operational experiences. Plant control systems were fully checked. During the pre-operational tests, several improvements in the system were made in terms of securing its safety margin and easy operation. Their performance was finally confirmed in July 1999 after completing the actual fuel loading.

(3) Start-up physics test[4.8.6)]

Fuel loading to the reactor started in July 1998, and the first criticality was attained on November 10, 1998. The cross section of the reactor core is shown in Fig. 4.8.8. Fuels were column-wise loaded from the outer fuel columns to the inner ones and 19 of the total 30 fuel columns made the reactor critical. The first criticality was attained almost in a shape of annular core, installing the outer ring of fuel columns and one inner fuel column leaving the other inner ones filled with dummy fuel blocks. The predicted minimum number of fuel columns attaining the first criticality was 16±1. The discrepancy between the predicted and the measured values was due to impurity and air contents in the dummy fuel blocks used for the calculations. The post calculation with revised graphite block composition showed that the number of critical fuel column is 19 as shown in Fig.4.8.9. The other inner fuel columns were filled in to give the full core by December 1998. In the course of fuel loading, low power physics tests were carried out for the 21, 24, and 27 fuel columns loaded core. These tests provide useful data for designing future annular cores of advanced HTGRs.

(4) Rise to Power test[4.8.7- 4.8.8)]

Rise to power tests started in September 1999, and reactor power was increased step-by-step to 10MW,

to 20MW and then finally to 30MW as shown in Fig. 4.8.10. Full power of 30MW-thermal and reactor outlet coolant temperature of 850°C was achieved in December 2001. Certificate of pre-operation test, that is, operation permit of the HTTR was issued in March 2002.The HTTR accomplished the maximum reactor outlet coolant temperature of 950°C in April 2004 in high temperature test operation. Operation permit for the high temperature test operation was issued in June 2004.

(5) Safety demonstration test[4.8.9- 4.8.10)]

In the HTTR, safety demonstration tests have been implemented since FY 2002 in order to demonstrate excellent inherent safety peculiar to the high-temperature gas reactor. In the first phase of the safety demonstration test, the control-rod withdrawal tests and the gas circulator tripping tests, etc., have demonstrated the inherent safety of the high-temperature gas furnace, and the experimental data required for the accuracy of the analysis evaluation at the time of the accident was obtained. From FY 2010, as the safety demonstration test of the second phase, the loss of forced cooling test, the loss of core cooling test, etc., simulating more severe accidents were conducted, and experimental data was obtained.

In the loss of core cooling test conducted in February 2010, the forced cooling of the reactor core is stopped without inserting control rods into the core and, furthermore, without cooling by the vessel cooling system (VCS) to verify safety evaluation codes to investigate the inherent safety of high-temperature gas-cooled reactor (HTGR) be secured by natural phenomena to make it possible to design a severe accident-free reactor.

The test of loss of forced cooling (LOFC) when one of two cooling lines in VCS lost its cooling function was carried out to simulate the partial loss of cooling function from the surface of RPV using the HTTR at the reactor thermal power of 9 MW, under the condition that the reactor power control system and the reactor inlet coolant temperature control system were isolated, and three helium gas circulators (HGCs) in the primary cooling system (PCS) were stopped. The test results showed that the reactor power immediately decreased to almost zero, which is caused by negative feedback effect of reactivity, and became stable as soon as HGCs were stopped as shown in Fig.4.8.11. From FY 2011 and beyond, we plan to continue the safety demonstration test such as the loss of core cooling test.

(6) Continuous operation[4.8.11- 4.8.12)]

To use the High-Temperature Gas-cooled Reactor (HTGR) system as a commercial reactor similar to the future HTGR ‘GTHTR300C,’ supplying stable high-temperature heat from the reactor to the heat utilization system such as the hydrogen production system over a prolonged period should be demonstrated.

In order to demonstrate to supply stable heat to heat utilization system for long-term, HTTR was conducted Rated/Parallel-loaded 30-days operation. Furthermore the 50-day high-temperature continuous operation with full power, which is the first long-term operation with a reactor outlet coolant temperature over 900°C, was achieved in March 2010 in the HTTR. In these continuous operations, JAEA evaluated the experimental data such as core burn-up, helium purity control, performance of high temperature

equipments, structural integrity in the core, etc. and demonstrated the nuclear thermal availability of heat source for thermo-chemical hydrogen production technology. In addition, we evaluated the obtained data and demonstrated that the fuel of HTTR developed in Japan has the world's highest quality. Furthermore, the performance of the reactor internal structure and the intermediate heat exchanger, which is the core of the technology for manufacturing and transporting high temperature gas, demonstrated that high temperature nuclear heat can be stably supplied to the utilization system for a long term.

In order to supply stable high-temperature heat from the reactor to the heat utilization system using the HTTR, the heat exchange performance and structure integrity of the intermediate heat exchanger (IHX) should be confirmed. In this paper, the heat exchange performance and structure temperature of the IHX were evaluated with the high-temperature continuous operation data and compared with the designed one or estimated one. As a result, it was confirmed that the IHX can exchange stable high-temperature heat from the primary coolant to the secondary helium, and the IHX structure temperature is under the allowable working temperature in the operation. Moreover, it was confirmed that the heat exchange performance is almost the same as the designed one and that the structure temperature estimated with the analysis code is almost the same as the measured one.

4.8.5 Operation procedure

(1) Operation manuals

The operation manual describes the operation of the HTTR, the method of facilities checking and correspondences for abnormal events, and it consists of 2400 pages of documents. The operation of the HTTR is managed based on the nuclear reactor facility safety regulations and the operation manuals, and is classified under the following phases.

- Pre-start up preparation,
- Preparation of reactor start up,
- Reactor start up,
- Steady state power operation,
- Inspection after stop.

Pre-start checks of the water system [pressurized water cooling facility, reactor container cooling facility, auxiliary cooling facility (including helium system)] and the confirmation of setting values for the measurement control system facility are carried out before the 24 hours monitoring works (= shift works by five teams).

Helium system (primary cooling facility, secondary helium cooling facility, primary and secondary helium purifying facilities, primary and secondary helium sampling facilities, etc.) are checked as “the pre-start checks of helium system combination facilities” in the shift works.

Each operation phases are shown as follows,

a) Pre-start up preparation

-Check of power supplies, valves include operation check

-Initial helium filling

b) Preparation of reactor start up

-Operation of helium gas circulators

- Refilling of helium gas

c) Reactor start up

-Power up from critical operation to 30% power

-Confirmations of operation state of equipment, radiation monitoring data and operation mode selection device

d) Steady state power operation

- Operation from 30% to 100% power

e) Reactor shutdown

- Power down from steady state power operation

(2) Operation data of helium coolant leak rate[4.8.13)]

The helium gas is used as the primary coolant in HTGR. The helium gas is easy to leak, and the primary helium leakage should be controlled tightly from the viewpoint of preventing the release of radioactive materials to the environment. Moreover from the viewpoint of preventing the oxidization of graphite and metallic material, the helium coolant chemistry should be controlled tightly. The primary helium leakage and the helium coolant chemistry during the operation is the major factor in the HTGR for commercialization of HTGR system. We have shown the design concept and the obtained operational experience on the primary helium leakage control and primary helium impurity control in the HTTR.

Figure 4.8.12 shows the evaluated primary helium leak rate. The primary helium leak rate is restricted 0.3 wt%/day in the HTTR from the viewpoint of preventing the release of radioactive materials to the environment and confirming the integrity of the pressure boundary. Therefore, the helium leakage should be controlled severely and watched during the operation. The four periodic inspections were experienced in the HTTR. It was confirmed that evaluated primary helium leak rates were within and much lower than the restricted one, and the variation caused by the aging of facility was not generated. The primary helium leak rate is much lower than the restricted value and the primary helium confinement technology used in the HTTR is very useful for the development of commercial HTGR.

(3) Impurities control technologies [4.8.14- 4.8.15)]

(a) Power rise procedure considering impurities behavior

For the reasons such as prevention of oxidation of the graphite structural material used in the core and prevention of carbon deposition due to reduction in the low temperature range, equipment for removing impurities in Helium gas and facilities for detecting impurities are provided as helium auxiliary facilities.

At the initial startup of the HTTR, the amount of impurities released from the graphite structural material of the core and the heat insulation used was presumed in advance, and furthermore, management standards for maintaining the structural integrity of graphite were set and the output was increased.

Therefore, clarifying the impurity characteristics in the coolant is indispensable for improving the operating technique of the high temperature gas reactor.

In the process of increasing the power during the operation up to the reactor outlet coolant temperature of 850 °C conducted in December 2001, in order to reduce the H_2O concentration, at reactor power where the reactor outlet coolant temperature does not exceed 800 °C, The reactor power was kept for about 1 month to reduce the chemical impurity concentration. Figure 4.8.13 shows the change in impurity concentration at the inlet of reactor at the reactor outlet coolant temperature of 850°C.

On the other hand, in the operation up to the reactor outlet coolant temperature of 950°C, which was carried out in April 2004, sufficient impurities were removed in the operation period of 850 °C, so the impurity concentration was lower than the operation at 850°C. Figure 4.8.14 shows the change in the impurity concentration at the inlet of the reactor in the operation up to 950°C.

Impurity concentration is an important controlled object for suppressing deterioration of graphite and refractory metal, but the behavior of impurities largely changes depending on the operation timing and the output to be reached. Furthermore, our recent study reveals that the emission characteristics of impurities decrease faster than we had assumed at design time. Our ongoing research is useful to rationally design facilities to remove impurities and to achieve efficient operation.

(b) Tritium transport data in primary / secondary coolant[4.8.16)]

The tritium concentration in the high-temperature engineering test reactor (HTR) was measured during high-temperature (950°C) continuous operation for 50days in 2010, which is the first measurement of tritium concentration in the secondary helium circuit during operation using the intermediate heat exchanger, to develop an assessment base for evaluating tritium behavior in the high temperature gas cooled reactor hydrogen-production system.

Helium was sampled at the locations shown in Fig. 4.8.15 and Fig. 4.8.16, and the tritium concentration contained in helium was measured with a liquid scintillation counter, and the results are shown in Fig. 4.8.17 and Fig.4.8.18.

Our this study shows that the concentration and total quantity of tritium in the secondary helium cooling system of the HTTR-iodine sulfur (IS) system can be maintained below the regulatory limits, which implies that the hydrogen production plant can be exempt from the safety function of the nuclear facility.

For this research we have built facilities to measure tritium with high accuracy and measured tritium in many places of HTTR. Tritium is a radionuclide that easily diffuses metals, and our measurement techniques and data are useful for safety handling of tritium management.

(4) Neutron detector for use at high temperature [4.8.17)]

Two types of neutron detector are used in the HTTR. One is a fission counter which is prepared for the WRM. It is used under a high temperature environment such as at 450°C in operation and 550°C in accident. The other is an uncompensated ionization chamber. It is prepared for the power range monitor (PRM) and can detect a low neutron flux level. The WRM and PRM are used in the power range from

10-8% to 35 % and from 0.1% to 120%, respectively. The WRMs are installed at the top of a permanent reflector in reactor pressure vessel (RPV). Then, several months are necessary for the replacement of WRM because access into the RPV is required. Figure 4.8.19 shows the arrangement of neutron detector for WRMs.

An event, in which one of WRMs was disable to detect the neutron flux in the reactor core, occurred just after the reactor was shut down. An electrical inspection method was proposed to detect the cable disconnection of the WRM from outside of the reactor. The inspection method uses the waveform observation of the characteristic impedance using the time domain reflectometry (TDR) and the electrostatic capacitance measuring method and so on.

The TDR is one of the cable damage detecting methods. By observing the change in the response mode of the reflected pulse as the characteristic impedance, it is possible to specify the damage mode such as disconnection. A TDR spectrum of normal WRM and intentionally short-circuited WRM were obtained as a mock-up test. As a result of the test, it was confirmed that the position where disconnection occurs in the WRM was correlated to the waveform of characteristic impedance. The TDR spectrum of the actual WRM was measured by the measurement method verified by the mock-up test, and it was found that the breaking point can be effectively estimated.

The inspection using the TDR was carried out and the data was acquired. To carry out the inspection using the TDR was enacted in HTTR operation manual, as the start-up check, based on the experience of the cable disconnection. These data is valuable and expected to contribute to the development of the cable disconnection prediction technology for future HTGRs. The development is expected to be contributed to shift from the time-based maintenance to the condition-based maintenance for the future HTGRs.

(5) Monitoring method of fuel movement for Safeguard [4.8.18)]

As of the safeguards approach in the HTTR facility, an unattended spent fuel flow monitor (UFFM) was applied to carry out an item counting of spent fuel blocks. The UFFM is so designed and fabricated as to be the compact and unique monitor system to verify a movement of spent fuel blocks in "difficult to access" area and reduce inspection efforts. This system consists of two detector packages, electronics and computer. One package consists of two ionization chambers and a He-3 counter. The IAEA acceptance tests were performed and it was confirmed the followings:

- All the detectors were functioning properly to measure a spent fuel block flow.
- The time difference between detector signals was sufficient to determine the direction of the spent fuel blocks.
- The UFFM was useful to carry out the item counting.

The UFFM was approved as the IAEA safeguards equipment in the safeguards approach in the HTTR.

(6) Troubleshooting database obtained from ~20 years of HTTR maintenance [4.8.19)]

Troubles experienced since 1997 before the first criticality are managed in the database. The database system now contains more than 1000 records dating from 1997. These are used in order not to experience

the same trouble in HTTR, but show what kind of equipment should be made more carefully in the future high temperature gas cooled reactor. When events were classified according to the HTTR systems, about half of all events occurred in just two systems: the instrumental and control system and the auxiliary reactor system. Based on an analysis of the database, four major lessons have been identified that may contribute to the design of future HTGRs:

- Performance degradations of the HGCs. Decreasing volumetric flow rates of HGCs were caused by abnormal abrasion of slide materials, and dust from the slide material was a potential source for ingress of impurities. Degradation in the performance of oil seals was caused by adopting inadequate materials. Designs of future HTGRs would benefit from evaluating the selection of adequate materials based on these kinds of events.
- Malfunction of the RSS in the reactivity control system. This event was caused by human error during fabrication. Design of future HTGRs would benefit from improvements in the motor that prevent oil ingress into the brake; quality control during manufacturing should also be strengthened.
- Problems with emergency gas turbine generators. Adoption of emergency gas turbine generators for the HTTR has generally proven to be successful. To improve the safety and the reliability of the emergency generators, future HTGRs would benefit by incorporating into the design preventive measures against rust due to water and sea salt and against extended operating times.
- Experience of the Great East Japan Earthquake. Sludge deposition, distorted fuel injection, and reduction in thickness of the combustor liner in an emergency gas turbine generator were caused by a long-time wave from a strong earthquake.

References

4.8.1) Y. Tachibana, et al., “Procedure to prevent temperature rise of primary upper shielding in high temperature engineering test reactor (HTTR)”, Nuclear Engineering and Design, 201, 2-3, pp.227-238 (2000).

4.8.2) S. Ueta, et al., “Shielding technology for upper structure of HTTR”, Annals of Nuclear Energy, 94, pp.72-79 (2016).

4.8.3) K. Sawa, et al., “Fabrication of the first-loading fuel of the High Temperature Engineering Test Reactor”, Journal of Nuclear Science and Technology, 36, 8, pp.683-690 (1999).

4.8.4) K. Sawa, et al., “Research and development on HTGR fuel in the HTTR project”, Nuclear Engineering and Design, 233, 1-3, pp.163-172 (2004).

4.8.5) S. Takada, et al., “Near term test plan using HTTR (high temperature engineering test reactor)”, Nuclear Engineering and Design, 271, pp.472-478 (2014).

4.8.6) N. Fujimoto, et al., “Start-up Core Physics Tests of High Temperature Engineering Test Reactor (HTTR), (II) First Criticality by an Annular Form Fuel Loading and Its Criticality Prediction

Method", Nippon Genshiryoku Gakkaishi, 42, 5, pp.458-464 (2000) (in Japanese).

4.8.7) S. Fujikawa, et al., "Rise-to-power test of the HTTR (high temperature engineering test reactor)", Transactions of the Atomic Energy Society of Japan, 1, 4, pp.361-372 (2002) (in Japanese).

4.8.8) S. Fujikawa, et al., "Achievement of reactor-outlet coolant temperature of 950° C in HTTR", Journal of Nuclear Science and Technology, 41, 12, pp.1245-1254 (2004).

4.8.9) Y. Tachibana, et al., "Plan for first phase of safety demonstration tests of the High Temperature Engineering Test Reactor (HTTR)", Nuclear engineering and design, 224, 2, pp.179-197 (2003).

4.8.10) K. Takamatsu, et al., "Experiments and validation analyses of HTTR on loss of forced cooling under 30% Reactor power", Journal of Nuclear Science and Technology, 51, 11-12, pp.1427-1443 (2014).

4.8.11) D. Tochio, et al., "Result of long-term operation of HTTR; Rated/parallel-loaded 30-days operation", JAEA-Technology 2009-005 (2009), 47p (in Japanese).

4.8.12) K. Takamatsu, et al., "High temperature continuous operation in the HTTR (HP-11); Summary of the test results in the high temperature operation mode", JAEA-Research 2010-038 (2010), 59p (in Japanese).

4.8.13) D. Tochio, et al., "Helium leak and chemical impurities control technology in HTTR", Journal of Nuclear Science and Technology, 51, 11-12, pp.1407-1412 (2014).

4.8.14) N. Sakaba, et al., "Coolant chemistry of the high temperature gas-cooled reactor 'HTTR'", Transactions of the Atomic Energy Society of Japan, 3, 4, pp.388-395 (2004) (in Japanese).

4.8.15) S. Hamamoto, et al., "Investigation of chemical characteristics of primary helium gas coolant of HTTR (high temperature engineering test reactor)", Nuclear Engineering and Design, 271, pp.487-491 (2014).

4.8.16) A. L. Dipu, et al., "Assessment of amount and concentration of tritium in HTTR-IS system based on tritium behavior during high-temperature continuous operation of HTTR", Annals of Nuclear Energy, 88, pp.126-134 (2016).

4.8.17) Y. Shimazaki, et al., "Development of the Prediction Technology of Cable Disconnection of In-Core Neutron Detector for the Future High-Temperature Gas-Cooled Reactors", Journal of Nuclear Engineering and Radiation Science, 2, 4, pp.041008-1 - 041008-5 (2016).

4.8.18) S. Nakagawa, et al., "Development of the Unattended Spent Fuel Flow Monitoring Safeguards System (UFFM) for the High Temperature Engineering Test Reactor (HTTR) (Joint research)", JAEA-Technology 2007-003 (2007), 24p.

4.8.19) A. Shimizu, et al., "Development of operation and maintenance technology for HTGRs by using HTTR (High Temperature engineering Test Reactor)", Nuclear Engineering and Design, 271, pp.499-504 (2014).

Table 4.8.1 History of HTTR operation time

Fiscal year	Operation name	Operation mode	Purpose
1998	First Criticality test	-	First criticality and criticality test
2000	1st phase rise-to-power test (PT-1)	RS/RP	Power-up test up to reactor power 9MW in rated operation
2000	2nd phase rise-to-power test (PT-2)	RS/RP	Power-up test up to reactor power 20MW in rated operation
2001	3rd phase rise-to-power test (PT-3)	HS/HP	Power-up test up to reactor power 20MW in high temperature test operation
	4th phase rise-to-power test (PT-4)	RS/RP	Power-up test up to reactor power 30MW in rated operation
2002	1st operation cycle	RP/RS	CR withdraw test at reactor power 9MW
	2nd operation cycle	RS	・CR withdraw test at reactor power 15MW ・A gas circulator trip test at reactor power 9MW
2003	3rd operation cycle	RP/RS	Automatic reactor scram (primary coolant flow rate of PPWC; Low due to malfunction of a relay for a G/C)
	4th operation cycle	RS	Two gas circulators trip test at reactor power 9MW
	5th operation cycle	RS	・CR withdraw test at reactor power 15MW ・A gas circulator trip test at reactor power 18MW ・Two gas circulators trip test at reactor power 18MW ・Coolant flow reduction test at reactor power 18MW
2004	5th phase rise-to-power test (PT-5)	HS/HP	Power-up test up to reactor power 100% in high temperature test operation
2004	6th operation cycle	RS	Automatic reactor scram (Differential of control rod position; Large due to operation error)
2005	7th operation cycle	RS	Automatic reactor scram (Loss of off-site electric power)
2006	8th operation cycle	RS	・CR withdraw test at reactor power 24MW ・Two gas circulators trip test at reactor power 24MW ・Coolant flow reduction test at reactor power 24MW
	9th operation cycle	RS	・Two gas circulators trip test at reactor power 30MW ・Coolant flow reduction test at reactor power 30MW
2006-2007	10th operation cycle	RP	Demonstrate 30-days full-power operation in rated operation
2009	11th operation cycle	HP	Demonstrate 50-days full-power operation in high temperature test operation
2010	12th operation cycle	RS	Loss of Core Coolant Flow Test (All-gas-circulator trip test) at reactor power 9MW
	13th operation cycle	RS	Loss of Core Cooling Test (All-gas-circulator trip test with VCS inactive) at reactor power 9MW

R: Rated operation mode　　S: Single loaded operation mode
H: High temperature test operation mode　　P: Parallel loaded operation mode

Table 4.8.2 Phases and remarks from design and manufacturing to reactor operation at full power

Phases	Test items	Remarks	Check items*2
Research and development	—	・Manufacturing and processing technologies of graphite and carbon material. ・Welding technologies of high temperature components.	
Manufacturing	—	・Manufacturing technologies of graphite and carbon components, high temperature components and structures, etc.	
Installation	—	・Acceptance tests ・Installation of equipment in the compact facility of HTTR reactor building and transport between narrow spaces.	
Pre-operation test	・Component functional test at site ・System functional test	To pick up initial failure/trouble	
	Whole system functional test	Non-nuclear heat up tests, etc.	(a), (b)
	Confirmation test	To check the countermeasures for defect	(a)
Startup core physics test	First criticality test	First critical: 19 columns (total: 30 columns)	(c)
	Core physics characteristics test	Annular core and full core tests	(c)
Power-up test	Up to 10MW test at 850 ℃	Preparations of high power operation	(a), (b), (c)
	UP to 20MW test at 850 ℃	—	
	UP to 20MW test at 950 ℃	To check heat leakage around core bottom	(a), (b)
	Full-power test at 850 ℃	—	
	Full-power test at 950 ℃	After reevaluation based on above tests	(a)

*1 Acceptance inspection standards for fuel, graphite, B_4C / C, which are characteristic materials of HTGR, were established.
*2 HTTR is devised so these three leakage phenomena – Heat, Helium, Radiation - can be detected at an early stage in consideration of characteristics of HTGR.
(a)Heat leakage, (b)Helium leakage, (c)Radiation leakage

Table 4.8.3 The inspection item, purpose, method and sampling rate in the HTTR fuel[4.8.4)] fabrication

Inspection item	Major purpose*	Method	Sampling rate
Fuel kernel			
^{235}U enrichment	B	Mass spectrometer analysis and gamma-ray spectrometer analysis	1 sample/enrichment
Diameter	B	Optical particle size analysis	1 sample (100 particles)/fuel kernel lot
Sphericity	A	Optical particle size analysis	3 samples (100 particles/sample)/fuel kernel lot
Density	B	Mercury substitution	3 samples/fuel kernel lot
O/U ratio	A	Oxidation and weighing	1 sample/fuel kernel lot
Impurities	A, B	Emission spectrometer analysis	1 sample/enrichment
Coated fuel particle			
Layer thickness	A	Solvent substitution or sink-float	3 samples/coated fuel particle lot
Optical anisotropy factor	A	Polarization photometer	1 sample (5 particles/sample)/enrichment
Diameter	B	Optical particle size analysis	1 sample (100 particles)/coated fuel particle lot
Appearance	A	Visual observation	1 sample (2000 particles)/coated fuel particle lot
Cross section	A	Ceramography	1 sample (20 particles)/coated fuel particle lot
Sphericity	A	Selection by vibration table	All coated fuel particles
Strength	A	Point crushing	30 particles/enrichment
Fuel compact			
^{235}U enrichment	D	Mass spectrometer analysis and gamma-ray spectrometer analysis	1 sample/enrichment
U content	B	gamma-ray spectrometer analysis	All fuel compacts
O/U ratio	A	Oxidation and weighing	1 sample/fuel compact lot
Graphite powder	A	Density, impurities, grain size and water content	1 sample/graphite powder lot
Binder	A	Contents, ash, melting point and impurities	1 sample/binder lot
Exposed uranium fraction	A	Deconsolidation and acid leaching	2 samples/fuel compact lot
SiC-failure fraction	A	Burn and acid leaching	3 samples/fuel compact lot
Packing fraction	B	Weighing and calculation	3 samples/fuel compact lot
Matrix density	A	Weighing and calculation	3 samples/fuel compact lot
Dimensions	C	Micrometer	All fuel compacts
Appearance	A	Visual observation	All fuel compacts
Marking	D	Visual observation	All fuel compacts
Strength	A	Compression	3 samples/enrichment
Cross section	A	Ceramography	1 sample/fuel compact lot
Impurities	B	Emission spectrometer analysis	1 sample/enrichment

*A: Irradiation performance, B: Nuclear design, C: Thermal-hydraulic design, D: Process control

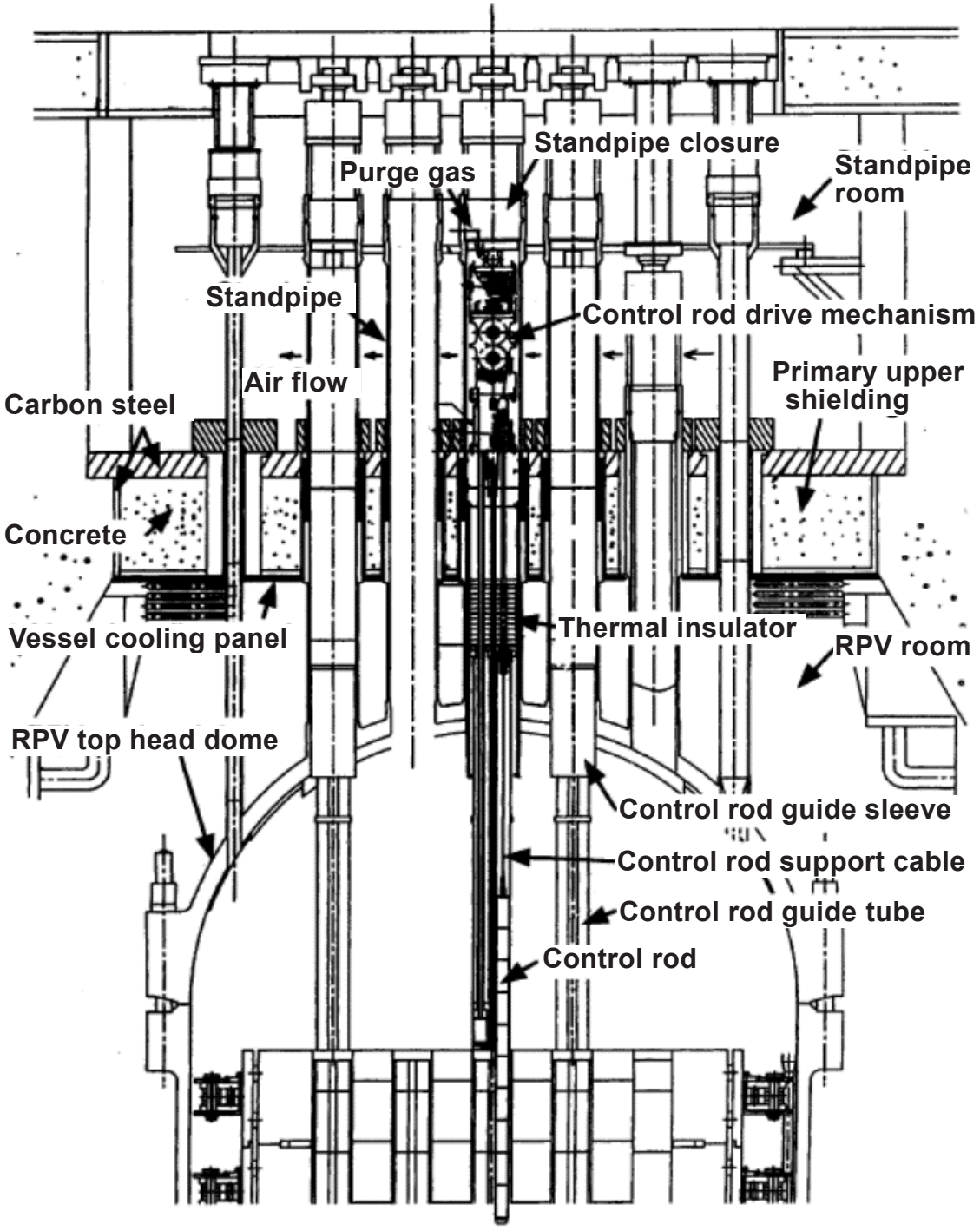

Fig. 4.8.1 Structure of standpipes, primary upper shielding, etc.[4.8.1)]

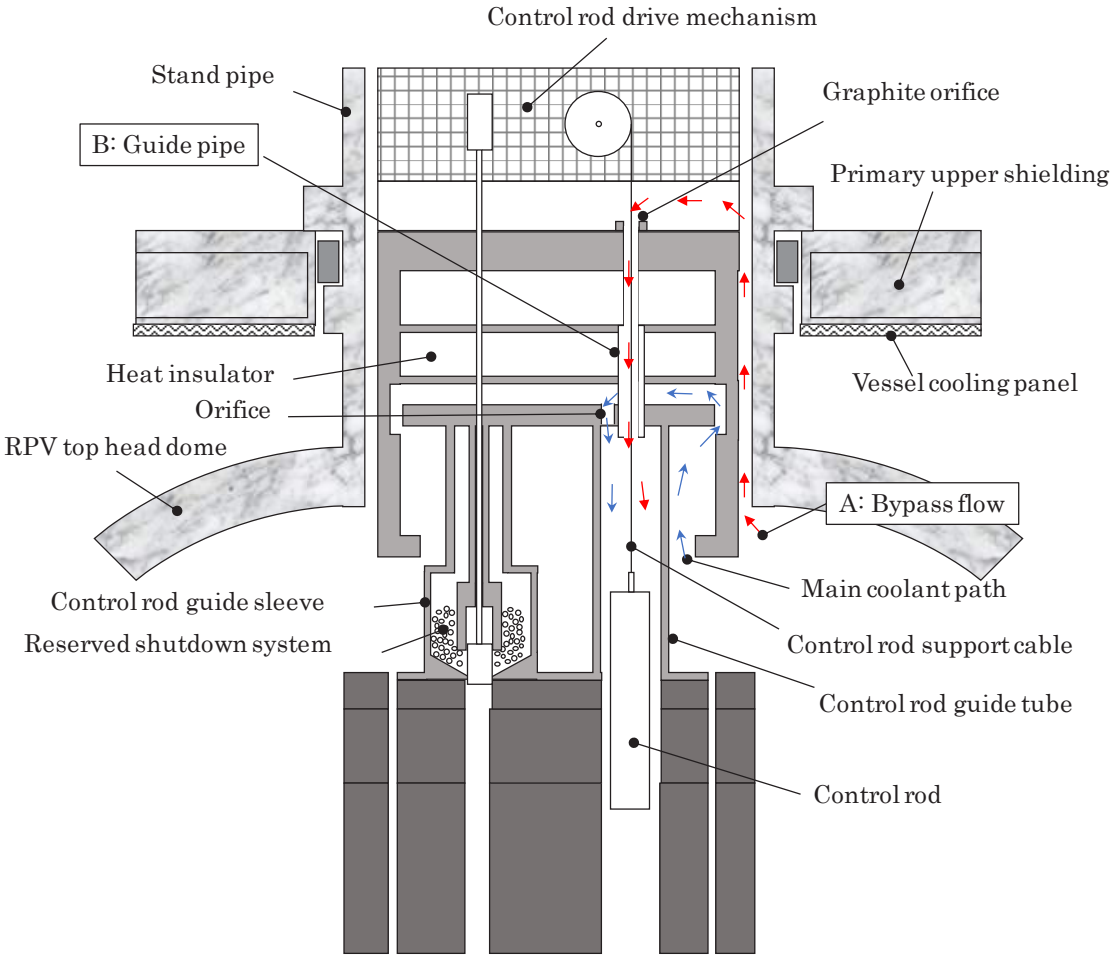

Fig. 4.8.2 Structure of inside of control rod standpipe before first countermeasure applied[4.8.1)]

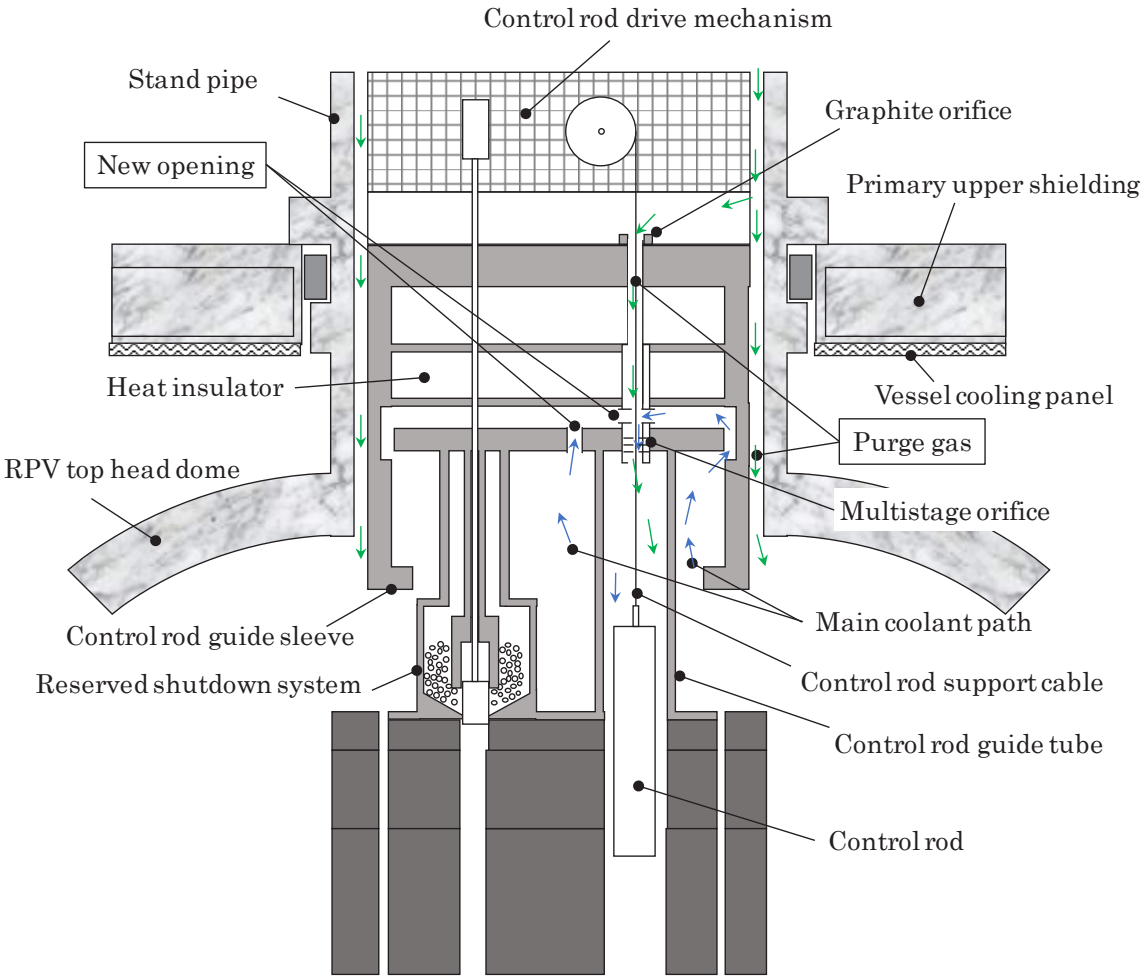

Fig. 4.8.3 Structure of inside of control rod standpipe before first countermeasure applied[4.8.1)]

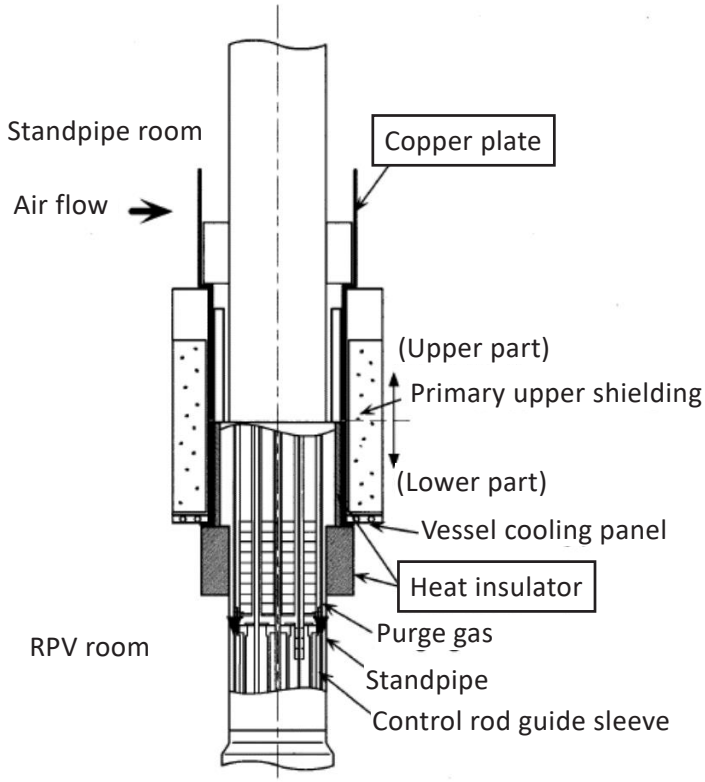

Fig. 4.8.4 Second countermeasure to prevent temperature rise of primary upper shielding[4.8.1)]

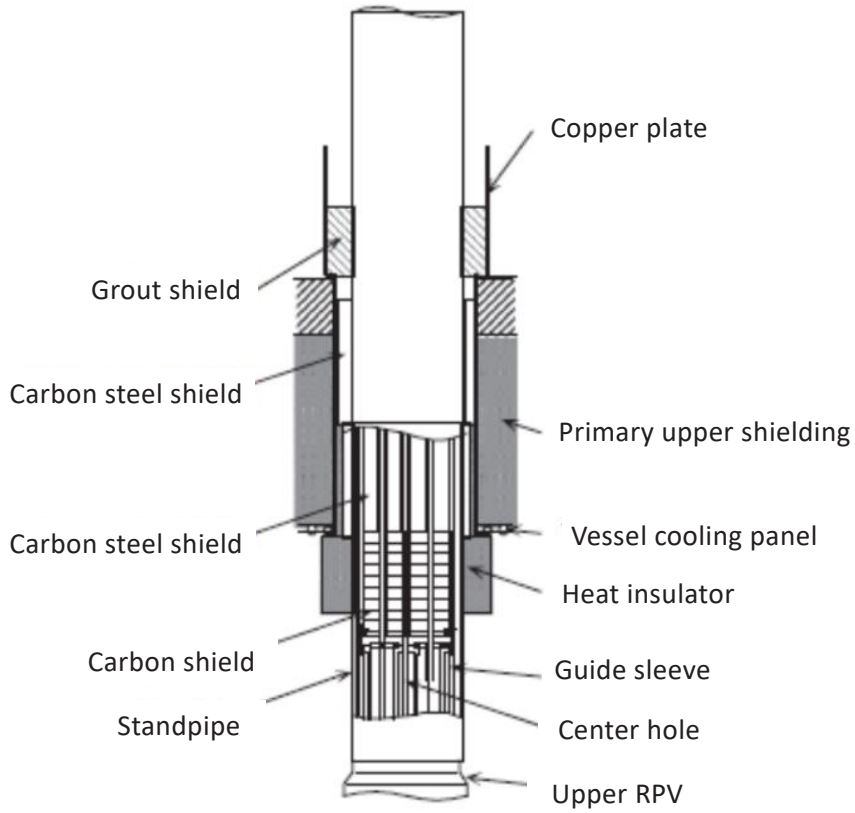

Fig. 4.8.5 Shielding structure of the standpipe[4.8.2)]

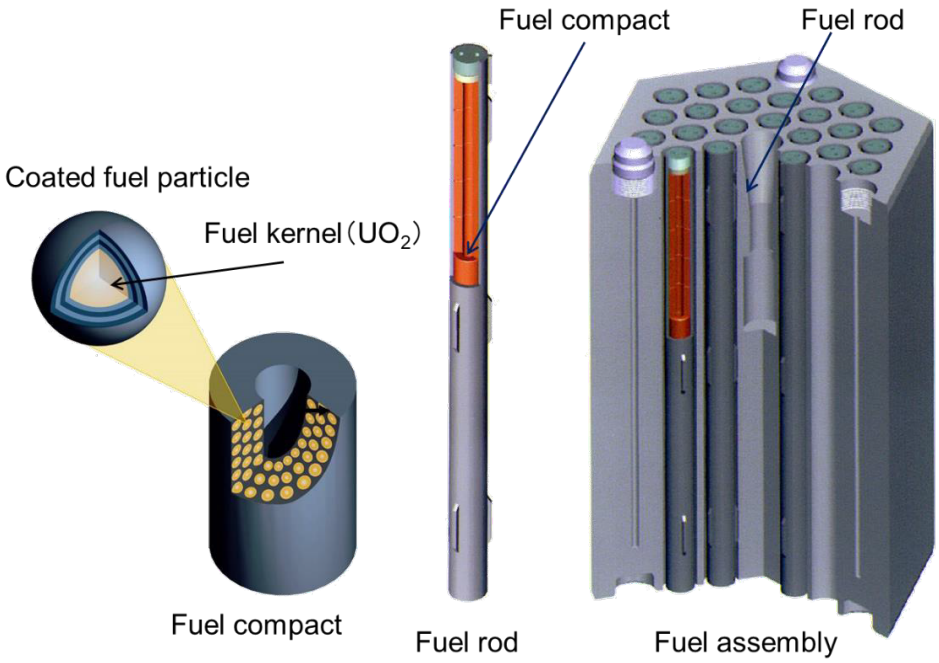

Fig. 4.8.6 HTTR fuel assembly

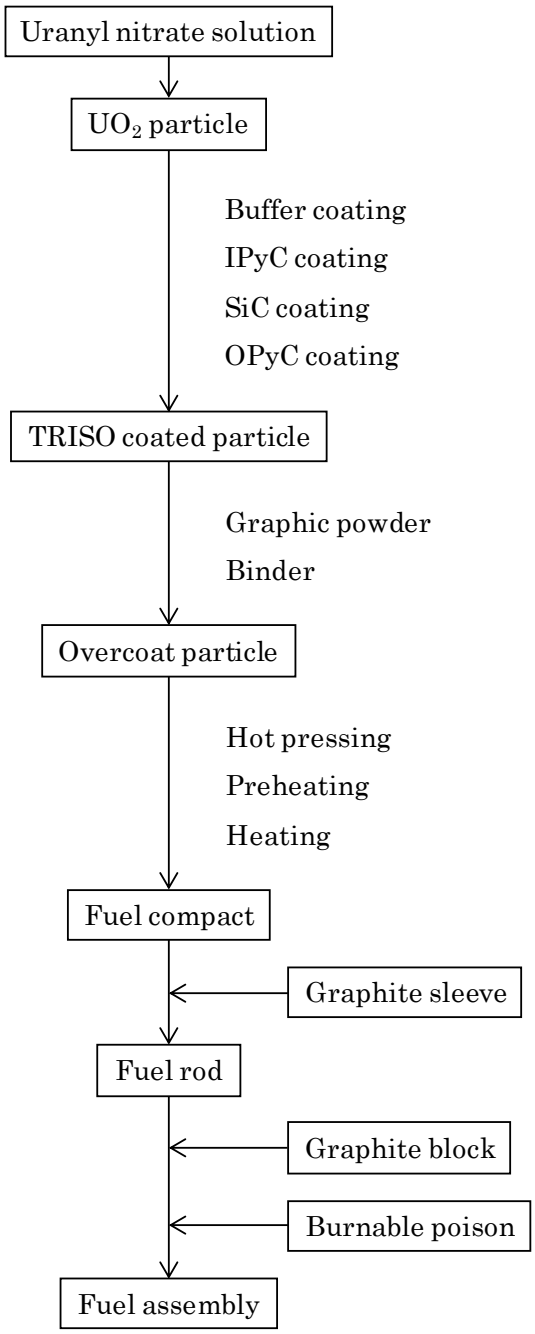

Fig. 4.8.7 Flow diagram of the fuel fabrication process

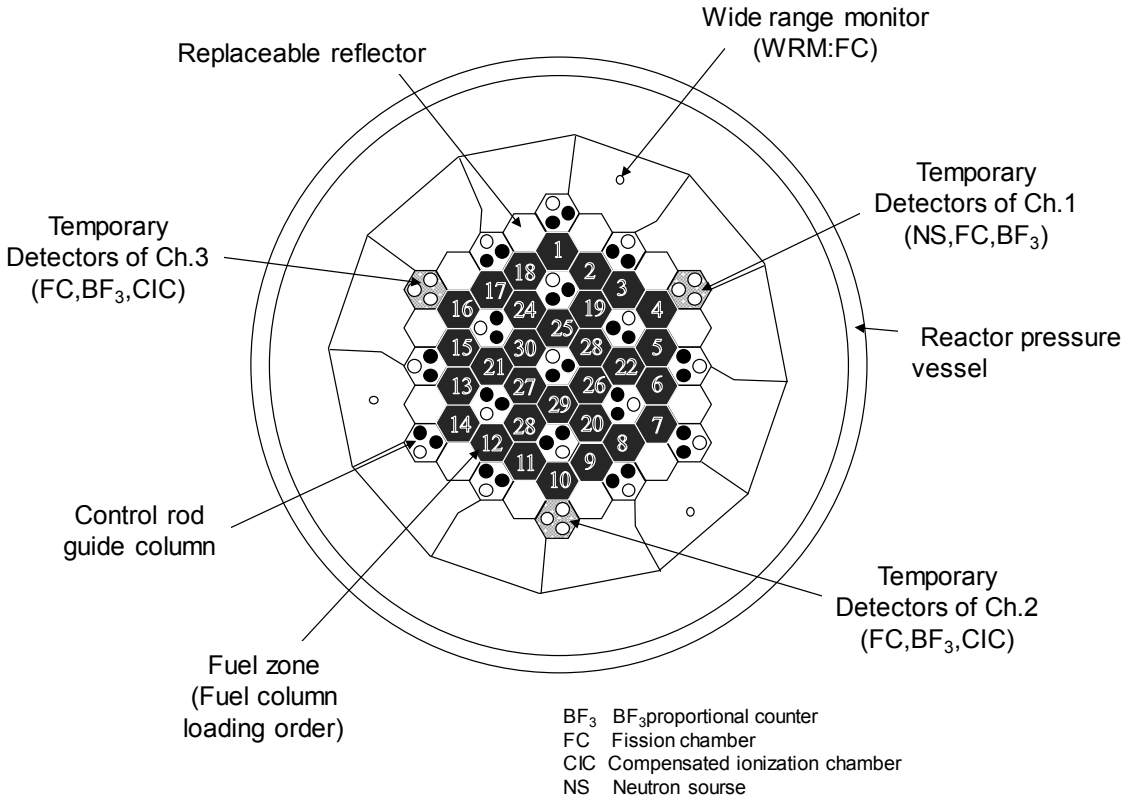

Fig. 4.8.8 Arrangement of temporary neutron detectors and fuel loading number

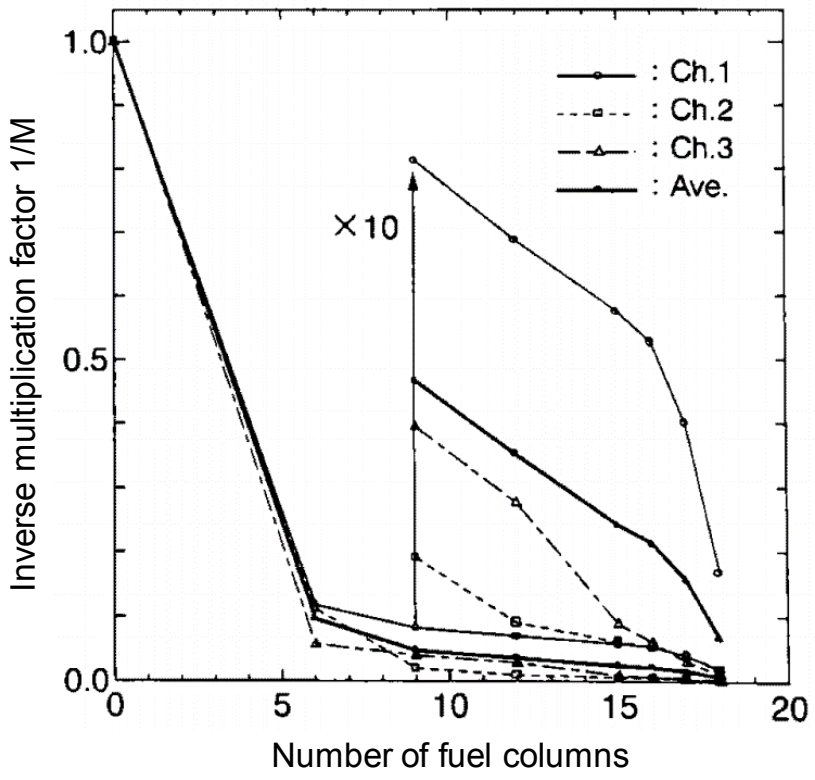

Fig. 4.8.9 Measured 1/M curves at fuel loading

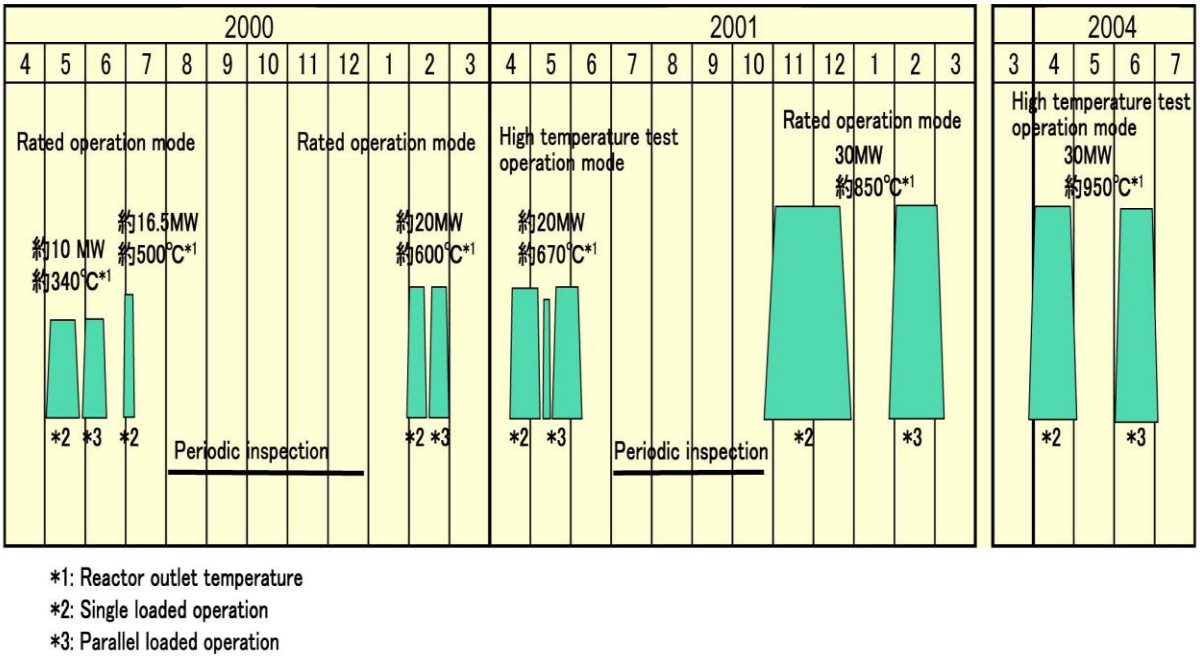

Fig. 4.8.10 Procedure for rise to power test of HTTR

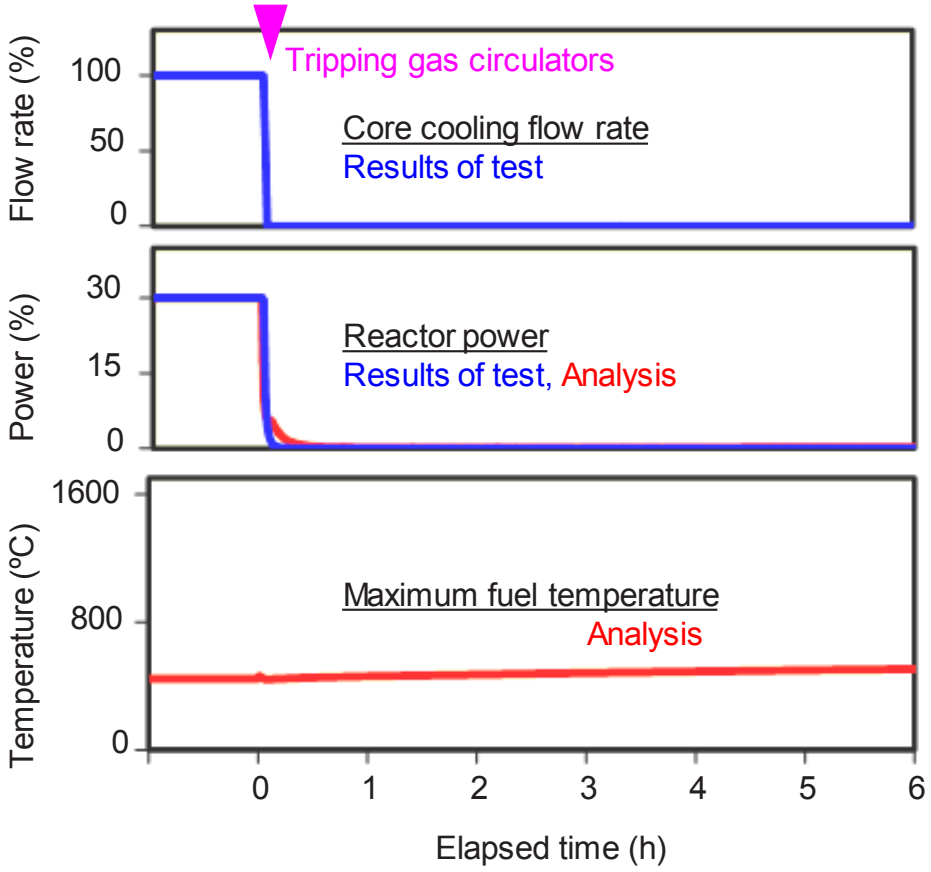

Fig. 4.8.11 Test result of loss of forced cooling (LOFC)

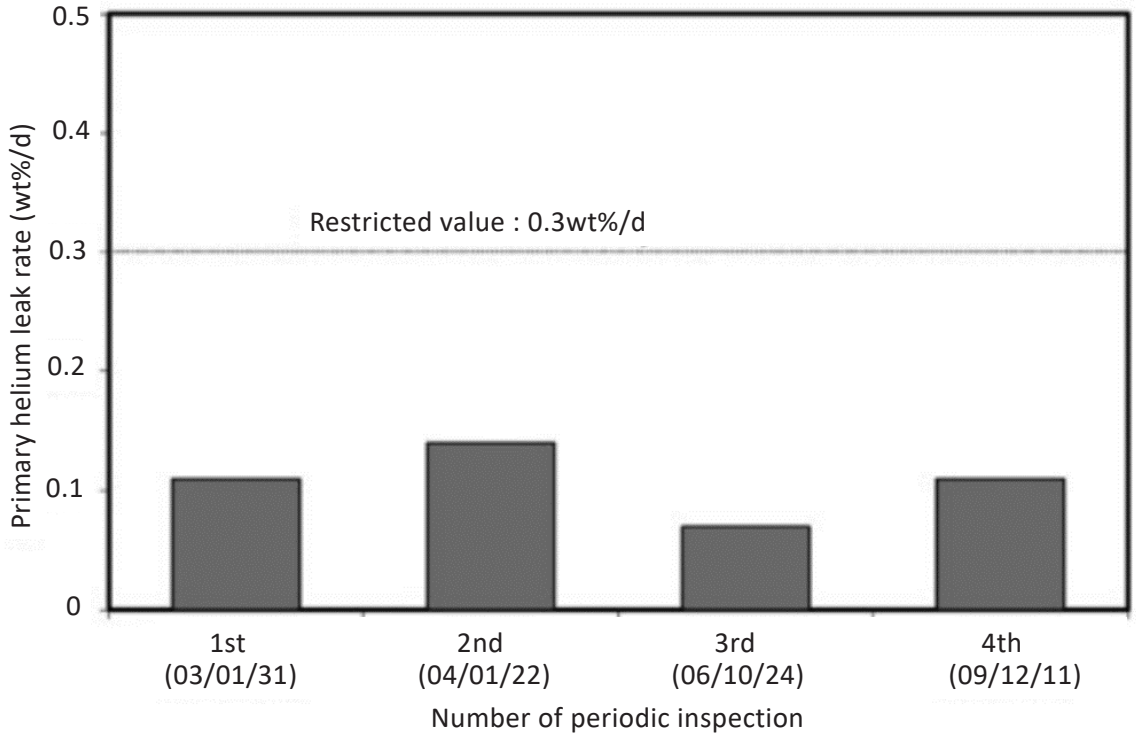

Fig. 4.8.12 Evaluated primary helium leak rate

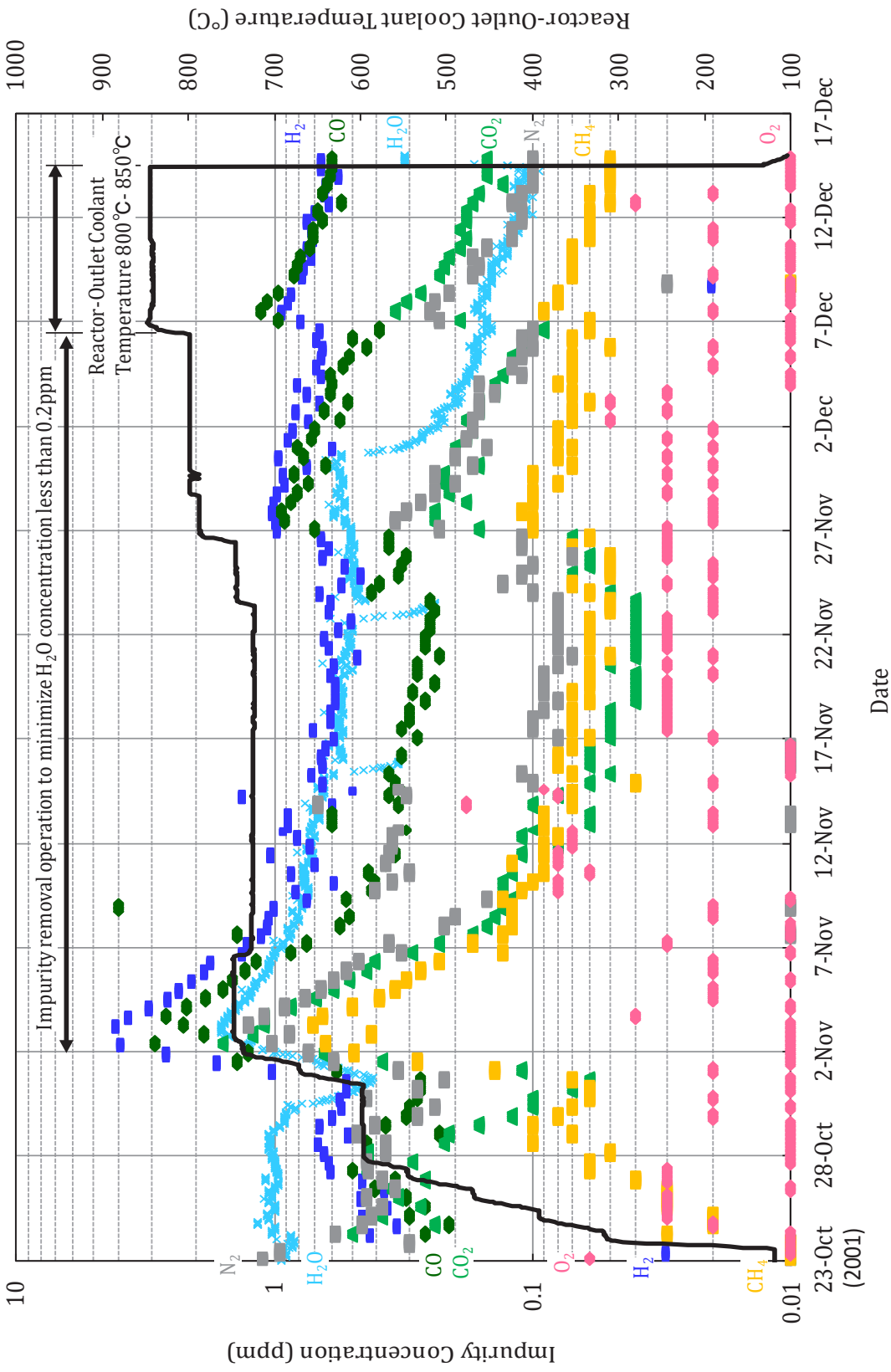

Fig.4.8.13 Chemical impurity behavior at the reactor-inlet obtained during the 850°C operation

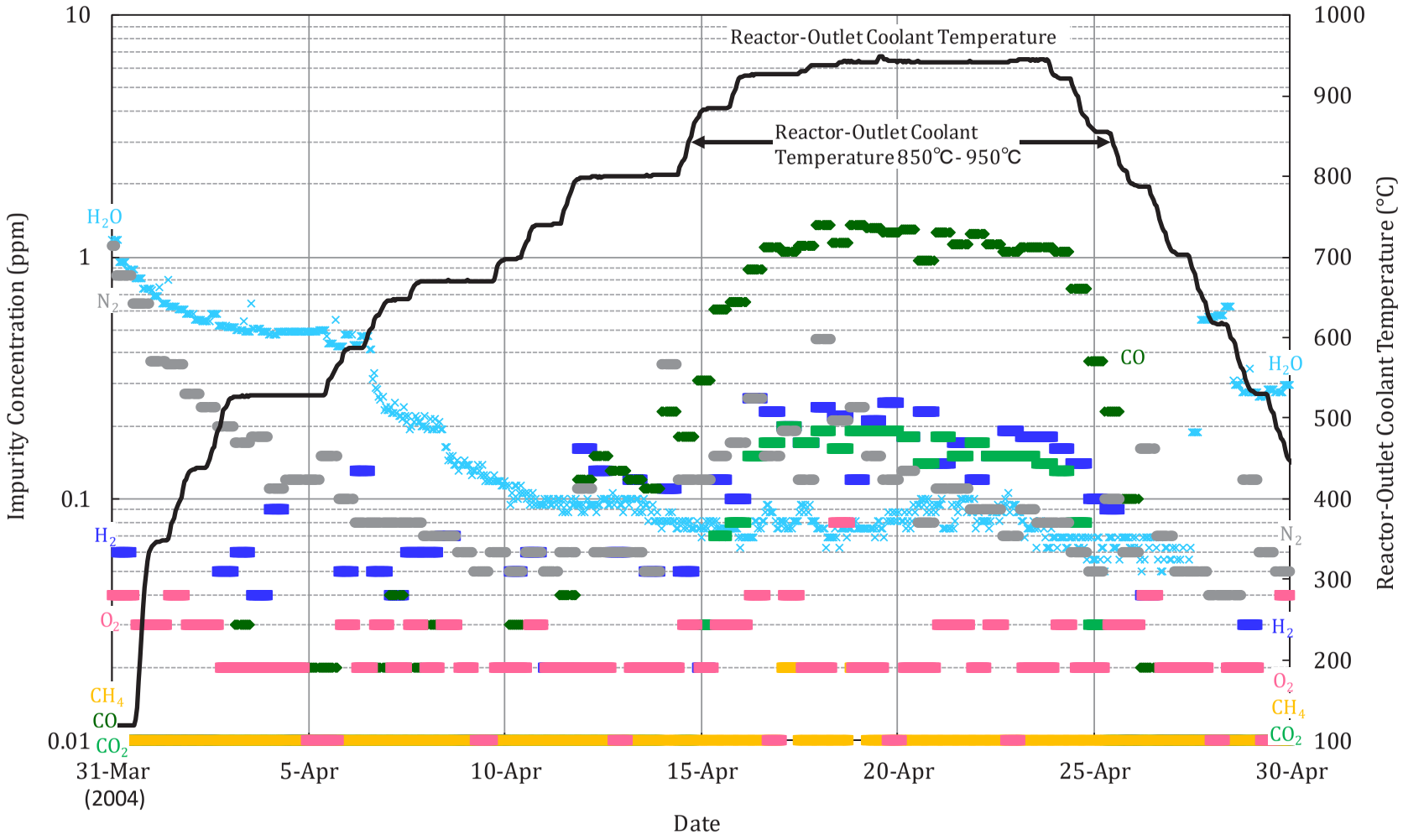

Fig.4.8.14 Chemical impurity behavior at the reactor-inlet obtained during the 950°C operation

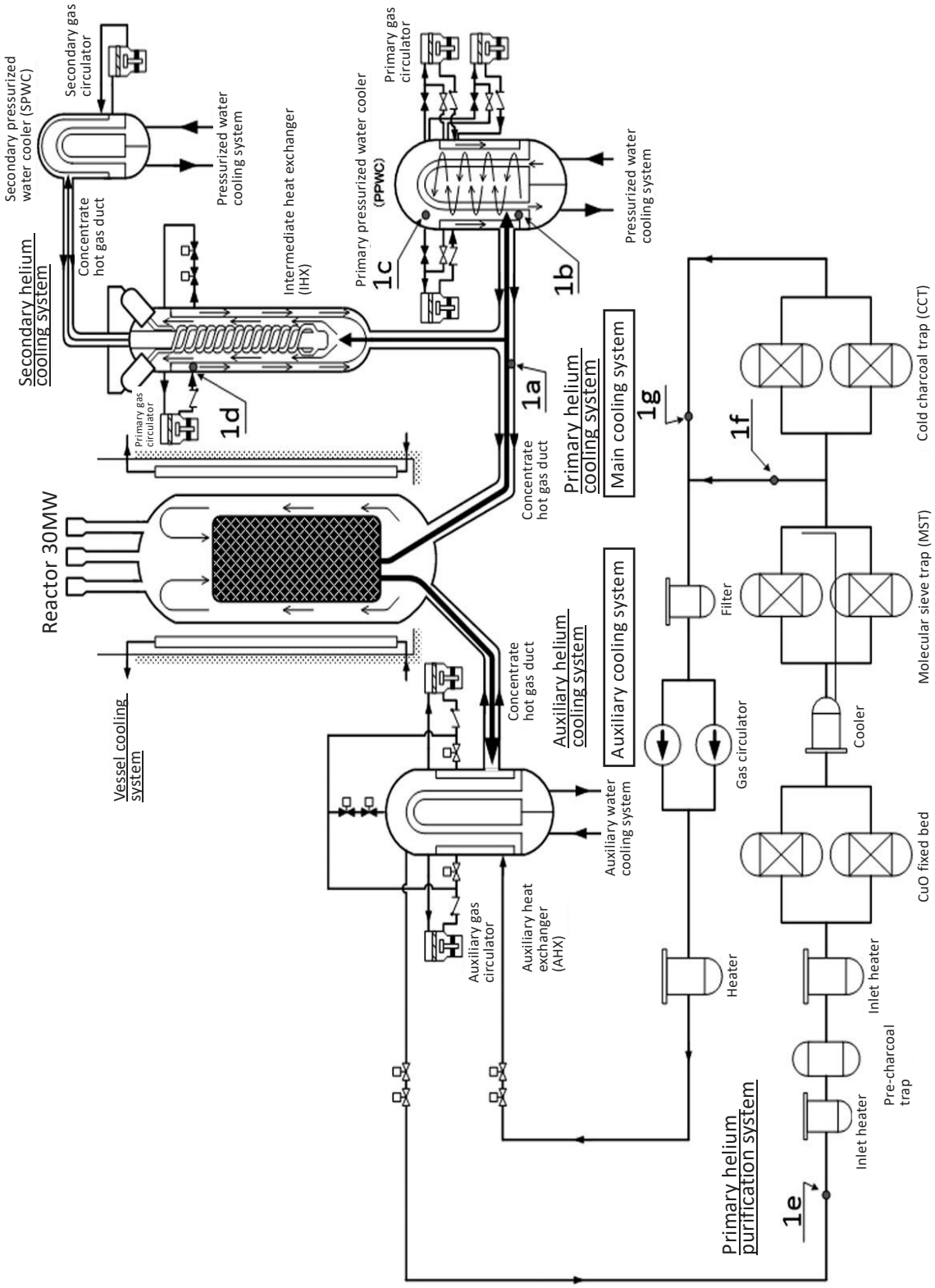

Fig. 4.8.15 Sampling points of primary helium gas

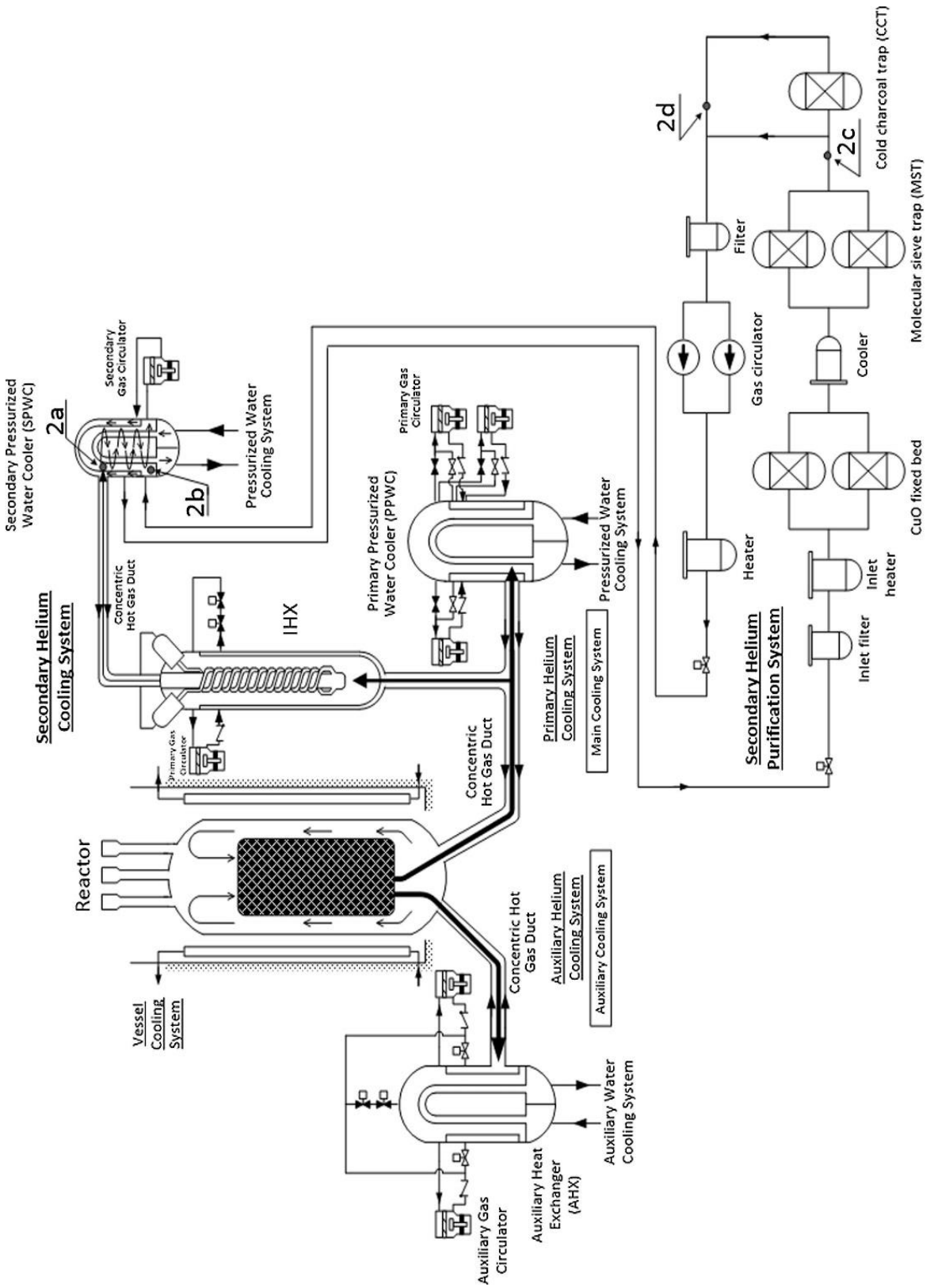

Fig. 4.8.16 Sampling points of secondary helium gas

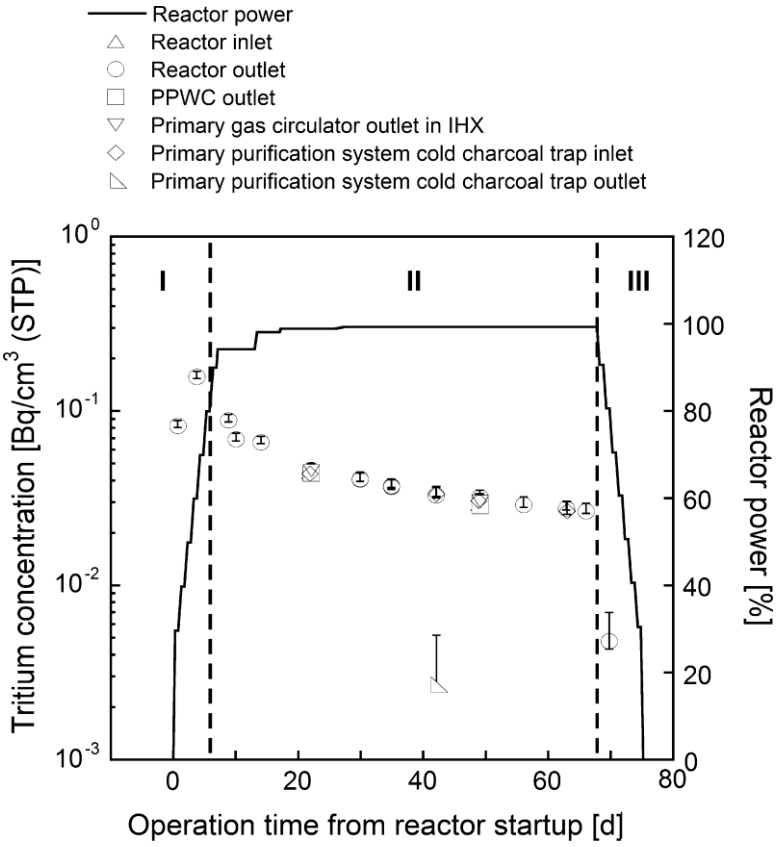

Fig. 4.8.17 Tritium concentration in primary helium gas

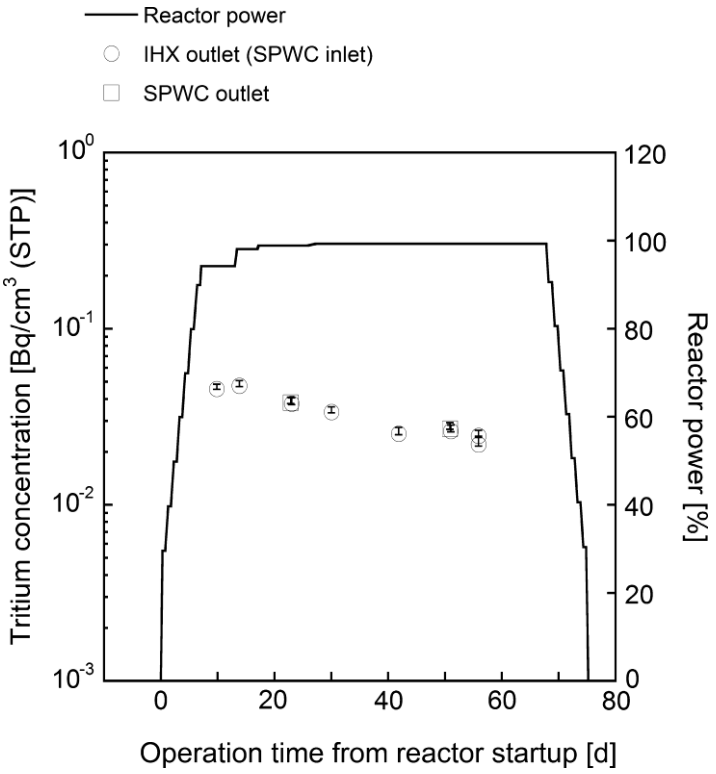

Fig. 4.8.18 Tritium concentration in secondary helium gas

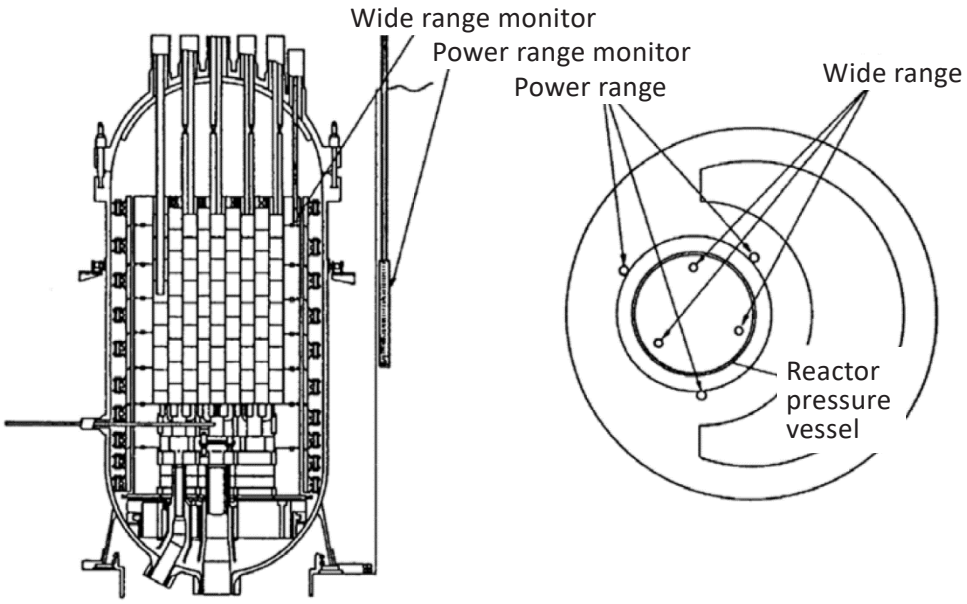

Fig. 4.8.19 Arrangement of neutron detector for WRMs and PRMs

4.9 Gas Turbine System for Power Generation

4.9.1 System design

The system design for HTGR direct gas turbine system needs to consider unique features of the closed-cycle, regenerative Brayton cycle. Several cycle parameters such as reactor outlet temperature, pressure ratio, turbine cooling flow rate, etc. should be optimized to maximize plant economics. These parameters heavily depend on system configuration and component specifications (cf. Table 4.9.1). For example, 1% increase in pressure drop reduces 0.7% of cycle efficiency. The pressure drop is determined by component design as well as flow rate in the system, which is strongly correlated with cycle pressure ratio pressure drop. Hence, the design requires iterative process and dedicated system design code is needed to determine optimum design point of the system. JAEA has a system design code of HTGR gas turbine system which includes design database of various reactors and gas turbines and which is verified by HTTR operation data. We have performed system design for several plants including commercial power generation plant[4.9.1), 4.9.2)], cogeneration plant [4.9.3)], and test plant [4.9.4)].

4.9.2 Aerodynamic design

Use of helium gas as working fluid is favorable in terms of avoiding losses due to sonic wave/boundary layer interactions because sonic speed of the helium gas is about three times of that of the air. However, the helium gas has approximately five times high specific heat than air which is used in industrial gas turbine, which leads to low volumetric flow rate, large number of blade rows and low blade height. If the blade height becomes too low, the efficiency may significantly decrease due to aerodynamic losses associated with surface and end wall boundary layer growth, secondary and clearance flows. In order to achieve compressor efficiency of more than 90%, a design target of commercial helium gas turbine with due considerations to assure 20% of surge margin, special consideration should be taken in aerodynamic design.

JAEA collaborates with Japanese gas turbine industry to develop original design techniques for helium compressor. Regarding the aerodynamic design, we decided to employ three dimensional blade airfoil to eliminate boundary layer flow separation on blade (cf. Fig.4.9.1). We also conducted 1/3 of full scale compressor tests to validate the design methods (cf. Fig.4.9.2). The measurement in the test includes internal flow path boundary layer measurements, airfoil performance measurements, inlet/outlet casing geometry performance measurements, and compressor efficiency and surge margin. As a result of a series of studies we have achieved improvement of performance prediction model over existing air-based model and confirmed that commercial scale compressor can attain efficiency of 91.5% (cf. Fig.4.9.3).

4.9.3 Shaft seal technology

One of the important design concerns in a helium gas turbine in direct cycle power generation plant is a leakage in a turbo machinery because the primary helium leakage is strictly limited in terms of safety. Especially, the shaft seal requires careful consideration when an external generator design is selected because the gas turbine shaft with a large diameter penetrates the power conversion vessel, which

constitutes the reactor pressure boundary.

We are proposing a hybrid shaft seal system which consists of multiple mechanical seals and a dry gas seal with multiple pressure controls. Figure 4.9.4 shows the concept of the proposed system. Currently, we are performing a conceptual design of the system. We are also investigating a test plan for element test to confirm the performance of the system. We will also install the shaft seal system to gas turbine to be connected to the HTTR in order to demonstrate sealing performance during transient conditions.

4.9.4 Turbine blade alloy

One of the most controversial topics for deployment of power conversion unit in a direct-cycle HTGR is the FP plate-out issues. Several past experiment results indicated that a large amount of FP may deposit on the power conversion unit if installed in the primary loop. Especially transport behavior of radioactive silver 110mAg has been paid attention because irradiation test results for TRISO coated fuel particle shows that SiC layer of the particle do not have sufficient capability to retain the FP. In addition, the amount of 110mAg generation in the fuel increases as fuel burnup increases. The silver released from the fuel to reactor coolant transport to power conversion system and deposit on the surface of the components. The deposited silver may diffuse deeply inside turbine blades. Radiological contamination of the gas turbine causes difficulty in maintenance because periodic inspections for the turbine require pulling out the turbine internals from power conversion vessels. This may results in high dose rate for plant workers because they must perform inspections at a short distance from radiological sources without shielding. According to our evaluation, dose level due to the plate-out has significant impact on the allowable working time for the inspection of gas turbine [4.9.5)].

JAEA in conjunction with Japanese industry has been tackling the issue. We have started a development of turbine blade alloy which can reduce the amount of FP plate-out to apply the inspection method used in conventional gas turbines. Our approach is to develop a turbine blade alloy which can reduce deposition rate of sliver. In order to establish a design strategy for the alloy, we are investigating correlation between silver diffusion behavior and alloy compositions and structures. Currently, we have been conducting silver diffusion test to representative turbine alloys (cf. Fig. 4.9.5).

References

4.9.1) X. Yan, et al., “Cost and performance design approach for GTHTR300 power conversion system”, Nuclear Engineering and Design, 226, 3, pp.351-373 (2003).

4.9.2) H. Sato, et al., “GTHTR300 - A nuclear power plant design with 50% generating efficiency”, Nuclear Engineering and Design, 275, pp.190-196(2014).

4.9.3) K. Kazuhiko, et al., “JAEA’s VHTR for Hydrogen and Electricity Cogeneration: GTHTR300C”, Nuclear Engineering and Technology, 39, 1, pp.9-20 (2007).

4.9.4) X. Yan, et al., “HTTR-GT/H2 Test Plant - System Design”, Proceedings of the 2016 International Topical Meeting on High Temperature Reactor Technology (HTR2016), pp.827-836 (2016).

4.9.5) S. Kosugiyama, et al., “Maintenance Methods and Procedures for the Power Conversion System of the Gas Turbine High Temperature Reactor 300 (GTHTR300)”, Transactions of the Atomic Energy Society of Japan, 2, 4, pp.532-545 (2003) (in Japanese).

Table 4.9.1 Cycle efficiency sensitivity to cycle parameters[4.9.1)]

Cycle parameters	Change in cycle parameter	Change in cycle efficiency [%]
Turbine inlet temperature	+50 °C	+1.5
Recuperator effectiveness	+1%	+0.8
Turbine cooling flow	+1%	-0.7
Pressure drop	+1%	-0.7
Compressor inlet temperature	+5°C	-0.6
Compressor efficiency	+1%	+0.5
Turbine efficiency	+1%	+0.4
Shaft seal leak flow	+1%	-0.4

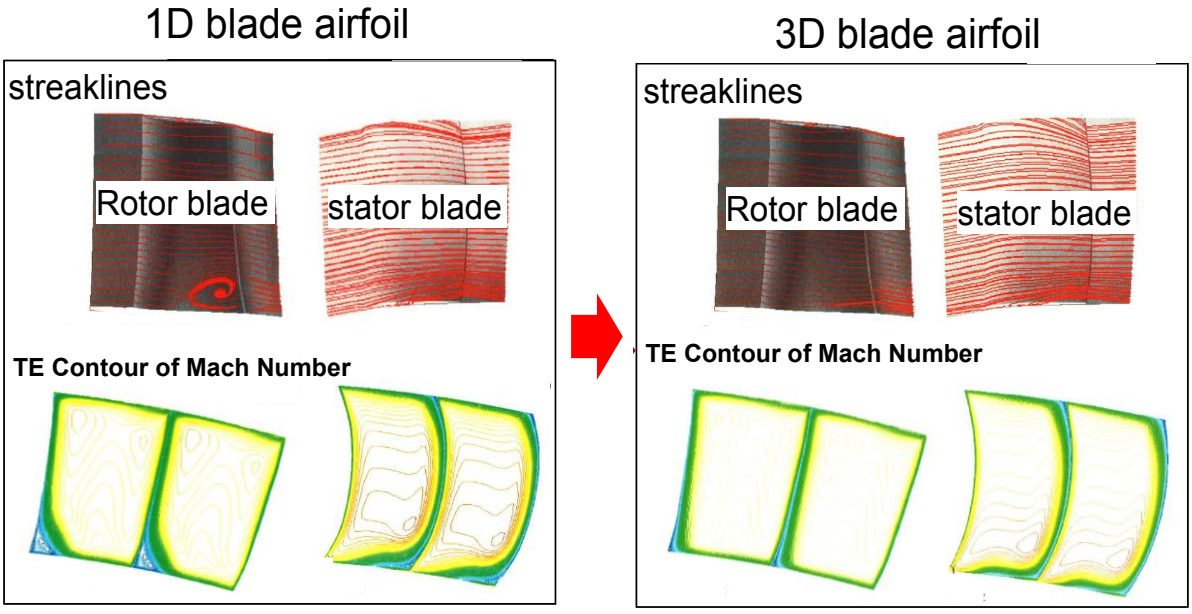

Fig.4.9.1 3D blade airfoil design

1/3 scale compressor

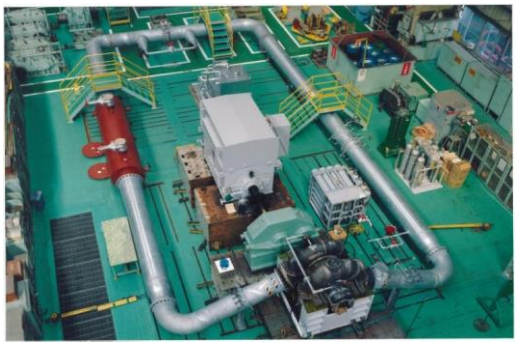

Test loop

1/3 scale compressor

Comparison between commercial and 1/3 scale compressors

	Commercial	1/3 scale
Stage number	20	4
Blade number/stage	72	72
Tip speed (m/s)	321	321
Rotational speed (rpm)	3600	10800
Pressure ratio	2.0	1.16

Test condition

Working fluid	Helium gas
Pressure	Max. 1.0MPa
Temperature	30°C

Test results

- Accurately predict commercial compressor performance by 3D CFD analysis and 1/3 scale test results
- Commercial compressor can attain efficiency of 91.5%

Fig.4.9.2 Mock-up scale compressor test

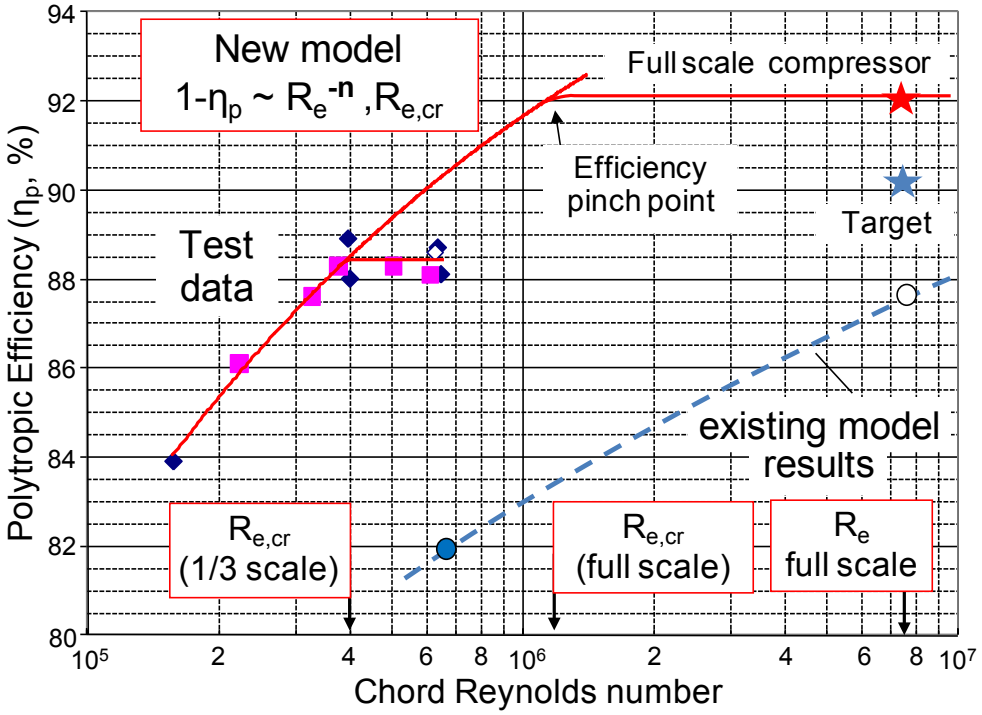

Fig.4.9.3 Commercial compressor performance prediction

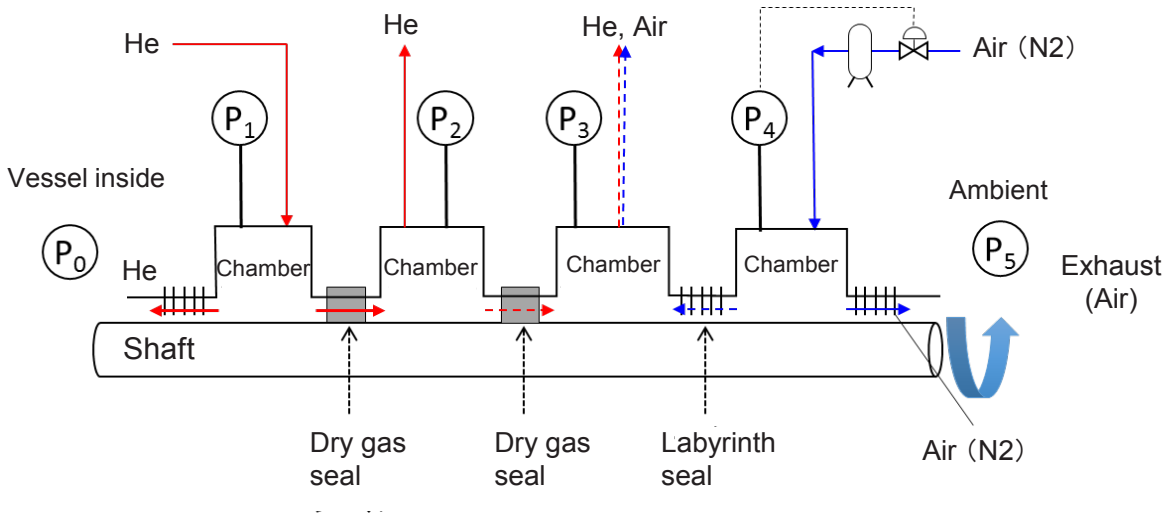

Fig.4.9.4 Concept of a hybrid shaft seal system

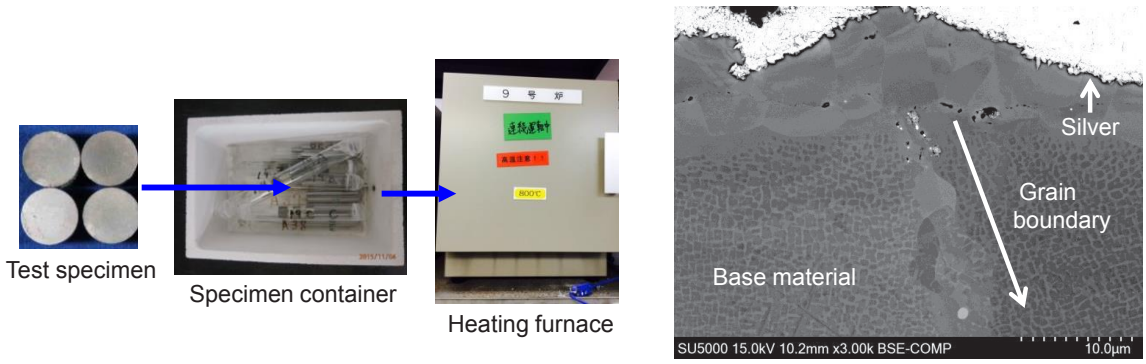

Fig.4.9.5 Silver diffusion test to turbine blade alloys

4.10 Iodine-Sulfur Process for Hydrogen Production

4.10.1 Outline of Iodine-Sulfur Process

A thermochemical water-splitting process offers the potential for the mass production of hydrogen at high levels of efficiency without using carbon dioxide, supplied with heat from HTGRs. This process is one of water-splitting methods to produce hydrogen by using chemical reactions. The iodine-sulfur (IS) process[4.10.1)] that uses iodine and sulfur compounds is most attractive thermochemical methods; as matter of fact, this method has been most deeply investigated while over 100 thermochemical processes using various chemicals have been proposed up to now. Fig. 4.10.1 is a chemical scheme of the IS process, in which iodine and sulfur compounds circulates to make the water-splitting by combining chemical reactions. This process is composed of the following chemical reactions:

SO_2 (g) + I_2 (aq) + 2H_2O (aq)→2HI (aq) + H_2SO_4 (aq) …… Bunsen reaction (ca. 100℃)
2HI (g)→H_2 (g) + I_2 (g) …… Hydrogen iodide decomposition (ca. 500℃)
H_2SO_4 (g)→H_2O (g) + SO_2 (g) + 0.5O_2 (g) ……Sulfuric acid decomposition (ca. 850℃)

where “aq” and “g” mean the aqueous phase and gaseous phase. The Bunsen reaction produces two acids, hydriodic acid (hydrogen iodide in water) and sulfuric acid, from water, and sulfur dioxide and iodine as raw materials in an aqueous solution. The mixed acid separates into two types of acid of its own accord (liquid-liquid phase separation). The acid, which is rich in HI, is HIx phase, while the acid, which is rich in H_2SO_4, is H_2SO_4 phase. After separation of the acids, they are purified and concentrated. Then, gasified HI/H_2SO_4 is separated from the solutions by distillation/vaporization, and decomposed in the other two reactions in the gaseous phases. The hydrogen iodide decomposes into iodine and hydrogen. The sulfuric acid decomposes into water, sulfur dioxide and oxygen. These three reactions as a whole force the water to split into hydrogen and oxygen. The products of the sulfur dioxide, the iodine and the water can be used again for the production of acids in the Bunsen reaction. The decomposition of sulfuric acid proceeds at temperatures of around 900℃ and absorbs heat. The decomposition of hydrogen iodide involves a small endothermic reaction around 500℃. The Bunsen reaction occurs exothermically at temperatures of about 100℃. These three reactions make a chemical cycle which converts water to hydrogen.

4.10.2. R&Ds of the IS process in JAEA

JAEA has conducted R&D on the IS process, in particular, on stable hydrogen production, high thermal efficiency for hydrogen production, stable operation of components in corrosive environments, and safety in integration of heat application system and the HTGR. Fig. 4.10.2 illustrates the R&D progress in JAEA. At the laboratory stage, 1 L/h of hydrogen production was accomplished[4.10.2-4.10.3)] for 48 by finding inhibition factors (side reactions etc.) and appropriate reaction conditions (temperature, composition). At the next basic engineering stage, a plant control technology, which almost automates the operation of hydrogen production, was developed for stable hydrogen production. Continues hydrogen production of 30 L/h for 1 week was carried out keeping the amount of hydrogen and oxygen generated at a

stoichiometric ratio (2:1) [4.10.4-4.10.5].

At present, the R&D is at the stage of industrial material components test. In the stage, Corrosion-resistant components made of industrial material of 100 L/h hydrogen production scale are developed, which are installed to a hydrogen production test facility to verify the soundness of plant-wide equipment and hydrogen production performance, etc. since 2014.

The test facility of hydrogen production was constructed applying appropriate practical structure materials selected for all the components considering operation condition and environment. Fluoroplastic lined steel, glass lined steel, SiC ceramic, and impervious graphite were applied for liquid environments. Hastelloy C276, a nickel based alloy, and SUS 316, a stainless steel, were used for vapor environments. Electric heaters are used to supply required heat.

Firstly, gastight function, gas distribution function, liquid flow and heating were confirmed as basic functions checking. After that, the processing rate data in each reactor (hydrogen production by HI decomposition reactor etc.), separation and gasification function (HI gas distillation etc.), were acquired. The entire process connecting the three process sections was operated in hydrogen production [4.10.6] for 8 hours at rate of 10 L / h in Feb. 2014, and in Oct. operation was extended to 31 hours at twice the hydrogen production rate (20 L/h). Through these operations, technical issues were obtained that prevention of clogging and stable control of solution composition in Bunsen reaction process are important for next longer operation. Currently, in order to achieve longer-term stable operation and to confirm the operation procedure including start-up and shutdown, improvements of equipment are under way. Besides, membrane technologies for improvement of thermal efficiency[4.10.7] and a strength evaluation method of ceramic reactors[4.10.8] are under development.

In future, a HTTR-GT/H_2 test, integration of a helium gas turbine power generation (GT) and hydrogen production with a high temperature test reactor (HTTR), a test reactor of HTGR settled in JAEA Oarai, is planned to establish safety design standards for connecting nuclear reactor and heat application systems.

4.10.3 Selection of Candidate Structural Materials

Corrosive chemicals should be used in the IS process because of the environments in which the chemical reactions and unit operations are proceeded. In the various phases and over a wide temperature range, corrosive halogens and sulfur compounds should be handled to work the process. Up to now, many investigations and screening tests of structural materials to fabricate corrosion-resistant equipment have been conducted[4.10.9-4.10.21] in representative process environments.

Candidate structural industrial materials have been selected from the viewpoint of corrosion resistance and commercial availability based on previous researches. Fig. 4.10.3 shows a brief outline of the candidates. For the gas phase environment, in the H_2SO_4 decomposition step, some refractory alloys that have been used in conventional chemical plants showed good corrosion resistance. In the HI decomposition step, a Ni-Cr-Mo-Ta alloy was found to show good corrosion resistance. For gas phase service, there are few concerns on structural materials. Meanwhile, the liquid phase environments are more severe than the gas phase environments. In HIx distillation at 20 bar, Ta showed excellent corrosion

resistance. Under boiling conditions of concentrated sulfuric acid under high pressure (e.g. 20 bar), ceramic materials containing silicone such as SiSiC, SiC, and Si_3N_4 showed excellent corrosion resistance. Because of the brittle behavior of ceramics, an H_2SO_4 vaporizer with a special concept, bayonet type reactor made of SiC tubs, was proposed[4.10.22]. For the Bunsen reaction step, fluoroplastic, glass, Zr, and Ta showed corrosion resistance, which can be applied using lining techniques.

4.10.4 Development of Corrosion Resistance Reactors

For industrialization the process components made of practical structural materials are essential. Fig. 4.10.4 shows developed corrosion resistance reactors which works in three main chemical reaction environments. For the Bunsen reactor[4.10.23-4.10.24], HI and H_2SO_4 are produced at around 100℃. Fluoroplastic lined steel is adapted because of its productivity. Solution in the storage tank is circulated in an external circuit consisting of a pump, a tubular reactor with a static mixer, a cooler; functions of the reactor, mixture of reactants, Bunsen reaction, heat removal, and separation of products, are separated to each component for operability.

The H_2SO_4 decomposer operates on H_2SO_4 liquid or vapor at about 900℃. Silicon carbide (SiC) is used as structural material because this high temperature and corrosive environment is too sever for application of metal materials. A bayonet type[4.10.25-4.10.26] reactor made of SiC tubes fixed on a glass-lined pipe is applied to integrate H_2SO_4 vaporization and decomposition in one reactor. This type has advantages that risk of leak decreases due to no sealing in high temperature part and that heat recovery is possible from high temperature H_2SO_4 decomposition product to low temperature H_2SO_4 solution through the SiC tube.

The HI decomposer decomposes HI to produce H_2 at around 400℃. Nickel based alloy is used for the reactor considering its thermal and corrosion resistance. A radial flow type fixed bed reactor[4.10.6] is used aiming stable reaction rate by prevention of ununiform flow.

4.10.5 Development of Thermal Efficiency Improvement Technology

R&D for higher hydrogen production thermal efficiency, development of membrane technique is one of essential tasks. HI should be separated from HIx solution produced in the Bunsen reaction. However, to separate pure HI is impossible by simple distillation because of pseudo-azeotropy of this mixture. To get over the pseudo-azeotro solution, concentration of HI with electro-electrodialysis (EED) was proposed[4.10.27] in JAEA. Fig. 4.10.5 is the schematic of the EED cell. HIx solution is fed to two cell compartments and HI is concentrated by electrochemical reactions at electrodes and permeation of H+ through a cation exchange membrane. Property of the membrane is an important factor for higher thermal efficiency. Radiation-induced grafted polymer membranes[4.10.28] are key material.

The EED cell consists of bipolar electrodes and a cation exchange membrane. HI in the HIx solution is concentrated by redox reactions of I2 on the surface of the electrodes. Developed EED cell stack is constructed by stacking several collector plates, electrodes, and membranes. Impervious graphite is used for the electrodes considering its conductivity and corrosion resistance[4.10.24].

References

4.10.1) J.H. Norman, et al., “Thermochemical Water-splitting for Hydrogen Production, Final Report (January 1975-December 1980)”, GRI-80/0105 (1981).

4.10.2) H. Nakajima, et al., “Closed-cycle continuous hydrogen production test by thermochemical IS process”, Kagaku Kogaku Ronbunshu, 24, 2, pp.352-355 (1998) (in Japanese).

4.10.3) H. Nakajima, et al., “A study on a closed-cycle hydrogen production by thermochemical water-splitting IS process”, Proceedings of 7th International Conference on Nuclear Engineering (ICONE-7), ICONE-7104, Tokyo, Japan, 6p (1999).

4.10.4) S. Kubo, et al., “A demonstration study on a closed-cycle hydrogen production by the thermochemical water-splitting iodine-sulfur process”, Nuclear Engineering and Design, 233, 1-3, pp.347-354 (2004).

4.10.5) K. Onuki, S. Kubo, et al., Chapter 17, “Thermochemical Iodine – Sulfur Process”, Nuclear Hydrogen Production Handbook, CRC Press, pp.461-498 (2011).

4.10.6) S. Kasahara, et al., “Current R&D status of thermochemical water splitting iodine-sulfur process in Japan Atomic Energy Agency”, International Journal of Hydrogen Energy, 42, 19, pp.13477-13485 (2017).

4.10.7) S. Kubo, et al., “Research and development on chemical reactors made of industrial structural materials and hydriodic acid concentration technique for thermochemical hydrogen production IS process”, JAEA-Technology 2015-028 (2015), 32p (in Japanese).

4.10.8) H. Takegami, et al., “Development of strength evaluation method for high-pressure ceramic components”, Nuclear Engineering and Design, 271, pp.253-256 (2014).

4.10.9) K. Onuki, et al., “Materials of Construction for the Thermochemical IS Process, (I)”, Journal of the Hydrogen Energy Systems Society of Japan, 18, 2, pp.49-56 (1994) (in Japanese).

4.10.10) K. Onuki, et al., “Materials of Construction for the Thermochemical IS Process, (II)”, Journal of the Hydrogen Energy Systems Society of Japan, 19, 2, pp.10-16 (1995) (in Japanese).

4.10.11) K. Onuki, et al., “Screening Tests on Materials of Construction for the Thermochemical IS Process”, Corrosion Engineering, 46, pp.141-149 (1997).

4.10.12) I. Ioka, et al., “Corrosion resistance of Fe-Si alloys in boiling sulfuric acid”, Zairyo (Journal of the Society of Materials Science, Japan), 46, 9, pp.1041-1045 (1997) (in Japanese).

4.10.13) M. Futakawa, et al., “Corrosion test of compositionally graded Fe-Si alloy in boiling sulfuric acid”, Corrosion Engineering, 46, pp.811-819 (1997).

4.10.14) N. Nishiyama, et al., “Corrosion resistance evaluation of brittle materials in boiling sulfuric acid”, Zairyo (Journal of the Society of Materials Science, Japan), 48, 7, pp.746-752 (1999) (in Japanese).

4.10.15) I. Ioka, et al., “The characterization of passive films on Fe-Si alloy in boiling sulfuric acid”, Journal of Materials Science Letters, 18, 8, pp.1497-1499 (1999).

4.10.16) Y. Kurata, et al., “High Temperature Tensile Properties of Metallic Materials Exposed to a Sulfuric Acid Decomposition Gas Environment”, Journal of the Japan Institute of Metals and

Materials, 65, 4, pp.262-265 (2001) (in Japanese).

4.10.17) R.L. Ammon, “Status of materials evaluation for sulfuric acid vaporization and decomposition application”, Proceedings of 4th World Hydrogen Energy Conference, California, USA, June 1982, 2, pp.623-644 (1982).

4.10.18) F. Coen Porisini, “Selection and evaluation of materials for the construction of a pre-pilot plant for thermal decomposition of sulfuric acid”, International Journal of Hydrogen Energy, 14, 4, pp.267-274 (1989).

4.10.19) Y. Imai, et al., “Corrosion resistance of metallic materials in high temperature gases composed of iodine, hydrogen iodide and water (Environment of the 3rd and 4th Stage Reactions)”, Boshoku Gizyutsu, 31, 11, pp.714-721 (1982) (in Japanese).

4.10.20) S. Kubo et.al., “Corrosion resistance of structural materials in high-temperature aqueous sulfuric acids in thermochemical water-splitting iodine-sulfur process”, International Journal of Hydrogen Energy, 38, 16, pp.6577-6585 (2013).

4.10.21) S. Kubo et.al., “Adaptability of Metallic Structural Materials to gaseous HI decomposition environment in thermochemical water-splitting iodine-sulfur process”, Corrosion Engineering, 62, 3, pp.104-111(2013).

4.10.22) F. Gelbald, et al., “Status of Initial Testing of the H_2SO_4 Section of the ILS Experiment”, SAND2007-7841 (2007).

4.10.23) S. Kubo et.al., “R&D Status on Thermochemical IS Process for Hydrogen Production at JAEA”, Energy Procedia, 29, pp.308-317 (2012).

4.10.24) N. Tanaka, et al., “IS Process Hydrogen Production Test for Components and System Made of Industrial Structural Material (I) - Bunsen and HI Concentration Section”, Proceedings of the 2016 International Topical Meeting on High Temperature Reactor Technology (HTR2016), HTR2016-18628, pp.1022-1028 (2016).

4.10.25) R. C. Moore, et al., “Sulfuric acid decomposition for the sulfur-based thermochemical cycles”, Nuclear Technology, 178, 1, pp.111-118 (2012).

4.10.26) H. Noguchi, et al., “IS Process Hydrogen Production Test for Components and System Made of Industrial Structural Material (II) - H_2SO_4 decomposition, HI Distillation, and HI Decomposition Section-”, Proceedings of the 2016 International Topical Meeting on High Temperature Reactor Technology (HTR2016), HTR2016-18629, pp.1029-1038 (2016).

4.10.27) K. Onuki, et al., “Electrodialysis of hydriodic acid in the presence of iodine”, Journal of Membrane Science, 175, 2, pp.171-179 (2000).

4.10.28) N. Tanaka, et al., “Effect of temperature on electro-electrodialysis of HI-I_2-H_2O mixture using ion exchange membranes”, Journal of Membrane Science, 411-412, pp.99-108 (2012).

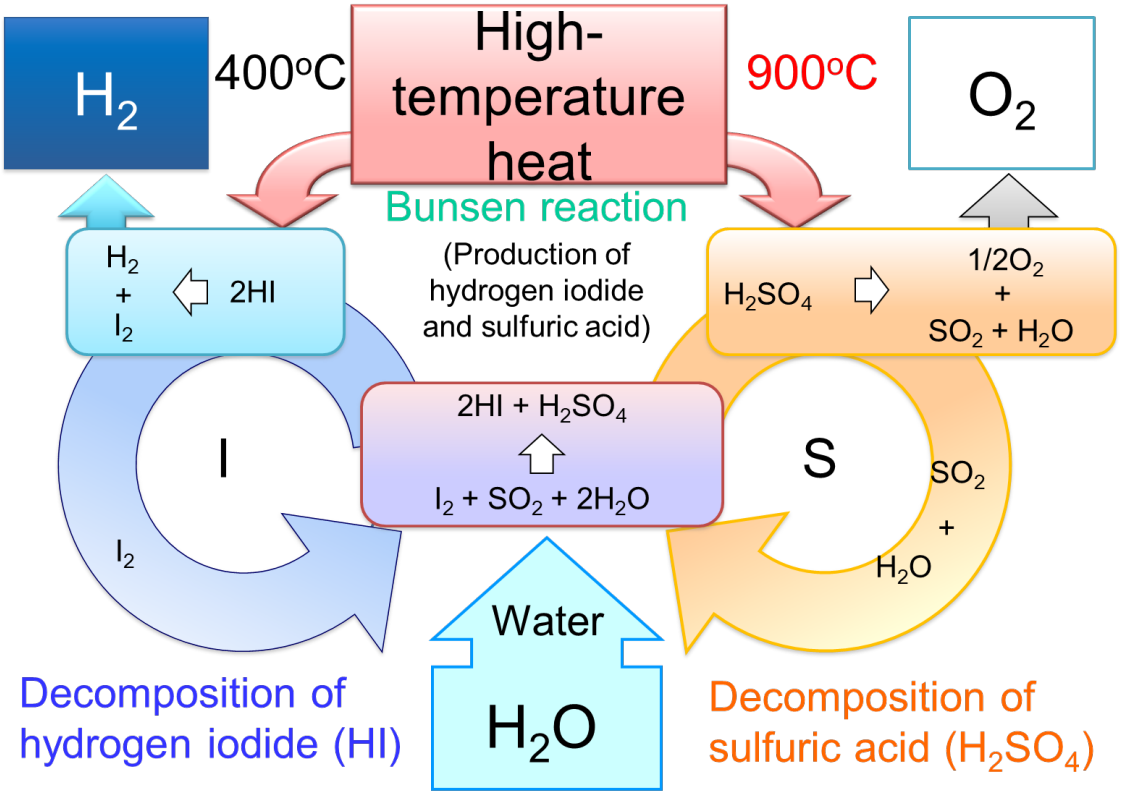

Fig.4.10.1 Brief chemical reaction scheme of the iodine-sulfur process for hydrogen production

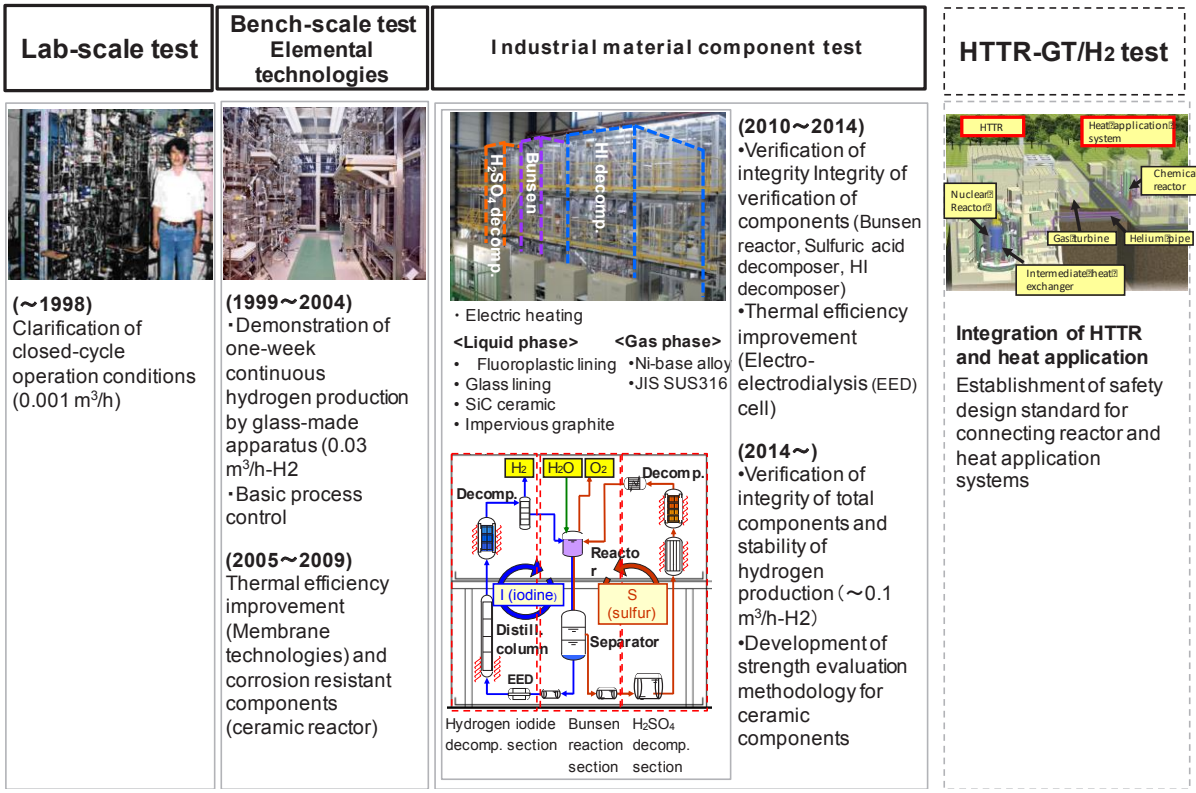

Fig.4.10.2 R&D progress of iodine-sulfur process in JAEA

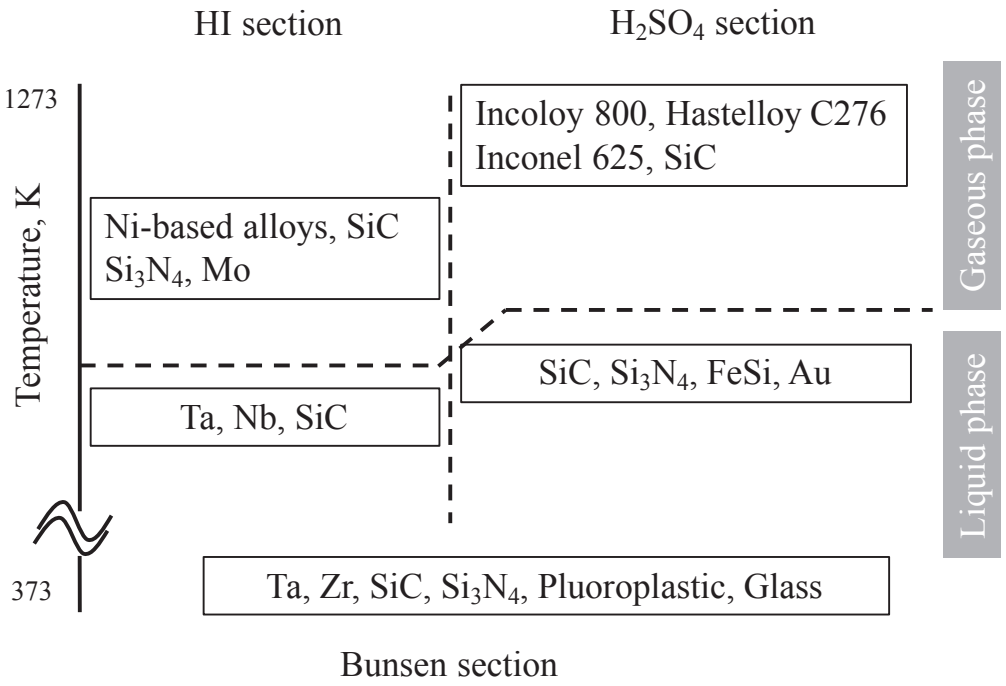

Fig.4.10.3 Candidate structural materials for prototypical environments of iodine-sulfur process. Fe -Si indicates high silicon iron

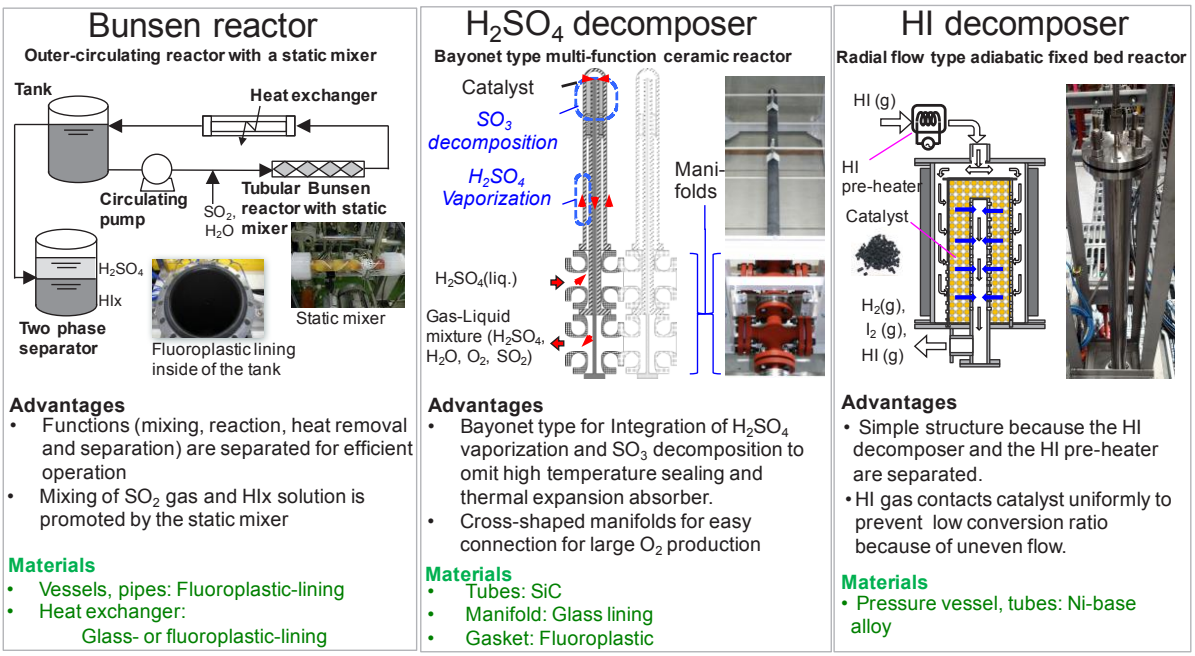

Fig.4.10.4 Developed corrosion resistance reactors made of practical structural materials

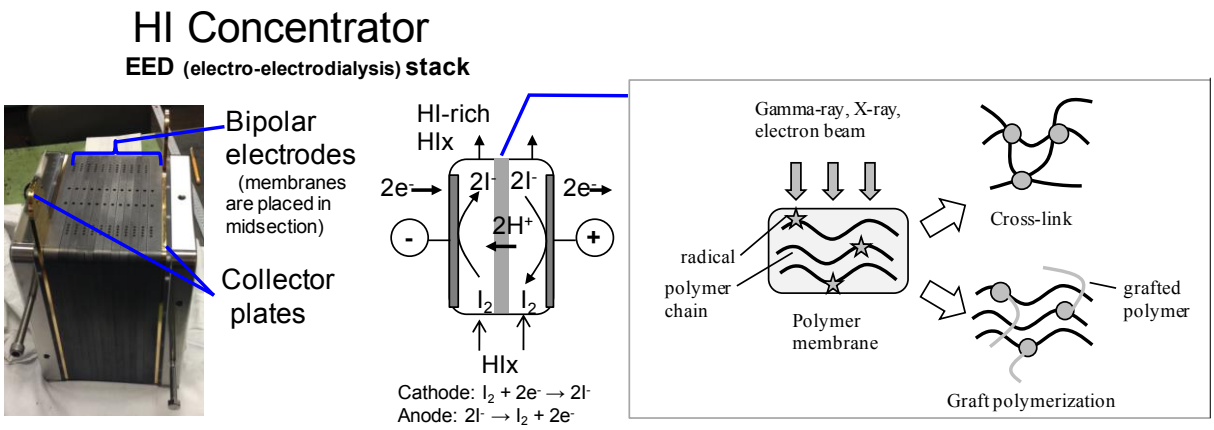

- Collector plates, electrodes and cation exchange membranes are assembled into a cell stack.

Materials

- Electrodes: Impervious graphite

- Cation exchange membrane by radiation-induced graft polymerization and cross-link process

Fig.4.10.5 Developed hydriodic acid concentrator to save required energy made of practical structural materials

4.11 Steam Reforming System for Hydrogen Production

4.11.1 Introduction

Heat application of nuclear energy to the steelmaking process was proposed in the 1960's. The concept of nuclear steelmaking is that reduction gases composed of hydrogen and carbon monoxide is produced by steam reforming of methane with heat of HTGR and supplied to a shaft furnace. In Japan, R&D of nuclear steelmaking was inaugurated in 1973 as a national project. The Engineering Research Association of Nuclear Steelmaking (ERANS), an industrial consortium of companies and institute, had promoted this project[4.11.1)].

Reflecting this project, JAEA considered hydrogen production system by steam reforming as one of the heat utilization systems of HTTR [4.11.2)]. Its technology matured on a fossil-fired plant enables the coupling with the HTTR in the early 2000's and technical solutions demonstrated by the coupling will contribute to other hydrogen production system such as IS process. A mock-up demonstration test was carried out to confirm safety, controllability and performance the steam reforming system under simulated operational conditions of the HTTR hydrogen production system [4.11.3-4.11.5)].

4.11.2 Design of HTTR steam reforming system

The HTTR hydrogen production system by steam reforming was designed to utilize the nuclear heat effectively and achieve hydrogen productivity competitive to that of a fossil-fired plant with operability, controllability and safety acceptable. Figure 4.11.1 shows a schematic flow diagram of HTTR hydrogen production system [4.11.2)]. The HTTR supplies nuclear heat of 10 MW at 950°C to the intermediate heat exchanger (IHX) and the heat of secondary helium is utilized by a steam reformer (SR) a super-heater and a steam generator (SG). Hydrogen is produced by steam reforming of methane ($CH_4+H_2O=CO+3H_2$). Table 4.11.1 shows design specifications of the HTTR hydrogen production system.

4.11.3 Mock-up Test Facility

The SR causes temperature fluctuation of the secondary helium by the fluctuation of chemical reaction at the start-up and the shut-down operation as well as malfunction or accident of the hydrogen production system. If the temperature fluctuation is transferred to the reactor, the reactor will be stopped. Therefore, the control technology should be developed to mitigate the temperature fluctuation within 10 °C at the SG outlet to prevent the scram of HTTR. JAEA proposed to use the SG as the thermal absorber installed downstream the SR in the secondary helium loop.

The hydrogen production capacity of mock-up test facility is 110 Nm^3/h and simulated key components downstream from the IHX of the HTTR hydrogen production system. Figure 4.11.2 shows the schematic flow diagram of the test facility and Table 4.11.1 shows design specifications of the mock-up test facility [4.11.3)]. An electric heater with 380kW was used as a heat source to heat helium gas up to 880°C at the SR inlet.

Figure 4.11.3 shows the view of the SR which has one bayonet-type catalyst tube made of Alloy 800H. The size of catalyst tube is approximately the same as those of the HTTR hydrogen production system.

In order to enhance the hydrogen production rate, disc-type fins, 2mm in height, 1mm in width and 3mm in pitch, were arranged around outer surface of the catalyst tube in the test facility[4.11.3)].

Figure 4.11.4 shows a schematic view of SG with 27 heat exchanger tubes. Helium gas flows inside of heat exchanger tubes and heat of helium gas is transferred to water of which holding quantity at the rated condition was 1.7m^3 and heat exchange rate between helium gas and water is 135kW at rated condition. The radiator was installed above the SG to cool a large quantity of steam produced in the SG in case of loss of chemical reaction and circulation of steam and condensed water circulate between the SG and the radiator[4.11.5)].

4.11.4 Operation Results

(1) Hydrogen production [4.11.4)]

The start-up of the HTTR hydrogen production system is required that the change of the secondary helium gas temperature at the outlet of the SG is within 10°C and the fluctuation of the pressure difference between helium and process gases (DP) is within the design pressure range of -0.5 MPa to 1.0MPa. In the start-up of the test facility, change of the SG outlet helium gas temperature and the DP were confirmed to satisfy above requirements in the condition that the SR inlet helium gas temperature was increased up to 880°C by 40°C/h, while the temperature rise speed of the HTTR hydrogen production system is 13°C /h. And pressure of the helium gas was increased from ambient pressure at room temperature to 4.1MPa at 880°C of the SR inlet helium gas temperature. The pressure of the process gas was controlled higher than 0.04MPa of that of helium gas, that is, the DP was controlled at 0.04MPa using a differential pressure control valve installed at the downstream of SR in the combustion line. During the start-up, nitrogen supplied in the SR was replaced with methane and steam to produce hydrogen above the SR inlet helium gas temperature of 700°C. The supply of steam was started before that of methane to prevent from coking on the catalyst, and the time interval between the supply of steam and that of methane was controlled within 1 hour in order to prevent from steam oxidation of the catalyst. The procedure of replacement of gases was as follows. First, flow rate of steam was increased from 0g/s at 700°C to rated value of 47g/s at 730°C. Then, flow rate of nitrogen was decreased from 30g/s at 730°C to 0g/s at 750°C and that of methane was increased from 0g/s at 730°C to rated value of 12g/s at 880°C.

Figure 4.11.5 shows flow rate of each gas, the DP, helium gas pressure at the SR inlet and helium gas temperatures change at the inlet and outlet of the SR and the SG during the start-up from 700°C to 880°C at the SR inlet. A horizontal axis is the time axis indicating an elapsed time from the start time of the increasing the helium gas temperature at the SR inlet from 700°C. At 0h, steam supply to the SR was started and supply flow rate was increased gradually to the rated value of 47g/s at 0.75h. Immediately, methane supply was started and nitrogen supply was stopped. Flow rate of methane increased drastically from 0g/s to 5.9g/s due to the characteristics of a control valve. After that, it increased gradually to the rated value of 12.0g/s at 880°C.

The SR inlet helium gas pressure could be controlled as a planned value and it increased from 3.7MPa at 700°C to 4.1MPa at 880 °C. At the moment of 0h, when water feed was started, the DP increased from

around 0.04MPa to 0.065MPa due to the increase of total flow rate in the SR and then it decreased immediately to around 0.04MPa. And at the moment of 0.75h, when methane feed was started, which means the start of the steam reforming reaction, the DP fluctuated due to the increase of total flow rate by produced hydrogen. The DP took minimum and maximum value of -0.04MPa and 0.10MPa, respectively, but its fluctuation range was extremely small compared to the design pressure range of -0.5MPa to 1.0MPa.

Increasing rate of the SR inlet helium gas temperature was 40°C per an hour, which is corresponding to the planned value. The SR outlet helium gas temperature decreased slightly in spite of the increase of the SR inlet helium gas temperature due to the increase of steam flow rate. And then, it decreased drastically at the moment of 0.75h, when methane feed was started, due to the start of the steam reforming reaction, and it took minimum value at 1.5h. The SG inlet helium gas temperature showed almost same temperature profile as that of the SR outlet helium gas temperature. It decreased from 591°C at 0h to 508°C at 1.5h. On the other hand, the SG outlet helium gas temperature decreased only 1.5°C during the start-up in spite of the change of the SG inlet helium gas temperature about 83°C. It was confirmed that thermal disturbance of the helium gas during the start-up could be mitigated by the SG.

Figure 4.11.6 shows hydrogen production rate during the start-up and a steady state. During the start-up, hydrogen production rate increased gradually from about 68m^3/h at the SR inlet helium gas temperature of 731°C to about 121m^3/h at 880°C with the increase of the helium gas temperature and methane flow rate. In the steady state, temperatures and pressures of helium and process gases were stable. And observed average flow rates of methane, steam and helium gas were 12.0g/s, 46.6g/s and 91.0g/s, respectively. Hydrogen production rate was stable and an average value between 14 and 40h was 120.2m^3/h.

(2) Loss of chemical reaction [4.11.5)]

The accident on the loss of chemical reaction in the SR is the severest one for the temperature fluctuation of the secondary helium gas. The simulation test was carried out to verify the control technology with the SG and the radiator against the temperature fluctuation of helium gas. Figure 4.11.7 shows feed flow rate of each gas to the chemical reactor, the SR, and hydrogen production rate, simulating the accident on loss of chemical reaction. A horizontal axis is the time axis indicating an elapsed time from the suspension of methane feed. Before the start of the test, flow rate of methane and steam could be controlled at each rated value, 12g/s and 47g/s, respectively. The helium temperature at inlet of SR was 880°C and hydrogen production rate showed stable value of about 120m^3/h. And it decreased to 0m^3/h due to the suspension of methane feed to the steam, and nitrogen was flowed instead of methane.

Figure 4.11.8 shows the helium gas temperatures of the SR and the SG, the steam flow rate of the radiator, and water pressures in the SG and the radiator. Before the loss of chemical reaction, the helium temperatures at the SR outlet and the SG inlet and the outlet were 632°C, 548°C and 262.5°C, respectively. At the elapsed time of 0h, when methane feed was stopped, the SR outlet helium gas temperature started to increase from 632°C to 837 °C at 1.2 hour due to the loss of chemical reaction. And it results in the

increase of the SG inlet helium gas temperature, and it increased from 548°C at 0h to 796°C at 1.4 hour. With increasing the pressure in the SG from 4.61 MPa to 4.75 MPa, and the helium temperature at the SG outlet increased from 262.5°C to 264.5°C. The circulation of steam and condensed water between the SG and the radiator was carried out at 4.75MPa.

After the start of the natural circulation, both of SG inside pressure and the radiator inlet pressure were kept decreasing. With changing the water pressure in the SG from 4.75MPa to 4.26MPa, the water temperature decreased from 260.2°C to 256.2°C. As a result, the SG outlet helium gas temperature decreased from 264.5°C to the minimum value of 261.3°C. Then, these pressures increased gradually because steam production rate in the SG became larger than the radiator inlet steam flow rate due to the increase of the SG inlet helium gas temperature. It results in the increase of both of the SG inside water temperature and the SG outlet helium gas temperature. Consequently, the SG inside pressure could be controlled about 4.3MPa, it means the water temperature in the SG could be controlled stable. On the other hand, the SG outlet helium gas temperature increased to 262.3 °C due to the increase of the helium gas temperature at the SG inlet. However, the fluctuation of helium gas temperature could be mitigated successfully in the range from -1.2°C to +2.0°C at the SG outlet, whereas SG inlet helium gas temperature increased 248°C at the loss of chemical reaction. It was within the target fluctuation range from -10°C to +10 °C at SG outlet, which is required from the HTTR operation.

As a result, it was confirmed that the SG can be used as a thermal absorber to mitigate the temperature fluctuation of the secondary helium gas caused by the chemical reactor. This technology can keep reactor operation at normal start-up and shut-down operation as well as malfunction or accident of the hydrogen production system.

4.11.5 Conclusion

By fabricating and operating a mockup model of hydrogen production system by steam reforming, the following results were obtained.

1) A steam reformer performing heat exchange with helium gas was developed. The disc-type fins on the surface of the catalyst tube were effective for promoting heat transfer with helium gas.
2) The control technology using a SG as a thermal absorber installed downstream from a chemical reactor in the secondary helium gas loop was developed to mitigate temperature fluctuation of the helium gas. By the simulation test with the mock-up test facility, it was confirmed that the SG could be used as the thermal absorber.
3) The operation procedures of the hydrogen production system by steam reforming were established including the normal start-up and shut-down methods working closely to the nuclear reactor, HTTR, and the irregular shut-down method against accidents such as loss of chemical reaction.

References

4.11.1) K. Tsuruoka, et al., “Design Study of Nuclear Steelmaking System”, Transactions of the Iron and Steel Institute of Japan, 23, 12, pp.1091-1101 (1983).

4.11.2) K. Hada, et al., “Design of a Steam Reforming System to be connected to HTTR”, JAERI-Conf 96-010, pp.229-240 (1996).

4.11.3) Y. Inagaki, et al., “Out-of-Pile Demonstration Test of Hydrogen Production System Coupling with HTTR”, Proceedings of 7th International Conference on Nuclear Engineering (ICONE-7), ICONE-7101, Tokyo, Japan, 10p. (1999).

4.11.4) H. Ohashi, et al., “Performance Test Results of Mock-up Test Facility of HTTR Hydrogen Production System”, Journal of Nuclear Science and Technology, 41, 3, pp.385-392 (2004).

4.11.5) Y. Inagaki, et al., “Research and Development on System Integration Technology for Connection of Hydrogen Production System to an HTGR”, Nuclear Technology, 157, 2, pp.111-119 (2007).

Table 4.11.1 Design specifications of HTTR hydrogen production system and mock-up test facility

Items	HTTR	Mock-up
Pressure Process-gas / helium-gas	4.5 / 4.1 MPa	
Temperature inlet at steam reformer Process-gas / helium-gas	450 / 880 °C	
Temperature outlet at steam reformer Process-gas / helium-gas	600 / 600 °C	600 / 650 °C
Natural gas feed	1296kg/h (81kmol/h)	43.2kg/h (2.7kmol/h)
Helium gas feed	8748kg/h	327.6 kg/h
Steam-carbon ratio (S/C)	3.5	2～4
Hydrogen product	3800Nm^3/h	110Nm^3/h
Heat source	Reactor(10MW)	Electric heater(380kW)

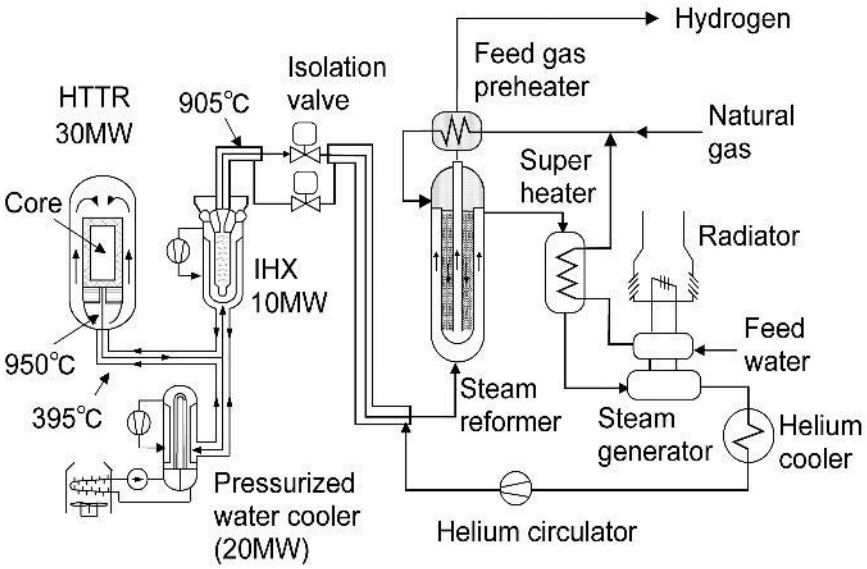

Fig. 4.11.1 Schematic flow diagram of HTTR hydrogen production system

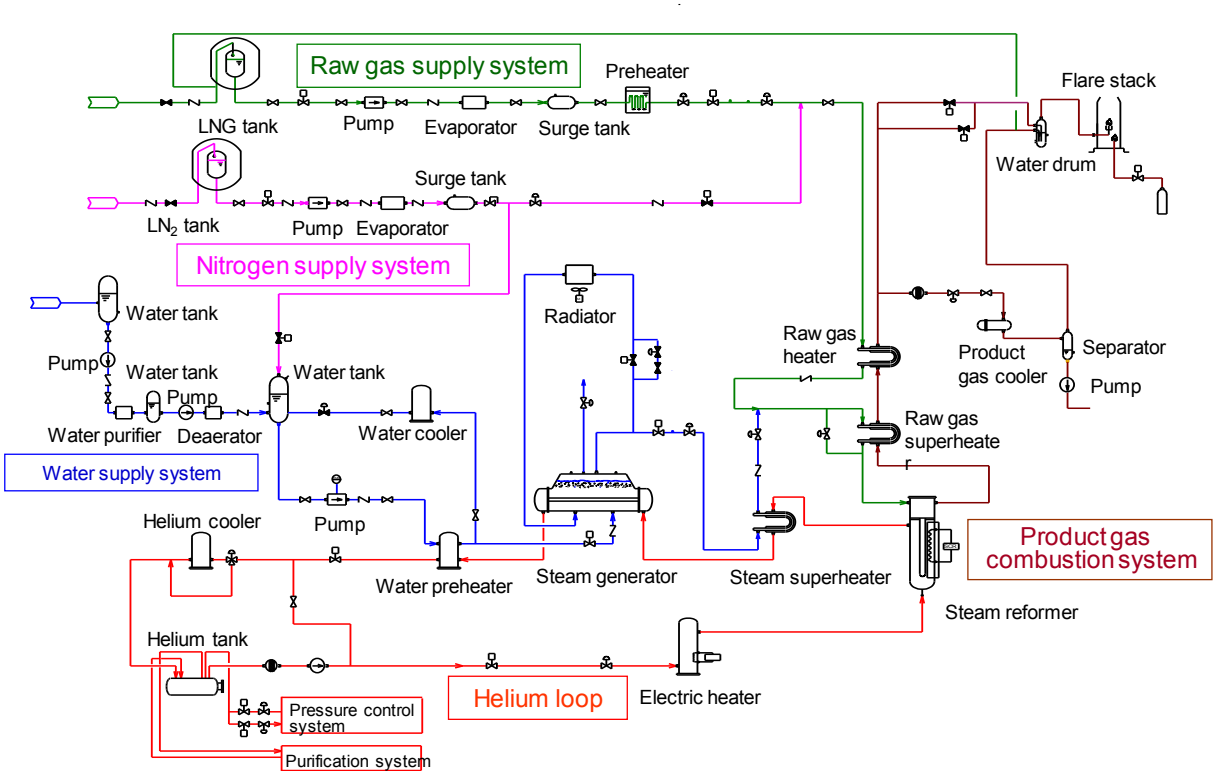

Fig. 4.11.2 Schematic flow diagram of mock-up test facility

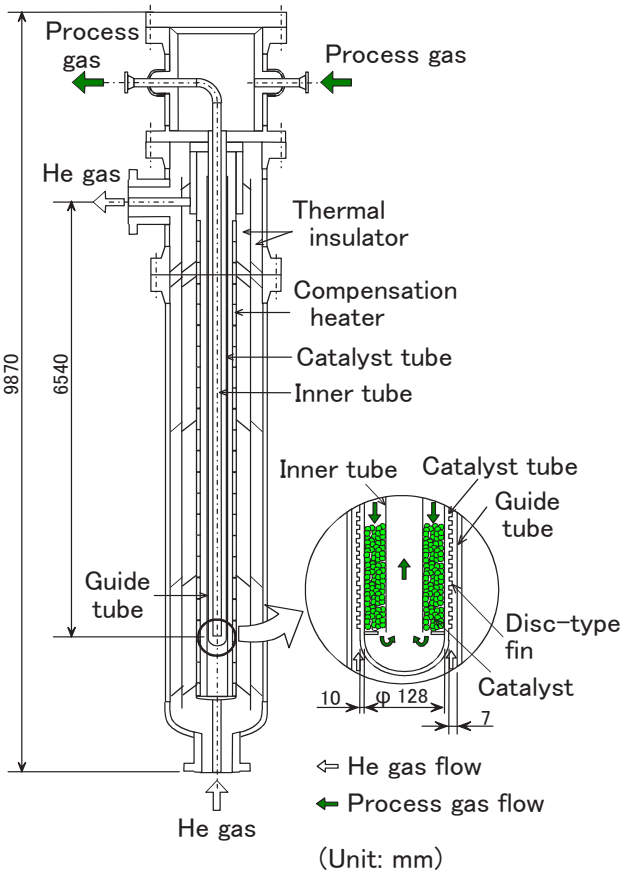

Catalyst tube

Fig. 4.11.3 Steam reformer

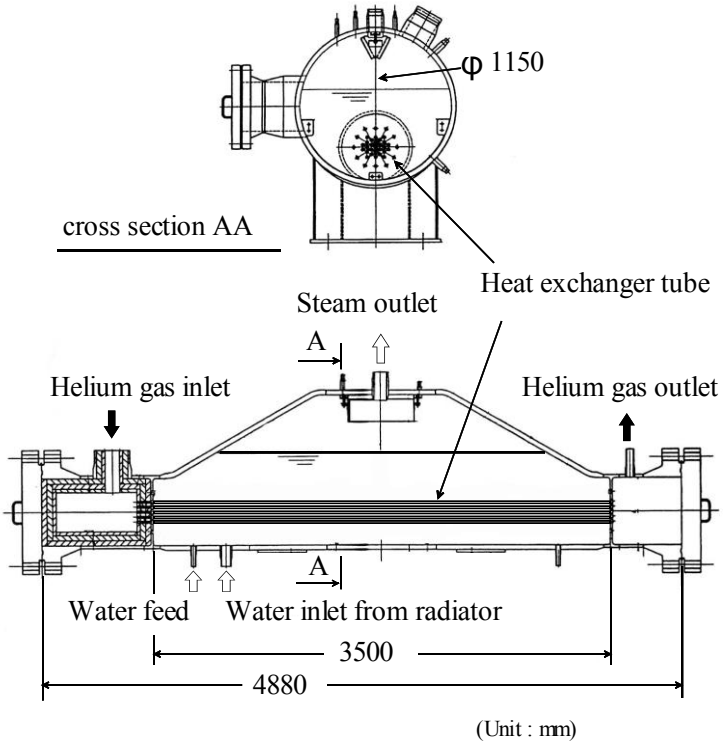

Fig. 4.11.4 Schematic view of steam generator

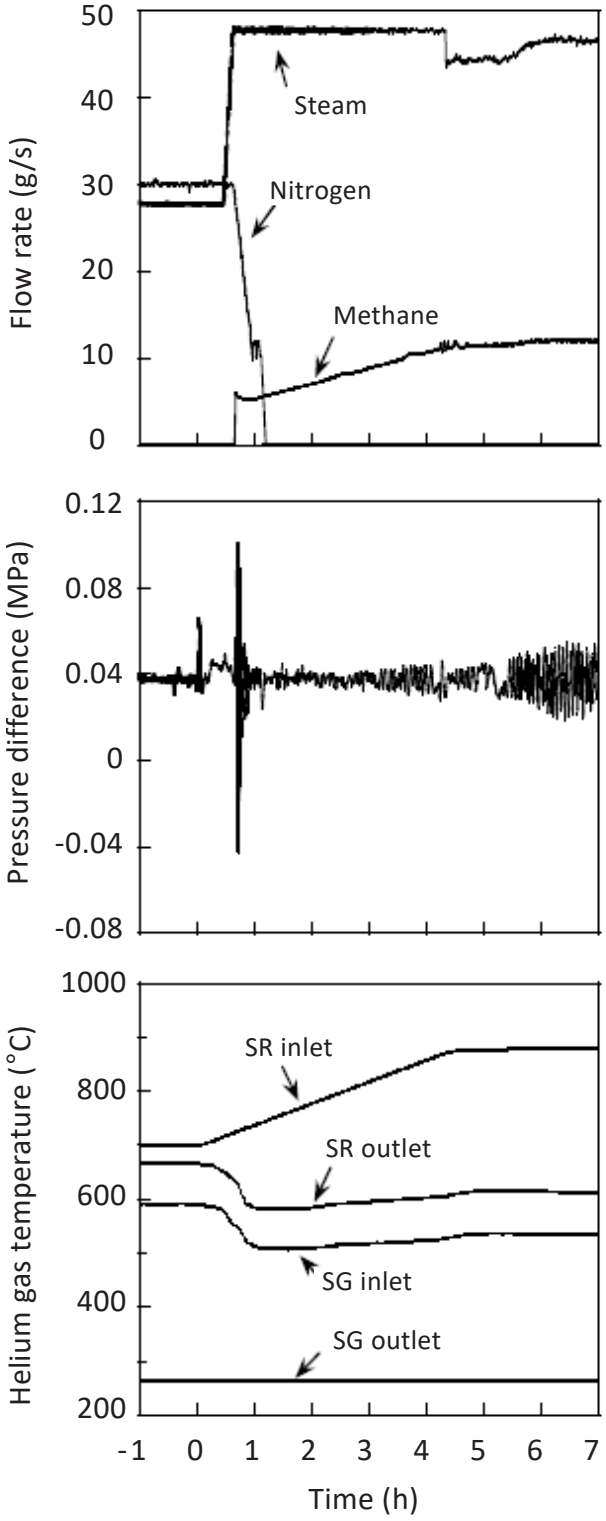

Fig. 4.11.5 Flow rates of each gas, pressure difference between helium and process gases at the reaction tube in steam reformer, helium gas pressure at stem reformer inlet and helium gas temperatures at inlet and outlet of steam reformer and steam generator during normal start-up.

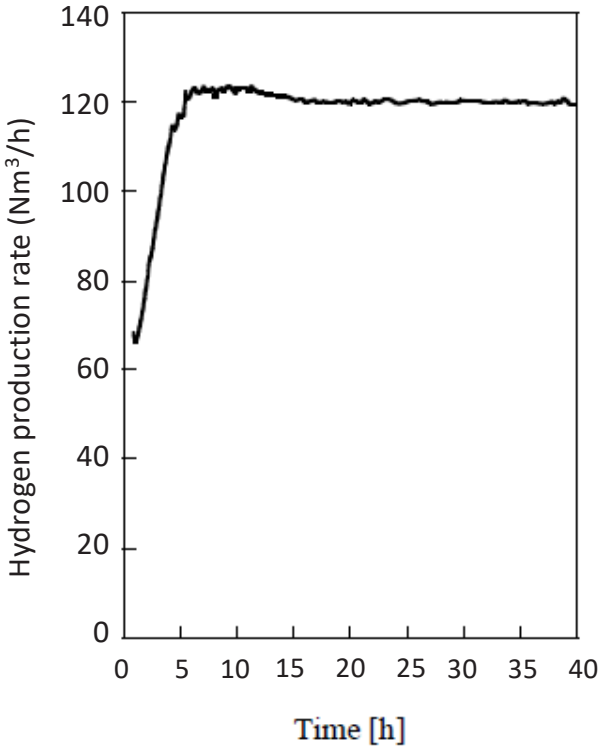

Fig. 4.11.6 Hydrogen production rate during start-up and steady state

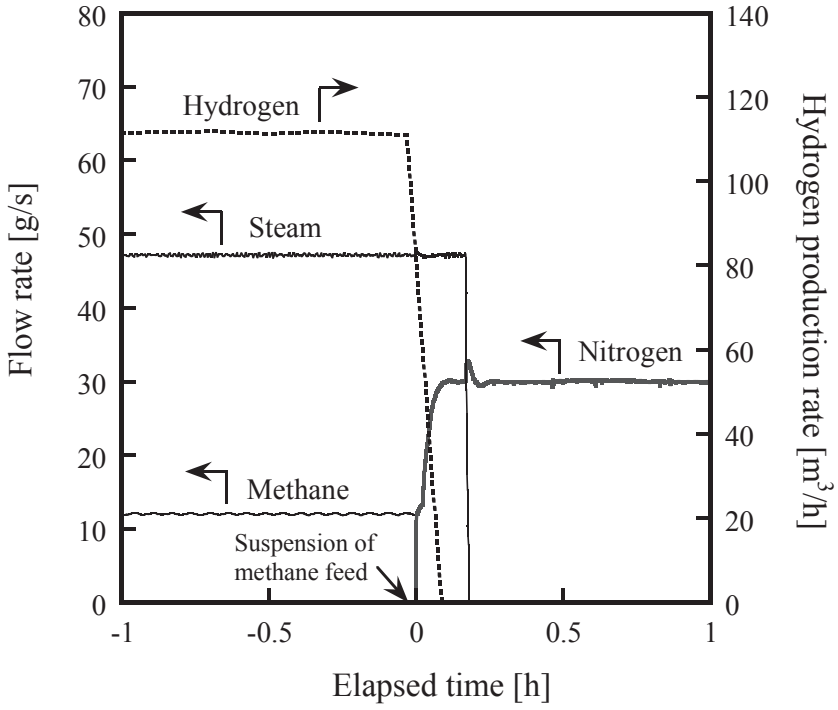

Fig. 4.11.7 Flow rate of each gas and hydrogen production rate in simulation test of accident on loss of chemical reaction

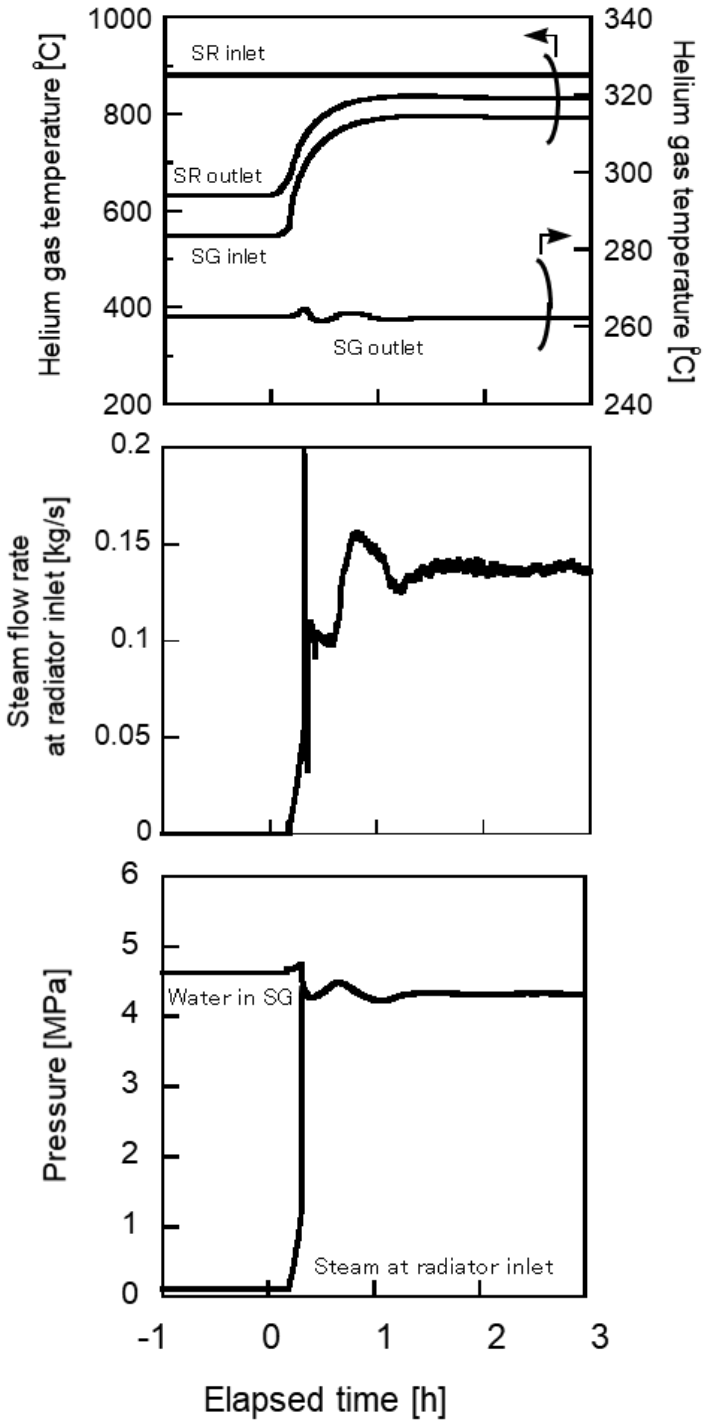

Fig. 4.11.8 Helium gas temperatures of steam reformer and steam generator, steam flow rate of the radiator, and water pressures in steam generator and radiator

5. Concluding Remarks

HTGR has a potential to solve the global warming issue to supply high temperature heat without CO_2 emission. Many countries have carried out the research and development on commercialization of HTGR for power generation and heat application. JAEA in cooperation with Japanese companies has developed world-highest-level HTGR technologies listed in Table 5.1. Japanese HTGR can operate at 950°C by optimized core design and new-developed heat resistant super alloy. This performance enable to realize high temperature heat application such as hydrogen production by thermochemical water-splitting. And JAEA constructed the test reactor, HTTR. Through HTTR design and operation, JAEA has many useful data and know-how to develop commercial HTGR.

Acknowledgments

The authors would like to express their appreciation to Dr. Kazuhiro SAWA, Director of Department of HTTR, and Mr. Tatsuo IYOKU, former Director of Department of HTTR, for their useful comments and advices.

Table 5.1 Japanese HTGR technologies (1/8)

Item	HTGR technologies	JAEA's patent, know-how, data	Manufactures' patent, know-how	Remarks
Neutronics /Thermal-hydraulics	Core coolant flow distribution technology to limit core bypass flow and increase effective coolant flow of the fuel	Seal technology to control bypass flow and core coolant flow distribution analysis technology based on HENDEL experimental data. HTTR experimental data of core pressure drop for validation of core coolant flow distribution analysis code.	Design technology of reactor internals to control bypass flow in core and design, fabrication and inspection technologies of core support structures (graphite and steel) Core restraint mechanism to control bypass flow between permanent reflectors.	Technology for prismatic HTGR Pebble bed HTGR: ・Difficult to control power density distribution ・Temperature rise is 100°C-200°C higher than that of prismatic HTGR with same power in DLOFC accident because of lower heat removal performance of the pebble bed
	Control technology of power density distribution to limit fuel temperature in normal operation and in accident.	Technology of fuel temperature analysis considering realistic hot spot factors to confirm that fuel integrity is securely guaranteed Technology of nuclear analysis method based on experiment data of VHTRC, etc., which apply to the core with different enrichment fuel assemblies and burnable poison (B_4C/C) Data of control rod position and power distribution in BOC obtained by HTTR operation; the data may be used for nuclear code validation		

Table 5.1 Japanese HTGR technologies (2/8)

Item	HTGR technologies	JAEA's patent, know-how, data	Manufactures' patent, know-how	Remarks
Fuel	Technologies for reducing as-fabricated failure fraction of TRISO coated fuel particle to limit radiation release Technologies for optimizing condition of fuel compaction process to prevent yield loss (HTTR experiences: 2.5×10^{-8} for through-coatings failure fraction, 8×10^{-5} for SiC-defective fraction which satisfy criteria of commercial reactor GTHTR300)	Developed through collaboration with Nuclear Fuel Industries, Ltd. Continuous coating method Design of fluidized bed Coating condition of each coating layer Optimizing fluidized particle condition Relationship between coating duration and internal flaw Compaction press temperature and velocity Removal of odd overcoated particle Control of compaction press condition Technologies and data accumulated through HTTR test operations Fission gas sampling data (Manually sampling measuring/evaluating technologies) Circulated radioactivity measuring data (Automated measuring technology by Fuel Failure Detection System) Plated-out fission products measuring data (Surface dose measuring technologies when exchanging filter of Primary Gas Circulator)	Unique technologies, exclusive of those jointly developed and owned with JAEA Mass production technologies of external gelation method (4.3kg-U per a batch) Vibrated dropping method Technologies to select good sphericity Mass production technologies of fluidized bed and chemical vapor deposition method (3.4kg-U per a batch) In-situ sampling system for TRISO coating inspection Fluidized particle condition Mass production technologies of overcoating device (3.4kg-U per a batch x 3 per 3 compact lots) Overcoated particle condition Sintering condition of fuel compact	HTTR criterion is less than 0.2 % for as-fabricated fuel failure fraction (which is sum of fractions both of through-coatings failure and SiC-defective). GTHTR300 criterion is less than 5×10^{-4} for as-fabricated fuel failure fraction (equivalent to limitation of radiation exposure evaluation).

Table 5.1 Japanese HTGR technologies (3/8)

Item	HTGR technologies	JAEA's patent, know-how, data	Manufactures' patent, know-how	Remarks
Graphite	High strength graphite production technology to withstand stress due to strain caused by temperature difference in graphite blocks and neutron irradiation High quality graphite production technology with less data dispersion leading to keep reference strength in high for design Design database including irradiation data: GTHTR 300 is designed to exchange fuel graphite blocks with an irradiation dose on the order of 5 dpa (displacement per atom). HTTR graphite database can be used for the GTHTR 300 without extension of irradiation database	【Design know-how】 Formulation of graphite structure design guidelines for graphite structures (IG-110, PGX, ASR-0RB) used in HTTR Formulation of design curves considering neutron irradiation and oxidation effects for graphite structures 【Database】 Formulation of reference strength (tension and compression) by statistical method based on acquired data such as tensile strength, compressive strength, longitudinal elastic modulus, thermal conductivity, coefficient of thermal expansion, etc. 【Inspection】 Formulation of graphite inspection standard Specification of inspection items, criteria and number of inspections necessary to guarantee quality Material, dimensional, visual and non-destructive inspections 【In-service inspection】 Formulation of in-service inspection method of graphite structure	【Production】 Following "process control item" is described. Grinding/mixing: Rotor speed Mixing: temperature, number of mixing Grinding/sieving: rotor speed CIP molding: pressure, time Primary firing: temperature, time Pitch impregnation: pressure, temperature, time Secondary firing: temperature, time Graphitization and high purity: temperature, time, halogen gas flow rate	Suppression of dispersion in product quality: since bulk density, true density, ash content, volatile content, linear expansion coefficient, graphitization property, etc. in raw materials affect the final quality of graphite products, strict acceptance inspections were carried out for properties of raw material coke. Cold isostatic pressure isotropic press (CIP) molding: technology that macroscopically makes isotropic properties of a product by injecting raw materials into a mold and pressurizing isotropically with water pressure Graphitization and purification: development and control of graphite crystals by heating up to about 3000°C to obtain predetermined physical properties

Table 5.1 Japanese HTGR technologies (4/8)

Item	HTGR technologies	JAEA's patent, know-how, data	Manufactures' patent, know-how	Remarks
Heat exchanger and metallic material	Intermediate heat exchanger is necessary to utilize high-temperature heat of 950°C, and material database (material strength standard, etc.) on high-temperature creep strength, corrosion resistance property, etc. used for heat exchanger tubes is necessary. Design standard of high-temperature heat exchanger	【Material (hastelloy XR as base material)】 Heat treatment method Material data (incl. He atmos.) 【Material (hastelloy XR as welding material)】 ・Component Filler material production technology Heat treatment condition after weld Welded data (incl. He atmos.) 【Design (High-temperature structure)】 Thermal expansion absorption mechanism (950°C, hastelloy XR) Design guidelines for high-temperature structure (including elastic creep analysis) 【Design (thermal-hydraulics)】 Steady heat transfer equation (He/He heat exchange) Thermal transient evaluation Heat-transfer enhancement technology	【Material (hastelloy XR as base material)】 Heat treatment method Material production technology 【Material (hastelloy XR as filler material)】 Component Filler material production technology Heat treatment condition after weld 【Design (high-temperature structure)】 Structural analysis 【Design (thermal-hydraulics)】 Steady heat transfer equation (He/He heat exchange) Heat-transfer enhancement technology 【Design (insulation structure)】 Insulator packing ratio optimization technology Liner installation, thermal expansion absorption, etc.	JAEA and Mitsubishi Materials Co., Ltd developed Hastelloy XR of superalloy with corrosion and heat resistance specifically for use in HTGRs. (available until 1000°C in accident) In addition, JAEA and Nippon Welding Rod Co., Ltd. developed filler material.

Table 5.1 Japanese HTGR technologies (5/8)

Item	HTGR technologies	JAEA's patent, know-how, data	Manufactures' patent, know-how	Remarks
Heat exchanger and metallic material (continu-ation)		【Design (insulation structure)】 Insulator data (equivalent thermal conductivity) Degradation prevention data of insulator (shot prevention) Natural convection prevention technology in insulation layer Insulator packing ratio optimization technology Liner installation, thermal expansion absorption, etc.【Operating experience】 High temperature test operation and rated operation data (950°C and 850°C) Structural integrity data (950° C and HTTR's continuous operation for 50 days) Aging degradation can be evaluated by surveillance test pieces in PPWC (hastelloy XR : tensile strength and bending strength). Tritium distribution data in systems (Evaluation of permeation amount through heat exchanger) 【ISI technology】 Damage inspection method by Eddy Current Testing (ET) and Ultrasonic Testing (UT) for helical coil made of hastelloy XR Measurement data of deposited dust in filters		

Table 5.1 Japanese HTGR technologies (6/8)

Item	HTGR technologies	JAEA's patent, know-how, data	Manufactures' patent, know-how	Remarks
Design Licensing Construction	Licensing experiences of HTTR	Experimental data necessary for establishing safety design philosophy (including documents) Experience of the HTTR safety review Sets of design criteria accepted by safety review (fuel, graphite components, high temperature components, etc.)		
	Seismic technologies especially for graphite components	Seismic classification philosophy (application for installment license) Seismic analysis code for graphite components Vibration tests data for verification of seismic analysis code Destruction tests data of core support structures (support post, permanent reflector block)	Fabrication technologies Quality control methods On-site installation technologies	One of important issues for HTGR design and licensing
	Safety evaluation technologies	Verified analysis codes accepted to licensing Test data and documents		
	Technologies to reduce heat loss	Design of thermal insulators	Fabrication technologies Quality control methods On-site installation technologies	Reflecting experiences through HTTR operation
	Shielding design technologies	Design technologies considering gaps due to thermal expansion		

Table 5.1 Japanese HTGR technologies (7/8)

Item	HTGR technologies	JAEA's patent, know-how, data	Manufactures' patent, know-how	Remarks
Operation Maintenance	Operation experiences	Operation manuals Education program for operators Troubleshooting database obtained from ~20 years of HTTR maintenance Periodic inspection procedures		
	Helium coolant control technologies	Operation data of leak rate		
	Impurities control technologies	Power rise procedure to control impurities in primary coolant based on operation experiences Tritium transport data in primary / secondary coolant		
	High temperature neutron detector in core	Inspection manual based on operation experiences	Fabrication technologies of in-core neutron detectors	
	Safeguards technologies	Monitoring and recording methods for fuel movement		

Table 5.1 Japanese HTGR technologies (8/8)

Item	HTGR technologies	JAEA's patent, know-how, data	Manufactures' patent, know-how	Remarks
Power generation technology	Power generation by helium gas turbines (novel technology) 【System design】 Power generation efficiency of 50% Being free of accident of water ingress into reactor core	A device with HTGR gas turbine power generation system of twin double-pipes layout, Patent JP4344839 System design code of HTGR gas turbine system which includes design database of various reactors and gas turbines and which is verified by HTTR operation data.		
	【Aerodynamic design】 To ensure high efficiency and reliable operation by reducing loss and separation of fluid around compressor blades.	Knowledges on aerodynamic design of helium compressors based on design and tests of 1/3 scale model (JAEA, MHI)	Experience accumulation of many designs of industrial gas turbines (MHI)	JAEA and MHI has verified the technology by 1/3 scale model test.
	【Shaft seal technology】 To minimize helium leakage of large diameter machinery shaft vessel penetration.	Patent is to be applied.		JAEA and MHI proposed a basic concept of leak reduction by dry gas seal system. Co-development is under way.
	【Reduction technology of FP deposition on turbine blades】 Development of turbine blade alloys with small FP deposition is required to permit maintenance.	Rotating equipment in nuclear facility. Patent Application JP 2014-105242 Knowledges on evaluation of FP deposition amount on components	Knowledges on casting of turbine blades by controlling chemical composition and crystal structure (IHI)	JAEA and IHI proposed the concept. Co-development is under way.

国際単位系（SI）

表１．SI 基本単位

基本量	SI 基本単位	
	名称	記号
長さ	メートル	m
質量	キログラム	kg
時間	秒	s
電流	アンペア	A
熱力学温度	ケルビン	K
物質量	モル	mol
光度	カンデラ	cd

表２．基本単位を用いて表されるSI組立単位の例

組立量	SI 組立単位	
	名称	記号
面積	平方メートル	m^2
体積	立方メートル	m^3
速さ，速度	メートル毎秒	m/s
加速度	メートル毎秒毎秒	m/s^2
波数	毎メートル	m^{-1}
密度，質量密度	キログラム毎立方メートル	kg/m^3
面積密度	キログラム毎平方メートル	kg/m^2
比体積	立方メートル毎キログラム	m^3/kg
電流密度	アンペア毎平方メートル	A/m^2
磁界の強さ	アンペア毎メートル	A/m
量濃度(a)，濃度	モル毎立方メートル	mol/m^3
質量濃度	キログラム毎立方メートル	kg/m^3
輝度	カンデラ毎平方メートル	cd/m^2
屈折率(b)	（数字の） 1	1
比透磁率(b)	（数字の） 1	1

(a) 量濃度（amount concentration）は臨床化学の分野では物質濃度（substance concentration）ともよばれる。
(b) これらは無次元量あるいは次元１をもつ量であるが、そのことを表す単位記号である数字の１は通常は表記しない。

表３．固有の名称と記号で表されるSI組立単位

組立量	SI 組立単位			
	名称	記号	他のSI単位による表し方	SI基本単位による表し方
平面角	ラジアン(b)	rad	1 (b)	m/m
立体角	ステラジアン(b)	sr(c)	1 (b)	m^2/m^2
周波数	ヘルツ(d)	Hz		s^{-1}
力	ニュートン	N		m kg s^{-2}
圧力，応力	パスカル	Pa	N/m^2	m^{-1} kg s^{-2}
エネルギー，仕事，熱量	ジュール	J	N m	m^2 kg s^{-2}
仕事率，工率，放射束	ワット	W	J/s	m^2 kg s^{-3}
電荷，電気量	クーロン	C		s A
電位差（電圧），起電力	ボルト	V	W/A	m^2 kg s^{-3} A^{-1}
静電容量	ファラド	F	C/V	m^{-2} kg^{-1} s^4 A^2
電気抵抗	オーム	Ω	V/A	m^2 kg s^{-3} A^{-2}
コンダクタンス	ジーメンス	S	A/V	m^{-2} kg^{-1} s^3 A^2
磁束	ウエーバ	Wb	Vs	m^2 kg s^{-2} A^{-1}
磁束密度	テスラ	T	Wb/m^2	kg s^{-2} A^{-1}
インダクタンス	ヘンリー	H	Wb/A	m^2 kg s^{-2} A^{-2}
セルシウス温度	セルシウス度(e)	℃		K
光束	ルーメン	lm	cd sr(c)	cd
照度	ルクス	lx	lm/m^2	m^{-2} cd
放射性核種の放射能(f)	ベクレル(d)	Bq		s^{-1}
吸収線量，比エネルギー分与，カーマ	グレイ	Gy	J/kg	m^2 s^{-2}
線量当量，周辺線量当量，方向性線量当量，個人線量当量	シーベルト(g)	Sv	J/kg	m^2 s^{-2}
酸素活性	カタール	kat		s^{-1} mol

(a)SI接頭語は固有の名称と記号を持つ組立単位と組み合わせても使用できる。しかし接頭語を付した単位はもはやコヒーレントではない。
(b)ラジアンとステラジアンは数字の１に対する単位の特別な名称で、量についての情報をつたえるために使われる。実際には、使用する時には記号radおよびsrが用いられるが、習慣として組立単位としての記号である数字の１は明示されない。
(c)測光学ではステラジアンという名称と記号srを単位の表し方の中に、そのまま維持している。
(d)ヘルツは周期現象についてのみ、ベクレルは放射性核種の統計的過程についてのみ使用される。
(e)セルシウス度はケルビンの特別な名称で、セルシウス温度を表すために使用される。セルシウス度とケルビンの単位の大きさは同一である。したがって、温度差や温度間隔を表す数値はどちらの単位で表しても同じである。
(f)放射性核種の放射能（activity referred to a radionuclide）は、しばしば誤った用語で"radioactivity"と記される。
(g)単位シーベルト（PV,2002,70,205）についてはCIPM勧告2（CI-2002）を参照。

表４．単位の中に固有の名称と記号を含むSI組立単位の例

組立量	SI 組立単位		
	名称	記号	SI 基本単位による表し方
粘度	パスカル秒	Pa s	m^{-1} kg s^{-1}
力のモーメント	ニュートンメートル	N m	m^2 kg s^{-2}
表面張力	ニュートン毎メートル	N/m	kg s^{-2}
角速度	ラジアン毎秒	rad/s	m m^{-1} s^{-1}=s^{-1}
角加速度	ラジアン毎秒毎秒	rad/s^2	m m^{-1} s^{-2}=s^{-2}
熱流密度，放射照度	ワット毎平方メートル	W/m^2	kg s^{-3}
熱容量，エントロピー	ジュール毎ケルビン	J/K	m^2 kg s^{-2} K^{-1}
比熱容量，比エントロピー	ジュール毎キログラム毎ケルビン	J/(kg K)	m^2 s^{-2} K^{-1}
比エネルギー	ジュール毎キログラム	J/kg	m^2 s^{-2}
熱伝導率	ワット毎メートル毎ケルビン	W/(m K)	m kg s^{-3} K^{-1}
体積エネルギー	ジュール毎立方メートル	J/m^3	m^{-1} kg s^{-2}
電界の強さ	ボルト毎メートル	V/m	m kg s^{-3} A^{-1}
電荷密度	クーロン毎立方メートル	C/m^3	m^{-3} s A
表面電荷	クーロン毎平方メートル	C/m^2	m^{-2} s A
電束密度，電気変位	クーロン毎平方メートル	C/m^2	m^{-2} s A
誘電率	ファラド毎メートル	F/m	m^{-3} kg^{-1} s^4 A^2
透磁率	ヘンリー毎メートル	H/m	m kg s^{-2} A^{-2}
モルエネルギー	ジュール毎モル	J/mol	m^2 kg s^{-2} mol^{-1}
モルエントロピー，モル熱容量	ジュール毎モル毎ケルビン	J/(mol K)	m^2 kg s^{-2} K^{-1} mol^{-1}
照射線量（X線及びγ線）	クーロン毎キログラム	C/kg	kg^{-1} s A
吸収線量率	グレイ毎秒	Gy/s	m^2 s^{-3}
放射強度	ワット毎ステラジアン	W/sr	m^4 m^{-2} kg s^{-3}=m^2 kg s^{-3}
放射輝度	ワット毎平方メートル毎ステラジアン	$W/(m^2$ sr)	m^2 m^{-2} kg s^{-3}=kg s^{-3}
酵素活性濃度	カタール毎立方メートル	kat/m^3	m^{-3} s^{-1} mol

表５．SI 接頭語

乗数	名称	記号	乗数	名称	記号
10^{24}	ヨタ	Y	10^{-1}	デシ	d
10^{21}	ゼタ	Z	10^{-2}	センチ	c
10^{18}	エクサ	E	10^{-3}	ミリ	m
10^{15}	ペタ	P	10^{-6}	マイクロ	μ
10^{12}	テラ	T	10^{-9}	ナノ	n
10^{9}	ギガ	G	10^{-12}	ピコ	p
10^{6}	メガ	M	10^{-15}	フェムト	f
10^{3}	キロ	k	10^{-18}	アト	a
10^{2}	ヘクト	h	10^{-21}	ゼプト	z
10^{1}	デカ	da	10^{-24}	ヨクト	y

表６．SIに属さないが、SIと併用される単位

名称	記号	SI 単位による値
分	min	1 min=60 s
時	h	1 h =60 min=3600 s
日	d	1 d=24 h=86 400 s
度	°	1°=(π/180) rad
分	’	1’=(1/60)°=(π/10 800) rad
秒	”	1”=(1/60)’=(π/648 000) rad
ヘクタール	ha	1 ha=1 hm^2=10^4m^2
リットル	L, l	1 L=1 l=1 dm^3=10^3cm^3=$10^{-3}m^3$
トン	t	1 t=10^3 kg

表７．SIに属さないが、SIと併用される単位で、SI単位で表される数値が実験的に得られるもの

名称	記号	SI 単位で表される数値
電子ボルト	eV	1 eV=1.602 176 53(14)×10^{-19}J
ダルトン	Da	1 Da=1.660 538 86(28)×10^{-27}kg
統一原子質量単位	u	1 u=1 Da
天文単位	ua	1 ua=1.495 978 706 91(6)×10^{11}m

表８．SIに属さないが、SIと併用されるその他の単位

名称	記号	SI 単位で表される数値
バール	bar	1 bar=0.1MPa=100 kPa=10^5Pa
水銀柱ミリメートル	mmHg	1 mmHg≈133.322Pa
オングストローム	Å	1 Å=0.1nm=100pm=10^{-10}m
海里	M	1 M=1852m
バーン	b	1 b=100fm^2=(10^{-12}cm)^2=$10^{-28}m^2$
ノット	kn	1 kn=(1852/3600)m/s
ネーパ	Np	SI単位との数値的な関係は、対数量の定義に依存。
ベル	B	
デシベル	dB	

表９．固有の名称をもつCGS組立単位

名称	記号	SI 単位で表される数値
エルグ	erg	1 erg=10^{-7} J
ダイン	dyn	1 dyn=10^{-5}N
ポアズ	P	1 P=1 dyn s cm^{-2}=0.1Pa s
ストークス	St	1 St =1cm^2 s^{-1}=$10^{-4}m^2$ s^{-1}
スチルブ	sb	1 sb =1cd cm^{-2}=10^4cd m^{-2}
フォト	ph	1 ph=1cd sr cm^{-2} =10^4lx
ガル	Gal	1 Gal =1cm s^{-2}=$10^{-2}ms^{-2}$
マクスウエル	Mx	1 Mx = 1G cm^2=10^{-8}Wb
ガウス	G	1 G =1Mx cm^{-2} =10^{-4}T
エルステッド(a)	Oe	1 Oe ≙ (10^3/4π)A m^{-1}

(a) ３元系のCGS単位系とSIでは直接比較できないため、等号「 ≙ 」は対応関係を示すものである。

表10．SIに属さないその他の単位の例

名称	記号	SI 単位で表される数値
キュリー	Ci	1 Ci=3.7×10^{10}Bq
レントゲン	R	1 R = 2.58×10^{-4}C/kg
ラド	rad	1 rad=1cGy=10^{-2}Gy
レム	rem	1 rem=1 cSv=10^{-2}Sv
ガンマ	γ	1 γ=1 nT=10^{-9}T
フェルミ		1 フェルミ=1 fm=10^{-15}m
メートル系カラット		1 メートル系カラット= 0.2 g = 2×10^{-4}kg
トル	Torr	1 Torr = (101 325/760) Pa
標準大気圧	atm	1 atm = 101 325 Pa
カロリー	cal	1 cal=4.1858J（「15℃」カロリー），4.1868J（「IT」カロリー），4.184J（「熱化学」カロリー）
ミクロン	μ	1 μ =1μm=10^{-6}m

（第8版，2006年）